Disruption of Endosomal Membrane by Cationic Vectors Drives Endosomal Release and Enables Successful Gene Delivery

By

Sriram Vaidyanathan

A dissertation submitted in partial fulfillment
of the requirements for the degree of
Doctor of Philosophy
(Biomedical Engineering)
in the University of Michigan
2016

Doctoral Committee

Professor Mark M. Banaszak Holl , Chair
Professor Robert T. Kennedy
Professor Bradford G. Orr
Professor Lonnie Shea
Professor David Sept

Dedication

This dissertation is dedicated to my parents (P.R Vaidyanathan and Lakshmi Iyer), uncle and aunt (Dr. P.R Hariharan and Brinda Hariharan) as well as the rest of my family.

Acknowledgements

I am grateful to Dr. Mark Banaszak Holl for being a tremendous mentor over the past few years. Mark's open door policy and his willingness to take a break from his work to work with his students is amazing. He has spent several hours every week discussing our experiments. I am very lucky to have such a kind, caring advisor who nurtured my scientific development.

I would like to thank my parents for always encouraging me and enabling me to study abroad in the United States. Their hard work and their personal values have always been a source of inspiration. Thanks to my little brother (Shravan) for being my best friend and always prompting me to push my boundaries. I am forever indebted to my Uncle and Aunt (P.R Hariharan and Brinda Hariharan) for being my "adopted" parents in America and welcoming me into their family. I would also like to thank my grandparents, uncles, aunts, cousins and the rest of my extended family for helping me with school work and supporting me all these years. I am extremely lucky to have such an amazing family.

Dr. Brad Orr has been my unofficial co-advisor as well as a constant source of support and encouragement over the years. His comments in our group meetings and help with mathematical models have been very useful. Dr. Michael Mayer was a great resource on my candidacy committee. I found our discussions on cell membrane biology and patch clamp methods very useful. I would like to thank Dr. Robert Kennedy for his useful suggestions on the microfluidic

patch clamp work and for serving on my committee. Thanks to Dr. Lonnie Shea and Dr. David Sept for serving on my committee. I would like to thank Maria Steele at the BME department for being the friendly face who welcomed me to Michigan and kept me on track with all the academic requirements.

I am fortunate to have so many great lab mates who have helped me learn and grow as a scientist over the years. I would like to thank Drs. Rebecca Matz and Rahul Rattan for teaching me the many cell and molecular biology techniques. I would like to specially acknowledge Becky's lab notebooks that are so detailed and allowed me to easily replicate her many procedures with great ease even several years later. Rahul has been an awesome collaborator and has helped me troubleshoot several microscopy experiments. Thanks to Dr. Casey Dougherty for being my lab buddy, allowing me to collaborate on her project and putting up with my cell culture lessons. I am glad that she did not hold the fact that I flipped our kayak in the Huron river against me! The electron microscopy lessons at the MIL with Dr. Mallory van Dongen were memorable. Dr. Ming Fang was nice enough to teach me to use chop sticks and I enjoyed our project maintaining her "pet" cells. I would like to acknowledge Meagan Cauble's efforts in teaching me bone biology and training me on the AFM. Rachel Merzel, Junjie Chen and Ted Ahn have been wonderful collaborators and lab-mates. I really value their company over the last few years. It has been a pleasure working with Milan Kaushik and Kevin Anderson. They were amazing collaborators who helped me grow as a mentor.

It has been a great fortune to work with everyone at MNIMBS. I would like to thank Dr. Pam Wong from MNIMBS for training me on their instruments and patiently helping me troubleshoot

my experiments in between her own experiments. Dr. Kasha and Alina Kotlyar has been a wonderful resource for my cell biology experiments. A special thanks to Dr. Mike Parise for managing the lab so efficiently.

I would like to acknowledge Dr. Kevin Otto for mentoring me through my undergrad at Purdue and developing my interest in research. My experience in the Otto group was very vital for helping me prepare for graduate research. Thanks to Andrew Pierce for being an extremely patient and caring graduate student mentor. Thanks to Matt McDermott for teaching me some chemistry.

Last but not the least, my time in Michigan has been so enjoyable because of all my friends. Janki Patel, Matthew Muckley, John Pitre, Nidhi Maley, Sydney Williams, Harish Balanethram and Paige Castle have been great company to share our highs and lows. I have really enjoyed our many nights out and all our parties. Vishnu Mani, Priyanka Pramanik, Pradeep Ranganathan, Swathi Maddali, Krishan Prem Kumar and Divya Sanghvi have been my family away from home. I really enjoyed all our time cooking together, the “unplanned” weekend trips and midnight birthday celebrations.

Table of Contents

List of Tables

List of Figures

List of Appendices

Chapter 1 Role of Cell Membrane-Vector Interactions in Successful Gene Delivery

Chapter will be submitted to Accounts of Chemical Research as a review

Introduction:

Gene therapy for the treatment of congenital disorders has been investigated with limited success.[1–5] Recent advances in genome editing such as the CRISPR/Cas system has resulted in a renewed interest in gene therapy.[6] The clinical success of gene therapy depends on the successful delivery of intact plasmid DNA (pDNA) to the nucleus of target cells.[7] Viral and non-viral delivery agents (vectors) are used to protect DNA from nucleases present in blood and tissue and also to promote cellular uptake.[8,9] Glybera, a gene therapy approved in Europe for exceptionally severe cases of lipoprotein lipase deficiency, uses a viral vector.[10,11] Although viral vectors enable tissue specific delivery and induce higher levels of gene expression than non-viral vectors, concerns have developed about adverse immune reactions.[9] Thus, strategies to improve the efficacy of non-viral vectors remain important. Successful vectors must overcome several hurdles including stability in blood, evading transport to liver and spleen due to capture by the reticular endothelial system, cellular uptake, and navigation of the intracellular transport mechanisms to reach the nucleus.[8,12] The challenges are substantially fewer when considering the use of vectors for gene delivery to cells in culture for biotechnology applications with cellular uptake, protection of intracellular nucleases, and intracellular transport to the nucleus remaining as the major hurdles. This account focuses on the key steps common to the challenges for both

gene therapy and biotechnology applications of a particular class of non-viral vector – polycationic polymers.

Polycationic polymers such as L-PEI, poly-l-lysine, and PAMAM dendrimers are able to bind and compact negatively charged pDNA and have been described as artificial histones.[13] The nanoscale polyplexes formed when mixing the two species are most commonly described by the ratio of cationic (or potentially cationic) nitrogen moieties (N) and the number of anionic phosphate groups (P) on the pDNA or oligonucleotide. Polyplexes formed with an N:P ratio >1 have a net positive charge that facilitates cellular uptake of the polyplexes through interactions with the negatively charged cell membrane. The interaction with the cell membrane leads to endocytosis of the polyplex and the initial placement of the polyplex into endosomes. Rate limiting processes for successful gene expression after this point include: 1) endosomal release,[14,15] 2) transport to specific organelles, 3) pDNA survival in cytosol,[16,17] 4) entry of pDNA into the nucleus[18–22] and 5) release of pDNA from the vector for transcription into mRNA (Figure 1.1).[23] Among these factors, transport of the DNA across the endosomal and nuclear membranes has been proposed to be the key roadblock to successful protein expression. [7]

Endosomal release of polyplexes formed using cationic polymers is proposed to be mediated by the proton sponge effect wherein buffering abilities of cationic vectors induces the swelling and rupture of endosomes releasing the nucleotide cargo into the cytosol.[14,15,24,25] However, studies tracking the colocalization of vector and pDNA labeled with pH sensitive fluorophores in single endosomes do not support this hypothesis.[26,27] Moreover, Hennink et al. synthesized a polymer with optimized buffering capacity and observed that the polymer did not exhibit good transfection abilities.[28] The second critical step of DNA transport into the nucleus has been proposed to be dependent on cell division;[18,20,29,30] however, multiple studies have now

demonstrated expression occurring without cell dvision.[21,31–35] Thus, the mechanisms of endosomal release and nuclear transport of polyplexes remains an area of active research.

Since 2004, our group has investigated the interactions of polycationic polymer and/or polyplexes with the cellular lipid membranes and how the interactions are related to successful gene delivery. Our studies were initially prompted by the observation that polycationic polymers induced the formation of nanoscale holes in supported lipid bilayers[36,37] and that this was a potential explanation of the observation that these materials induced porosity into cell[38–40] and internal organelle membranes.[41]

Interactions of cationic vector/polyplex with lipid bilayers in cells could affect subsequent gene delivery either at the cell membrane level (H1-H3) or at the internal organelle membrane (H4) level according to the following hypotheses. For each hypothesis, we have referenced our studies testing this idea.

H1: Increased cell membrane permeability induced by polyplexes allows diffusion of polyplexes across the cell membrane into the cytosol (avoiding the need for endosomal release).[17,42]

H2: Polyplex interaction with lipid rafts in the cell membrane enables endocytosis in pathways resulting in increased transport of polyplexes to the nucleus.[43,44]

H3: Increased cell membrane permeability and/or increased internal organelle membrane permeability activates cellular inflammatory mechanisms and/or cytosolic nucleases resulting in DNA degradation in the cytosol. [17,35]

H4: Increased failure of endosomal membrane integrity enables DNA to cross endosome and nuclear membranes.[44]

In this account, we first describe our studies of the interaction of cationic polymers and model supported lipid bilayers. We then discuss studies examining the stable intercalation of cationic polymers into mammalian cell membranes and the quantitative measurement of partition coefficients. We further connect these results to studies that investigated the subsequent release of DNA from endosomes, the degradation of DNA in the cytosol, and nuclear transport that results in gene expression. Our studies show that

1. Increased cell membrane permeability by polyplexes did not result in more cellular uptake and did not necessarily lead to high gene expression. [17,42,45] Hence, H1 was inconsistent with our studies.
2. Polyplex transport to endoplasmic reticulum and Golgi apparatus by L-PEI and G5 PAMAM did not explain differences in gene expression, inconsistent with H2.[44]
3. Although cells exposed to polyplexes show increased inflammatory responses and slowed cell division, the cells still showed high gene expression.[35] Thus, we ruled out H3.
4. Partitioning of free vectors (L-PEI, jetPEI > G5 PAMAM), but not polyplexes, into the cell membrane predicted <u>both</u> endosomal release and successful gene expression. Our studies also showed that polymers and polyplexes intercalate in the cell membrane for > 15 minutes. The addition of free L-PEI (an effective vector) to cells preloaded with G5 PAMAM polyplexes resulted in intact DNA release into the cytosol and a > 10-fold increase in gene expression. [44]

Our results in the context of other studies support H4 that the intercalation of cationic polymers promotes the failure of the endosomal membrane and enables the release of DNA cargo. Several studies have observed that free cationic polymers are vital for successful gene delivery.

Moreover, Zuhorn et al have observed endosomal release that leaves behind intact vesicles. Several other studies have showed that the toxicity of cationic polymers is due to internal organelle permeability induced by these materials.[46] Although our experiments did not measure partitioning of vectors into endosomal/internal organelle membranes directly, our results are consistent with the hypothesis that both endosomal and internal organelle membrane failure is due to the intercalation of cationic polymers. Further studies are necessary to understand the mechanism of this membrane failure in greater detail.

Interaction of free cationic polymer and polyplexes with lipid bilayers

The interaction of cationic materials with the cell membrane has been proposed to be important for understanding both the cytotoxicity of these materials as well as cellular uptake.[40] Our group was interested in directly observing these interactions in order to understand the mechanism of defect formation and membrane intercalation. We considered several possibilities such as i) free pores ii) polymer supported pores iii) a carpet of polymers on the bilayer and iv) polymers intercalated into the membrane (Figure 1.2D). Multiple studies using AFM showed that several cationic polymers (G5 PAMAM, G7 PAMAM, poly-L-lysine, DEAE-Dextran, PEI) and inorganic nanoparticles (Au-NH_2 and SiO_2-NH_2) induce new defects or enlarged preexisting defects in supported lipid bilayers made using DMPC.[36,38,39,47] In addition, the cationic materials induced defects and removed lipid from liquid phase lipid bilayers to a much greater extent than from gel phase bilayers.[37,48] In contrast to cationic materials, neutral materials required orders of magnitude greater concentrations to induce defects in supported lipid bilayers;[36,38] however, for neutral G5 PAMAM formed by acetylation of the terminal amines we observed ready intercalation into the lipid bilayer.[49]) In supported lipid bilayer studies, AFM evidence was observed consistent with all three defect structures: free pore, polymer supported pores, and

carpeting or intercalating polymer. This was further supported by dynamic light scattering and phosphorous NMR measurements suggested that defects were free pores which resulted from the formation of dendrimer filled lipid vesicles.[36,49] The formation of lipid-cationic polymer complexes was also further supported by molecular dynamics simulations.[50–52] Other computational models have showed the feasibility of dendrimer insertion into the lipid bilayer.[53] Subsequent solid state NMR experiments also supported the intercalation of dendrimers within lipid bilayers.[54]

Quantifying the interactions of free cationic polymer and polyplexes with cell membranes:

A major limitation of supported lipid bilayers is that they do not accurately represent cell membrane properties such as the presence of multiple lipids, proteins, cholesterol, and sugar groups. Several groups (including ours) have investigated changes in cell membrane permeability induced by cationic materials in cells by measuring the leakage of proteins and small molecule dyes.[38–40] The results indicate that although several polymers induce increased cell permeability to LDH and small molecule dyes as well as reduce cell viability, branched PEI (bPEI) induced cell membrane permeability and cell death at lower concentrations than other cationic polymers. This ability of bPEI to induce increased permeability and cytotoxicity was attributed to its higher charge density.[39] The AFM studies suggested the increased cell membrane permeability and cytotoxicity could result from the formation of pores in lipid bilayers.[39,55] Although the dye leakage studies provided quantitative information regarding cell membrane permeability, it was difficult to understand the impact of cell membrane permeability on gene expression in a given cell. Therefore, we used flow cytometry to relate changes in cell membrane permeability with activation of cytosolic nucleases as well as gene expression. Furthermore, we

used whole cell patch clamp experiments to quantify cell membrane permeability to ions on a single cell level.

Manual patch clamp experiments exhibited increased currents across cell membrane as a function of cationic polymer exposure. The magnitude of individual current events ranged from 0.2-2 nA consistent with free pore (i) or supported pore (ii) defects between 1-350 nm^2 in area.[56] The predicted size of current passing defects consisting of carpeted (iii) or intercalated (iv) regions is less clear but presumably larger than the size predicted for pores. Unlike cells exposed to cationic polymers, cells exposed to an antimicrobial peptide (AMO-3) exhibited discrete currents events consistent with a pore of ~2 nm diameter as predicted by other studies.[57,58]

Manual patch clamp experiments were extremely sensitive in detecting cell membrane currents of ~ 50 pA. However, the process was labor intensive, provided data from only a few cells, and did not allow for precise control over compound concentrations. To address these limitations, we used an automated microfluidic patch clamp system (the Ionflux-16) that enabled us to measure cell membrane conductivities of 20 cells simultaneously, precise control over polyplex/vector exposure time (1 s) and concentrations.[17,45,59] The IonFlux-16 also allowed us to assess the intactness of the treated cells using fluorescence microscopy. We observed that both cationic vectors and polyplexes increased membrane currents across cells to about 30-40 nA (Figure 1.3). This was less than the open channel currents of 70-80 nA observed when cells are completely dissolved by the detergent SDS.[59] Increasing the concentration of cationic vectors to 100-times the concentrations used in polyplexes formulations still did not increase the membrane currents above 40 nA. This indicated that the cationic polymers saturate the cell membrane at concentrations used in polyplexes. Moreover, the increase in cell membrane conductivity induced within 60 s was not reversible for over 15 minutes. Since free pores induced by

sonoporation repair in 5 s, the free pore model seen in supported lipid bilayers does not appear to be the source of the current in cell membranes. Instead cationic polymers and polyplexes appear to intercalate stably in the cell membrane and increase membrane permeability by either a supported pore (ii), carpet (iii) or intercalation (iv) model.[52] Finally, we further quantified the amount of polymer/polyplex partitioned in the cell membrane at equilibrium.

In order to distinguish between the four hypotheses in the introduction (H1-H4), we then compared the intercalation of different cationic polymers and polyplexes to gene expression. We observed that polymers inducing high gene expression (jetPEI, L-PEI) in HEK293A cells had higher partition constants in the cell membrane and induced cell membrane permeability at lower concentrations than G5 PAMAM, which induced gene expression in few cells.[45] Similarly, the magnitude of cell membrane currents induced by the intercalation of free polymers (jetPEI ~ LPEI > BPEI~ G5 PAMAM), but not polyplexes, predicted the ability of polyplexes to induce gene expression in HeLa cells (jetPEI ~ LPEI > BPEI~ G5 PAMAM).[17] Flow cytometry experiments investigating the relationship between the polyplex-induced influx of propidium iodide dye and gene expression also did not observe any correlation with gene experession.[60] These results are also broadly consistent with other data in showing that polyplex induced cell membrane permeability does not predict successful gene delivery. [17,22,42,61]

In our experiments, increased cell membrane permeability by polymers did not result in increased cellular uptake of polyplexes.[17] These results are inconsistent with H1. The partitioning of polymers into the cell membrane can explain inflammation and apoptosis associated with these agents. For example, Mukherjee et al showed that apoptotic pathways could be triggered by in Ca^{2+} levels was caused by the influx of Ca^{2+} from the extracellular fluid as well as release

from endoplasmic reticulum.[55] Similarly, Reineke et al showed that colocalization of PEI with the mitochondria and attributed the interaction of PEI with the mitochondria as a cause for cytotoxicity.[62] Since the lipid bilayers in a cell are cycled rapidly, polymer intercalation into the cell membrane may explain apoptotic pathways triggered by cationic vector induced leakiness of internal organelles. However, polymers that partition strongly into the cell membrane resulting in higher membrane permeabilization also induce higher gene expression and induce more inflammation. Thus, cellular defense mechanisms triggered by the process are not the limiting factors in enabling successful gene expression (H3). This suggests that the intercalated polymer influences subsequent gene expression either by mediating transport in specific pathways (H2) or by mediating endosomal release (H4). We used fluorescence microscopy experiments to further understand these processes.

Cellular Uptake and Intracellular Transport of Cationic Polymers and Polyplexes:

In studying polyplex transport, polymer transport has often been treated as control experiments. Our membrane interaction studies suggest that polymer transport may in fact be as important as polyplex transport. Polyplexes have been shown to be taken up by both clathrin and caveolin mediated endocytosis as well as macropinocytosis. [63,64] Multiple studies have observed that gene expression was abolished if caveolin mediated pathways were inhibited. [65,66] Conese et al. suggested that polyplexes escape endosomes more easily in caveolin mediated pathways.[64] Our group found that the internalization of G5 PAMAM dendrimers and polyplexes was not GM1/caveolin pathway dependent in multiple cell lines.[43,67] Other studies have suggested that the transport of polyplexes to the Golgi apparatus and ER by caveolin mediated pathways may be involved in the subsequent transport of polyplexes to the nucleus.[68–70]

Although polyplexes have been observed in the ER and Golgi apparatus, it is unclear if these polyplexes are responsible for subsequent gene expression. To address this question, we used a small oligonucleotide molecular beacon (OMB) labeled with a FRET dye pair to distinguish intact DNA responsible for therapeutic activity from degraded DNA. [44] The degradation of pDNA by cytosolic nucleases has been proposed to be one of the factors limiting gene delivery to the nucleus.[34] We observed that co-localization of intact DNA by jetPEI and G5 PAMAM polyplexes in the Golgi apparatus and ER in HEK293A cells was identical and thus did not explain the 100-fold difference in gene expression. However, the release of OMB into the cytosol (jetPEI >> G5 PAMAM) quantitatively predicted the gene expression induced by polyplexes (jetPEI >> G5 PAMAM) (Figure 4). Specifically, OMBs delivered using jetPEI were released into the cytosol but the OMBs delivered using G5 PAMAM were confined to vesicles. Moreover, the release of G5 PAMAM polyplexes from vesicles could be triggered by the co-incubation, pre-incubation or post-incubation of L-PEI with cells treated using G5 PAMAM polyplexes resulting in a >10-fold increase in GFP expression. Lipofectamine also achieved this 10-fold increase in gene expression, OMB release into the cytosol and transport to the nucleus but only if it was added to cells at the same time as G5 PAMAM polyplexes suggesting that has to be incorporated into the polyplexes. Previous studies by other groups have shown that the addition of free L-PEI enhances gene expression although they did not provide a mechanism of action.[71–75] These results support H4 and indicate that free cationic polymer intercalated in endosomal membranes induces failure of the endosomal membrane that enables successful gene expression.

According to this new model, jetPEI/L-PEI is successful in mediating endosomal escape in a larger fraction of cells because it can intercalate and disrupt endosomal membranes at much

lower concentrations than G5 PAMAM. Apart from explaining the ability of L-PEI to release polyplexes already trapped in endosomes, the model can also better explain the wide difference in gene expression induced by L-PEI and G5 PAMAM despite their similar buffering abilities. Moreover, the model is also consistent with a recent report by Zuhorn et al. that the release of nucleotides from endosomes leaves behind intact endosomes as opposed to the ruptured endosomes proposed by the proton sponge hypothesis.[46] They observed that the release of cargo from endosomes happened within a few seconds. This is more consistent with a new intercalation event at the endosome level rather than prolonged leakiness starting from endosome budding at the cell membrane. More studies will be necessary to understand the mechanism of cationic polymer interactions with the endosomal bilayer.

The addition of L-PEI also resulted in OMB presence in the nucleus within 4 h. It was unclear if the presence of L-PEI was necessary for the nuclear uptake of the OMB, although the quick presence of OMB in the nucleus rules out cell division as an explanation for nuclear uptake. Reineke et al have observed that although L-PEI and other polymers with high gene expression induce nuclear membrane permeability,[22,61] pDNA transfer into the nucleus increased dramatically in the presence of cytosolic extracts.[22] Polyplexes microinjected into the cytosol have been shown to induce higher gene expression than bare pDNA.[34] It is also unclear from our data if the nuclear membrane was penetrated by intact polyplexes or freecationic polymer. Free polymers have been shown to diffuse freely in the cytosol.[76,77] Thus, it is possible that the nuclear membrane could be made permeable by the free polymer and it easier for polyplexes to penetrate the nucleus.

The interaction of cationic vectors and DNA in polyplexes is also interesting since DNA in polyplexes is protected from nucleases but needs to be released inside the nucleus for

transcription into mRNA. We have also probed the DNA-vector interactions in polyplexes using NMR and fluorescence based techniques and observed that polyplexes are highly dynamic systems in which free nucleotides and vectors exchange with polyplexes rapidly. [78,79] The OMB experiments indicate that the DNA release from polymers and nuclease protection are not the critical parameters that enable successful gene expression.

Conclusion:

Identifying the physicochemical properties of cationic polymers critical to optimize gene expression would aid in the development of new vectors. The buffering ability of polymers has been historically considered important for optimal endosomal release, [14,15,24,25,34]although several studies have disagreed with this hypothesis.[26,27] Moreover, the proton sponge model does not explain the transport of polyplexes to the nucleus and the cytotoxicity induced by the cationic vectors. Our experiments indicate that the intercalation of free polymers into the lipid membranes promotes endosomal release, nuclear entry and gene expression in the following steps and enable successful gene expression in the following steps (Figure 1.5): [44]

1. Polyplexes delivered to the cell release free vector, smaller polyplexes, and free DNA either near the cell membrane or inside vesicles

2. Free cationic polymer released from polyplexes intercalates into the cell plasma membrane and then circulates to endosomal membranes and disrupts them.

The effectiveness of PEI in permeabilizing membranes has been attributed to its higher charge density [39,80] . It is unclear if the higher partition constant in the lipid membrane is also related to this property. Our model explains all the physiological effects of polyplexes (endosomal, mitochondrial and nuclear permeabilization) using the same physicochemical

property. Studies supporting our model mainly use two polymers L-PEI and G5 PAMAM. Future studies using other cationic polymers and lipids with different transfection abilities and physicochemical properties (hydrophobicities, charge density and vector architecture (branched vs linear)) will be necessary to validate the proposed model. Although our model mainly focused on understanding gene delivery, the same strategy may also be used to improve the efficacy of other therapeutic systems in which endosomal release is a limiting factor.

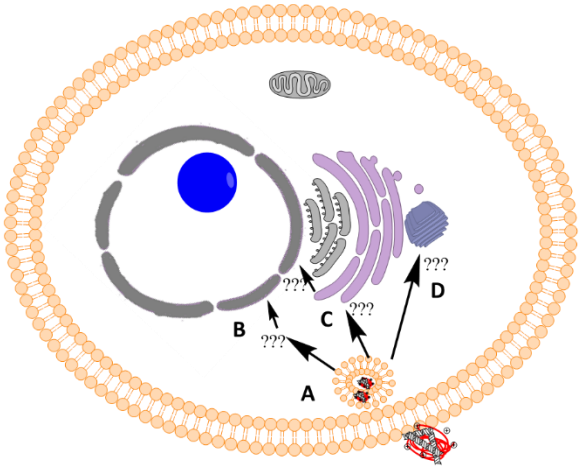

Figure 1.1. Polyplex transport in cells. A. Polyplexes are internalized into endosomes. B. Endosomal release has been suggested to be a critical step in enabling subsequent transport of DNA to the nucleus. C-D. Polyplexes have also been observed in internal organelles such as the Endoplasmic reticulum and Golgi apparatus, even though it is unclear if the polyplexes in these organelles are active in enabling gene expression.

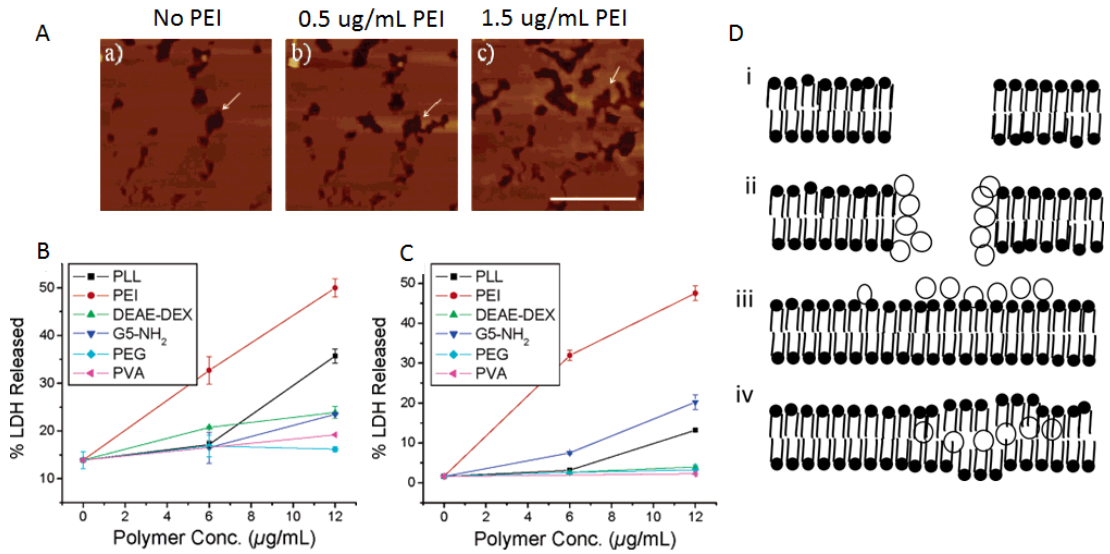

Figure 1.2: Cationic Polymers form defects in lipid bilayers and cell membranes. PEI enhanced the size of existing defects in supported lipid bilayers. B. Although many cationic polymers induced LDH release from KB cells, PEI induced significantly more LDH release at much lower concentrations. C. PEI also induced the most LDH release in Rat2 cells. D. Cationic materials could form three types of defects in lipid bilayers (i) free pores (ii) polymer supported pores (iii) a carpet of polymers or (iv) polymer intercalated bilayer.

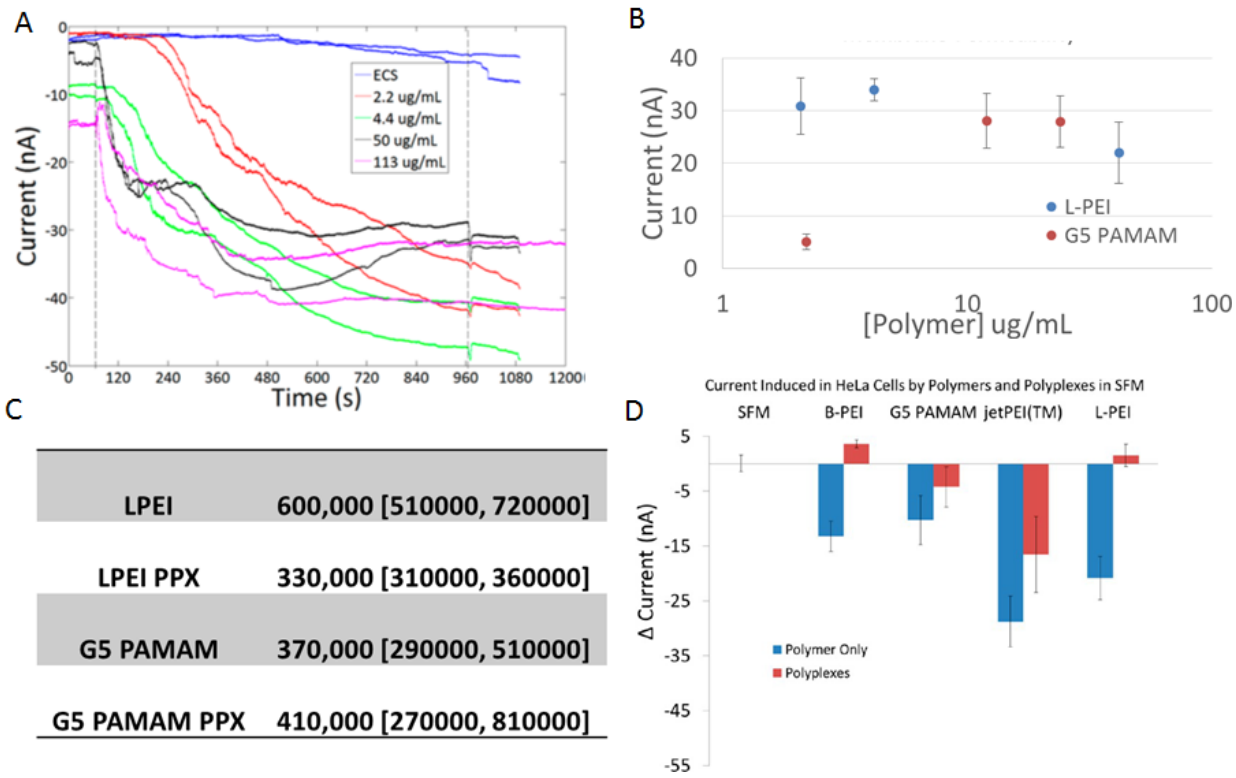

LPEI	600,000 [510000, 720000]
LPEI PPX	330,000 [310000, 360000]
G5 PAMAM	370,000 [290000, 510000]
G5 PAMAM PPX	410,000 [270000, 810000]

Figure 1.3: Free vector intercalation predicts gene expression. A. PEI induced increased cell membrane currents of HEK 293A cells starting at 2.2 ug/mL. The overall level of current never increased beyond -50 nA even at a concentration of 113 ug/mL indicating that cells were still intact. Dissolution of cells with agents such as SDS resulted in currents > -70 nA. B. L-PEI induced increased membrane currents at much lower concentrations than G5 PAMAM. C. Free L-PEI had a higher partition constant into HEK293A cell membranes than free G5 PAMAM. Partition constants of polyplexes were not different within error. D. Free cationic vectors also induced increased membrane currents in HeLa cells with L-PEI and jetPEI showing the greatest increase and showing the greatest gene expression. Currents induced by polyplexes could not predict gene expression.

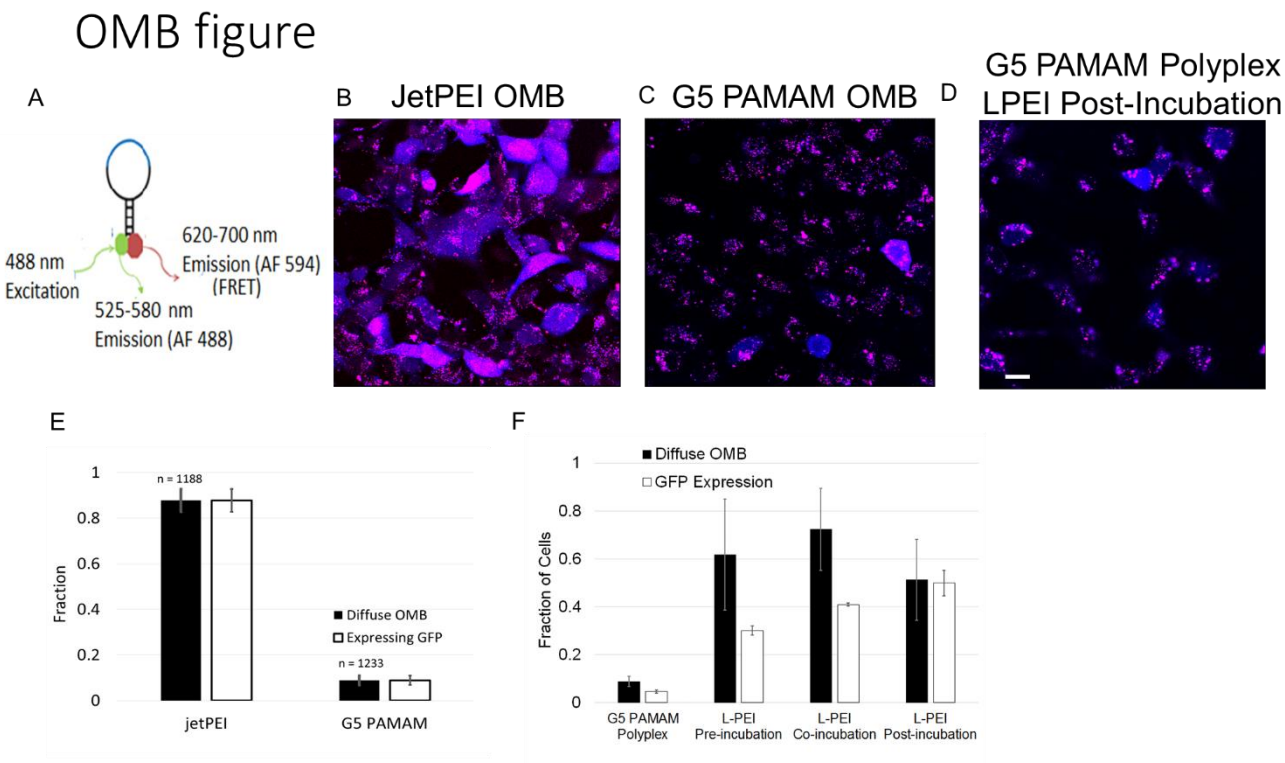

Figure 1.4: Free vector induced endosomal release predicts gene expression. A. OMB employed for FRET studies. B. OMB delivered using jetPEI polyplexes (N:P 10:1) exhibits diffuse distribution at 4h. C. OMB delivered using G5 PAMAM polyplexes (N:P 10:1) were confined to vesicles with few cells showing diffuse OMB distribution. D. Treatment of cells with L-PEI for 1 h following 3 h G5 PAMAM polyplex incubation results in diffuse, cytosolic OMB distribution. E. The fraction of cells (n = total number of cells counted from 10 images each obtained from 3 biological replicates) showing diffuse OMB distribution in the cytosol (jetPEI = 88 ± 5 %, G5 PAMAM = 9 ± 2 %) corresponds to the fraction of cells expressing GFP (jetPEI = 80 ± 5 %, G5 PAMAM 4 ± 1 %). F. Pre-incubation, co-incubation and post-incubation of L-PEI with G5 PAMAM polyplexes increases both fraction of cells displaying diffuse OMB and fraction of cells expressing GFP by >10-fold.

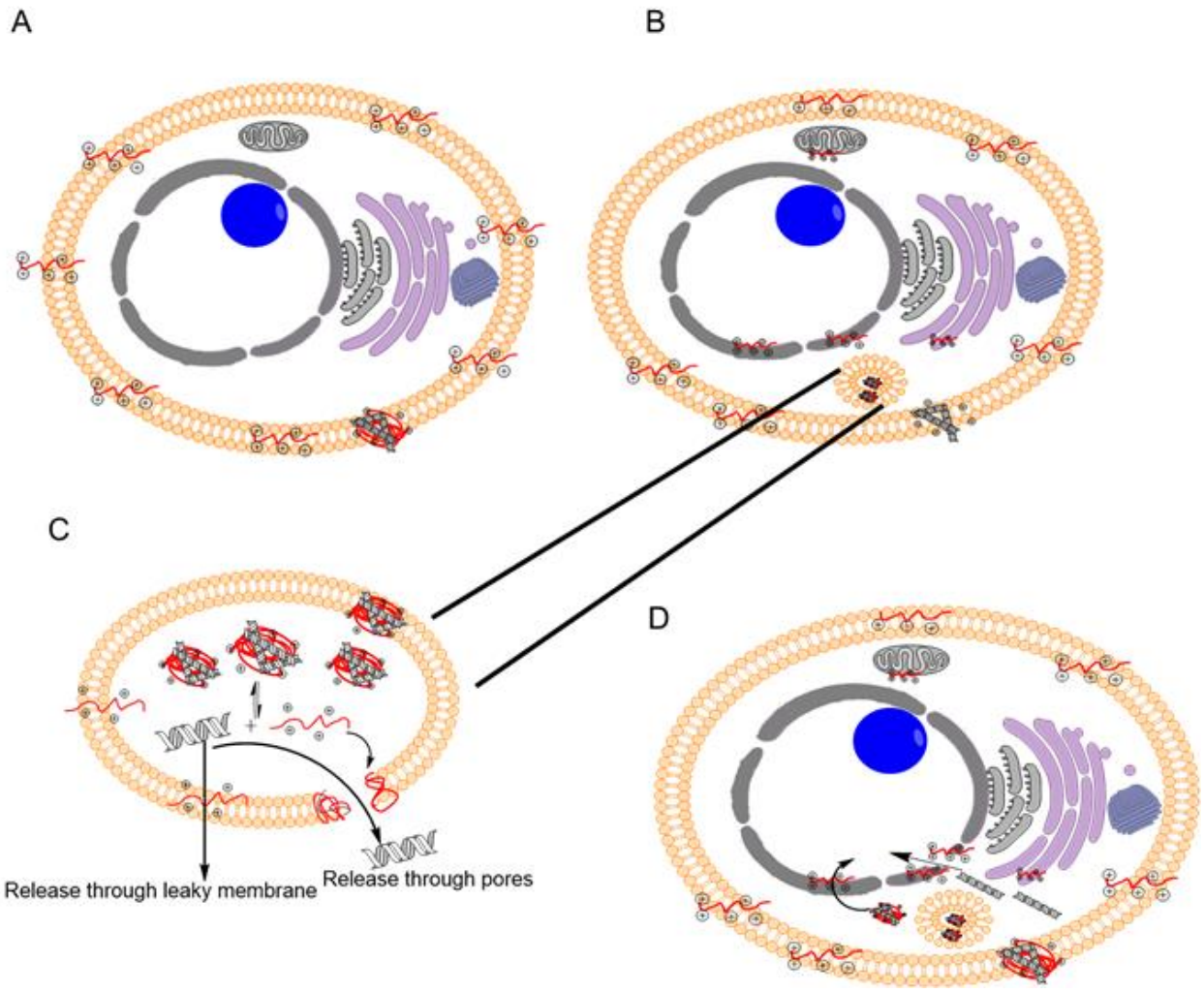

Figure 1.5: Membrane intercalation model of endosmal release. A. Free cationic polymer intercalates into the plasma membrane and/or is released from associated polyplexes. B. Cationic polymer is dispersed into internal cellular membranes via lipid recycling pathways. Polyplexes are endocytosed. C. Cationic polymer intercalated into endosomal membranes induces membrane permeability and facilitates release of genetic material into the cytosol. D. We hypothesize that cationic polymer associated with the nuclear membrane via lipid recycling and/or cytosolic pathways induces permeabilization and facilitates transport into the nucleus.

REFERENCES:

(1) Griesenbach, U.; Geddes, D. M.; Alton, E. W. F. W. Gene Therapy Progress and Prospects: Cystic Fibrosis. *Gene Ther 13*, 1061–1067.

(2) Griesenbach, U.; Alton, E. W. F. W. Gene Transfer to the Lung: Lessons Learned from More than 2 Decades of CF Gene Therapy. *Adv. Drug Deliv. Rev.* **2009**, *61*, 128–139.

(3) Cavazzana-Calvo, M.; Hacein-Bey, S.; Basile, G. de Saint; Gross, F.; Yvon, E.; Nusbaum, P.; Selz, F.; Hue, C.; Certain, S.; Casanova, J.-L.; *et al.* Gene Therapy of Human Severe Combined Immunodeficiency (SCID)-X1 Disease. *Science (80-.).* **2000**, *288*, 669–672.

(4) Pawliuk, R.; Westerman, K. A.; Fabry, M. E.; Payen, E.; Tighe, R.; Bouhassira, E. E.; Acharya, S. A.; Ellis, J.; London, I. M.; Eaves, C. J.; *et al.* Correction of Sickle Cell Disease in Transgenic Mouse Models by Gene Therapy. *Science (80-.).* **2001**, *294*, 2368–2371.

(5) Cavazzana-Calvo, M.; Payen, E.; Negre, O.; Wang, G.; Hehir, K.; Fusil, F.; Down, J.; Denaro, M.; Brady, T.; Westerman, K.; *et al.* Transfusion Independence and HMGA2 Activation after Gene Therapy of Human [bgr]-Thalassaemia. *Nature* **2010**, *467*, 318–322.

(6) Gori, J. L.; Hsu, P. D.; Maeder, M. L.; Shen, S.; Welstead, G. G.; Bumcrot, D. Delivery and Specificity of CRISPR/Cas9 Genome Editing Technologies for Human Gene Therapy. *Hum. Gene Ther.* **2015**, *26*, 443–451.

(7) Nguyen, J.; Szoka, F. C. Nucleic Acid Delivery: The Missing Pieces of the Puzzle? *Acc. Chem. Res.* **2012**, *45*, 1153–1162.

(8) Yin, H.; Kanasty, R. L.; Eltoukhy, A. A.; Vegas, A. J.; Dorkin, J. R.; Anderson, D. G. Non-Viral Vectors for Gene-Based Therapy. *Nat Rev Genet* **2014**, *15*, 541–555.

(9) Nguyen, J.; Szoka, F. C. Nucleic Acid Delivery: The Missing Pieces of the Puzzle? *Acc. Chem. Res.* **2012**, *45*, 1153–1162.

(10) Ross, C. J. D.; Twisk, J.; Meulenberg, J. M.; Liu, G.; Van Den Oever, K.; Moraal, E.; Hermens, W. T.; Rip, J.; Kastelein, J. J. P.; Kuivenhoven, J. A.; *et al.* Long-Term Correction of Murine Lipoprotein Lipase Deficiency with AAV1-Mediated Gene Transfer of the Naturally Occurring LPLS447X Beneficial Mutation. *Hum. Gene Ther.* **2004**, *15*, 906–919.

(11) Gaudet, D.; de Wal, J.; Tremblay, K.; Déry, S.; van Deventer, S.; Freidig, A.; Brisson, D.; Méthot, J. Review of the Clinical Development of Alipogene Tiparvovec Gene Therapy for Lipoprotein Lipase Deficiency. *Atheroscler. Suppl.* **2010**, *11*, 55–60.

(12) Blanco, E.; Shen, H.; Ferrari, M. Principles of Nanoparticle Design for Overcoming Biological Barriers to Drug Delivery. *Nat Biotech* **2015**, *33*, 941–951.

(13) Bielinska, A. U.; Chen, C.; Johnson, J.; Baker, J. R. DNA Complexing with Polyamidoamine Dendrimers: Implications for Transfection. *Bioconjug. Chem.* **1999**, *10*, 843–850.

(14) Akinc, A.; Thomas, M.; Klibanov, A. M.; Langer, R. Exploring Polyethylenimine-Mediated DNA Transfection and the Proton Sponge Hypothesis. *J. Gene Med.* **2005**, *7*, 657–663.

(15) Boussif, O.; Lezoualc'h, F.; Zanta, M. A.; Mergny, M. D.; Scherman, D.; Demeneix, B.; Behr, J. P. A Versatile Vector for Gene and Oligonucleotide Transfer into Cells in Culture and in Vivo: Polyethylenimine. *Proc. Natl. Acad. Sci. U. S. A.* **1995**, *92*, 7297–7301.

(16) Pollard, H.; Toumaniantz, G.; Amos, J. L.; Avet- Loiseau, H.; Guihard, G.; Behr, J. P.; Escande, D.; Avet-Loiseau, H.; Guihard, G.; Behr, J. P.; *et al.* Ca2+- sensitive Cytosolic Nucleases Prevent Efficient Delivery to the Nucleus of Injected Plasmids. *J. Gene Med.* **2001**, *3*, 153.

(17) Rattan, R.; Vaidyanathan, S.; Wu, G. S.-H.; Shakya, A.; Orr, B. G.; Banaszak Holl, M. M. Polyplex-Induced Cytosolic Nuclease Activation Leads to Differential Transgene Expression. *Mol. Pharm.* **2013**, *10*, 3013–3022.

(18) Brunner, S.; Sauer, T.; Carotta, S.; Cotten, M.; Saltik, M.; Wagner, E. Cell Cycle Dependence of Gene Transfer by Lipoplex, Polyplex and Recombinant Adenovirus. *Gene Ther.* **2000**, *7*, 401–407.

(19) Lechardeur, D.; Lukacs, G. L. Nucleocytoplasmic Transport of Plasmid DNA: A Perilous Journey from the Cytoplasm to the Nucleus. *Hum. Gene Ther.* **2006**, *17*, 882–889.

(20) Mortimer, I.; Tam, P.; MacLachlan, I.; Graham, R. W.; Saravolac, E. G.; Joshi, P. B. Cationic Lipid-Mediated Transfection of Cells in Culture Requires Mitotic Activity. *Gene Ther.* **1999**, *6*, 403–411.

(21) Dowty, M. E.; Williams, P.; Zhang, G.; Hagstrom, J. E.; Wolff, J. a. Plasmid DNA Entry into Postmitotic Nuclei of Primary Rat Myotubes. *Proc. Natl. Acad. Sci. U. S. A.* **1995**, *92*, 4572–4576.

(22) Grandinetti, G.; Reineke, T. M. Exploring the Mechanism of Plasmid DNA Nuclear Internalization with Polymer-Based Vehicles. *Mol. Pharm.* **2012**, *9*, 2256–2267.

(23) Itaka, K.; Harada, A.; Yamasaki, Y.; Nakamura, K.; Kawaguchi, H.; Kataoka, K. In Situ Single Cell Observation by Fluorescence Resonance Energy Transfer Reveals Fast Intra-Cytoplasmic Delivery and Easy Release of Plasmid DNA Complexed with Linear Polyethylenimine. *J. Gene Med.* **2004**, *6*, 76–84.

(24) Behr, J.-P. The Proton Sponge: A Trick to Enter Cells the Viruses Did Not Exploit. *Chim. Int. J. Chem.* **1997**, *51*, 1–2.

(25) Sonawane, N. D.; Szoka, F. C.; Verkman, A. S. Chloride Accumulation and Swelling in Endosomes Enhances DNA Transfer by Polyamine-DNA Polyplexes. *J. Biol. Chem.* **2003**, *278* , 44826–44831.

(26) Kulkarni, R. P.; Mishra, S.; Fraser, S. E.; Davis, M. E. Single Cell Kinetics of Intracellular, Nonviral, Nucleic Acid Delivery Vehicle Acidification and Trafficking. *Bioconjug. Chem.* **2005**, *16*, 986.

(27) Benjaminsen, R. V; Mattebjerg, M. A.; Henriksen, J. R.; Moghimi, S. M.; Andresen, T. L.

The Possible “proton Sponge” Effect of Polyethylenimine (PEI) Does Not Include Change in Lysosomal pH. *Mol. Ther.* **2012**, *21*, 149–157.

(28) Funhoff, A. M.; van Nostrum, C. F.; Koning, G. A.; Schuurmans-Nieuwenbroek, N. M. E.; Crommelin, D. J. A.; Hennink, W. E. Endosomal Escape of Polymeric Gene Delivery Complexes Is Not Always Enhanced by Polymers Buffering at Low pH. *Biomacromolecules* **2004**, *5*, 32–39.

(29) Grosse, S.; Thévenot, G.; Monsigny, M.; Fajac, I. Which Mechanism for Nuclear Import of Plasmid DNA Complexed with Polyethylenimine Derivatives? *J. Gene Med.* **2006**, *8*, 845–851.

(30) Tseng, W.-C.; Haselton, F. R.; Giorgio, T. D. Mitosis Enhances Transgene Expression of Plasmid Delivered by Cationic Liposomes. *Biochim. Biophys. Acta - Gene Struct. Expr.* **1999**, *1445*, 53–64.

(31) Dean, D. A. Import of Plasmid DNA into the Nucleus Is Sequence Specific. *Exp. Cell Res.* **1997**, *230*, 293–302.

(32) Wilson, G. L.; Dean, B. S.; Wang, G.; Dean, D. A. Nuclear Import of Plasmid DNA in Digitonin-Permeabilized Cells Requires Both Cytoplasmic Factors and Specific DNA Sequences. *J. Biol. Chem.* **1999**, *274* , 22025–22032.

(33) Ludtke, J. J.; Sebestyen, M. G.; Wolff, J. A. The Effect of Cell Division on the Cellular Dynamics of Microinjected DNA and Dextran. *Mol Ther* **2002**, *5*, 579–588.

(34) Pollard, H.; Remy, J.-S.; Loussouarn, G.; Demolombe, S.; Behr, J.-P.; Escande, D. Polyethylenimine but Not Cationic Lipids Promotes Transgene Delivery to the Nucleus in Mammalian Cells. *J. Biol. Chem.* **1998**, *273*, 7507–7511.

(35) Matz, R. L.; Erickson, B.; Vaidyanathan, S.; Kukowska-Latallo, J. F.; Baker, J. R.; Orr, B. G.; Banaszak Holl, M. M. Polyplex Exposure Inhibits Cell Cycle, Increases Inflammatory Response, and Can Cause Protein Expression without Cell Division. *Mol. Pharm.* **2013**, *10*, 1306–1317.

(36) Mecke, A.; Uppuluri, S.; Sassanella, T. M.; Lee, D.-K.; Ramamoorthy, A.; Baker, J. R.; Orr, B. G.; Banaszak Holl, M. M. Direct Observation of Lipid Bilayer Disruption by Poly(amidoamine) Dendrimers. *Chem. Phys. Lipids* **2004**, *132*, 3–14.

(37) Mecke, A.; Lee, D.-K.; Ramamoorthy, A.; Orr, B. G.; Banaszak Holl, M. M. Synthetic and Natural Polycationic Polymer Nanoparticles Interact Selectively with Fluid-Phase Domains of DMPC Lipid Bilayers. *Langmuir* **2005**, *21*, 8588–8590.

(38) Hong, S.; Bielinska, A. U.; Mecke, A.; Keszler, B.; Beals, J. L.; Shi, X.; Balogh, L.; Orr, B. G.; Baker, J. R.; Banaszak Holl, M. M. Interaction of Poly (amidoamine) Dendrimers with Supported Lipid Bilayers and Cells: Hole Formation and the Relation to Transport. *Bioconjug. Chem.* **2004**, *15*, 774–782.

(39) Hong, S.; Leroueil, P. R.; Janus, E. K.; Peters, J. L.; Kober, M. M.; Islam, M. T.; Orr, B. G.; Baker Jr, J. R.; Banaszak Holl, M. M. Interaction of Polycationic Polymers with Supported Lipid Bilayers and Cells: Nanoscale Hole Formation and Enhanced Membrane Permeability. *Bioconjug. Chem.* **2006**, *17*, 728–734.

(40) Fischer, D.; Li, Y.; Ahlemeyer, B.; Krieglstein, J.; Kissel, T. In Vitro Cytotoxicity Testing of Polycations: Influence of Polymer Structure on Cell Viability and Hemolysis. *Biomaterials* **2003**, *24*, 1121–1131.

(41) Moghimi, S. M.; Symonds, P.; Murray, J. C.; Hunter, a C.; Debska, G.; Szewczyk, A. A Two-Stage Poly(ethylenimine)-Mediated Cytotoxicity: Implications for Gene Transfer/therapy. *Mol. Ther.* **2005**, *11*, 990–995.

(42) Prevette, L. E.; Mullen, D. G.; Holl, M. M. B. Polycation-Induced Cell Membrane Permeability Does Not Enhance Cellular Uptake or Expression Efficiency of Delivered DNA. *Mol. Pharm.* **2010**, *7*, 870.

(43) Hong, S.; Rattan, R.; Majoros, I. J.; Mullen, D. G.; Peters, J. L.; Shi, X.; Bielinska, A. U.; Blanco, L.; Orr, B. G.; Baker Jr, J. R. The Role of Ganglioside GM1 in Cellular Internalization Mechanisms of Poly (amidoamine) Dendrimers. *Bioconjug. Chem.* **2009**, *20*, 1503–1513.

(44) Vaidyanathan, S.; Chen, J.; Orr, B. G.; Banaszak Holl, M. M. Cationic Vector Intercalation into the Lipid Membrane Enables Intact Polyplex DNA Escape from Endosomes for Gene Delivery. *Submitted* **2016**.

(45) Vaidyanathan, S.; Anderson, K. B.; Merzel, R. L.; Jacobovitz, B.; Kaushik, M. P.; Kelly, C. N.; van Dongen, M. A.; Dougherty, C. A.; Orr, B. G.; Banaszak Holl, M. M. Quantitative Measurement of Cationic Polymer Vector and Polymer–pDNA Polyplex Intercalation into the Cell Plasma Membrane. *ACS Nano* **2015**, *9*, 6097–6109.

(46) ur Rehman, Z.; Hoekstra, D.; Zuhorn, I. S.; Rehman, Z. ur; Hoekstra, D.; Zuhorn, I. S. On the Mechanism of Polyplex-and Lipoplex-Mediated Delivery of Nucleic Acids: Real-Time Visualization of Transient Membrane Destabilization Without Endosomal Lysis. *ACS Nano* **2013**, *7*, 3767–3777.

(47) Leroueil, P. R.; Berry, S. A.; Duthie, K.; Han, G.; Rotello, V. M.; McNerny, D. Q.; Baker Jr, J. R.; Orr, B. G.; Holl, M. M. Wide Varieties of Cationic Nanoparticles Induce Defects in Supported Lipid Bilayers. *Nano Lett.* **2008**, *8*, 420–424.

(48) Erickson, B.; Dimaggio, S. C.; Mullen, D. G.; Kelly, C. V; Leroueil, P. R.; Berry, X. S. A.; Baker, J. R.; Orr, B. G.; Holl, M. M. B. Interactions of Poly (amidoamine) Dendrimers with Survanta Lung Surfactant : The Importance of Lipid Domains. **2008**, *149*, 11003–11008.

(49) Mecke, A.; Majoros, I. J.; Patri, A. K.; Baker, J. R.; Banaszak Holl, M. M.; Orr, B. G. Lipid Bilayer Disruption by Polycationic Polymers: The Roles of Size and Chemical Functional Group. *Langmuir* **2005**, *21*, 10348–10354.

(50) Kelly, C. V; Leroueil, P. R.; Nett, E. K.; Wereszczynski, J. M.; Baker, J. R.; Orr, B. G.; Banaszak Holl, M. M.; Andricioaei, I. Poly(amidoamine) Dendrimers on Lipid Bilayers I: Free Energy and Conformation of Binding. *J. Phys. Chem. B* **2008**, *112*, 9337–9345.

(51) Kelly, C. V; Leroueil, P. R.; Orr, B. G.; Banaszak Holl, M. M.; Andricioaei, I. Poly(amidoamine) Dendrimers on Lipid Bilayers II: Effects of Bilayer Phase and Dendrimer Termination. *J. Phys. Chem. B* **2008**, *112*, 9346–9353.

(52) Kelly, C. V; Liroff, M. G.; Triplett, L. D.; Leroueil, P. R.; Mullen, D. G.; Wallace, J. M.; Meshinchi, S.; Baker, J. R.; Orr, B. G.; Banaszak Holl, M. M. Stoichiometry and Structure of Poly(amidoamine) Dendrimer−Lipid Complexes. *ACS Nano* **2009**, *3*, 1886–1896.

(53) Ginzburg, V. V; Balijepalli, S. Modeling the Thermodynamics of the Interaction of Nanoparticles with Cell Membranes. *Nano Lett.* **2007**, *7*, 3716–3722.

(54) Smith, P. E. S.; Brender, J. R.; Dürr, U. H. N.; Xu, J.; Mullen, D. G.; Banaszak Holl, M. M.; Ramamoorthy, A. Solid-State NMR Reveals the Hydrophobic-Core Location of Poly(amidoamine) Dendrimers in Biomembranes. *J. Am. Chem. Soc.* **2010**, *132*, 8087–8097.

(55) Arvizo, R. R.; Miranda, O. R.; Thompson, M. A.; Pabelick, C. M.; Bhattacharya, R.; Robertson, J. D.; Rotello, V. M.; Prakash, Y. S.; Mukherjee, P. Effect of Nanoparticle Surface Charge at the Plasma Membrane and Beyond. *Nano Lett.* **2010**, *10*, 2543–2548.

(56) Chen, J.; Hessler, J. A.; Putchakayala, K.; Panama, B. K.; Khan, D. P.; Hong, S.; Mullen, D. G.; Dimaggio, S. C.; Som, A.; Tew, G. N.; *et al.* Cationic Nanoparticles Induce Nanoscale Disruption in Living Cell Plasma Membranes. *J. Phys. Chem. B* **2009**, *113*, 11179–11185.

(57) Yang, L.; Gordon, V. D.; Trinkle, D. R.; Schmidt, N. W.; Davis, M. A.; DeVries, C.; Som, A.; Cronan, J. E.; Tew, G. N.; Wong, G. C. L. Mechanism of a Prototypical Synthetic Membrane-Active Antimicrobial: Efficient Hole-Punching via Interaction with Negative Intrinsic Curvature Lipids. *Proc. Natl. Acad. Sci.* **2008**, *105*, 20595–20600.

(58) Yang, L.; Gordon, V. D.; Mishra, A.; Som, A.; Purdy, K. R.; Davis, M. A.; Tew, G. N.; Wong, G. C. L. Synthetic Antimicrobial Oligomers Induce a Composition-Dependent Topological Transition in Membranes. *J. Am. Chem. Soc.* **2007**, *129*, 12141–12147.

(59) Vaidyanathan, S.; Orr, B. G.; Banaszak Holl, M. M. Detergent Induction of HEK 293A Cell Membrane Permeability Measured under Quiescent and Superfusion Conditions Using Whole Cell Patch Clamp. *J. Phys. Chem. B* **2014**, *118*, 2112–2123.

(60) Prevette, L. E.; Mullen, D. G.; Banaszak Holl, M. M. Polycation-Induced Cell Membrane Permeability Does Not Enhance Cellular Uptake or Expression Efficiency of Delivered DNA. *Mol. Pharm.* **2010**, *7*, 870–883.

(61) Grandinetti, G.; Smith, A. E.; Reineke, T. M. Membrane and Nuclear Permeabilization by Polymeric pDNA Vehicles: Efficient Method for Gene Delivery or Mechanism of Cytotoxicity? *Mol. Pharm.* **2012**, *9*, 523–538.

(62) Grandinetti, G.; Ingle, N. P.; Reineke, T. M. Interaction of Poly(ethylenimine)-DNA Polyplexes with Mitochondria: Implications for a Mechanism of Cytotoxicity. *Mol. Pharm.* **2011**, *8*, 1709–1719.

(63) Rejman, J.; Conese, M.; Hoekstra, D. Gene Transfer by Means of Lipo- and Polyplexes: Role of Clathrin and Caveolae-Mediated Endocytosis. *J. Liposome Res.* **2006**, *16*, 237–247.

(64) Rejman, J.; Bragonzi, A.; Conese, M. Role of Clathrin- and Caveolae-Mediated Endocytosis in Gene Transfer Mediated by Lipo- and Polyplexes. *Mol Ther* **2005**, *12*,

468–474.

(65) van der Aa, M. A. E. M.; Huth, U. S.; Häfele, S. Y.; Schubert, R.; Oosting, R. S.; Mastrobattista, E.; Hennink, W. E.; Peschka-Süss, R.; Koning, G. A.; Crommelin, D. J. A. Cellular Uptake of Cationic Polymer-DNA Complexes via Caveolae Plays a Pivotal Role in Gene Transfection in COS-7 Cells. *Pharm. Res.* **2007**, *24*, 1590–1598.

(66) McLendon, P. M.; Fichter, K. M.; Reineke, T. M. Poly(glycoamidoamine) Vehicles Promote pDNA Uptake through Multiple Routes and Efficient Gene Expression via Caveolae-Mediated Endocytosis. *Mol. Pharm.* **2010**, *7*, 738–750.

(67) Qi, R.; Mullen, D. G.; Baker, J. R.; Holl, M. M. B. The Mechanism of Polyplex Internalization into Cells: Testing the GM1/Caveolin-1 Lipid Raft Mediated Endocytosis Pathway. *Mol. Pharm.* **2010**, *7*, 267.

(68) Reilly, M. J.; Larsen, J. D.; Sullivan, M. O. Polyplexes Traffic through Caveolae to the Golgi and Endoplasmic Reticulum En Route to the Nucleus. *Mol. Pharm.* **2012**, *9*, 1280–1290.

(69) Ingle, N. P.; Xue, L.; Reineke, T. M. Spatiotemporal Cellular Imaging of Polymer-pDNA Nanocomplexes Affords in Situ Morphology and Trafficking Trends. *Mol. Pharm.* **2013**, *10*, 4120–4135.

(70) Fichter, K. M.; Ingle, N. P.; McLendon, P. M.; Reineke, T. M. Polymeric Nucleic Acid Vehicles Exploit Active Interorganelle Trafficking Mechanisms. *ACS Nano* **2013**, *7*, 347–364.

(71) Boeckle, S.; von Gersdorff, K.; van der Piepen, S.; Culmsee, C.; Wagner, E.; Ogris, M. Purification of Polyethylenimine Polyplexes Highlights the Role of Free Polycations in Gene Transfer. *J. Gene Med.* **2004**, *6*, 1102–1111.

(72) Dai, Z.; Gjetting, T.; Mattebjerg, M. A.; Wu, C.; Andresen, T. L. Elucidating the Interplay between DNA-Condensing and Free Polycations in Gene Transfection through a Mechanistic Study of Linear and Branched PEI. *Biomaterials* **2011**, *32*, 8626–8634.

(73) Yue, Y.; Jin, F.; Deng, R.; Cai, J.; Chen, Y.; Lin, M. C. M.; Kung, H.-F.; Wu, C. Revisit Complexation between DNA and Polyethylenimine - Effect of Uncomplexed Chains Free in the Solution Mixture on Gene Transfection. *J. Control. Release* **2011**, *155*, 67–76.

(74) Ruponen, M.; Arkko, S.; Urtti, A.; Reinisalo, M.; Ranta, V.-P. Intracellular DNA Release and Elimination Correlate Poorly with Transgene Expression after Non-Viral Transfection. *J. Control. Release* **2009**, *136*, 226.

(75) Perevyazko, I. Y.; Bauer, M.; Pavlov, G. M.; Hoeppener, S.; Schubert, S.; Fischer, D.; Schubert, U. S. Polyelectrolyte Complexes of DNA and Linear PEI: Formation, Composition and Properties. *Langmuir* **2012**, *28*, 16167–16176.

(76) Seksek, O.; Biwersi, J.; Verkman, A. . Translational Diffusion of Macromolecule-Sized Solutes in Cytoplasm and Nucleus. *J. Cell Biol.* **1997**, *138*, 131–142.

(77) Lukacs, G. L.; Haggie, P.; Seksek, O.; Lechardeur, D.; Freedman, N.; Verkman, A. S. Size-Dependent DNA Mobility in Cytoplasm and Nucleus. *J. Biol. Chem.* **2000**, *275*,

1625–1629.

(78) Prevette, L. E.; Nikolova, E. N.; Al-Hashimi, H. M.; Banaszak Holl, M. M. Intrinsic Dynamics of DNA-Polymer Complexes: A Mechanism for DNA Release. *Mol. Pharm.* **2012**, *9*, 2743–2749.

(79) Shakya, A.; Dougherty, C. A.; Xue, Y.; Al-Hashimi, H. M.; Banaszak Holl, M. M. Rapid Exchange Between Free and Bound States in RNA–Dendrimer Polyplexes: Implications on the Mechanism of Delivery and Release. *Biomacromolecules* **2016**, *17*, 154–164.

(80) Roser, M.; Fischer, D.; Kissel, T. Surface-Modified Biodegradable Albumin Nano- and Microspheres. II: Effect of Surface Charges on in Vitro Phagocytosis and Biodistribution in Rats. *Eur. J. Pharm. Biopharm.* **1998**, *46*, 255–263.

Chapter 2 : Detergent Induction of HEK 293A Cell Membrane Permeability Measured Under Quiescent and Superfusion Conditions using Whole Cell Patch Clamp

Published as: Detergent Induction of HEK 293A Cell Membrane Permeability Measured under Quiescent and Superfusion Conditions Using Whole Cell Patch Clamp. *J. Phys. Chem. B* **2014**, *118*, 2112–2123.

INTRODUCTION

Detergents are employed for a wide variety applications in biology including dissolving cell membranes,[1,2,3,4] isolating membrane components such as proteins,[5] transport of agents such as drug and genes into the cell,[6] adjuvants in vaccination,[7] and providing aqueous solubility to hydrophobic and/or nanoscale materials.[8] In part, this wide variety of roles stems from the ability to vary both the head group size and charge of a detergent, as well as the length and shape of the hydrocarbon tail. However, a common detergent such as sodium dodecyl sulfate (SDS) is able to play many of the roles described above by varying concentration. This great variety of applications indicates the detergent/membrane interaction is multifaceted and has substantial continued promise for biological manipulation. In order to fulfill this promise, increased understanding of the balance between the roles in enhanced transport, membrane permeability, and overall dissolution of the cell membrane must be understood.

The theory of detergent interaction with cell plasma membranes has been developed using homogeneous phospholipid bilayer models. The interaction is generally proposed to go through a three-stage equilibrium model (see supplementary material, Figure A.1) as the detergent/lipid (D/L) ratio increases: [1-4]

I) intercalation of non-micellar detergent into the bilayer

II) equilibrium coexistence of phospholipid-saturated D/L micelles with detergent-saturated phospholipid bilayer

III) dissolution of detergent-saturated phospholipid bilayer into D/L micelles.

These three stages, although a simplification when considering detergent interaction with a cell plasma membrane containing numerous other components including proteins and cholesterol,[5,9] nevertheless provides a starting point for considering the detergent/plasma membrane interaction and the experiments used to probe the biophysical outcomes. There are also three steps considered as important for the kinetics of the detergent/lipid bilayer interaction[4]

i) insertion into the outer leaflet of the bilayer, ranging from milliseconds to seconds

ii) equilibration between the outer and inner leaflets, ranging from milliseconds to days

iii) equilibration between the inner leaflet and the inner aqueous compartment occurring over minutes to days

When considering the interaction of detergents with most cell types, both the thermodynamic and kinetic aspects described above fail to take account of active processes, particularly lipid cycling between the outer cell plasma membrane and the inner cellular membranes, which can serve to replenish lipid and other components, as well as transport detergent to the cell interior. For most eukaryotic cell types, the plasma membrane represents less than 5% of the cells total membrane composition.[10] In this regard, the structure and dynamics of most eukaryotic cell plasma membranes differs substantially from that of lipid bilayer vesicle models or that of red blood cells (erythrocytes), in which the plasma membrane is the only membrane present. Another significant difference between physiological exposure of cells to detergent as compared to both

model bilayer systems and most *in vitro* cell models is the choice of quiescent versus flowing systems. Most cell-based experiments to date have been performed as quiescent experiments using erythrocytes,[11-14] although HeLa[15] and B16[16] cells have also been employed. The erythrocyte studies generally use hemolysis as a primary assay for membrane permeability, although the ability of this assay to effectively test Stage I intercalation events has been questioned.[13] Studies testing whether detergent-induced transbilayer lipid motion (flip-flop) was an early Stage I event that could be directed related to cell membrane leakage determined that flip-flop and permeability were independent events.

In studies with a variety of positively charged nanomaterials including synthetic mimics of antimicrobial peptides, antimicrobial peptides, proteins, polymers, and particles on eukaryotic cells such as KB, Rat2, HeLa, and HEK293A, we and others noted that cell plasma membranes showed evidence of membrane leakage (lactate dehydrogenase (LDH), propidium iodide (PI), and fluorescein assays; increased membrane current) caused by disruption of the membrane and/or membrane pore formation far below concentrations that induced lysis.[17-22] In model membrane systems, we and others have noted that the direct introduction of nanoscale holes or pores, membrane thinning and membrane intercalation.[17,18,,23-30] Increased membrane current was ascribed to structural membrane disruption or pore formation because the current induction was not cation specific and lacked rectification, as would be observed for ion-channel based changes in current.[19] With these findings in hand, and considering the extensive studies discussed above using detergents that also have a rich nanoscale structure, we were interested exploring the Stage I to II interactions of detergent with eukaryotic cell membranes. In particularly, we wanted to take advantage of the sensitivity of electrical measurements using whole cell patch clamp as a complementary approach to the hemolysis studies most common in the literature.

In this paper, we examine the interaction of SDS, CTAB, and ORB with HEK 293A cells using automated planar patch clamp (Ionflux 16^{TM}). The following major conclusions were reached: 1) detergent partitions from solution to cell plasma membrane much faster (seconds) than detergent exchanges between the plasma membrane and internal cell membranes (minutes) 2) detergent-induced cell membrane permeability does not decrease after removal of detergent from the external solution over time period of > 15 minutes, even with active equilibration with internal membranes 3) XTT assays indicated ranges of detergent-induced cell plasma membrane permeability that were not acutely toxic 4) the relative activity of SDS, CTAB, and ORB for the induction of membrane permeability HEK 293A cells was quantified for both superfusion and quiescent conditions 5) whole cell patch clamp measurement of current induction was employed to obtain partition coefficients for SDS, CTAB, and ORB with the HEK 293A cells.

The Ionflux 16 uses the whole cell patch clamp configuration to measure the changes in membrane conductance for 16 groups of twenty cells in 8 independent patterns (320 patched cells per experimental run) (Figure 2.1). This instrument has a number of advantages/differences as compared to traditional whole cell patch clamp[19] using a single cell/electrode combination including: 1) simultaneous ability to run multiple repeats and/or multiple exposure concentrations 2) sub-second ability to change concentration 3) continuous superfusion environment 4) ready post-hoc analysis following electrical characterization of all 320 cells using fluorescence microscopy. Electrical characterization of cell plasma membrane permeability was obtained for all three detergents under dynamic exposure most closely related to thermodynamic Stages I-II and kinetic Stages i-iii. For SDS exposure, progression to Stage III occurred as concentration increased as evidence by the observation of open channel currents. For both CTAB and ORB, intercalation did not result in progression to Stage III (membrane

dissolution), consistent with the elegant physical chemical studies of Seelig et al. [31] and Xia and Onyuksel[32] on lipid bilayer models that the head group dramatically effects tendency towards micellization. Consistent with their results, we observe SDS inducing micellization and complete dissolution of the cells for a 2 mM exposure whereas the cell plasma membranes remain intact up to 10 and 1.4 mM for CTAB and ORB, respectively. Considering the ability of each detergent to induce membrane permeability prior to micellization occurring, we find that the relatively activity as a function of concentration under flow conditions is 1: 20: 14 for SDS, CTAB, and ORB, respectively.

In order to understand the nature of detergent induced membrane permeability further, we also subjected cells to detergent exposure for 10 s – 300 s and monitored if the membrane currents returned to baseline levels. For SDS (at sub-solubilizing concentrations), CTAB and ORB, we observed that the increase in membrane permeability caused within 10 s of detergent exposure was not reversible for over 15 minutes. Further work is necessary to determine if this increased membrane permeability can be chronic and its long term impact on cellular function *in vitro* and *in vivo*.

In order to understand the impact of changes in lipid concentration on the detergent induced membrane permeability, we also performed experiments under quiescent, equilibrium conditions by mixing detergent with varying numbers of cells followed by patching the cells and measuring the resulting membrane currents. Partitioning assays have been widely used in literature to measure the lipid bilayer composition and partition constant of detergents in the bilayer.[1-4,11-13,33-37]

The concentration of detergent required to induce a given magnitude of membrane permeability is linearly related to the lipid concentration. At a fixed membrane perturbation

level, the amount of total detergent in the system is constant as presented in equation 1 where D_b denotes detergent in bilayer and D_w the detergent in water. [1-4]

$$D_{total} = D_b + D_w \quad (1)$$

R_b is the ratio of detergent to lipid (L) in the bilayer for a given level of membrane disruption as given in equation 2. [1-4] Substituting equation (2) in (1) results in equation 3.

$$R_b = \frac{D_b}{L} \quad (2)$$

$$D_{Total} = R_b * L + D_w \quad (3)$$

The partitioning of detergent into the lipid membrane can be described by a model (equation 4) where the mole fraction of detergent in the bilayer (X_b) is related to the detergent in water (D_w) through a partition constant (K).[1-4]

$$X_b = \frac{D_b}{D_b + L} = K * D_w \quad (4)$$

The substitution of equations 2, 4 in equation 3 results in equation 5 . [1-4]

$$D_T = R_b * L + \frac{R_b}{(R_b+1)*K} \quad (5)$$

This experiment thus allows us to readily compare our patch clamp derived data with extensive literature in the field. We have determined the partition constants of SDS, CTAB and ORB in the membrane to be 23000 M^{-1}, 55000 M^{-1}, and 39000 M^{-1}, respectively. Fluorescence experiments for ORB indicated that detergent intercalated into the outer leaflet was internalized into the inner cellular membranes over the approximately 20 minute time period of these experiments. The combination of the whole cell patch clamp data and XTT viability data suggest there is a range, ≤ 0.2 mM for SDS and ≤ 1 mM for CTAB and ORB, where detergent exposure can cause long-term plasma membrane permeability without causing acute toxicity.

The results from our experiments indicate that additional work is needed to understand the role of low doses of these classes of materials on inducing inflammatory responses.

EXPERIMENTAL METHODS

SDS and CTAB were obtained from Sigma-Aldrich (Sigma-Aldrich; St. Louis, MO). ORB was obtained from Life technologies (Carlsbad, CA). Other reagents were obtained from Fisher Scientific unless mentioned otherwise.

Ensemble Whole-Cell Patch Clamp Using IonFlux 16^{TM}:

Solutions: Extracellular solution (ECS) consisted of 138 mM NaCl, 4 mM KCl, 1.8 mM $CaCl_2$, 1 mM $MgCl_2$, 10 mM HEPES and 5.6 mM glucose adjusted to pH 7.45 using NaOH. Intracellular solution (ICS) consisted of 100 mM potassium aspartate, 30 mM KCl, 5 mM $MgCl_2$, 5 mM EGTA, 4mM Tris ATP, and 10 mM HEPES adjusted to pH 7.2 using KOH. SDS and CTAB stock solutions were made by dissolving the detergents in ECS to obtain a final concentration of 10 mM. Other concentrations were obtained by serial dilution of the stock solution in ECS. 10 mg of Octadecyl rhodamine B (ORB) was dissolved in 0.5 mL DMSO (final stock concentration 27.4 mM). 100µL of stock was added to 1.9 mL of ECS to obtain 1.37 mM ORB in ECS+5% DMSO. Lower concentrations of ORB were obtained by performing serial dilutions in ECS.

Determining Critical Micelle Concentrations of Detergents in ECS: The fluorimetric method described by Chattopadhyay and London was used to determine the CMC of SDS and CTAB in the ECS.[38] Briefly, 10µL of 1 mM of Diphenyl-(1,6)-Hexatriene (DPH) dissolved in tetrahydrofuran was added to detergents dissolved in ECS. The fluorescence of these samples was measured using FluoroMax-2 (Horiba Instruments Inc.). The excitation wavelength was

358nm. Emission was measured from 400 nm - 500 nm. Above the CMC, when detergents are present as micelles, DPH is incorporated into the micelles and there is a sharp increase in fluorescence.

Cell Culture Materials: DMEM High Glucose with Sodium Pyruvate and Glutamine (Thermo scientific) was the base media (DMEM). Complete media was made by adding 50 mL of Fetal Bovine Serum, 5 mL of Non-essential Amino Acids (Thermo Scientific) and 5mL of Penicillin-Streotomycin to 500 mL DMEM. Serum Free Media (SFMII) for suspension culture of HEK 293A cells was purchased from Invitrogen. Detachin was purchased from Gelantis Inc. PBS (1X) without Ca^{2+} and Mg^{2+} was obtained from Thermo Scientific.

Cell Preparation for Whole Cell Patch Clamp: HEK 293A cells (Cat. No. CRL-1573; ATCC; passages 12-17) were cultured in 175 cm^2 flasks in complete media at 37C and 5% CO_2. The cells were cultured to ~90% confluency (~20-25 million cells). The cells were suspended by first washing with 10 mL of PBS and suspended by treatment with 5 mL Detachin at 37 °C for 5 minutes. 5 mL of compete media was added and the cells were triturated. The suspension was centrifuged at 1000 rpm for 2 minutes (220 x g) and the supernatant was discarded. The cells were suspended in SFM II supplemented with 25 mM HEPES and Pen-Strep, placed in a 25 cm^2 suspension flask and shaken at 75 rpm for 5 minutes. Employing SFMII as opposed to the regular serum free DMEM resulted in a roughly three-fold increase in cell count and was critical for achieving improved seal resistance in each trapping zone. The cells were triturated and counted using a cytometer at this stage. The suspension was centrifuged at 1000 rpm for 2 minutes. The cells were suspended in (ECS). The cells were centrifuged, re-suspended in ECS to a concentration of 8 to 12 million cells/mL and loaded in the IonFlux-16^{TM} 96 well microfluidic plate.

Staining with PKH26: In order to determine if cells were present and intact at the patch clamp sites after experimental treatments including exposure to ECS, SDS and CTAB, we stained cells with membrane dye PKH26 according to the instructions from Sigma-Aldrich. Briefly, ~20 million cells were suspended in serum free media using Detachin as described above. The cells were centrifuged at 1400 rpm (431 x g) for 1 minute. The supernatant was discarded and the cells were suspended in serum free DMEM. The cells were once again centrifuged at 1400 rpm and suspended in 1 mL Diluent C. 4 µL of PKH26 (1mM in ethanol) was dissolved in 1 mL of Diluent C. The cell suspension was mixed with the PKH26 solution and incubated for 5 minutes with periodic mixing every 5 minutes. 10 mL of complete media was added to stop the staining process. The cells were washed with complete media 3 times and suspended in SFM II. The cells were then counted and suspended in ECS for use in the whole cell patch clamp experiments.

Whole Cell Patch Clamp using Ionflux 16™

The IonFlux 16™ consists of a 96 well microwell plate etched with microfluidic channels at the plate bottom as previously described by Ionescu-Zanetti et al. (Figure 2.1).[39] Solutions flow over patched cells giving a superfusion environment for detergent exposure. Each plate is divided into 8 patterns containing two zones that trap 20 cells each. The current trace obtained by each electrode is the combined current from 20 cells. Each pattern has eight wells for compound addition that are independently controlled pneumatically. Each pattern has an IN well which was loaded with cells suspended in ECS. Before the experiment, the plate was "preprimed" for two minutes. During the preprime step, the IN well was filled with ECS. The trap wells were filled with ICS and the compound wells had compound solutions. After the preprime step, the IN well was filled with cells suspended in ECS. The experiment consisted of four phases: Prime, Trap,

Break and Data Acquisition. The timeline and pressure settings for the four phases are provided in supplementary material (Figure A.2). In the trap phase, the fluid in the main channel flowed in pulses (no flow for 4.2 s, followed by fluid flowing for 0.8 s), which allowed cells to be trapped. The trapped cells were perforated using a rectangular pressure pulse of amplitude 4 psi for 10 s during the break phase. During the data acquisition phase, the main channel and the trap pressures were constant at 0.16 psi and 6 mm Hg respectively. The voltage for data acquisition was set at -70 mV and the sampling rate was 500 Hz. The data was collected in frames that lasted 30 s followed by a 0.3 s period when no data was collected.

Detergent exposure after patching:

Once the cells were trapped, they were exposed to ECS for 120 s, following which they are exposed to detergents at different concentrations. Cells were exposed to SDS and CTAB for 900 s and exposed again to ECS for 120 s. Cells were treated with ORB for 600 s and treated with ECS again for 120 s. A schematic of the experimental protocol is provided in supplementary material (Figure S2).

Data Analysis: The current vs time trace files were exported and processed using Microsoft Excel and MATLAB. The change in membrane current upon exposure to the detergents for different lengths of time was calculated. The time averages of current from 7.2s -11.2 s after exposure (72.6 to 76.6s) and from 931 to 935 s after exposure (991.6 to 995.6 s) were subtracted with time average of current just before detergent exposure (60.6 – 64.6 s). For cells exposed to ORB the time average current 10 minutes after exposure (666.6 to 670.6 s) was subtracted from the time average current immediately before exposure (60.6-64.6 s). One way analysis of

variance (ANOVA) followed by Tukey's multicomparison test was performed to determine the statistical significance of the difference in current changes across different treatments.

Quiescent experiments using cells pre-treated with detergent:

Partitioning assay have been widely used to measure the lipid bilayer composition and partition constant of detergents in the bilayer.[1-4,11-13,33-37] In this experiment, different numbers of HEK 293A cells were pre-treated with detergent followed by whole cell patch clamp measurements to evaluate the detergent partitioning into the membrane as a function of lipid concentration.

A fixed number of cells (e.g 5 million cells) were suspended in ECS and incubated with various concentrations of detergents for 15 minutes. The suspension was then centrifuged at 1000 rpm. The cells were resuspended in ECS and patched using the IF-16. The current vs time trace files were exported and the time averaged current from the first four minutes was used as a measure of membrane permeability. This process was repeated for four different cell counts (1.5 million, 5 million, 10 million and 15 million cells).

For CTAB alone, the partitioning behavior was also probed using a trypan blue assay. Trypan blue is a dye that is excluded from cells when the cell membrane is not compromised. In this experiment, cells were pretreated with CTAB as described above but trypan blue assay was used as a membrane permeability marker instead of whole cell patch clamp.

Experimental Design and Data Analysis: In order to compare membrane perturbation induced by SDS, CTAB, and ORB at thermodynamic Stage I and determine partition coefficients, the change in membrane behavior is generally measured at the onset of perturbation.[12,33] This approach is also taken because the plateau reached upon after substantial exposure can be the

result differing physical states including complete cell solubilization (SDS) or saturation of the cell plasma membrane with detergent (CTAB, ORB). Figure A.4 provides an example of this behavior and method of calculation for the trypan blue assay for CTAB.

For the whole cell patch clamp study, it was difficult to identify the point of onset of increase in current due to the variability in the patch quality of cells. Hence, we used the following three step method to estimate the detergent concentrations required for the onset of increased permeability (Figure A.5) and calculate partition constants.

1. The rate of increase in current from control levels till a current level of ~ 50 nA was measured (Figure A.5). The inverse of this slope provides us a measure of the amount of detergent necessary to increase the current by 1 nA.
2. Upon examination of multiple data sets, current changes of ~ 15 nA were determined to represent a reliable magnitude of change to indicate an detergent-induced current increase. The detergent necessary to increase the current by 1 nA was multiplied by 15 to obtain an estimate for detergent necessary to induce membrane currents of 15 nA.
3. The detergent concentrations at the onset of increased membrane permeability were then plotted with respect to the lipid concentration and fit with a linear model. The lipid concentration in cells was estimated from literature to be 10^9 lipid molecules per cell membrane.[10] The slope and intercept of this line were R_b and D_w respectively. The partition constant K was calculated using equation 6.

$$K = \frac{R_b}{(R_b+1)*\text{Intercept}} \tag{6}$$

In step 1, a current level of 50 nA was used to calculate the slope because the cells treated using SDS, CTAB and ORB, are in a comparable physical state corresponding to thermodynamic Stage I-II of the partition model. Higher current levels represent the current after cells have been

solubilized by SDS. At a current level of 50 nA, the cells were not solubilized when visualized using PKH26 and ORB and gave a cell count that did not differ from the control.

XTT assay: XTT kits from Sigma-Aldrich were used for this experiment. HEK293A cells were plated in a 96 well tissue culture plate at a density of 100,000 cells per well and incubated overnight at 37°C and 5% CO_2. Cells were incubated with SDS, CTAB, ORB or ECS for 20 minutes. The supernatant was then removed and 50 µL of PBS was added to each well. 50 parts of solution A was mixed with 1 part of solution B to prepare the XTT reagent. 30 µL of this reagent were added to each well and incubated at 37° C and 5% CO_2 for 2 hours. The absorbance of the well was then measured at 490 nm and 690 nm and the difference in absorbance between the two wavelengths was calculated. A large difference would indicate more viable cells. The percent viability was then calculated with respect to cells treated with ECS.

RESULTS

The critical micelle concentrations (CMCs) of SDS and CTAB in ECS were determined to be 0.8-1 mM and 0.03-0.06 mM, respectively. The CMC values in water were also obtained giving values of 6-8 mM and 1-2 mM, respectively, consistent with the published data in the literature.[38] Line drawings of the detergent structures are provided in Figure A.3.

The change in current as a function of time measured for patched cells exposed to 0.004 to 2 mM SDS is presented in Figure 2.2. Each trace is the total current measured across 20 cells. Cells exposed to 0.2 mM SDS (number of traces, n=11) and 2 mM SDS (n=8) exhibited an initial sharp increase in current when compared to the ECS controls. On average, the current increase started between 2 to 3 s and 1 s, respectively, for cells treated with 0.2 mM and 2 mM SDS. For

cells treated with 0.2 mM SDS, the initial change in current lasted 3 to 4 s. The current then increased slowly for the next 67 ± 25 s. This was followed by a faster increase in current which reached ~50 nA at the end of 15 minutes. The currents for cells exposed to 2 mM SDS eventually reached open channel current levels. Except for one trace that took 871s after exposure to reach open channel current level, other traces reached open channel current in 120 ± 61 s.

The difference between the pre-exposure current and the currents at 7.2-11.2 s and 931 – 935 s after exposure are presented in Figure 2.2B. One-way analysis of variance indicated the change in current in the first 7.2-11.2 s after compound release was significantly different between the treatments ($p < 0.001$). Tukey's multiple comparisons analysis indicated that the current increases caused by 0.2 mM and 2 mM SDS were significantly different from the control and from each other ($\alpha = 0.05$). Similarly, the mean change in current 931 to 935s after exposure to detergents was significantly different for the different treatments ($p < 0.001$).

The change in current as function of time measured for patched cells exposed to 0.001 to 10 mM CTAB is presented in Figure 2.3. The introduction of CTAB at 0.0001 mM (n = 4) and 0.001 mM (n = 4) did not cause a change in conductance as compared to the controls. The introduction of CTAB at 0.01 mM (n = 8), which is still below CMC, caused a slow increase in current that eventually reached ~1/3 of the open channel current. The exposure of cells to CTAB at 0.1 mM (n=10), 1 mM (n = 12) and 10 mM (n = 4) caused a rapid increase in membrane current that reached a steady state between -40 to -70 nA. The times of onset for the change in current after compound release were 2 to 3 s for 0.1 mM CTAB and 1s for both 1 mM and 10 mM CTAB .

ANOVA indicated that the mean current increases at 7.2 to 11.2 s and 931-935 s after detergent exposure between all the treatments were significantly different ($p < 10^{-5}$). At the 7.2 to 11.2s time point, Tukey's multiple comparison test indicates that the current changes produced by 0.1 mM, 1 mM and 10 mM CTAB were significantly different from the ECS controls, 0.0001 mM and 0.001 mM CTAB ($\alpha = 0.05$). At the 931 to 935 s time point, the current increases produced by 0.01 mM, 0.1 mM, 1 mM and 10 mM CTAB were significantly different from the ECS controls, 0.0001 mM and 0.001 mM CTAB ($\alpha = 0.05$). Unlike SDS, a CTAB concentration as much as 200 times higher than the CMC did not result in open channel current levels.

The exposure of cells to detergents caused significant changes in the membrane currents observed by whole cell patch clamp. The currents in some traps treated with 2 mM SDS reached open channel levels; however, currents in traps treated with 0.2 mM SDS, 0.1 mM, 1 mM and 10 mM CTAB remained steady at approximately half the open channel levels.

These steady state current levels could be either due to 20 intact, but leaky cells, or a mixture of intact cells and dissolved cells leading to open channels in some fraction of the 20 trapping sites per zone. Fluorescence microscopy was employed to distinguish between these two possibilities. In order to determine if cells were intact after treatment with the various concentrations of SDS and CTAB in the microfluidic plates, we stained cells with PKH26. PKH26 is a dye that localizes to the cell membrane. The cells were then patched and treated with detergents, as described in the previous section. Figures 2.2 C-F and 2.3 C-H show the fluorescent images of cells stained with PKH26 after treatment with detergents for 15 minutes. Cells treated with ECS, 0.04 mM SDS and 0.001 mM CTAB were intact as indicated by their fluorescent perimeter. This is consistent with the observation that cells do not display an increase in permeability when treated with detergents at these concentrations. Cells treated with 0.2 mM

SDS and 0.1 mM to 10 mM CTAB were also intact even though they display substantially increased membrane currents. The patterns treated with 2 mM SDS do not show any intact cells, consistent with the measured open channel current levels.

As an alternative approach to employing PKH26, we also employed Octadecyl Rhodamine B (ORB), a positively charged amphiphilic, fluorescent detergent. This approach provided the opportunity to explore the relationship between intercalation and current increase at the lowest concentration exposures. The change in current as function of time measured for patched cells exposed to 0.035 to 1.4 mM ORB is presented in Figure 2.4. ORB at 0.035 mM, 0.14 mM and 1.4 mM increased membrane current significantly when compared with the controls. Current induced by 0.014 mM ORB is significantly different from ECS control but not 0.007 mM ORB. Fluorescence microscopy images (Figure 2.4 C-F) reveal that the cells are fluorescent and intact after exposure to ORB at all three concentrations for 10 minutes.

Figure 2.5 presents the current induced after cells are exposed to SDS, CTAB and ORB for 900 s. SDS and ORB induce increased membrane permeability at 0.2 and 0.14 mM respectively, while CTAB induces membrane permeability at 0.01 mM. CTAB induces permeability at concentrations 20 times less than SDS and 14 times less than ORB. The relative activity of SDS: CTAB: ORB is thus 1: 20: 14 as measured by this method.

The metabolic activity of cells exposed to SDS, CTAB and ORB as measured by the XTT assay is presented in Figure 2.6. Cells exposed 0.004 to 0.2 mM SDS, 0.001 – 0.1 mM CTAB and 0.0137-0.137 mM ORB do not show a loss in metabolic activity. Cells exposed to 2 mM SDS, 1 mM and 10 mM CTAB and 1.37 mM ORB show reduced metabolic activity.

Detergents can increase membrane permeability either by removing lipids from the membrane or by forming stable pores in the membrane. In order to further probe the reversibility of the current induction in the plasma membrane, we exposed cells to detergents at sub-solubilization concentrations for 10 s, 30 s or 300s followed by ECS for 900 s (Figure 2.7) . Cells were exposed to 0.2 mM SDS, 0.1 mM CTAB and 0.137 mM ORB. The exposure of cells to SDS, CTAB and ORB for 10 s is sufficient to cause increased membrane permeability. The increased permeability induced within 10 s is not reversible, even fifteen minutes after exposure for all three materials. This result is once again consistent with the hypothesis that the increased permeability is caused by the intercalation of detergents in the cell membrane.

The experiments discussed so far have all been for detergent exposure under superfusion conditions. The vast majority of experiments in the literature have examined detergent exposure under quiescent conditions.[11-13,33-37] In order to compare our superfusion-based data to quiescent data we treated cell with varying amounts of detergent and then patched the cells to make the current measurements (Figure 2.8 A-C). The amount of detergent necessary to induce membrane conductivity increased with the cell number. Cells treated with the highest concentrations of SDS reached the open channel current plateau of the Ionflux-16 instrument since the cells were fully solubilized. Cells exposed to CTAB and ORB remained intact even at the highest concentrations and their current plateaus arise from detergent saturation of plasma membrane.

The detergent concentrations at the onset of increased membrane permeability were calculated, plotted with respect to the lipid concentration, and fit using a linear model (Figure 2.9). The values of R_b and K were calculated as in equation 5 (Table 2.1). The ratio of detergent to lipid in the bilayer at the onset of increased permeability was 2.0 for SDS, 0.3 for CTAB and 0.4 for ORB. The partition constants (K) for SDS, CTAB and ORB are 23000 M^{-1}, 55000 M^{-1} and

39000 M^{-1}, respectively. The partition constant of CTAB measured using the trypan blue assay is 48000 M^{-1}

There is an error associated with estimates of R_b and the intercept obtained using a linear regression of the data in Figure 2.9 that can be employed to estimate the error in K (full details provided in supplementary information). Employing the error in R_b and the intercept, a range of values for the partition constant (K) for SDS [16300 - 39200], CTAB [29000 - 476000], and ORB [24000 - 99000] were obtained. The partition constant of CTAB measured using the trypan blue assay ranged from 37000 to 67000 M^{-1}. Ranges are provided rather than the standard deviation because K is not a linear function of R and the the mean estimate of K calculated from R and D_w is not the midpoint of the distribution of K. Literature values for K for liposomes and erythrocytes reported to date gave no error term.[12, 33]

Table 2.1. Rb and K values for SDS, CTAB and ORB

Material	**Line Equation**	**R^2**	**R_b ± Standard Error**	**D_w ± Standard Error**	**K (Average) [Lower bound, Upper Bound]**
SDS	2 X + 28.7	0.96	2 ± 0.4	29± 10	23000 , [16300, 39200]
CTAB	0.3 X + 4.2	0.79	0.3 ± 0.1	4.2 ± 2.8	55000 , [29000, 476000]
ORB	0.4 X + 7.3	0.87	0.4 ± 0.1	7.3 ± 3.1	39000, [24000, 99000]

DISCUSSION

The changes in transmembrane currents observed in cells treated with different concentrations of SDS can be categorized into three groups (numbered 1-3 in Figure 2.2A): 1) Traces that show no change in membrane conductivity compared to controls 2) Traces that show a rapid change in

conductivity within 2 s of exposure to detergents and then reach a steady state current that is less than the open channel current and 3) traces that show a rapid increase in current that reaches open channel levels over a few minutes. Traces from cells exposed to 2 mM SDS are in group 3. Visualization of these patch sites for PKH 26 stained cells indicates complete solubilization of cells (Figure 2.2 E). By way of contrast, CTAB did not solubilize cells even at 200 times the CMC. Current traces of cells exposed to 0.2 mM SDS and 0.1-10 mM CTAB fall into group 2 and PKH26 stained cells are readily visible in the patch sites (Figure 2.3). Current traces from cells exposed to ECS, 0.004 to 0.04 mM SDS and 0.0001-0.001 mM CTAB belong to group 1 and also exhibit readily visualized PKH26 stained cells. Cells treated with 0.01 mM CTAB exhibited behavior midway between groups I and II with both a slower rate of current increase and final current values that did not reach the saturated limited.

In group 2, all twenty PKH26 stained cells in a trap were intact after exposure to detergents for ten minutes. Thus, the steady state current is not caused by the incomplete solubilization of cells causing some fraction of the trapping sites to exhibit open channel current values. This observation is consistent with the hypothesis that the increased membrane permeability is caused by detergent intercalation in the membrane. This hypothesis is further supported by the fact that ORB, which is known to localize in the membrane, also induces increased membrane permeability (Figure 2.4).

It has been suggested that detergent micelles are required for the solubilization of lipid membranes,[9] or that solubilization occurs near CMC.[5,16] Evidence has also been presented that micelles are not necessary for solubilization.[32] In our experiments, SDS solubilized cells above CMC. By way of contrast, CTAB does not solubilize cells even at concentrations 200 times above CMC. Thus, the presence of detergent micelles alone is not a sufficient criterion for the

complete solubilization of cell membranes. Moreover, the effect of 0.2 mM SDS (below CMC) on membrane current and cell viability is similar to the effect of 0.1 mM CTAB (above CMC) in spite of the different aggregation states. This suggests that the aggregation state of free detergent in solution does not influence membrane solubilization. Rather, our cell-level studies agree with the physical chemical studies of Seelig et al. [31] and Xia and Onyuksel[32] on lipid bilayer models that it is the degree of incorporation into the membrane, head group shape and charge of the detergent that determine the efficiency of cell membrane solubilization by detergents. This process may also be affected by the cycling of lipid from the membrane within the cell. From our study, it is seen that the detergent partitioning occurs in the scale of a few seconds as compared to the several minutes needed for lipid recycling.

Several models have been proposed for the perturbation of lipid membranes by detergents. Detergents can increase conductivity by intercalating in the membrane and disrupting normal lipid packing, forming stable detergent lined pores, or forming lipid-lined pores due to the formation of mixed micelles. In our whole cell patch clamp experiments under superfusion conditions, the increased membrane conductivity induced by these detergents is not reversible. The fact that the pores induced by SDS, CTAB and ORB are not reversible over 15 minutes indicates the detergent is intercalated in the membrane and/or stabilizing any pores formed. The detergent could be intercalated in the membrane and cause membrane bending or thinning, as in a carpet model,[40] or it could form stable detergent-lined pores as has been reported for barrel-stave [41,42]and toroidal pore models.[43,44] The data reported here cannot distinguish between these two possibilities, in part because the amplifier response is averaged over 20 patched cells. This prevents clear resolution of single pore formation and the type of comparison we could make with X-ray structural data when performing single cell patch clamp studies.[19,45] By way of

comparison, apparently unstabilized and detergent-free, pores formed by sonoporation are reversible over 5-20 s[46] and unstabilized pores in giant unilamellar vesicles close in about 100 ms.[47] One possible factor that could confound the IonFlux-16 reversibility experiment is the adsorption of detergent in the walls of the microfluidic channel during the 10-300 s exposure and subsequent release when cells are exposed to ECS alone (Figure 2.7D). To address this concern, we modeled the exponential release of detergent from a monolayer adsorbed in the channel wall between the compound release site and trap site where cells are located. Results presented in Figure A.6 show that the cells are exposed to concentrations much lower than the concentrations necessary to induce membrane permeability.

The results in Table 2.1 show that the ratio of detergent to lipid in the bilayer at the onset of increased membrane permeability is 7 and 5 times greater for SDS when compared to CTAB and ORB, respectively. The partition constant for SDS in POPC and POPC/POPG vesicles has been determined by Beck, Seelig et al. to be 33,000 and 37,000 M^{-1} respectively.[31] Another study by Tan, Seelig et al. reported the partition constant of SDS in POPC and POPC/POPG small and large unilamellar vesicles to range from 12,500 M^{-1} to 70,000 M^{-1} depending on the size and composition of the vesicles as well as the temperature.[37] Our observation of 23000 M^{-1} is thus within the range predicted from studies of vesicle models. Beck, Seelig et al. also report a K of 350,000 M^{-1} for CTAB in POPC vesicles. Our partition constants of 55000^{-1} M^{-1} (patch clamp) and 48000 M^{-1} (trypan blue) measured for HEK 293A cells are substantially smaller and differ substantially from the value determined using a vesicle model.

During the estimation of partition constants for charged detergents into well-defined lipid systems such as liposome, the electrostatic interaction of the detergent with the membrane is also

taken into account. This is because the concentration of a charged detergent near the surface of the charged cell membrane need not be equal to the bulk detergent concentration in the aqueous phase.[4,31,37] The local concentration of the SDS, CTAB and ORB near the membrane surface is affected by the membrane surface charge density, buffer composition etc.[4,31,37] Thus, K is a function of R_b, D_w and the surface potential (ψ_0) as described by equation 3. The overall partition constant K is related to the partition constant that accounts for electrostatic interactions as described by equation 3.[4,31,37] In equation 7, z is the charge of the detergent head group, F_0 is Faraday's constant, R is the gas constant, T is the temperature and ψ_0 is the membrane surface potential.

$$K_{electrostatic} = \frac{K_{overall}}{(e^{-\frac{zF_0\psi_0}{RT}})} \quad (7)$$

In our experiment, the membrane surface potential of cells was not readily available since it could be affected by a number of biological factors such as the presence of additional proteins, sugar moieties on the surface, physiological state of the cell etc. In addition, the lipid membrane is cycled through the cell and it is unclear how the surface potential would be affected by that process. Hence, the binding constants calculated in this work are overall binding constants that do not take into account electrostatic interactions.

Based on the XTT assay, the detergent treated cells in group 2 can be further differentiated as cells with increased membrane currents that do not exhibit reduced metabolic activity (2a) and cells with increased membrane current that show decreased metabolic activity (2b). Group 2a is represented by cells exposed to 0.2 mM SDS and 0.1 mM CTAB, while 2b consists of cells exposed to 1 mM and 10 mM CTAB. Thus, at least at certain concentrations, detergents increase membrane permeability to ion flow without reducing metabolic activity and without damaging, to the limit of our optical resolution, the structure of the cell. Moreover, the cells treated with

0.137 mM ORB are fluorescent, show increased membrane currents and are metabolically active. This shows that an amphiphilic molecule with a charged head group can intercalate in cell membranes, cause increased membrane conductivity, but not reduce the metabolic activity of the cells.

CONCLUSION

Detergents increased the transmembrane conductivity of cells very rapidly, on the order of a few seconds. SDS and CTAB increased membrane conductivity of cells even when their bulk concentration was below CMC. The experiments support previous conclusions that detergent head group charge and shape affects cell membrane solubilization. Fluorescence microscopy images indicated that cells with increased conductivity were intact. Patch clamp experiments combined with microscopy also showed that ORB both intercalates in the membrane and increases membrane conductivity significantly. The increased membrane conductivity induced by detergents at sub-solubilizing concentrations does not decrease once compound exposure is stopped. These results suggest intercalated detergent remains in the plasma membrane for at least 15 minutes. Moreover, our studies provide partition constants for SDS, CTAB and ORB in non-erythrocytic mammalian cell membranes.

SUPPORTING INFORMATION

Schematic of detergent – cell membrane interaction (A.S1); Description of IonFlux 16 ™; Line diagrams of detergents used in study (A.S3); Membrane partitioning of CTAB using trypan blue assay (A.S4); Estimation of detergent concentration at the onset of membrane permeability (A.S5); Amount of detergent released from microfluidic channel wall (A.S6); Estimation of error in partition constant estimate.

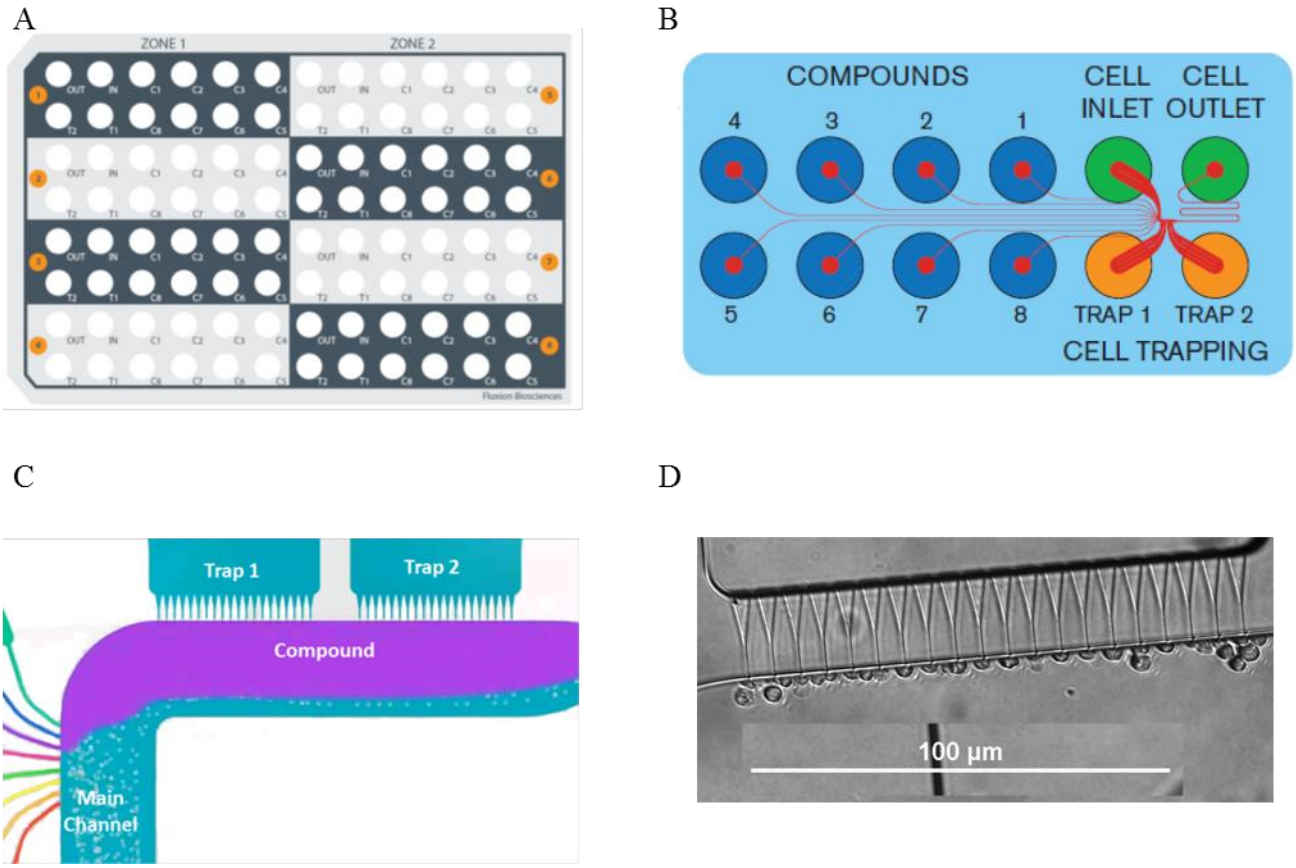

Figure 2.1. Ionflux 16^{TM} Description. (A) Ionflux 16^{TM} consists of a 96 well plate with 8 patterns (colored in grey and black and numbered in orange circles). (B) Each pattern has two trap wells (Trap 1, Trap 2) that are filled with ICS. Cells are loaded in the "INLET" wells and waste is collected in the "OUTLET" well. Compounds are loaded in wells C1 to C8. (C) A zoomed in view of the trap zones. The cells suspended in ECS flow in the "Main Channel" which flows past the trap zones. When a compound is released, the laminar flow ensures that the compound and ECS streams do not mix. (D) shows cells trapped in a trap zone. (Figures 2.1A-2.1C were developed by Fluxion Biosciences).

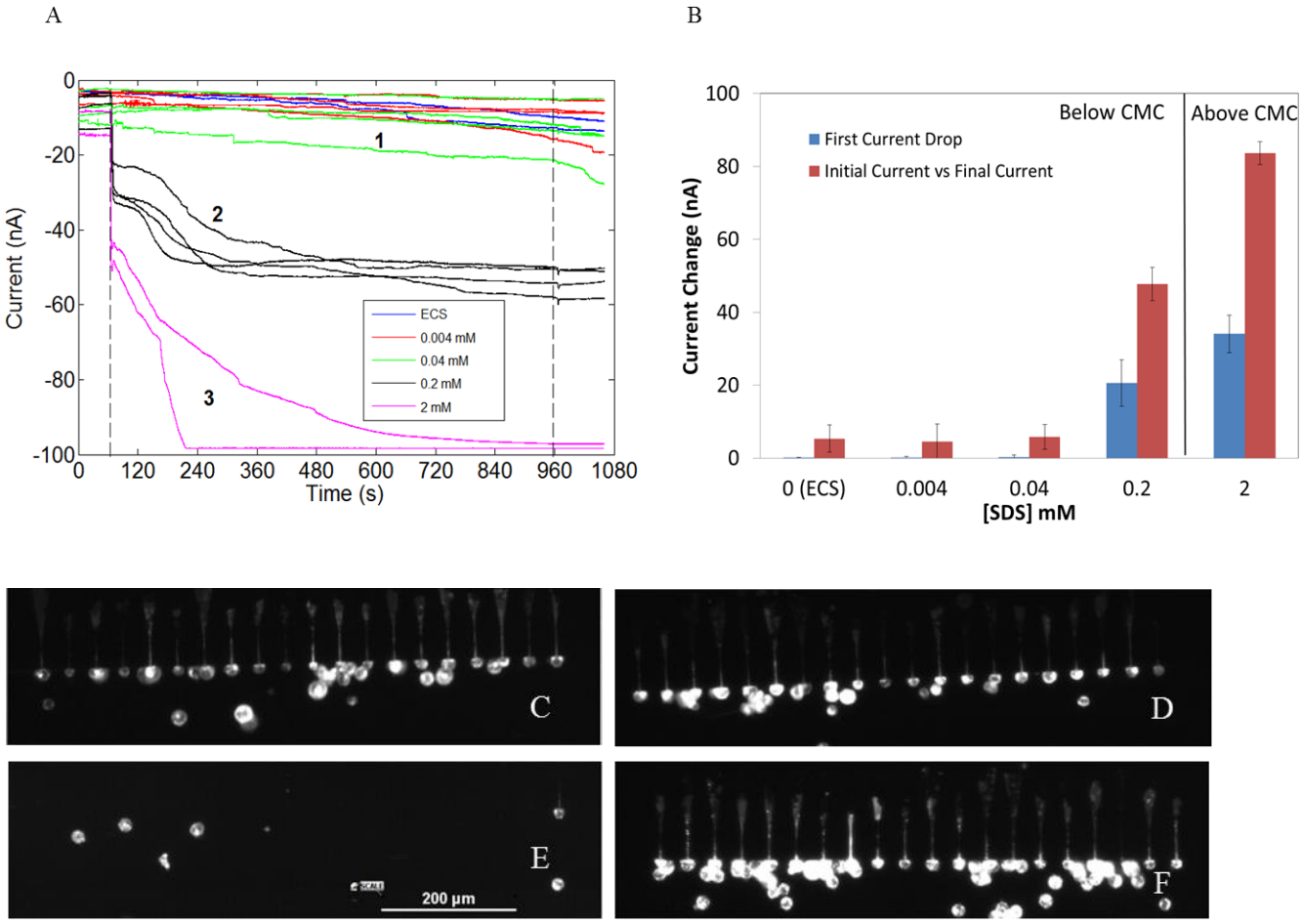

Figure 2.2. Membrane Permeability Induced by SDS. (A) The exposure of HEK293A cells to 0.004 mM and 0.04 mM SDS does not result in an increase in conductivity when compared to the ECS controls. Exposure to 0.2 mM and 2 mM SDS caused a large and sudden increase in conductivity within 1-3 s. The CMC of SDS is ~0.8 mM. Thus, SDS causes increased cell permeability even below CMC. (B) The difference between current before exposure to detergents, 7-11 s after detergent release and 931-935 s after detergent release were calculated. One way ANOVA combined with Tukey test indicates that the current changes caused by 0.2 mM and 2 mM SDS are significantly different from the current changes caused by ECS, 0.04 mM SDS and 0.004 mM SDS. (C) Fluorescent image of HEK293A cell exposed to 0.04 mM SDS shows intact cells. This is consistent with the absence of an increase in current. (D) Cells treated with 0.2 mM SDS are still intact after exposure for 10 minutes. This implies that the observed increase in current is due to the increased permeability of the membrane. (E) Cells treated with 2 mM SDS are not present in the trap region. This is consistent with current levels similar to open channel current levels. (F) Cells treated with just the ECS are intact after 10 minutes.

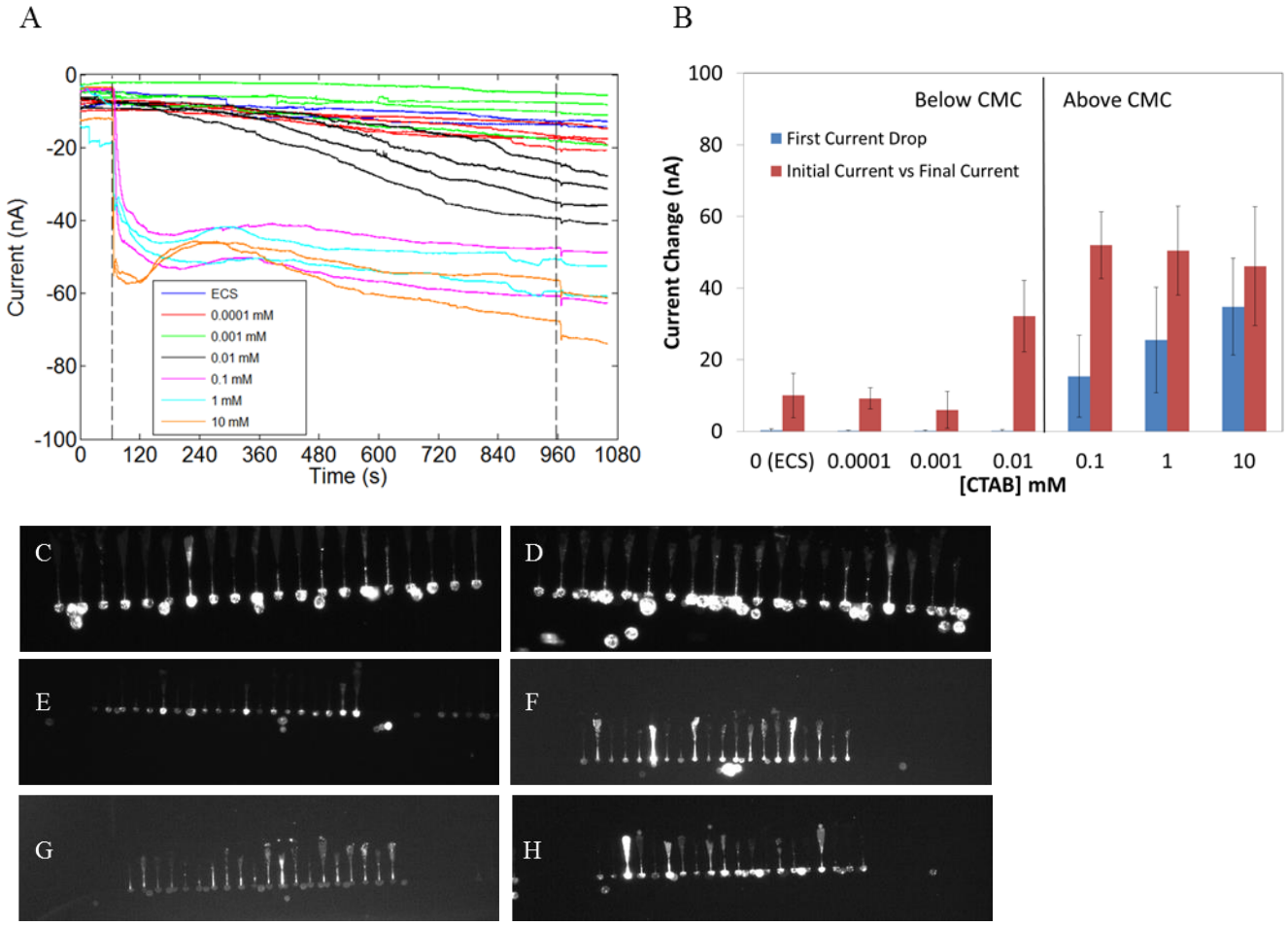

Figure 2.3. Membrane Permeability Induced by CTAB. (A)The exposure of HEK293A cells to ECS, 0.0001 mM, and 0.001 mM CTAB did not result in an increase in conductivity. Exposure to 0.01 mM CTAB caused a delayed increase in conductivity. The exposure of cells to 0.1 mM CTAB causes a large and sudden increase in conductivity within 1-3 s after exposure. The CMC of CTAB is ~0.06 mM. Thus, CTAB caused increased cell permeability even below CMC. (B) The difference between current before exposure to detergents, 7-11 s after detergent release and 931-935 s after detergent release were calculated. One-way ANOVA combined with Tukey test indicates that the current changes caused by 0.01-10 mM CTAB are significantly different from the current changes caused by ECS, 0.0001 mM CTAB and 0.001 mM CTAB. (C,D) Fluorescent images of HEK293A cells treated with 0.001 mM and 0.01 mM CTAB show that the cells are intact. This is consistent with the absence of an increase in current. (E-G) Cells treated with 0.1 mM, 1 mM and 10 mM CTAB are still intact after exposure for 10 minutes. This implies that the observed increase in current is due to the increased permeability of the membrane. (H) Cells treated with just ECS are intact after 10 minutes.

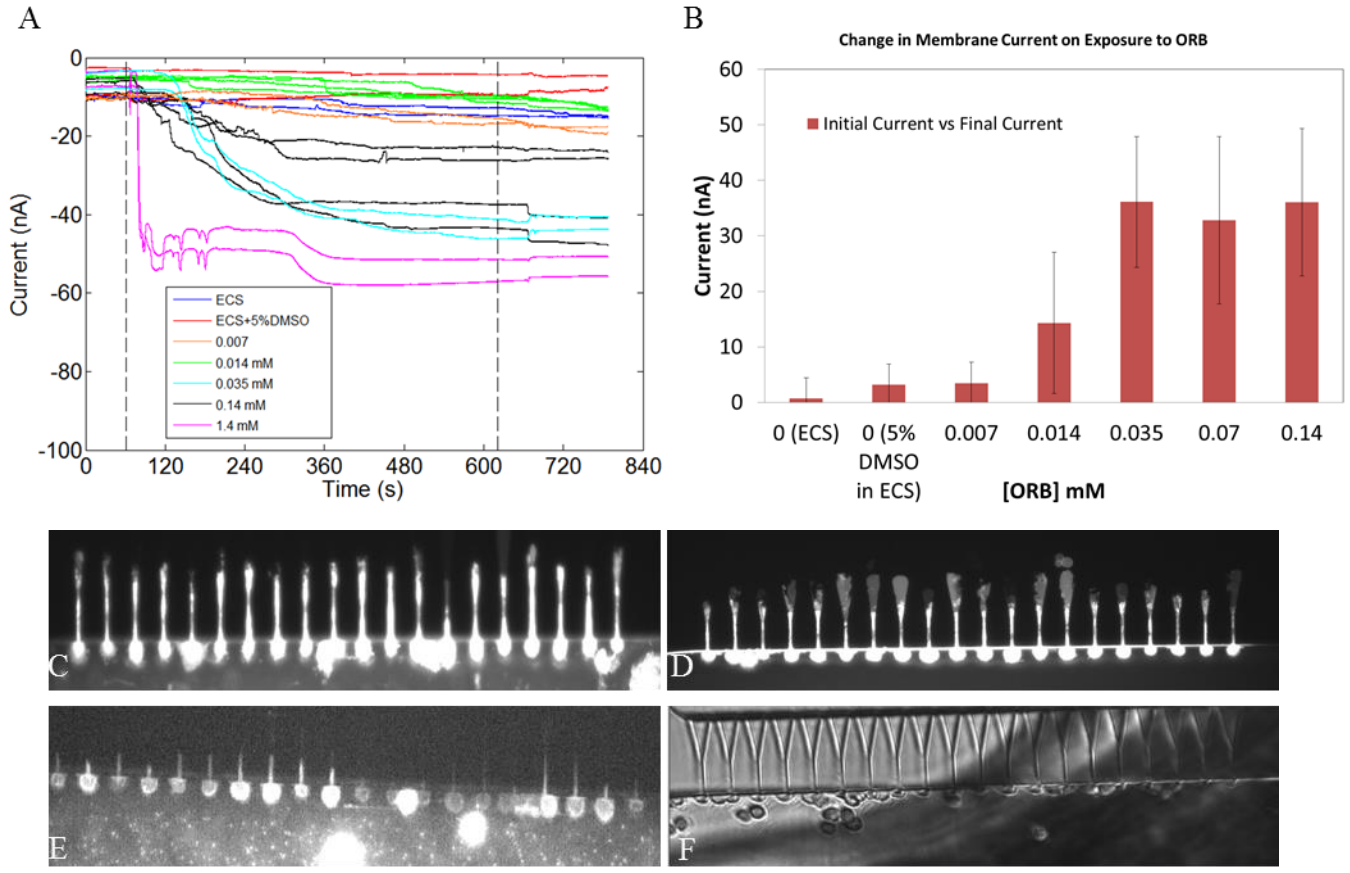

Figure 2.4. Membrane Permeability Induced by ORB. (A) The exposure of HEK293A to 0.035 - 1.4 mM ORB results in an increase in conductivity within 2-50 s that is not seen in the 5% DMSO and ECS controls. (B) The difference between current before exposure to detergents and 931-935 s after detergent release were calculated. One way ANOVA combined with Tukey test indicates that the current changes caused by 0.035 mM, 0.14 mM and 1.4 mM ORB are significantly different from the current changes caused by ECS, 0.007 mM and 0.014 mM. Current induced by 0.014 mM ORB is significantly different from ECS control but not 0.007 mM ORB (C) Fluorescent image of HEK293A cells treated with 1.37 mM ORB indicates that cells are intact after 10 minute exposure even though they exhibit a change in conductivity. (D) Cells treated with 0.137 mM ORB are still intact after exposure for 10 minutes. This implies that the observed increase in current for the 0.137 mM ORB is due to the increased permeability of the membrane. (E) Cells treated with 0.0137 mM ORB are fluorescent but do not exhibit a change in membrane conductivity (F) Bright field image of cells treated with just 5% DMSO in ECS are intact after 10 minutes.

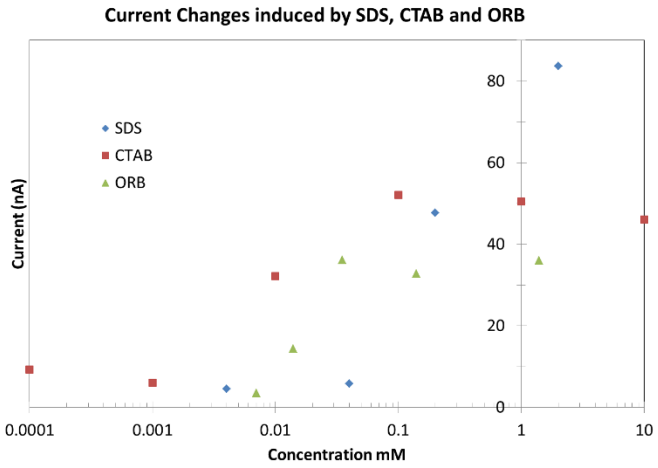

Figure 2.5. Change in Membrane Currents Induced by Detergents. Figure shows the change in current 900 s after exposure to SDS, CTAB and ORB dissolved in ECS. SDS and ORB induce increased membrane permeability at 0.2 mM respectively, while CTAB and ORB induce membrane permeability at 0.01 mM and 0.014 mM respectively. CTAB induces permeability at concentrations 20 times less than SDS and 14 times less than ORB. The relative activity of SDS:CTAB:ORB is thus 1:20:14 as measured by this method.

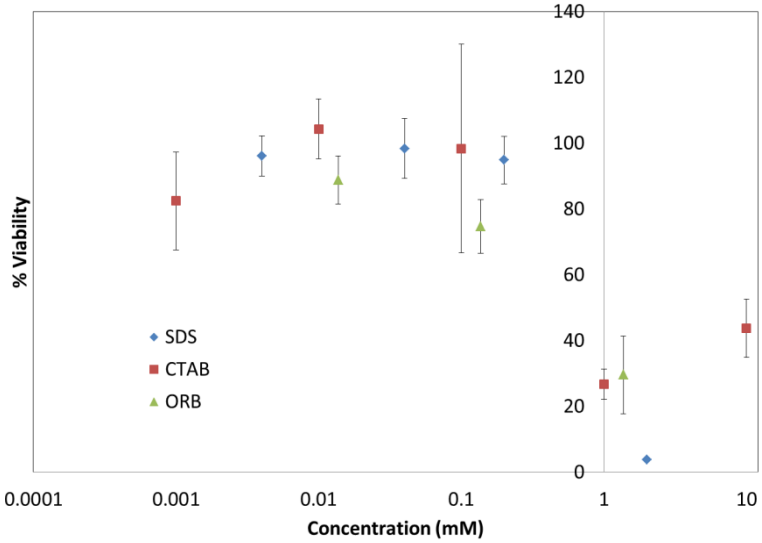

Figure 2.6. Mitochondrial Toxicity Induced by Detergents. Figure shows the percent of metabolically active cells after exposure to SDS, CTAB and ORB dissolved in ECS compared to cells exposed to ECS alone. All three compounds cause reduced cell viability at concentrations greater than 1 mM.

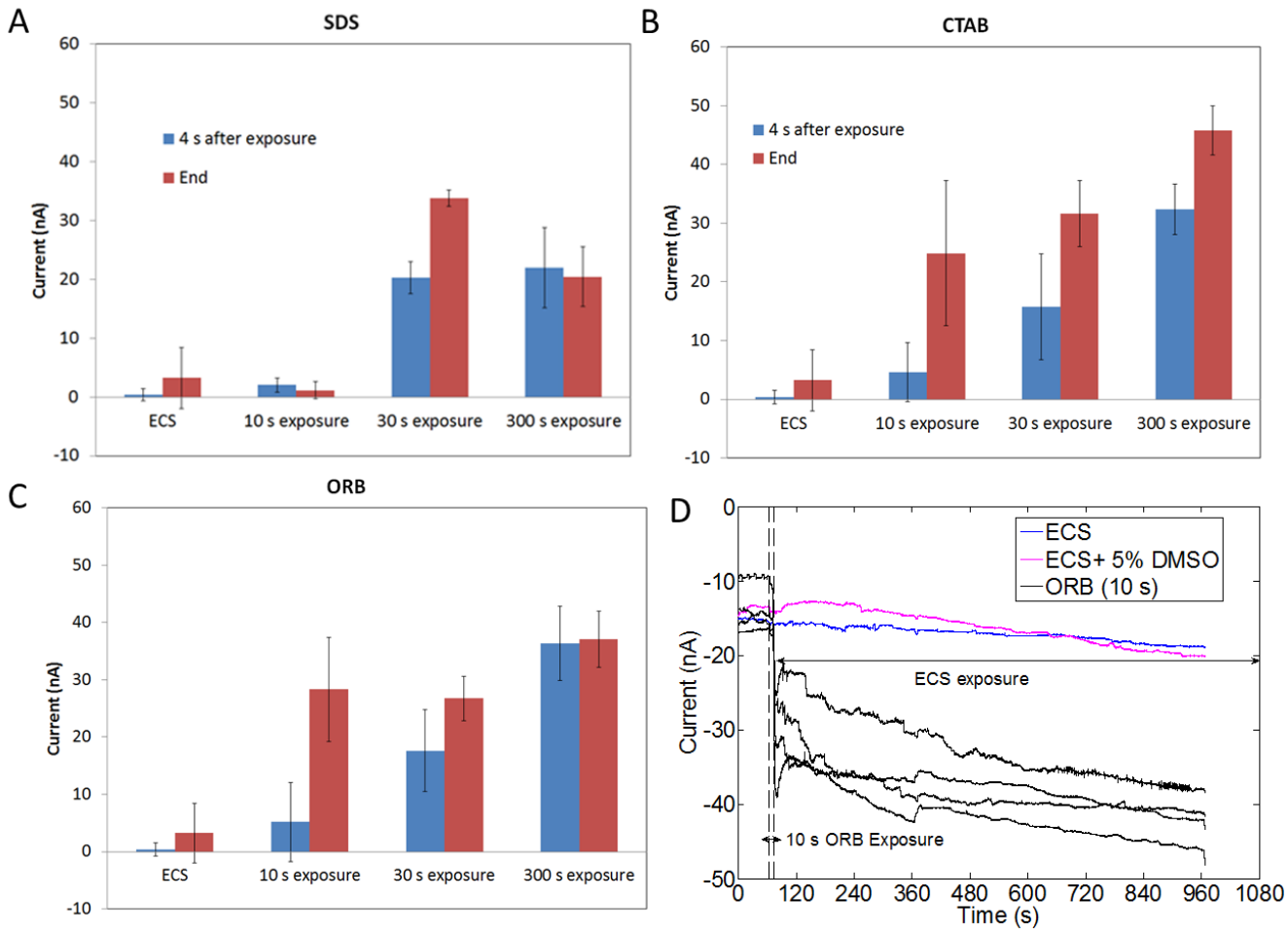

Figure 2.7. Increased Membrane Permeability by Detergents not Reversible. (A) The increased conductivity induced in HEK293 A by 0.2 mM SDS after 30 s of exposure is not reversed at the end of the experiment (600s). (B) The increased conductivity induced in HEK293 A by 0.1 mM CTAB after 10 s of exposure is not reversed at the end of the experiment (600s). (C) The increased conductivity induced in HEK293 A by 0.137 mM ORB after 10 s of exposure is not reversed at the end of the experiment (600s). (D) Exemplar figure showing current traces of cells exposed to ORB for 10 s in comparison to control current traces from cells exposed to only ECS or ECS+ 5% DMSO. The dotted lines marked with the double arrow indicated the time when cells were exposed to ORB.

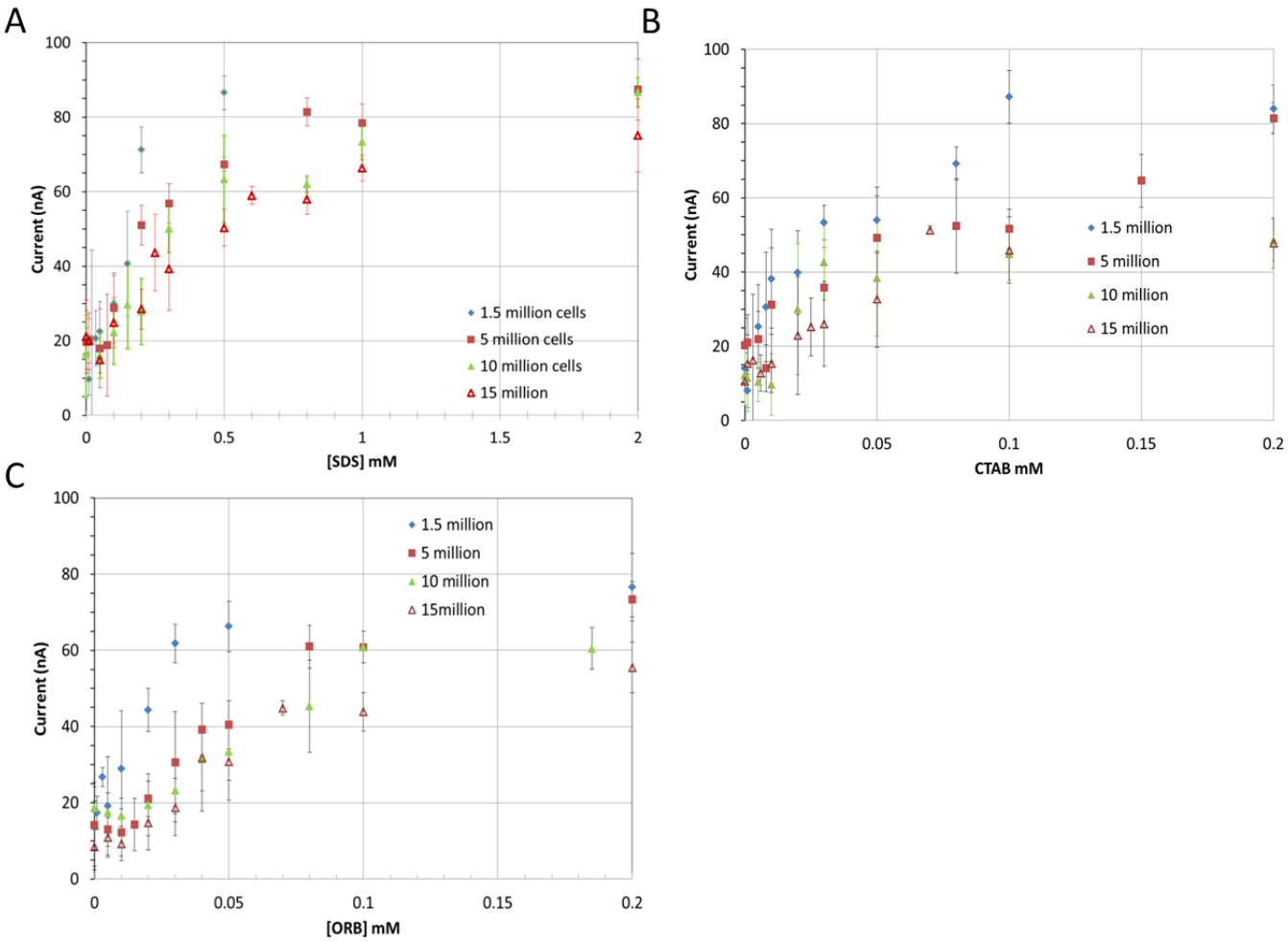

Figure 2.8. Increased Membrane Conductivity in Cells Pre-treated with Detergents. Increasing numbers of HEK 293 A cells require increasing concentrations of (A) SDS, (B) CTAB, (C) ORB to induce the same amount of conductivity.

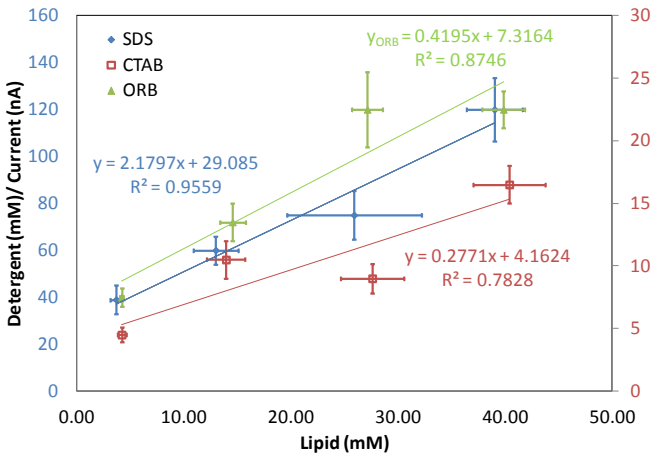

Figure 2.9. Detergent Concentration to Induce Cell Membrane Permeability Dependent on Cell number. Detergent concentrations at the onset of increased permeability in current increases with increasing cell count and then further fit with a line.

REFERENCES

1. Heerklotz, H.; Seelig, J. Correlation of Membrane/Water Partition Coefficients of Detergents with the Critical Micelle Concentration. *Biophys. J.* **2000**, *78*, 2435-2440.

2. Lichtenberg, D.; Ahyayauch, H.; Alonso, A.; Goni, F. M. Detergent Solubilization of Lipid Bilayers: A Balance of Driving Forces. *Trends Biochem. Sci.* **2013**, *38*, 85-93.

3. Lasch, J. Interaction of Detergents with Lipid Vesicles. *Biochim. Biophys. Acta.* **1995**, *1241*, 269-292.

4. Heerklotz, H. Interactions of Surfactants with Lipid Membranes. *Q. Rev. Biophys.* **2008**, *41*, 205-264.

5. Kragh-Hansen, U.; le Maire, M.; Møller, J. V. The Mechanism of Detergent Solubilization of Liposomes and Protein-Containing Membranes. *Biophys. J.* **1998**, *75*, 2932-2946.

6. van der Woude, I.; Wagenaar, A.; Meekel, A. A.; ter Beest, M. B.; Ruiters, M. H.; Engberts, J. B.; Hoekstra, D. Novel Pyridinium Surfactants for Efficient, Nontoxic in Vitro Gene Delivery. *Proc. Natl. Acad. Sci. U. S. A.* **1997**, *94*, 1160-1165.

7. Hamouda, T.; Myc, A.; Donovan, B.; Shih, A. Y.; Reuter, J. D.; Baker, J.,J R. A Novel Surfactant Nanoemulsion with a Unique Non-Irritant Topical Antimicrobial Activity Against Bacteria, Enveloped Viruses and Fungi. *Microbiol. Res.* **2001**, 156, 1-7.

8. Sau, T. K.; Murphy, C. J. Seeded High Yield Synthesis of Short Au Nanorods in Aqueous Solution. *Langmuir* **2004**, *20*, 6414-6420.

9. Deo, N.; Somasundaran, P. Disintegration of Liposomes by Surfactants: Mechanism of Protein and Cholesterol Effects. *Langmuir* **2003**, *19*, 2007-2012.

10. Alberts, B. In *Molecular biology of the cell;* Garland Science: New York, 2002.

11. Preté, P. S. C.; Malheiros, S. V. P.; Meirelles, N. C.; de Paula, E. Quantitative Assessment of Human Erythrocyte Membrane Solubilization by Triton X-100. *Biophys. Chem.* **2002**, *97*, 1-5.

12. Preté, P. S. C.; Gomes, K.; Malheiros, S. V. P.; Meirelles, N. C.; de Paula, E. Solubilization of Human Erythrocyte Membranes by Non-Ionic Surfactants of the Polyoxyethylene Alkyl Ethers Series. *Biophys. Chem.* **2002**, *97*, 45.

13. Preté, P. S. C.; Domingues, C. C.; Meirelles, N. C.; Malheiros, S. V. P.; Goñi, F. M.; de Paula, E.; Schreier, S. Multiple Stages of Detergent-Erythrocyte Membrane interaction—A Spin Label Study. *Biochim. Biophys. Acta* **2011**, *1808*, 164-170.

14. Goñi, F. M.; Alonso, A. Spectroscopic Techniques in the Study of Membrane Solubilization, Reconstitution and Permeabilization by Detergents. *Biochim. Biophys. Acta* **2000**, *1508*, 51-68.

15. Koley, D.; Bard, A. J. Triton X-100 Concentration Effects on Membrane Permeability of a Single HeLa Cell by Scanning Electrochemical Microscopy (SECM). *Proc. Natl. Acad. Sci. U. S. A.* **2010**, *107*, 16783-16787.

16. Partearroyo, M. A.; Ostolaza, H.; Goñi, F. M.; Barberá-Guillem, E. Surfactant-Induced Cell Toxicity and Cell Lysis. *Biochem. Pharmacol.* **1990**, *40*, 1323-1328.

17. Hong, S.; Bielinska, A. U.; Mecke, A.; Keszler, B.; Beals, J. L.; Shi, X.; Balogh, L.; Orr, B. G.; Baker, J. R.,Jr; Banaszak Holl, M. M. Interaction of Poly(Amidoamine) Dendrimers with Supported Lipid Bilayers and Cells: Hole Formation and the Relation to Transport. *Bioconjug. Chem.* **2004**, *15*, 774-782.

18. Hong, S.; Leroueil, P. R.; Janus, E. K.; Peters, J. L.; Kober, M. M.; Islam, M. T.; Orr, B. G.; Baker, J. R.,Jr; Banaszak Holl, M. M. Interaction of Polycationic Polymers with Supported Lipid Bilayers and Cells: Nanoscale Hole Formation and Enhanced Membrane Permeability. *Bioconjug. Chem.* **2006**, *17*, 728-734.

19. Chen, J.; Hessler, J. A.; Putchakayala, K.; Panama, B. K.; Khan, D. P.; Hong, S.; Mullen, D. G.; Dimaggio, S. C.; Som, A.; Tew, G. N.; *et al*. Cationic Nanoparticles Induce Nanoscale Disruption in Living Cell Plasma Membranes. *J. Phys. Chem. B* **2009**, *113*, 11179-11185.

20. Leroueil, P. R.; Hong, S.; Mecke, A.; Baker Jr, J. R.; Orr, B. G.; Banaszak Holl, M. M. Nanoparticle Interaction with Biological Membranes: Does Nanotechnology Present a Janus Face? *Acc. Chem. Res.* **2007**, *40*, 335-342.

21. Carmona-Ribeiro, A. M.; de Melo Carrasco, Letícia Dias. Cationic Antimicrobial Polymers and their Assemblies. *Int. J. Mol. Sci.* **2013**,*14*, 9906-9946.

22. Sgolastra, F.; deRonde, B. M.; Sarapas, J. M.; Som, A.; Tew, G. N. Designing Mimics of Membrane Active Proteins. *Acc. Chem. Res.* **2013**, *46*, 2977-2987.

23. Mecke, A.; Lee, D.; Ramamoorthy, A.; Orr, B. G.; Banaszak Holl, M. M. Membrane Thinning due to Antimicrobial Peptide Binding: An Atomic Force Microscopy Study of MSI-78 in Lipid Bilayers. *Biophys. J.* **2005**, *89*, 4043-4050.
24. Mecke, A.; Majoros, I. J.; Patri, A. K.; Baker, J. R.; Banaszak Holl, M. M.; Orr, B. G. Lipid Bilayer Disruption by Polycationic Polymers: The Roles of Size and Chemical Functional Group. *Langmuir* **2005**, *21*, 10348-10354.
25. Li, S.; Malmstadt, N. Deformation and Poration of Lipid Bilayer Membranes by Cationic Nanoparticles. *Soft Matter* **2013**, *9*, 4969-4976.
26. Schulz, M.; Olubummo, A.; Binder, W. H. Beyond the Lipid-Bilayer: Interaction of Polymers and Nanoparticles with Membranes. *Soft Matter* **2012**, *8*, 4849-4864.
27. Lin, J.; Alexander-Katz, A. Cell Membranes Open "Doors" for Cationic Nanoparticles/Biomolecules: Insights into Uptake Kinetics. *ACS Nano* **2013**, *7*, 10799-10808.
28. Carney, R. P.; Astier, Y.; Carney, T. M.; Voïtchovsky, K.; Jacob Silva, P. H.; Stellacci, F. Electrical Method to Quantify Nanoparticle Interaction with Lipid Bilayers. *ACS Nano* **2013**, *7*, 932-942.
29. Mishra, A.; Lai, G. H.; Schmidt, N. W.; Sun, V. Z.; Rodriguez, A. R.; Tong, R.; Tang, L.; Cheng, J.; Deming, T. J.; Kamei, D. T. Translocation of HIV TAT Peptide and Analogues Induced by Multiplexed Membrane and Cytoskeletal Interactions. *Proc. Natl. Acad. Sci. U.S.A.* **2011**, *108*, 16883-16888.
30. Leroueil, P. R.; Berry, S. A.; Duthie, K.; Han, G.; Rotello, V. M.; McNerny, D. Q.; Baker, J. R.,Jr; Orr, B. G.; Holl, M. M. Wide Varieties of Cationic Nanoparticles Induce Defects in Supported Lipid Bilayers. *Nano Lett.* **2008**, *8*, 420-424.

31. Beck, A.; Li-Blatter, X.; Seelig, A.; Seelig, J. On the Interaction of Ionic Detergents with Lipid Membranes Thermodynamic Comparison of n-Alkyl-$N^{+}(CH_3)_3$ and n-Alkyl-SO_4^{-}. *J. Phys. Chem. B* **2010**, *114*, 15862-15871.

32. Xia, W. J.; Onyuksel, H. Mechanistic Studies on Surfactant-Induced Membrane Permeability Enhancement. *Pharm. Res.* **2000**, *17*, 612-618.

33. Heerklotz, H.; Seelig, J. Leakage and Lysis of Lipid Membranes Induced by the Lipopeptide Surfactin. *Eur. Biophys. J.* **2007**, *36*, 305-314.

34. Heerklotz, H.; Seelig, J. Titration Calorimetry of Surfactant-Membrane Partitioning and Membrane Solubilization. *Biochim. Biophys. Acta* **2000**, *1508*, 69-85.

35. de la Maza, A.; Parra, J. L. Vesicle-Micelle Structural Transition of Phosphatidylcholine Bilayers and Triton X-100. *Biochem. J.* **1994**, *303*, 907-914.

36. de la Maza, A.; Coderch, L.; Gonzalez, P.; Parra, J. L. Subsolubilizing Alterations Caused by Alkyl Glucosides in Phosphatidylcholine Liposomes. *J. Control. Release* **1998**, *52*, 159-168.

37. Tan, A.; Ziegler, A.; Steinbauer, B.; Seelig, J. Thermodynamics of Sodium Dodecyl Sulfate Partitioning into Lipid Membranes. *Biophys. J.* **2002**, *83*, 1547.

38. Chattopadhyay, A.; London, E. Fluorimetric Determination of Critical Micelle Concentration Avoiding Interference from Detergent Charge. *Anal. Biochem.* **1984**, *139*, 408-412.

39. Spencer, C. I.; Li, N.; Chen, Q.; Johnson, J.; Nevill, T.; Kammonen, J.; Ionescu-Zanetti, C. Ion Channel Pharmacology Under Flow: Automation Via Well-Plate Microfluidics. *Assay Drug Dev. Technol.* **2012**, *10*, 313-324.

40. Pouny, Y.; Rapaport, D.; Mor, A.; Nicolas, P.; Shai, Y. Interaction of Antimicrobial Dermaseptin and its Fluorescently Labeled Analogs with Phospholipid Membranes. *Biochemistry.* **1992**, *31*, 12416-12423.

41. Baumann, G.; Mueller, P. A. Molecular Model of Membrane Excitability. *J. Supramol. Struct.* **1974**, *2*, 538-557.

42. He, K.; Ludtke, S. J.; Worcester, D. L.; Huang, H. W. Neutron Scattering in the Plane of Membranes: Structure of Alamethicin Pores. *Biophys. J.* **1996**, *70*, 2659-2666.

43. Matsuzaki, K. Magainins as Paradigm for the Mode of Action of Pore Forming Polypeptides. *Biochim. Biophys. Acta* . **1998**, *1376*, 391-400.

44. Ludtke, S. J.; He, K.; Heller, W. T.; Harroun, T. A.; Yang, L.; Huang, H. W. Membrane Pores Induced by Magainin. *Biochemistry* **1996**, *35*, 13723-13728.

45. Yang, L.; Gordon, V. D.; Trinkle, D. R.; Schmidt, N. W.; Davis, M. A.; DeVries, C.; Som, A.; Cronan, J. E.; Tew, G. N.; Wong, G. C. Mechanism of a Prototypical Synthetic Membrane-Active Antimicrobial: Efficient Hole-Punching Via Interaction with Negative Intrinsic Curvature Lipids. *Proc. Natl. Acad. Sci. U.S.A.* **2008**, *105*, 20595-20600.

46. Zhou, Y.; Kumon, R. E.; Cui, J.; Deng, C. X. The Size of Sonoporation Pores on the Cell Membrane. *Ultrasound Med. Biol.* **2009**, *35*, 1756-1760.

47. Sandre, O.; Moreaux, L.; Brochard-Wyart, F. Dynamics of Transient Pores in Stretched Vesicles. *Proc. Natl. Acad. Sci. U.S.A.* **1999**, *96*, 10591-10596

Chapter 3 Quantitative Measurement of Cationic Polymer Vector and Polymer/pDNA Polyplex Intercalation into the Cell Plasma Membrane

Published as: Quantitative Measurement of Cationic Polymer Vector and Polymer–pDNA Polyplex Intercalation into the Cell Plasma Membrane. *ACS Nano* **2015**, *9*, 6097–6109.

INTRODUCTION

Nanoscale polymer/oligonucleotide complexes have been employed for the delivery of plasmid DNA (pDNA) into cells in order to alter protein expression.[1–3] Cytotoxicity caused by cationic surface charge is a major concern regarding these polymer delivery vectors.[4–7] In particular, the cationic nanomaterials interact with the cell membranes and nuclear membranes changing the membrane porosity and membrane potential, increasing intracellular calcium concentrations, and inducing inflammatory responses.[6,8–12] These toxicity mechanisms present a challenge in gene delivery since the positive charge of gene delivery vectors is necessary to complex DNA effectively and thus protect against degradation by cellular enzymes. Moreover, the cationic charge of DNA-vector complexes (polyplexes) has been proposed to facilitate adsorptive endocytosis. Thus, understanding the mechanism of interaction of cationic vectors and nanoscale polyplexes with the cell membrane, and the influence of this interaction on gene expression, can enable the design of vectors that are both less cytotoxic and more effective gene delivery agents.

Several previous studies have characterized the nature of defects formed by the cationic nanomaterials in both model systems and in living cell membranes. [4,8,13–17] Computational

methods have proposed several models for cationic polymer-induced cell membrane permeability, including the formation of free pores, polymer supported pores, and a carpet mechanism for cationic polymer induced cell membrane permeability (Figure 3.1).[5,18–24]

Atomic force microscopy (AFM) experiments on supported lipid bilayers have provided evidence for both free and polymer-supported pores formed by cationic nanoparticles.[4,8,13,14,16,17] Although these studies provide a framework for understanding the cell membrane-cationic polymer interactions, the supported lipid bilayers have a much simpler lipid composition than living cell membranes. They are devoid of membrane proteins, cholesterol, and glycolipids. Building on these previous studies, manual whole cell patch clamp experiments in HEK 293A cells have shown that cationic polymers induce transient increases in current (0.1 to 10 sec) along with an overall increase in membrane conductivity that is consistent with 1-21 nm diameter pores or even larger carpeted regions.[15] Recently, Heja et al. examined neurons present in brain slices and observed that the membrane permeability induced by generation five poly(amidoamine) (G5 PAMAM) dendrimers is not reversible over a time period of several minutes.[25] This observation is consistent with either a supported pore or a carpet model for the cationic polymer-cell membrane interactions, but it is not consistent with an unsupported pore model since these are known to close on the order of 5 seconds.[26] Although significant progress has been made in understanding the characteristics of the supported pores, it is unclear if the mechanism of pore formation changes based on nanoparticle concentration. In addition, most studies to date have used cationic polymer vectors and not the cation polymer/oligonucleotide vectors that are used in gene delivery applications. In a previous paper, we demonstrated that ~50-200 nm polyplexes consisting of both cationic vector and oligonucleotide induced changes in cell membrane conductivity.[27] However, the polyplex-cell membrane interaction has not been

studied in detail (*e.g.* concentration dependence, partition constant etc). Both the shielding of charges by DNA in the polyplex and the relative dynamics of the cationic species and pDNA[28] likely change as function of polycation vector structure. The impacts of concentration and complexation with nucleotides on membrane uptake and disruption are unknown. Moreover, despite the importance of the initial interaction with the cell membrane, quantitative studies to measure the uptake of cationic vectors and polyplexes into the cell membrane have not been performed and the equilibrium partition constants have not been obtained. Partition constants have been of great value for developing quantitative models of cell-detergent interactions and will aid in the development of quantitative models of other nanomaterial-cell membrane interactions.[29–44]

We previously used the Ionflux-16 (IF-16), an automated whole cell patch clamp instrument, and a trypan blue assay to characterize the partitioning of detergents in the cell membrane of HEK 293A cells[42] and to measure increased membrane conductivity induced by polyplexes in HeLa cells.[27] To investigate the mechanism of interaction of polymers and polyplexes with the cell membrane and to understand the role of these membrane interactions in gene transfection, we used the IF-16 and trypan blue assays to test hypotheses 1 and 2 generated from our previous work,[13,15] as well as new hypothesis (3) regarding the relationship of vector charge density to partition constant.

H1: the magnitude of membrane current induced by cationic vectors increases with solution charge concentration

H2: the increased membrane current induced by the cationic vectors is reversible, thus supporting a free pore mechanism

H3: the partition constant is linearly related to the charge density of the vectors and polyplexes.

Our experiments show that:

1. Contrary to H1, after a threshold concentration is reached, cationic polymers and polyplexes induce a saturated level of cell membrane conductivity over a wide concentration range. The magnitude of membrane conductivity changes and the time scales of polyplex interactions are similar to the conductivity changes induced by free polymers. This similarity suggests that the observed plasma membrane activity is based on the intercalation of the cationic vector alone. The combination of the polyplex and cationic polymer data indicates that in both cases, after an external threshold concentration is reached, the amount of cationic vector partitioned into the cell plasma membrane remains constant over the range of therapeutically relevant concentrations.

2. The vector-cell membrane interaction is stable for at least 15 minutes, which is consistent with two models: a carpet mechanism or the formation of polymer-supported pores (H2).

3. Extension of the trypan blue assay to the cationic vectors alone yielded quantitative partition constants for the vectors that increase as a function of charge density. Polyplexes made from the cationic vectors did not follow this trend (H3). In particular, polyplexes made using linear poly(ethyleneimine) (L-PEI), which had the highest charge density, showed a decrease in the membrane partition constant as compared to the free polymer.

The induction of long lasting membrane porosity provides a mechanism for the toxicity and may also be partially responsible for the inflammatory response previously reported after cells were exposed to cationic polymer vectors and polyplexes.[8,12,13]

RESULTS AND DISCUSSION

Particle Size and Zeta Potential: Table 3.1 shows the measured zeta potentials of the free vectors (G5 PAMAM, L-PEI, jetPEI, and N-[1-(2,3-dioleoyloxy)propyl]-N,N,N-trimethylammonium methyl-sulfate (DOTAP)) and of the N:P 10:1 polyplexes, as well as the Z-averaged diameters of the polyplexes as measured by dynamic light scattering (DLS). Polyplexes made using L-PEI and jetPEI showed a decrease in zeta potential as compared to the free polymer whereas G5 PAMAM and DOTAP polyplexes had zeta potentials similar to that of free vectors. The polymer vectors gave polyplexes with diameters of 200-300 nm and the lipid DOTAP gave polyplexes with a diameter of 500-600 nm.

Table 3.1. Z-averaged diameters of polyplexes (N:P=10) measured using dynamic light scattering; zeta-potentials of free vectors and polyplexes

Material	Diameter (nm)	Zeta Potential (mV)
jetPEI	-	40 ± 6
jetPEI Polyplex	212 ± 41*	26 ± 3
L-PEI	-	39 ± 3
L-PEI Polyplex	210 ± 19*	24 ± 1
G5 PAMAM[45]	6.2 ± 0.2#	32 ± 7
G5 PAMAM Polyplex	280 ± 42*	36 ± 1
DOTAP	-	56 ± 2
DOTAP Polyplex	564 ± 54*	53 ± 1

* = Z-average from light scattering
# = hydrodynamic diameter from diffusion NMR measurements

Concentration dependence of cell plasma membrane currents induced by free vectors and polyplexes: Currents induced by free polymers and N:P 10:1 polyplexes at a variety of concentrations are presented in Figures 3.2-3.7 and summarized in Table 3.2. Representative traces of induced currents for the vectors G5 PAMAM, L-PEI, and DOTAP are presented in Figure 3.2. The commercial transfection agent jetPEI can only be analyzed in terms of molar

amine concentration since molar mass is not provided by the vendor, so this data is plotted separately in Figure 3.3. All three cationic polymers initiated changes in plasma membrane conductivity. As the concentration of cationic polymer to which the cells were exposed increased, an increase in membrane current was observed, which plateaued at ~ 30 – 40 nA. This plateau was independent of the cationic vector employed and was the maximum current observed over a wide range of concentrations. Exposure of the cells to two orders of magnitude greater concentrations of polymer did not induce a further increase in current. However, the time required to induce membrane currents did decrease as the concentration of polymer was increased. The 30 – 40 nA magnitude of the current plateau was significantly less than the open channel currents of 60-70 nA observed for the microfluidic device when cells were not present at the patch site.

By way of contrast to the cationic polymers, only ~50% of traces from cells exposed to the cationic lipid DOTAP resulted in an increase in membrane current. The current change in the sub-group with increased current was 10 ± 3 nA and had a rate of change of 0.016 ± 0.004 nA/ms. The magnitude of change in current is 1/3-1/2 of the current change induced by cationic polymers. The remaining traces, which showed an increase in current, had a current change of 1 ± 1 nA and exhibited an average rate of change of 0.004 ± 0.003 nA/ms, similar to that of the controls. A similar bifurcation of results was obtained when cells were exposed to a range of 39.2 µg/mL to 196 µg/mL DOTAP (corresponding to N:P=10:1 to N:P = 50:1) (Figure 3.2C). By comparing multiple experiments across multiple plates, we are able to rule out possible plate-based effects such as a systematic difference as a result of pattern location. Possible biological origins, such as capturing different representative populations of cells, also seems unlikely based on modeling of likely changes in current based on random trapping of different cell phenotypes

(full details in supplementary materials). Therefore, the origin of this reproducible bifurcation in behavior remains unknown. The general conclusion can still be drawn, however, that the smaller increase in current for DOTAP as compared to the polymer vectors is consistent with the lipid structure, which has two fatty acid chains capable of stably integrating into the cell membrane and laterally diffusing instead of remaining localized to stabilize a membrane pore.

Representative traces of membrane currents of cells exposed to cationic gene delivery agents G5 PAMAM, L-PEI, jetPEI, and DOTAP at the total polymer concentrations used in for transfection[12,15,27] are presented in Figure 3.4. The membrane current traces correspond to the polymer concentrations present when 0.8 µg of DNA in 500 µL of media is used to make polyplexes with N:P=10:1. Figure 3.5 illustrates traces of membrane currents of cells exposed to polyplexes with concentrations of polymers identical to those used in transfection studies and in Figure 3.4. G5 PAMAM polyplexes and jetPEI polyplexes induced an increase in current at N:P = 10:1 while L-PEI polyplexes required an N:P > 10:1 to induce an increase in current. The rate of current change seen in cells exposed to L-PEI polyplexes of N:P = 10 (0.02 nA/ms) was higher than the cell-only controls (0.004 ± 0.003 nA/ms). DOTAP polyplexes did not induce an increase in membrane current. The rate of current change after exposure to DOTAP was also not different from cell-only controls.

The statistical significance of the changes in membrane conductivity was determined using one-way ANOVA followed by Tukey's multi-comparison test. The ANOVA indicated that the mean change in current was not equal between all the groups. Tukey's multi-comparison test indicated that the currents induced by jetPEI, jetPEI polyplexes, G5 PAMAM, G5 PAMAM polyplexes, and L-PEI were significantly different from the mean current change seen in the controls. Current changes induced by DOTAP polyplexes and L-PEI polyplexes were not

Table 3.2: Changes in membrane currents induced by polymers and polyplexes.

Material	Δ Current (nA) ± St.Dev	Time for Current Increase (s)
ECS (Control)	1.6 ± 2	NA
Polymers		
G5 PAMAM (~ 2.2 µg/mL)	5 ± 3	N/A
G5 PAMAM (~ 12 µg/mL)*	33 ± 7	65 ± 60
G5 PAMAM (~ 24 µg/mL)	25 ± 7	20 ± 11
G5 PAMAM (~ 48 µg/mL)	18 ± 7	14 ± 2
L-PEI (2.2 µg/mL)*	31 ± 5	178 ± 50
L-PEI (4.4 µg/mL)	31 ± 2	40 ± 20
L-PEI (50 µg/mL)	22 ± 6	7 ± 2
L-PEI (113 µg/mL)	17 ± 5	6 ± 3
jetPEI (65 µM)*	32 ± 4	120 ± 56
jetPEI (130 µM)	27 ± 8	11 ± 3
DOTAP (36.4 µg/mL)*	6 ± 4	N/A
DOTAP (73 µg/mL)	5 ± 6	N/A
DOTAP (196 µg/mL)	4 ± 3	N/A
Polyplexes		
G5 PAMAM (N:P = 10)	34 ± 14	245 ± 85
G5 PAMAM (N:P = 20)	38 ± 2	25 ± 18
L-PEI Polyplexes (N:P = 10)	9 ± 4	452 ± 89
L-PEI Polyplexes (N:P = 18)	38 ±5	82 ± 40
L-PEI Polyplexes (N:P = 20)	30 ± 7	20 ± 5
jetPEI polyplexes(N:P = 5)	5 ± 3	N/A
jetPEI polyplexes(N:P = 10)	36 ± 6	93 ± 55
jetPEI polyplexes(N:P = 20)	31± 4	10 ± 2
DOTAP Polyplexes (N:P = 10)	4 ± 5	N/A

* Indicates that the cationic vector concentration is same as total cationic vector concentration present for N:P = 10 polyplexes with 0.8 µg DNA per well

significantly different from the controls. Approximately 50% of traces from cells treated using DOTAP showed an increase in membrane current (10 ± 3 nA), but this increase was much smaller than the increase in current observed from cells treated using the other cationic polymers.

Although all cationic polymers induced increased membrane conductivity, they did so at different absolute concentrations. However, based upon the estimated charge concentrations for each polymer, the magnitude of current induced by the polymers was related to the total charge

concentration in solution (Figure 3.6). In order to further confirm that if the increased conductivity induced by cationic polymers was dependent on charge, cells were treated with G5 PAMAM with different numbers of surface amine groups neutralized by acetylation (26%-80%). Changes in the membrane conductivity of cells were measured using the IF-16. Cells treated by G5 PAMAM with 80% acetylation showed a significantly smaller increase in membrane conductivity. Amine-terminated G5 PAMAM dendrimers acetylated to 26%, 40%, and 80% induced an increase in membrane currents of 29 ± 10, 30 ± 3 and 7 ± 5 nA, respectively (Figure 3.7). Thus, increasing levels of acetylation on G5 PAMAM reduced the membrane current induced by G5 PAMAM. Our observations indicate that the increase in porosity in the cell plasma membrane is related to the total cationic charge concentration, as previously reported.[4–6,8] However, our measurements also demonstrate that membrane permeability approaches a plateau as concentration increases.

The ability of the different vectors to induce the expression of green fluorescent protein (GFP) in HEK 293A cells was also assessed. G5 PAMAM, jetPEI, L-PEI, and DOTAP induced GFP expression in <1%, 80%, 80%, and 21% of the cells, respectively (Figure 3.8). Figure B.1 presents the membrane currents induced by the jetPEI, L-PEI, and G5 PAMAM polyplexes at N:P ratios other than 10:1. The jetPEI polyplexes with N:P ranging from 5:1 to 20:1 and L-PEI polyplexes with N:P ranging from 10-20:1 all induce GFP expression in greater than 80% of cells. However, increased currents are only induced by some polyplex formulations. For example, jetPEI polyplexes induce gene expression at N:P = 5:1, 10:1, and 20:1, but increased currents are observed only for N:P = 10:1 and 20:1. Similarly, G5 PAMAM polyplexes induce increased membrane currents but induce transfection in only ~ 1 % of cells. These results suggest that differences in transfection efficiency as a function of cationic vector are due to differences

in transport subsequent to adsorptive endocytosis. We previously reached a similar conclusion in a study examining transfection efficiency and membrane conductivity in HeLa cells. The uptake of propidium iodide was measured after exposure of cells to polymer for 3 hours and whole cell patch clamp was employed to measure membrane permeability.[27] With regard to these Ionflux™ patch-clamp studies, it should be noted that the cells in the patch clamp experiment were exposed to gene delivery agents and polyplexes/lipoplexes for only 15 minutes. For transfections, cells were exposed to polyplexes for 3 hours.

Overall, the cationic polymers and their polyplexes induced increased membrane conductivity in HEK 293A cells. This is broadly consistent with the results of previous studies using manual patch clamp and fluorescence techniques, which indicated that cationic polymers and nanoparticles (metal and silica) induce increased membrane permeability to dyes, proteins and ions.[4,6–8,13,15] Our experiments further show that beyond a threshold concentration, the exposure of cells to increasing concentrations of jetPEI, L-PEI, and G5 PAMAM results in a saturated membrane current of 30-50 nA over a broad concentration range. Thus, these results provide an important new perspective to the relationship between membrane conductivity and vector and/or polyplex charge concentration (H1). Specifically, the materials exhibit a saturation threshold over a broad concentration range prior to reaching concentrations capable of lysing the cell.

We have previously shown that the exposure of HEK 293A cells to the cationic detergents cetyl trimethylammonium bromide (CTAB) and octadecyl rhodamine B (ORB) result in a similar saturating current level.[42] The microfluidic patch-clamp technique is capable of detecting solubilization of cells, such as by the anionic detergent sodium dodecyl sulfate (SDS). By way of contrast to the saturating currents, solubilization of cells by SDS resulted in open channel

currents > 70 nA.[42] Thus, the results indicate that the gene delivery polymers saturate the cell membrane over a broad concentration range but do not cause cell lysis.

Intactness of Cells Treated using Polymers and Vectors: Two experiments were employed to determine if the increase in membrane currents is caused by the dissolution of patched cells. In one experiment, patched cells treated with cationic vectors and polyplexes were exposed to a fluorescent detergent, ORB, for 10 s. As indicated in fluorescence micrographs of the patching regions (Figure 3.4 (C-G) and Figure 3.5 (C-G)), cells remained on all patching sites after 15 minutes of exposure independent of treatment condition. As an alternate approach, cells were treated using fluorescently labeled G5 PAMAM. Experiments using amine-terminated G5 PAMAM labeled with TAMRA dye resulted in increased current and showed that the cells were labeled by material after 10 minutes of exposure (Figure B.2A). By way of contrast, TAMRA dye-labeled acetylated G5 PAMAM did not increase membrane currents and also did not stain cells (Figure B.2B). These results are consistent with the smaller increase in currents observed in cells treated with partially acetylated G5 PAMAM dendrimers. The concentrations of cationic polymers contained in polyplexes with N:P = 10:1 and 20:1 have been optimized for transfection *via* LDH, XTT assays and do not induce cell lysis.[8] Higher concentrations of cationic polymers show reduced cell viability when measured using LDH and XTT assays.

Currents Induced by Vectors are Not Reversible for Over 15 minutes: The experiments described so far, have shown that polymers and polyplexes saturate the cell membrane and induce an increase in membrane conductivity. Understanding if the interaction is reversible can enable us to understand if the intercalation results in transient pores or more stable structures such as a supported pore or carpet. Cells were exposed to free G5 PAMAM and L-PEI for short periods (10-600 s) and then allowed to recover in the presence of ECS alone. Unlike traditional

patch-clamp methods where a substantial time-lag exists in changing solution concentration[15] the microfluidic Ionflux™ flow system allows rapid exchange of solution with full exchange in <1 s. Exposure of cells to 20 µg/mL G5 PAMAM for 60 seconds increased membrane current by ~30 nA at the end of the experiment (600 seconds later) (Figure 3.9). Exposure of cells to L-PEI (2.2 µg/mL) required 300 seconds to induce membrane permeability. However, the permeability induced after 300 seconds is not reversible for up to 1100 seconds (Figure 3.10).

The increased membrane conductivities induced by both G5 PAMAM and L-PEI are not reversible for over 15 minutes. These results suggest that H2 is incorrect at least for G5 PAMAM and L-PEI in HEK 293A cells. A possible alternate explanation for the increased conductivity would be the lysing of a few of the 20 cells present at a given patch site. Such lysing would also result in an increased current that is not reversible. The increased membrane currents could be caused by either the lysing of a small fraction of the cells present in a trapping zone or by an increase in membrane conductivity of intact cells present in the trap zone.

Figure 3.4C-G and Figure 3.5C-G show cells stained with a fluorescent detergent ORB for 10 s at the end of experiments where cells had been exposed to polymers for 900 seconds. It is seen that the cells are intact in all of these cases. Thus, increase membrane current is due to the increased membrane conductivity induced by polymers and not due to the lysing of a subset of the 20 trapped cells.

Heja *et al*. showed that the membrane conductivity of neurons in brain slices of rats increased irreversibly after exposure to G5 PAMAM, consistent with supported pore or carpet models.[25] By way of contrast, increases in membrane currents caused by unsupported pores induced by sonoporation have been shown to be reversible on the timescale of only 5 seconds.[26]

Our experiments extend their results to other polymers and also cultured mammalian cells. Our results reported here are also consistent with the formation of supported pores or a carpet mechanism, as opposed to an unsupported pore. One factor that could possibly confound the IonFlux-16 reversibility experiment is the adsorption of polymers in the walls of the microfluidic channel during the 10-300 second exposure and subsequent release when cells are exposed to ECS alone **(**Figure 3.9 and Figure 3.10). To address this concern, we modeled the exponential release of polymer from a monolayer adsorbed on the channel wall between the compound release site and the trap site where cells are located. Results presented in Figure B.3 show that the cells are exposed to G5 PAMAM and L-PEI at concentrations that are 50 and 12 times lower, respectively, than the concentrations necessary to induce membrane permeability.

Several studies have shown that calcium ions, dyes such as propidium iodide and large proteins such as LDH leak from cells in the presence of cationic vectors.[6,8,13,47,48] The prolonged presence of cationic polymers on the cell membrane may explain the influx of such molecules, dyes and proteins. Cationic polymers and nanoparticles have been shown to induce changes in the mitochondrial outer membrane potential and induce the release of mitochondrial proteins such as cytochrome c.[9] In the case of linear and branched PEI, it has been suggested that the mitochondrial membrane damage is due to the formation of channels in the mitochondria.[9] The transfer by lipid cycling of stable pores from the plasma membrane may provide a mechanism for the mitochondrial membrane damage induced by these materials.

Measurement of Partition Constants for G5 PAMAM, L-PEI, DOTAP and their Polyplexes: The experiments using IF-16 showed that cationic polymers and polyplexes saturate the cell plasma membrane and remain in the membrane for greater than 15 minutes. However, they did not provide any information on the relative amounts of the polymers and polyplexes

partitioned in the membrane. To probe this question we employed a trypan blue assay and previously reported partition models to quantify the partition constants of the cationic material (free L-PEI, G5 PAMAM, DOTAP and their respective polyplexes) bound to the cell membrane.[29–32,42] Briefly, the total polymer concentration (P_T) at a given level of cell membrane perturbation is linearly related to the total lipid concentration (L) as described in equation 1. In equation 1, R_b is the ratio of polymer to lipid in the cell membrane and P_w is the polymer partitioned into the water phase. The partition constant K can be calculated using equation 2. The detailed mathematical model[29–32] describing equations 1 and 2 is provided in the supplementary material.

Table 3.3 presents the partition constants and related parameters for the L-PEI, G5 PAMAM, DOTAP and their polyplexes.

$$P_T = R_b * L + P_w \quad (1)$$

$$K = \frac{R_b}{(R_b+1)*P_w} \quad (2)$$

Figure **3.11** shows the linear models used to calculate the partition constants for the polymers and polyplexes. The percentages of cells that were trypan blue positive when treated with varying concentrations of cationic vectors and polyplexes are shown in Figures S4-S6. The vector/polyplex concentration necessary to induce trypan blue permeability increases as the cell count increases in all cases as shown in Figure 3.11. Figure B.4 also shows the L-PEI concentration necessary to induce trypan blue permeability is greater for polyplexes than for free polymer. The lower partition constant for polyplexes as compared to the free polymer indicates that polyplexes do not intercalate into the membrane to the same degree as free polymer at the same polymer concentration. The partition

constants of G5 PAMAM polyplexes and DOTAP polyplexes were not significantly different from the partition constant of the free G5 PAMAM and free DOTAP respectively.

The calculated partition constant for L-PEI is higher than the partition constant for G5 PAMAM, which is in turn higher than the partition constant of DOTAP. This observation is consistent with the higher charge density on L-PEI as compared to G5 PAMAM and DOTAP. Thus, the results are consistent with H3 for free cationic polymers. The partition constants of polyplexes do not exhibit this trend. The partition constant for L-PEI polyplexes is lower than the partition constants of free L-PEI. However, the partition constants for DOTAP polyplexes and G5 PAMAM polyplexes were similar to the partition constant for their respective free polymers. Interestingly, the observation that L-PEI polymer and polyplexes behave differently than DOTAP and G5 PAMAM is also consistent with the observations from the patch clamp experiments.

L-PEI polyplexes did not induce current at N:P=10:1 but an equivalent concentration of free L-PEI induced increased current. In contrast, G5 PAMAM polyplexes at N:P=10:1 and an equivalent concentration of free G5 PAMAM both induced increased currents. This means the L-PEI polyplexes at N:P=10:1 had a lower surface charge than G5 PAMAM polyplexes at N:P=10:1 even though the bulk positive to negative charge ratios were the same. Both the trypan blue assay and the IonFlux experiments suggest that charge shielding by DNA was stronger for L-PEI polyplexes than G5 PAMAM polyplexes.

Table 3.3: Estimates for R_b and K for L-PEI, L-PEI Polyplexes, G5 PAMAM, and G5 PAMAM Polyplexes

Material	**Line eqn.**	**R^2**	R_b	P_w	K **(M^{-1})**
LPEI	y = 0.057x + 0.077	0.99	0.057 ± 0.002	0.077 ± 0.011	600,000 [510000,720000]
LPEI PPX	y = 0.052x + 0.16	0.92	0.052 ± 0.001	0.16 ± 0.01	330,000 [310000 , 360000]
G5	y = 0.080x + 0.22	0.97	0.080 ± 0.008	0.22 ± 0.04	370,000 [290000 , 510000]
G5 PPX	y = 0.072x + 0.16	0.96	0.072 ± 0.009	0.16 ± 0.06	410,000 [270000 , 810000]
DOTAP	y = 1.4x + 4.6	0.85	1.4 ± 0.2	4.6 ± 2.2	140,000 [86000,310000]
DOTAP PPX	y = 1.4x + 5.1	0.85	1.4 ± 0.2	5.1 ± 2.2	120,000 [78000,230000]

Indeed, jetPEI polyplexes and L-PEI polyplexes both exhibited a decrease of about 15 mV in zeta potential compared to the free polymers, but the G5 PAMAM polyplexes and DOTAP polyplexes did not show such a decrease (Table 3.1). Therefore, the observed differences in partition constants between polyplexes made using L-PEI and G5 PAMAM are consistent with the zeta potentials. Our group previously investigated the G5 PAMAM-DNA interaction using NMR and showed it to be highly dynamic, consisting of rigid DNA and mobile dendrimer.[28] This may be the reason why the G5 PAMAM polyplexes have a similar zeta potential as the free G5 PAMAM. Similar NMR studies using L-PEI polyplexes may help determine if the DNA-polymer interactions are different in those polyplexes. Further biological studies are necessary to determine if the differences in DNA-polymer interactions seen in L-PEI and jetPEI induce better

gene expression as a result of protecting DNA from degradation, by aiding its transport to the nucleus through some other mechanism, or perhaps combination of both mechanisms.

The results of this study are most directly relevant to cell transfections carried out in serum-free media. These conditions are typically employed because they optimize pDNA transfection and protein expression when employing polycationic vectors. Additional studies are needed to better understand the polyplex/membrane interactions under *in vivo* conditions such as the vitreous humor of the eye and intramuscular and subcutaneous tissue.

CONCLUSIONS

We studied the mechanism of interaction of cationic vectors and polyplexes with the cell membrane with the aim of developing less toxic and more effective gene delivery agents. We determined that cationic polymers and polyplexes exhibit a threshold behavior with respect to both uptake into the cell plasma membrane and induction of cell membrane conductivity over a wide concentration range (H1). Moreover, the persistence of the induced membrane current upon the removal of the cationic vectors and polyplexes indicates that the cell is unable to clear the polymer from the plasma membrane. These observations suggest that the polymers and polyplexes intercalate into the membrane and form a stabilized pore or carpet structure (H2). To quantify the amount of material bound to cells, we extended the methods used to quantify membrane partitioning of detergents to cationic polymers and polyplexes. Our results showed that free cationic vectors with a relatively higher charge density also exhibit a larger partition constant (H3), but this trend was not observed in the case of polyplexes. The induction of long lasting cell membrane porosity characterized in this paper provides a mechanism for the toxicity

and the induction of inflammatory pathways observed in cells upon exposure to cationic gene delivery vectors.[6,9,12]

EXPERIMENTAL METHODS

Materials: G5 PAMAM dendrimers were obtained from Dendritech, Inc. jetPEI and L-PEI were obtained from Polysciences, Inc. DMEM High Glucose with Sodium Pyruvate and Glutamine (Life technologies) was the base media. Complete media was made by adding 50 mL of fetal bovine serum, 5 mL of Non-essential Amino Acids (Thermo Scientific) and 5 mL of penicillin-streptomycin to 500 mL DMEM. Serum Free Media (SFM-II) for suspension culture of HEK 293A cells, PBS (1X) without Ca^{2+} and Mg^{2+}, and Octadecyl Rhodamine B (ORB) were purchased from (Life technologies). Detachin was purchased from Genlantis, Inc. Other reagents were obtained from Fisher Scientific unless otherwise specified. Amine-terminated and acetylated G5 PAMAM dendrimer containing one TAMRA dye per dendrimer (G5-NH_2-$TAMRA_1$ and G5-Ac-$TAMRA_1$) were prepared according to literature methods.[49,50]

Solutions: Extracellular solution (ECS) consisted of 138 mM NaCl, 4 mM KCl, 1.8 mM $CaCl_2$, 1 mM $MgCl_2$, 10 mM HEPES and 5.6 mM glucose adjusted to pH 7.45 using NaOH. Intracellular solution (ICS) consisted of 100 mM potassium aspartate, 30 mM KCl, 5 mM $MgCl_2$, 5 mM EGTA, 4mM Tris ATP, and 10 mM HEPES adjusted to pH 7.2 using KOH.

Estimation of charge concentrations: The charge concentrations for G5 PAMAM were obtained using potentiometric titration with NaOH as described by Mullen et al.[46] We assumed a concentration of 7.5 mM charged amines for jetPEI as instructed by the manufacturer. For L-PEI, we used the average number of amines in a 25 kDa polymer to estimate the charge concentration. We assumed that all of the DOTAP tertiary amine groups were charged.

Polyplexes for Gene Expression Study and Patch Clamp: Polyplexes containing 0.8 µg DNA with N:P ratio of 10 were made by adding equal volumes of polymer to DNA in water. Here, N and P represent the cationic amine groups in the vector and the anionic phosphate groups in the DNA, respectively. At N:P = 10:1, polyplexes are positively charged. The mixture of polymer and DNA was allowed to incubate for 20 minutes. For studying GFP expression, 50 µL of polyplex solution was added to 80,000 cells plated in 450 µL of serum free DMEM. For patch clamp experiments, 50 µL of polyplex solution was added to 450 µL of ECS.

Whole-Cell Patch Clamp using IonFlux 16: The IonFlux 16 (IF-16) patch clamp instrument is capable of simultaneously trapping 20 cells in 16 trapping zones.[51] Electrical properties of each group of 20 cells are measured with dedicated amplifiers. The ensemble of cells is located in eight independently controllable microfluidic environments. Thus, the cells in two different trapping zones experience the same microfluidic environment. This allowed for simultaneous measurement of the changes in cell membrane conductivity in response to interactions with different polymer and polyplex materials.

The methods for the whole cell patch operation and cell preparation have been previously described in detail.[20] Briefly, HEK 293A cells were cultured in 175 cm^2 flasks in complete medium at 37 °C and 5% CO_2. Cells were cultured to ~95% confluency (~20-25 million cells). The cells were suspended by treatment with 5 mL of Detachin at 37 °C for 5 minutes, after which 5 mL of complete media was added. The cell suspension was centrifuged for 2 minutes at 1,000 rpm and resuspended in 9.6 mL SFM-II and 0.4 mL 1 M HEPES for suspension culture. The suspension was placed in a 25 cm^2 suspension flask and shaken at 75 rpm at 35 °C for 5 minutes. In the meantime, cells were counted with a cytometer. The cell suspension from the flask was centrifuged once again at 1,000 rpm for 2 minutes, resuspended in ECS to a

concentration of 8-12 million cells/mL, and thoroughly triturated. The cells were loaded into the IF-16 96-well microfluidic plate at 250 µL per well.

The current *vs.* time trace files were exported and processed using Microsoft Excel and MATLAB. Initial current magnitudes less than -15 nA indicated a sufficient quality of patching for each ensemble of cells. Traces with starting currents above -15 nA were not included in the analysis. The time averaged current from 4 seconds preceding the exposure of the cells to polymer/polyplex (60-64 seconds from the start of the experiment) were compared with the time averaged current following exposure of the cells to polymer/polyplex at 965-969 seconds from start. One-way analysis of variance (ANOVA) coupled with Tukey's multi-comparison tests were performed to evaluate the statistical significance of the difference in the current changes across different the different compounds. Current time traces were also evaluated by measuring their rate of current change. The i/t traces were fit using a linear model in MATLAB, and the slope magnitude was employed to determine if the traces differed significantly.

Polyplexes for Partition Assay: Polyplexes were generated in ECS by adding polymer to plasmid DNA at N:P=10. The polymer concentration in the polyplex solution that was added to the cells was intentionally varied, but N:P was always maintained at 10. The polyplexes were allowed to incubate for 20 minutes prior to being added to the cells.

Trypan Blue Partition Constant Assay:[30,34,35,42] A fixed number of cells (*e.g.* 1 million cells) was suspended in ECS and incubated for 30 minutes with a range of concentrations of polymers/polyplexes. The solutions of cells and polymer/polyplexes were mixed every 10 minutes. The suspensions were then centrifuged at 1,000 rpm, and the cells were resuspended in ECS. Finally, the cells were treated with trypan blue, and the number of trypan blue positive cells was counted using a hemocytometer. This process was completed for four different cell

counts (100,000, 500,000, 1 million, and 3 million cells). The polymer concentrations at the onset of trypan blue uptake above baseline were then plotted with respect to the lipid concentration and the results fit with a linear model. The lipid concentration in cells was estimated from literature to be 10^9 lipid molecules per cell membrane.[52] The slope and intercept of this line were R_b and P_w respectively (equation1). K was then estimated using Equation 2. The mathematical model describing the relationship between R_b, P_w and K is described in supplementary material. The error associated with estimates of R_b and P_w obtained using the linear regression can be employed to estimate the error in K (full details provided in supplementary information).

GFP Expression in HEK 293A Cells: HEK 293A cells were plated in 12 well polystyrene plates at 80,000 cells/well in 1 mL of complete DMEM and allowed to grow overnight. Polyplexes containing endotoxin free plasmid encoding GFP were made at N:P=10:1. Before transfection, cells were placed in 450 µL of serum free DMEM and 50 µL of polyplex solution containing 0.8 µg of GFP plasmid were added to the cells. After 3 hours, the media was aspirated and replaced with 1 mL of complete DMEM. GFP expression in cells was measured using flow cytometry 24 hours after the polyplexes were added to cells.

Flow Cytometry: Complete media was aspirated and the cells were washed three times with 1 mL of Ca^{2+}- and Mg^{2+}-free PBS. The cells were suspended with 200 µL of trypsin and incubated at 37˚C for 2 minutes. The trypsinization process was stopped by adding 1 mL of cold PBS with Ca^{2+} and Mg^{2+}. The cell suspension was centrifuged and the cells resuspended in 400 µL of Ca^{2+}- and Mg^{2+}-free PBS. Flow cytometry was performed using an Accuri C6 flow cytometer. The cells were excited by a 488 nm laser, and the fluorescence emission was measured at 525 ± 25 nm. A total of 10,000 events were counted for each sample.

Size and Zeta Potential Measurements: The polyplexes of N:P=10:1 were prepared as described above, but suspended in 450 µL of water instead of ECS. A Malvern Zetasizer Nano ZS (Worchestershire, U.K) instrument with a 4 mW He-Ne laser operating at 633 nm with a 173° scattering angle was used to measure particle size by dynamic light scattering. The refractive index used for the measurements was 1.59. Data from five measurements each consisting of 5 repeats was used to calculate the hydrodynamic diameter. Zetapotentials were measured using the same instrument. About 600 µL of polyplex solutions were loaded into DTS1060 cells, which were then placed in the instrument.

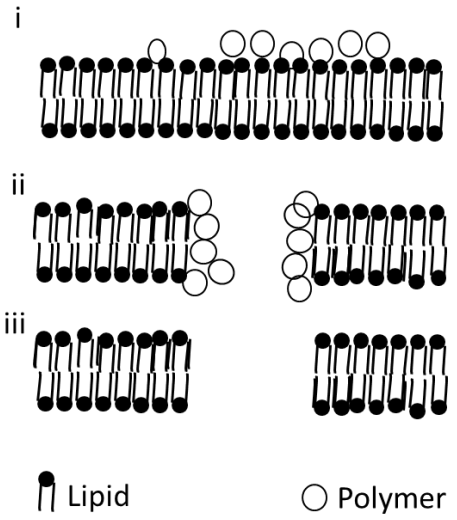

Figure 3.1: Models of Polymer Induced Cell Membrane Defects. Polymer intercalation can produce increased permeability by (i) the formation of a carpet mechanism where the polymer is intercalated randomly across the lipid membrane or (ii) through the formation of polymer supported pores or (iii) through the formation of free pores.

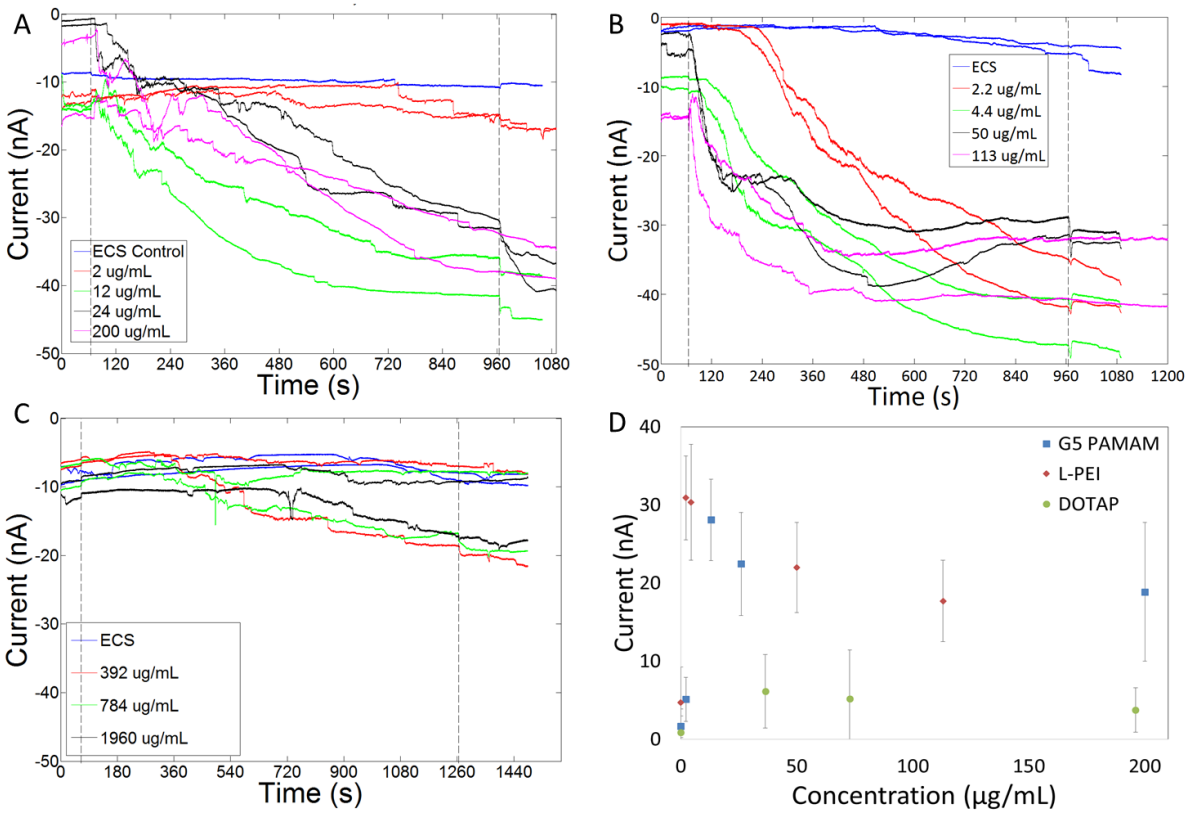

Figure 3.2: Increased Membrane Conductivity Induced by Free L-PEI, G5 PAMAM and DOTAP. Membrane currents of cells exposed to G5-PAMAM (A), L-PEI (B) and DOTAP (C). As the concentration of cationic polymers increased the current induced did not change. Some cells exposed to DOTAP showed a small increase in current. Average increase in current induced by the different vectors are shown in D. In figures A-C, the first dotted line at 65 s indicates the release of the free cationic vectors resulting in exposure of these compounds to the cells. The second dotted line denotes the end of compound exposure.

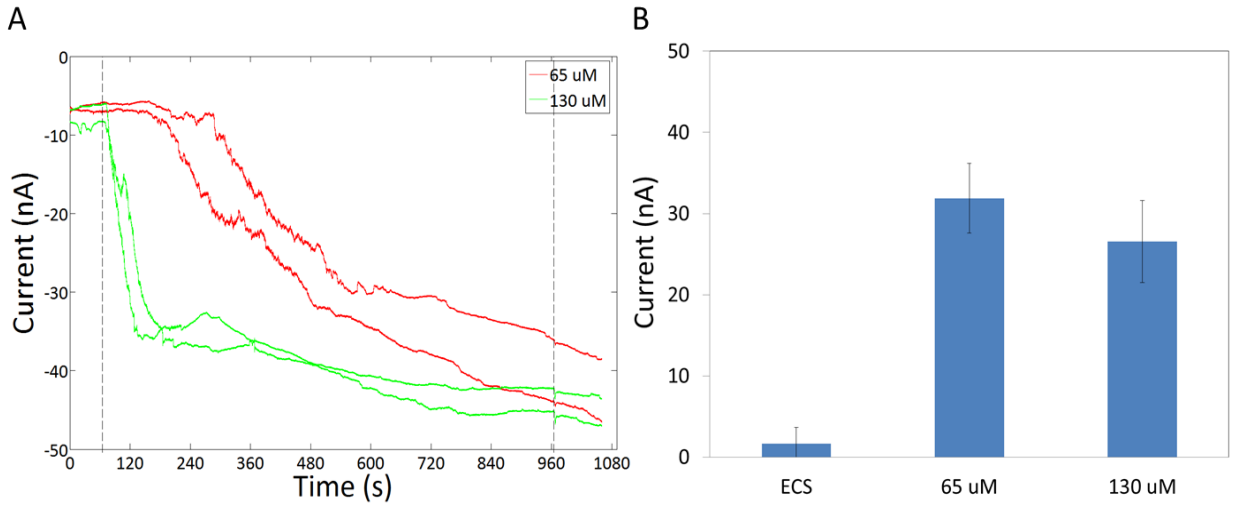

Figure 3.3: Increased Membrane Conductivity Induced by jetPEI. As the concentration of jetPEI dendrimers is increased the current induced does not change. A) Representative traces for cells treated with jetPEI. The first dotted line at 65 s indicates the release of the free jetPEI resulting in exposure of cells to jetPEI. The second dotted line denotes the end of jetPEI exposure. B) Average increase in current induced by the jetPEI at different concentrations.

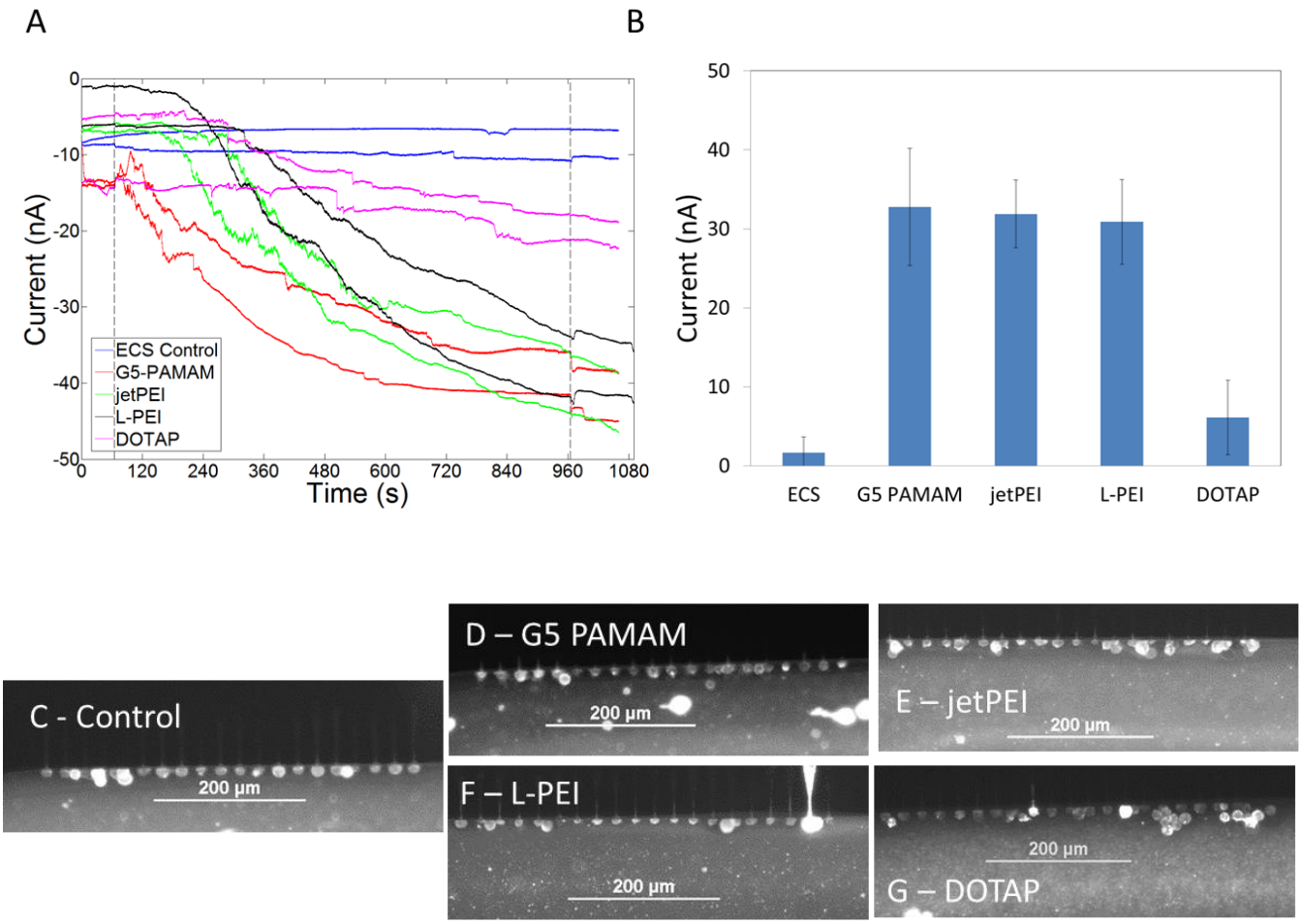

Figure 3.4: Membrane Conductivity Changes Induced by Free Vectors at Gene Delivery Concentrations. Gene delivery agents G5 PAMAM, jetPEI , L-PEI, and DOTAP induce increased membrane currents. A) Representative traces for cells treated with the three polymers. Increased membrane current induced by G5 PAMAM (red) plateaus between 600 s – 740 s. Currents induced by jetPEI and L-PEI plateau at ~ 40 – 50 nA at higher concentrations. The first dotted line at 65 s indicates the release of the free cationic vectors resulting in exposure of these compounds to the cells. The second dotted line denotes the end of compound exposure. B)

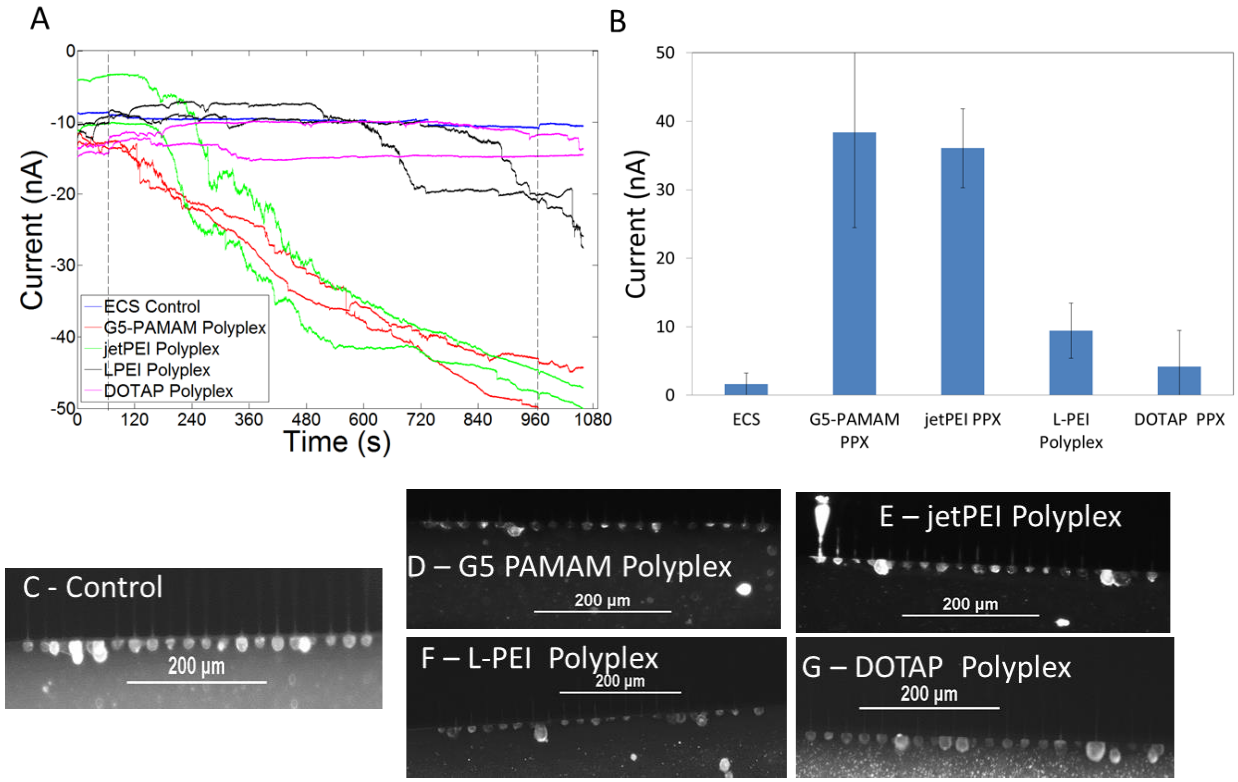

Figure 3.5: Membrane Conductivity Changes Induced by Polyplexes. Polyplexes made using G5 PAMAM and jetPEI (N:P = 10) in ECS induce increased membrane currents. A) Representative traces for cells treated with the polyplexes. The first dotted line at 65 s indicates the release of the polyplexes resulting in exposure of cells to polyplexes. The second dotted line denotes the end of polyplex exposure. B) Average increase in current induced by the polyplexes. C-E) Fluorescence images illustrating that cells exposed to polyplexes made using the different gene delivery agents are intact after 900 seconds of exposure. Average increase in current induced by the polymers. Cationic polymers jetPEI, LPEI and G5 PAMAM increase membrane permeability greater than DOTAP. C-E) Fluorescence images illustrating that cells exposed to the different gene delivery agents are intact after 900 s of exposure.

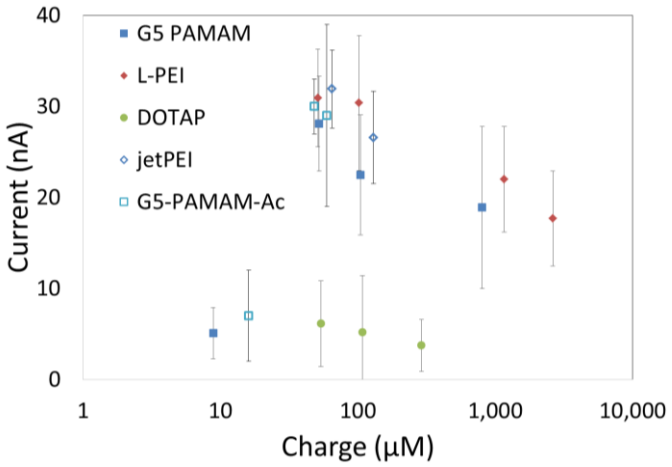

Figure 3.6: Membrane Current Changes as a Function of Charge Concentration. Current induced by polymer at different charge concentrations is similar for the three cationic polymers. DOTAP induces much less current compared to the polymers.

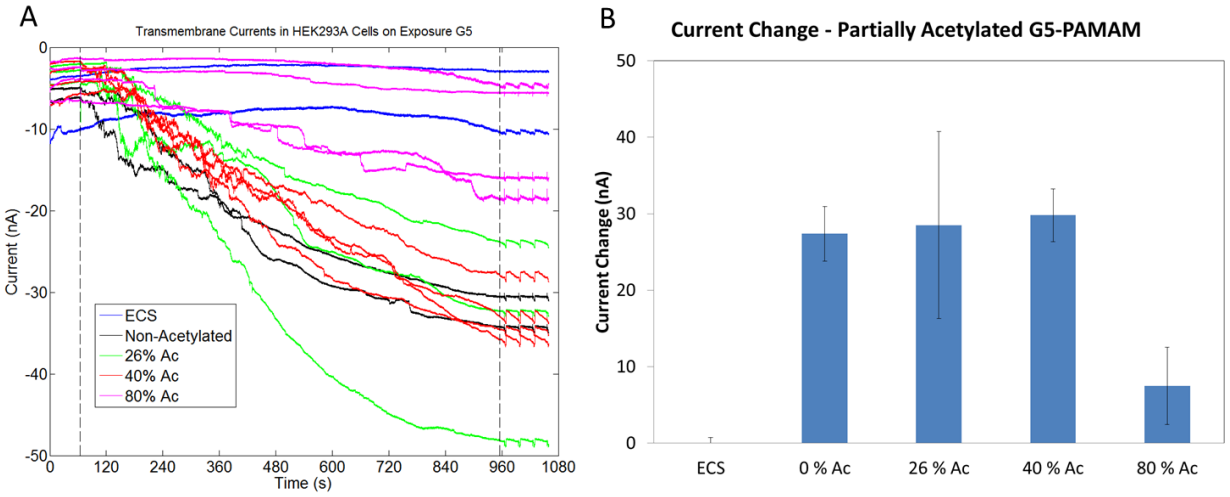

Figure 3.7: Membrane Permeability Induced by Acetylated G5 PAMAM. Cells exposed to G5 PAMAM acetylated to different levels. G5 PAMAM with 80% of the primary amines acetylated did not induce membrane permeability. A) The first dotted line at 65 s indicates the release of the G5 PAMAM resulting in exposure of cells to G5 PAMAM. The second dotted line denotes the end of G5 PAMAM exposure.

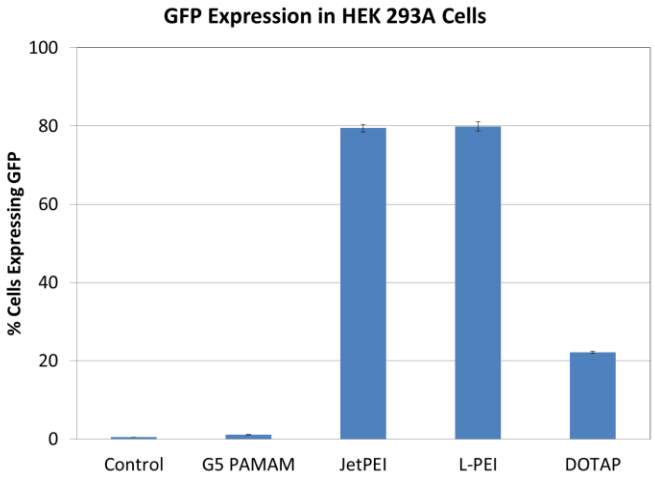

Figure 3.8: GFP Expression by Polyplexes. Expression of GFP in HEK 293 A cells transfected using G5 PAMAM, jetPEI, L-PEI and DOTAP 24 h after transfection

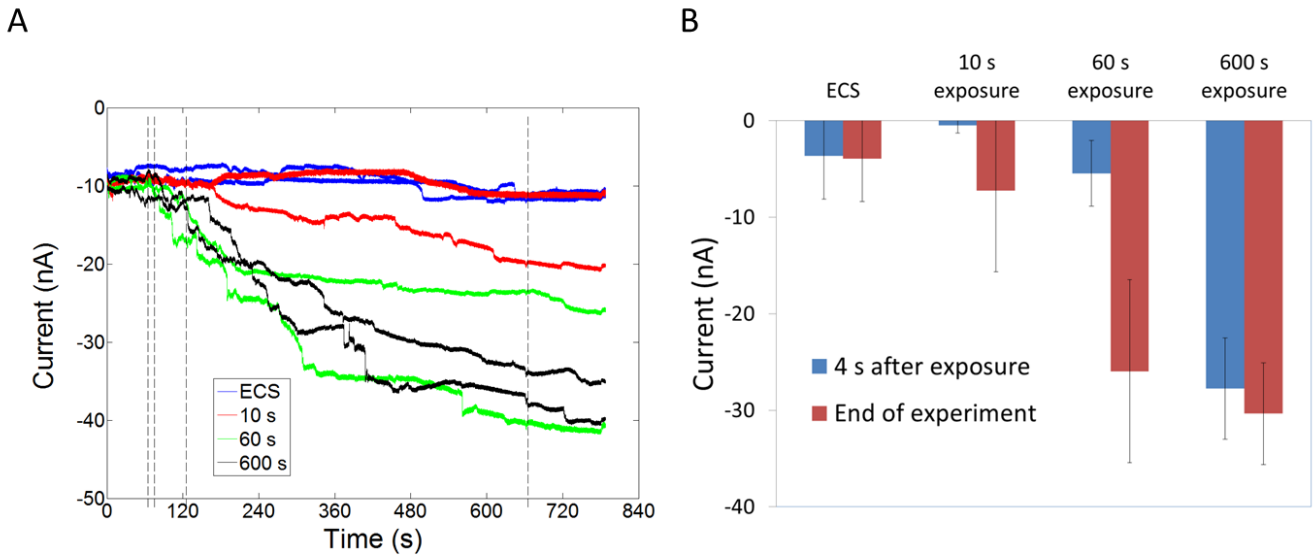

Figure 3.9: Reversibility of Membrane currents Induced by G5 PAMAM. Exposure of HEK 293 A cells to G5 PAMAM for 60 seconds induced increased membrane permeability that is not reversible for over 900 seconds. A) Representative current traces. The first dotted line indicates the release of G5 PAMAM at 65 s. Subsequent dotted lines indicate 10 s, 60 s and 600s from release of G5 PAMAM respectively when G5 PAMAM exposure was stopped and cells were exposed to ECS alone. B) The difference between currents at 65 s and subsequent time points.

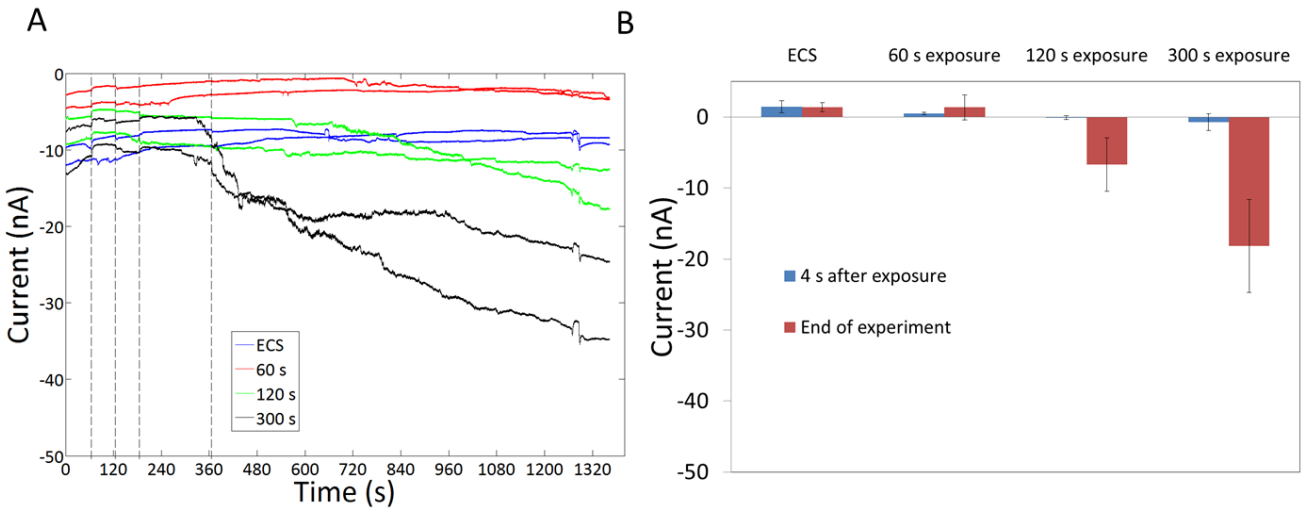

Figure 3.10: Reversibility of Membrane currents Induced by L-PEI. Exposure of HEK 293 A cells to L-PEI for 300 s causes increased membrane permeability that is then not reversible for over 900 s. A) Representative current traces. The first dotted line at 65 s indicates the release of L-PEI at 65 s. Subsequent dotted lines indicate 60 s, 120 s and 300s from release of L-PEI respectively when L-PEI exposure was stopped and cells were exposed to ECS alone. B) The difference between currents at 65 s and at different time points.

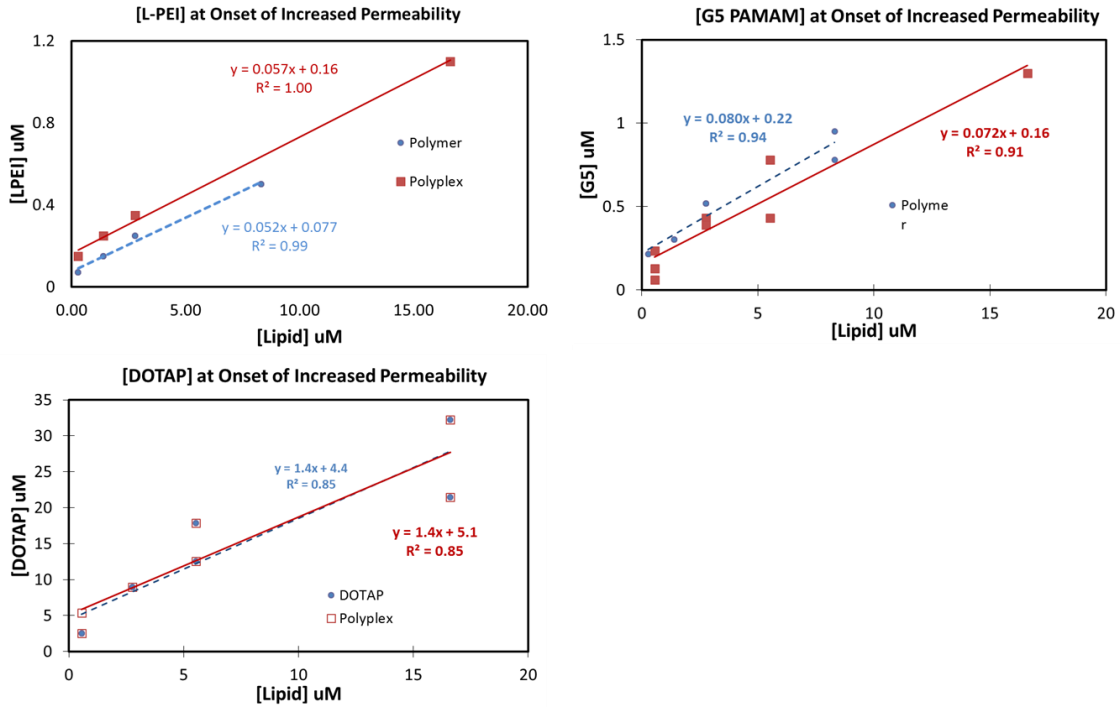

Figure 3.11: Increased Membrane Permeability Induced by Free Vectors and Polyplexes Dependent on Cell Number. Onset of increased trypan blue permeability induced by L-PEI , G5 PAMAM, and DOTAP and their polyplexes as a function of lipid concentrations. It is seen

that L-PEI polyplexes induce increased permeability at higher concentrations than the free polymer. Such an observation was true for G5 PAMAM polyplexes only in some trials.

REFERENCES:

(1) Nguyen, J.; Szoka, F. C. Nucleic Acid Delivery: The Missing Pieces of the Puzzle? *Acc. Chem. Res.* **2012**, *45*, 1153–1162.

(2) Mintzer, M. A.; Simanek, E. E. Nonviral Vectors for Gene Delivery. *Chem. Rev.* **2009**, *109*, 259–302.

(3) Wang, A. Z.; Langer, R.; Farokhzad, O. C. Nanoparticle Delivery of Cancer Drugs. *Annu. Rev. Med.* **2012**, *63*, 185–198.

(4) Leroueil, P. R.; Berry, S. A.; Duthie, K.; Han, G.; Rotello, V. M.; McNerny, D. Q.; Baker Jr, J. R.; Orr, B. G.; Holl, M. M. Wide Varieties of Cationic Nanoparticles Induce Defects in Supported Lipid Bilayers. *Nano Lett.* **2008**, *8*, 420–424.

(5) Lin, J.; Zhang, H.; Chen, Z.; Zheng, Y. Penetration of Lipid Membranes by Gold Nanoparticles: Insights into Cellular Uptake, Cytotoxicity, and Their Relationship. *ACS Nano* **2010**, *4*, 5421–5429.

(6) Arvizo, R. R.; Miranda, O. R.; Thompson, M. A.; Pabelick, C. M.; Bhattacharya, R.; Robertson, J. D.; Rotello, V. M.; Prakash, Y. S.; Mukherjee, P. Effect of Nanoparticle Surface Charge at the Plasma Membrane and Beyond. *Nano Lett.* **2010**, *10*, 2543–2548.

(7) Huhn, D.; Kantner, X. K.; Geidel, X. C.; Brandholt, S.; Cock, I. De; Soenen, S. J. H.; Gil, P. R.; Montenegro, J.; Braeckmans, K.; Nienhaus, G. U.; *et al.* Polymer-Coated Nanoparticles Interacting with Proteins and Cells: Focusing on the Sign of the Net Charge. *ACS Nano* **2013**, *7*, 3253–3263.

(8) Hong, S.; Leroueil, P. R.; Janus, E. K.; Peters, J. L.; Kober, M. M.; Islam, M. T.; Orr, B. G.; Baker Jr, J. R.; Banaszak Holl, M. M. Interaction of Polycationic Polymers with Supported Lipid Bilayers and Cells: Nanoscale Hole Formation and Enhanced Membrane Permeability. *Bioconjugate Chem.* **2006**, *17*, 728–734.

(9) Moghimi, S. M.; Symonds, P.; Murray, J. C.; Hunter, a C.; Debska, G.; Szewczyk, A. A Two-Stage Poly(ethylenimine)-Mediated Cytotoxicity: Implications for Gene Transfer/therapy. *Mol. Ther.* **2005**, *11*, 990–995.

(10) Grandinetti, G.; Smith, A. E.; Reineke, T. M. Membrane and Nuclear Permeabilization by Polymeric pDNA Vehicles: Efficient Method for Gene Delivery or Mechanism of Cytotoxicity? *Mol. Pharmaceutics* **2012**, *9*, 523–538.

(11) Grandinetti, G.; Ingle, N. P.; Reineke, T. M. Interaction of Poly(ethylenimine)-DNA Polyplexes with Mitochondria: Implications for a Mechanism of Cytotoxicity. *Mol. Pharmaceutics* **2011**, *8*, 1709–1719.

(12) Matz, R. L.; Erickson, B.; Vaidyanathan, S.; Kukowska-Latallo, J. F.; Baker, J. R.; Orr, B. G.; Banaszak Holl, M. M. Polyplex Exposure Inhibits Cell Cycle, Increases Inflammatory Response, and Can Cause Protein Expression without Cell Division. *Mol. Pharmaceutics* **2013**, *10*, 1306–1317.

(13) Hong, S.; Bielinska, A. U.; Mecke, A.; Keszler, B.; Beals, J. L.; Shi, X.; Balogh, L.; Orr, B. G.; Baker, J. R.; Banaszak Holl, M. M. Interaction of Poly (amidoamine) Dendrimers with Supported Lipid Bilayers and Cells: Hole Formation and the Relation to Transport. *Bioconjugate Chem.* **2004**, *15*, 774–782.

(14) Erickson, B.; DiMaggio, S. C.; Mullen, D. G.; Kelly, C. V.; Leroueil, P. R.; Berry, S. a.; Baker, J. R.; Orr, B. G.; Holl, M. M. B. Interactions of Poly(amidoamine) Dendrimers with Survanta Lung Surfactant: The Importance of Lipid Domains. *Langmuir* **2008**, *24*, 11003–11008.

(15) Chen, J.; Hessler, J. A.; Putchakayala, K.; Panama, B. K.; Khan, D. P.; Hong, S.; Mullen, D. G.; Dimaggio, S. C.; Som, A.; Tew, G. N.; *et al.* Cationic Nanoparticles Induce Nanoscale Disruption in Living Cell Plasma Membranes. *J. Phys. Chem. B* **2009**, *113*, 11179–11185.

(16) Mecke, A.; Lee, D.-K.; Ramamoorthy, A.; Orr, B. G.; Banaszak Holl, M. M. Membrane Thinning due to Antimicrobial Peptide Binding: An Atomic Force Microscopy Study of MSI-78 in Lipid Bilayers. *Biophys. J.* **2005**, *89*, 4043–4050.

(17) Mecke, A.; Majoros, I. J.; Patri, A. K.; Baker, J. R.; Banaszak Holl, M. M.; Orr, B. G. Lipid Bilayer Disruption by Polycationic Polymers: The Roles of Size and Chemical Functional Group. *Langmuir* **2005**, *21*, 10348–10354.

(18) Lee, H.; Larson, R. G. Lipid Bilayer Curvature and Pore Formation Induced by Charged Linear Polymers and Dendrimers: The Effect of Molecular Shape. *J. Phys. Chem. B* **2008**, *112*, 12279–12285.

(19) Lee, H.; Larson, R. G. Multiscale Modeling of Dendrimers and Their Interactions with Bilayers and Polyelectrolytes. *Molecules* **2009**, *14*, 423–438.

(20) Lee, H.; Larson, R. G. Coarse-Grained Molecular Dynamics Studies of the Concentration and Size Dependence of Fifth- and Seventh-Generation PAMAM Dendrimers on Pore Formation in DMPC Bilayer. *J. Phys. Chem. B* **2008**, *112*, 7778–7784.

(21) Lee, H.; Larson, R. G. Molecular Dynamics Simulations of PAMAM Dendrimer-Induced Pore Formation in DPPC Bilayers with a Coarse-Grained Model. *J. Phys. Chem. B* **2006**, *110*, 18204–18211.

(22) Kelly, C. V; Leroueil, P. R.; Nett, E. K.; Wereszczynski, J. M.; Baker, J. R.; Orr, B. G.; Banaszak Holl, M. M.; Andricioaei, I. Poly(amidoamine) Dendrimers on Lipid Bilayers I: Free Energy and Conformation of Binding. *J. Phys. Chem. B* **2008**, *112*, 9337–9345.

(23) Kelly, C. V; Leroueil, P. R.; Orr, B. G.; Banaszak Holl, M. M.; Andricioaei, I. Poly(amidoamine) Dendrimers on Lipid Bilayers II: Effects of Bilayer Phase and Dendrimer Termination. *J. Phys. Chem. B* **2008**, *112*, 9346–9353.

(24) Yan, L.-T.; Yu, X. Enhanced Permeability of Charged Dendrimers across Tense Lipid Bilayer Membranes. *ACS Nano* **2009**, *3*, 2171–2176.

(25) Nyitrai, G.; Keszthelyi, T.; Bota, A.; Simon, A.; Toke, O.; Horvath, G.; Pal, I.; Kardos, J.; Heja, L. Sodium Selective Ion Channel Formation in Living Cell Membranes by Polyamidoamine Dendrimer. *Biochim. Biophys. Acta* **2013**, *1828*, 1873–1880.

(26) Zhou, Y.; Kumon, R. E.; Cui, J.; Deng, C. X. The Size of Sonoporation Pores on the Cell Membrane. *Ultrasound Med. Biol.* **2009**, *35*, 1756–1760.

(27) Rattan, R.; Vaidyanathan, S.; Wu, G. S.-H.; Shakya, A.; Orr, B. G.; Banaszak Holl, M. M. Polyplex-Induced Cytosolic Nuclease Activation Leads to Differential Transgene Expression. *Mol. Pharmaceutics* **2013**, *10*, 3013–3022.

(28) Prevette, L. E.; Nikolova, E. N.; Al-Hashimi, H. M.; Banaszak Holl, M. M. Intrinsic Dynamics of DNA-Polymer Complexes: A Mechanism for DNA Release. *Mol. Pharmaceutics* **2012**, *9*, 2743–2749.

(29) Heerklotz, H.; Seelig, J. Correlation of Membrane/Water Partition Coefficients of Detergents with the Critical Micelle Concentration. *Biophys. J.* **2000**, *78*, 2435–2440.

(30) Lichtenberg, D.; Ahyayauch, H.; Alonso, A.; Goni, F. M. Detergent Solubilization of Lipid Bilayers: A Balance of Driving Forces. *Trends Biochem. Sci.* **2013**, *38*, 85–93.

(31) Lasch, J. Interaction of Detergents with Lipid Vesicles. *BBA - Rev. Biomembranes* **1995**, *1241*, 269–292.

(32) Heerklotz, H. Interactions of Surfactants with Lipid Membranes. *Q. Rev. Biophys.* **2008**, *41*, 205–264.

(33) Preté, P. S. C.; Malheiros, S. V. P.; Meirelles, N. C.; de Paula, E. Quantitative Assessment of Human Erythrocyte Membrane Solubilization by Triton X-100. *Biophys. Chem.* **2002**, *97*, 1–5.

(34) Preté, P. S. C.; Gomes, K.; Malheiros, S. V. P.; Meirelles, N. C.; de Paula, E. Solubilization of Human Erythrocyte Membranes by Non-Ionic Surfactants of the Polyoxyethylene Alkyl Ethers Series. *Biophys. Chem.* **2002**, *97*, 45–54.

(35) Preté, P. S. C.; Domingues, C. C.; Meirelles, N. C.; Malheiros, S. V. P.; Goñi, F. M.; de Paula, E.; Schreier, S. Multiple Stages of Detergent-Erythrocyte Membrane interaction—A Spin Label Study. *BBA - Biomembranes* **2011**, *1808*, 164–170.

(36) Heerklotz, H.; Seelig, J. Leakage and Lysis of Lipid Membranes Induced by the Lipopeptide Surfactin. *Eur. Biophys. J.* **2007**, *36*, 305–314.

(37) Heerklotz, H.; Seelig, J. Titration Calorimetry of Surfactant-Membrane Partitioning and Membrane Solubilization. *Biochim. Biophys. Acta* **2000**, *1508*, 69–85.

(38) De la Maza, A.; Parra, J. L. Vesicle-Micelle Structural Transition of Phosphatidylcholine Bilayers and Triton X-100. *Biochem. J.* **1994**, *303*, 907–914.

(39) De la Maza, A.; Coderch, L.; Gonzalez, P.; Parra, J. L. Subsolubilizing Alterations Caused by Alkyl Glucosides in Phosphatidylcholine Liposomes. *J. Control. Release* **1998**, *52*, 159–168.

(40) Tan, A.; Ziegler, A.; Steinbauer, B.; Seelig, J. Thermodynamics of Sodium Dodecyl Sulfate Partitioning into Lipid Membranes. *Biophys. J.* **2002**, *83*, 1547–1556.

(41) Beck, A.; Li-Blatter, X.; Seelig, A.; Seelig, J. On the Interaction of Ionic Detergents with Lipid Membranes Thermodynamic Comparison of N-Alkyl-+N(CH3)3 and N-Alkyl-SO4−. *J. Phys. Chem. B* **2010**, *114*, 15862–15871.

(42) Vaidyanathan, S.; Orr, B. G.; Banaszak Holl, M. M. Detergent Induction of HEK 293A Cell Membrane Permeability Measured under Quiescent and Superfusion Conditions Using Whole Cell Patch Clamp. *J. Phys. Chem. B* **2014**, *118*, 2112–2123.

(43) Lichtenberg, D.; Opatowski, E.; Kozlov, M. M. Phase Boundaries in Mixtures of Membrane-Forming Amphiphiles and Micelle-Forming Amphiphiles. *BBA - Biomembranes* **2000**, *1508*, 1–19.

(44) Cócera, M.; López, O.; Pons, R.; Amenitsch, H.; de la Maza, A. Effect of the Electrostatic Charge on the Mechanism Inducing Liposome Solubilization: A Kinetic Study by Synchrotron Radiation SAXS. *Langmuir* **2004**, *20*, 3074–3079.

(45) Van Dongen, M. A.; Orr, B. G.; Banaszak Holl, M. M.; Dongen, M. A. Van; Orr, B. G.; Holl, M. M. B. Diffusion NMR Study of Generation-Five PAMAM Dendrimer Materials. *J. Phys. Chem. B* **2014**, *118*, 7195–7202.

(46) Mullen, D. G.; Desai, A.; Van Dongen, M. a.; Barash, M.; Baker, J. R.; Banaszak Holl, M. M. Best Practices for Purification and Characterization of PAMAM Dendrimer. *Macromolecules* **2012**, *45*, 5316–5320.

(47) Prevette, L. E.; Mullen, D. G.; Banaszak Holl, M. M. Polycation-Induced Cell Membrane Permeability Does Not Enhance Cellular Uptake or Expression Efficiency of Delivered DNA. *Mol. Pharmaceutics* **2010**, *7*, 870–883.

(48) Kim, S. T.; Saha, K.; Kim, C.; Rotello, V. M. The Role of Surface Functionality in Determining Nanoparticle Cytotoxicity. *Acc. Chem. Res.* **2013**, *46*, 681–691.

(49) Dougherty, C. A.; Furgal, J. C.; van Dongen, M. A.; Goodson, T.; Banaszak Holl, M. M.; Manono, J.; DiMaggio, S. Isolation and Characterization of Precise Dye/Dendrimer Ratios. *Chem. Eur. J.* **2014**, *20*, 4638–4645.

(50) Dougherty, C. A.; Vaidyanathan, S.; Orr, B. G.; Banaszak Holl, M. M. Fluorophore:Dendrimer Ratio Impacts Cellular Uptake and Intracellular Fluorescence Lifetime. *Bioconjugate Chem.* **2015**.

(51) Spencer, C. I.; Li, N.; Chen, Q.; Johnson, J.; Nevill, T.; Kammonen, J.; Ionescu-Zanetti, C. Ion Channel Pharmacology Under Flow: Automation *Via* Well-Plate Microfluidics. *Assay Drug Dev. Technol.* **2012**, *10*, 313–324.

(52) Alberts, B.; Johnson, A.; Lewis, J.; Raff, M.; Roberts, K.; Walter, P. The Lipid Bilayer. In *Molecular biology of the cell*; Garland Science: New York, 2002.

Chapter 4 Fluorophore:Dendrimer Ratio Impacts Cellular Uptake and Intracellular Fluorescence Lifetime

Published as: Fluorophore:Dendrimer Ratio Impacts Cellular Uptake and Intracellular Fluorescence Lifetime. *Bioconjugate Chem.* **2015** *26* (2), 304-315

INTRODUCTION

Cationic polymers are employed for a variety of biological applications involving transport of the polymer into cells including transfection agents for oligonucleotides, antibacterial agents, and drug delivery agents.[1-5] In order to probe the uptake and cellular localization properties, the polymer is often modified with fluorescent dye.[6] In this case, it is important to understand how the presence of dye modifies the behavior of the polymer. Such dye-modified polymers are also of interest as models for the biodistribution behavior of the polymer when it is modified with multiple hydrophobic moieties, such as targeting agents or drugs. Dye:polymer conjugates are often complex mixtures. Dye conjugated to a large excess of reactive sites on the polymer will result in a Poisson distribution of dye:polymer particle ratios that is superimposed on the molecular weight (MW) distribution of the base polymer.[7, 8] Materials containing a large degree of dispersion in both MW and hydrophobicity per particle are expected to exhibit a range of biological uptake and distribution behavior.[9-12] An additional complication is the impact of dye conjugation. Specifically the impact that the localization of multiple dyes on a given polymer particle has on the photophysical properties of the dye. This high effective concentration of dye

can result in substantial differences in both fluorescence intensity and lifetime per polymer particle.[6, 13, 14] Given the importance of dye-conjugates to probing the mechanisms of cationic polymers as antibacterial agents and as vectors for gene and drug delivery, we have explored the ways in which employing distributions of dye-conjugates impacts interpretations of cell uptake and localization for polycationic polymers.

The generation of systematically varied dye:polymer ratios for a cationic polymer is a challenging problem. Most commonly, a mean variation in dye:polymer ratio is achieved under stochastic reaction conditions that generate a statistical distribution of ratios and a mixture of hydrophobic and photophysical properties. The distribution of ratios is quite broad with substantial overlap of materials for different means, making comparisons between different conjugate averages difficult to interpret. Table 4.1 provides an illustrative example for the case of stochastic conjugates containing an average of 1-4 dyes for generation 5 poly(amidoamine) (G5 PAMAM) dendrimer. For these cases, the population of the mean percentage varies between about 1/5th and 1/3rd of the total material.

Table 4.1. Statistical conjugation heterogeneity for a G5 PAMAM (G5-dye$_n$) containing 93 arms and 1-4 conjugated dyes.

	Percentage of each dye:dendrimer ratio										
Avg n	0	1	2	3	4	5	6	7	8	9	10
1	36.6	**37.0**	18.5	6.1	1.5	0.3	0.1	-	-	-	-
2	13.2	27.1	**27.4**	18.2	9.0	3.5	1.1	0.3	0.1	-	-
3	4.7	14.7	22.5	**22.8**	17.1	10.1	5.0	2.0	0.7	0.2	0.1
4	1.7	7.0	14.5	19.8	**20.0**	16.0	10.5	5.9	2.8	1.2	0.5

For each value of n, the percentage for the mean value is highlighted in bold.

In order to prepare a set of cationic polymer samples containing a uniform dye:polymer ratio across all particles in the sample, it is necessary to decouple the number of dyes per particle from the particle MW. This is synthetically challenging since a large polymer particle will generally have more functional attachment sites, and therefore have a statistically greater chance of multiple dye conjugation. We achieved the decoupling of conjugation number from MW by separating a stochastic mixture of TAMRA dye conjugates based on the differential hydrophobicity imparted to each dendrimer particle by the presence of dye. In this study, we report the semi-preparative reverse-phase high performance liquid chromatography (rp-HPLC) fractionation of the stochastic mixture of dye:dendrimer ratios in G5-NH_2-$TAMRA_{1.5(avg)}$ into samples containing a single dye:dendrimer ratio (n = 1-4) as well as a sample containing n >5: G5-NH_2-$TAMRA_n$ (n = 1 - 4, 5+). Characterization of the precise dye:dendrimer ratio fractions was carried out by analytical reverse-phase ultrahigh performance liquid chromatography (rp-UPLC), ^{1}H NMR spectroscopy, and MALDI-TOF mass spectrometry.

With this new set of precise ratio dye conjugates available, we tested the following implicit and explicit hypotheses that underlie previous literature studies employing mixtures containing stochastic distributions of dye:polymer ratios:

H1) Uptake of cationic polymers can be quantified by measuring the change in mean fluorescence of cells using flow cytometry.

H2) The components of a stochastic distribution of dye:polymer ratios have a similar collective trend in terms of environmental lifetime response, so the mixture can be used to probe internal cellular environments.

H3) The changes in environment-based lifetime response are large as compared to difference in lifetime response associated with differences in dye:polymer ratio.

The three hypotheses were tested by measuring the uptake, fluorescence emission, and fluorescence lifetime of G5-NH_2-$TAMRA_n$ (n = 1 - 4, 5+, 1.5_{avg}) in HEK293A cells using flow cytometry, fluorimetry, and fluorescence lifetime imaging microscopy (FLIM). In addition, fluorescence emission and lifetime control experiments were performed in aqueous solutions with controlled pH, ionic strength, and biomolecule concentration to test the impacts of these conditions on the fluorescence properties. We show that contrary to the expectations of H1, mean fluorescence is a poor measure for comparing the relative cellular uptake of differing dye:polymer ratios. FLIM studies of the dye-conjugates taken up into the HEK293A cells suggest the fluorescence lifetime response to the cellular environment is very sensitive to the dye:polymer ratio, raising concerns about H2 and H3. These studies indicate caution should be exercised when interpreting FLIM data for stochastic dye mixtures in biological systems. \ Biological systems have the capacity for fractionating a sample,[9-12, 15] much like an HPLC column, prior to the fluorescence measurement. For such a system, this study indicates that it is critical to know the dye:polymer ratio dependent properties of the material being measured in order to accurately compare fluorescence intensities or to make use of differences in fluorescence lifetime.

RESULTS AND DISCUSSION

The importance of cationic polymers for biological applications has led to a number of recent studies addressing the use of dye conjugates. Mier et al. studied the stochastic conjugation of multiple dyes including fluorescein, rhodamine, coumarin, and dansyl to PAMAM dendrimers.[16]

With the exception of dansyl, they found that fluorescence intensity decreased as the mean number of dyes per dendrimer increased. The intensity decrease was attributed to a combination of a small Stokes shift leading to quenching and the high effective concentration that results from multiple dyes conjugated to the same polymer core. By way of contrast, in dansyl-modified PAMAM materials, fluorescence increased with increasing dye:dendrimer ratio, presumably due to the large Stokes shift of 195 nm. Schroeder et al. examined Cy3 and Cy5 dye optical properties conjugated to generation 5 (G5) PAMAM or G6 PAMAM dendrimer in order to create a new set of materials for biological imaging with enhanced stability and increased accuracy in single molecule imaging.[17] Dendrimer mixtures with an average of 8 Cy5 dyes gave slower photobleaching compared to free dye with a 6 to 10 fold increase in photobleaching lifetime value for the G5 PAMAM conjugates. The dendrimer conjugates with an average of 14 Cy5 dyes on G6 PAMAM showed a ~17 fold increase in photobleaching lifetime value. The mean conjugation numbers employed in this case generate mixtures with <0.5% of the material having zero or one dye. This eliminates the most dramatic difference in effective local concentration and the related variation in photophysical properties that occurs when the dye:polymer ratio changes from 1 to 2. Wagner et al. employed stochastically prepared G3 PAMAM dendrimer conjugated to a mean of 1 Alexa Fluor 555 dye to quantify the rate constant of dendrimer uptake in Caplan-1 cells.[18] Interestingly, reverse-phase high performance liquid chromatography (rp-HPLC) did not resolve different species as being present in this case, although separation has been achieved for other dye ligands.[14] In this study, an effective mass transfer coefficient was determined for the mixture of dye:dendrimer ratios present in the sample. Many additional studies addressing the uptake of polycationic polymer-dye conjugates have been discussed in a series of comprehensive reviews.[6] These studies are of broad interest because the

level of hydrophobicity is known to alter a polymer's ability to permeate cell membranes,[19] as well as impact transfection efficiency,[20-24] biodistribution,[15] and pharmokinetics.[25, 26] Colocalization of polymer-fluorophore conjugates based on surface functionality[17, 27] has also been shown. In all cases, the presence of broad conjugation heterogeneity in the stochastic mixtures of polymer-dye conjugates has prevented a detailed understanding of what fraction or fractions of the conjugates are providing the desired biological activity.

In order to focus this study on the impact of dye conjugation heterogeneity, it was necessary to employ a cationic polymer that contained a minimal MW distribution while remaining convenient for generating a systematic change in the dye:polymer ratio. In addition, the polymer MW must be large enough to accommodate a number of dyes and still maintain good water solubility for all dye:polymer ratios. We selected G5 PAMAM dendrimer as this material is readily available commercially, has excellent water solubility, and has a sufficiently large MW (theoretically 28,826 Da) to maintain solubility upon conjugation with multiple dyes. In addition, we have developed rp-HPLC protocols that remove all of the trailing generations (G1-G4; 1,430 to 14,215 Da MW) as well as the dimer, trimer, and tetramer oligomers (~50,000 to 120,000 Da range) typically present in G5 PAMAM dendrimer.[28] The purified G5 PAMAM material obtained from the rp-HPLC purification has an average of 93 primary amine terminal arms per particle (as compared to the theoretical 128 arms), a M_n of 25,130 Da, and a M_w of 27,140 Da (M_n/M_w = 1.08). The full mass range of the isolated monomer G5 PAMAM material was 21,000 to 30,000 Da.

Isolation and Characterization of Dendrimer-TAMRA conjugates. Direct conjugation of TAMRA to G5 PAMAM dendrimer results in a Poisson distribution of dye:dendrimer ratios (Scheme 4.1a). The material was separated using semi-preparative rp-HPLC (Scheme 4.1b) into

fractions containing precise dye:dendrimer ratios (n = 1-4) as well as a sample where n ≥ 5. The isolated fractions were reinjected into an analytical UPLC to determine purity (Scheme 4.1c) and further characterized using ^{1}H NMR spectroscopy, emission and absorption measurements, MALDI-TOF-MS, and fluorescence lifetime imaging microscopy (FLIM).

Analytical UPLC provides the most sensitive measure of the number of dyes present per dendrimer particle.[14] The shift resulting from the addition of each dye to the dendrimer scaffold for the first two dyes is substantially larger than the breadth of the peak resulting from the MW distribution of the G5 PAMAM dendrimer (Scheme 4.1c). As the number of dyes increases, the incremental value of the hydrophobicity induced shift decreases. The UPLC method detects the dye:dendrimer particle ratio induced shifts in the context of the full defect structure of the polymer, which generates the observed peak width.[14] The number of dyes measured for each fraction G5-NH_2-$TAMRA_n$ are n = 0.0, 1.0, 2.0, 3.0, 4.0, and an average of 6.8 dye:dendrimer for the n ≥ 5 fraction (Table C.1). The average number of TAMRA dyes per dendrimer was also assessed using ^{1}H NMR spectroscopy by comparing the integration of the TAMRA protons to the integration of the internal protons in the G5 PAMAM dendrimer (1,210 protons).[7, 29] The averages of n = 0.0, 0.9, 1.8, 3.3, 4.5, and 6.9 are in reasonable agreement with the UPLC data. The NMR values are less reliable than the UPLC values because a) the isolated fraction does not fully represent the material used to determine the internal proton count of 1,210, thus introducing error into the comparison of the integrated ratios and b) we are determining the ratio by comparing a small number of TAMRA protons to a large number of dendrimer protons. MALDI-TOF-MS was also used to characterize each isolated fraction (Table C.1, Figure C.1). A trend towards higher mass was observed as n increased from 1 to 4 as well as for 5+; however, obtaining dye:dendrimer ratios from such data is inaccurate because we are sampling a different

subfraction of the entire MW distribution for each G5-NH_2-$TAMRA_n$ (see the HPLC separation in Scheme 4.1b). The impact of the differential subfractionation is highlighted by the 300 Da decrease observed when comparing G5-NH_2-$TAMRA_o$ to G5-NH_2-$TAMRA_1$. In our previous work discussing the synthesis of related dye:dendrimer conjugates, we compared the relative ability of UPLC, ^{1}H NMR spectroscopy, and MALDI-TOF-MS data to assign dye:dendrimer ratios in detail.[14]

The impact of the dye:dendrimer ratio on photophysical properties was assessed using a combination of FLIM and absorption and emission spectroscopies (Figure 4.1). The absorption and emission spectra were obtained for 0.1 mg/mL G5-NH_2-$TAMRA_n$ solutions in water, which corresponds to roughly 3-4 μM solutions. As expected for this concentration of dye, the absorption spectrum for G5-NH_2-$TAMRA_1$ exhibited a single maximum at 560 nm.[14, 30] Although the total solution concentration for dye in G5-NH_2-$TAMRA_2$ was still micromolar, the absorption now showed the classic two peak pattern, at 525 and 560 nm, typically associated with formation of TAMRA dimers in highly concentrated solutions.[30] This pattern provided additional evidence for the absence of $n \geq 2$ materials in the sample assigned as G5-NH_2-$TAMRA_1$. In addition, the relative intensity ratio of the 525 and 560 nm peaks indicated little if any n = 1 material was present in the G5-NH_2-$TAMRA_2$ sample. The two peaks remained present, and the 525 nm peak grew in relative intensity as n increased. For all these samples, the local concentration of dye, which is restricted on each dendrimer particle to a hydrodynamic sphere of 3.1 nm radius,[31] was on the order of 10 M. The impact of the dye:dendrimer ratio was also observed in the fluorescence spectra taken in water. The most fluorescent material, as a function of dendrimer concentration, is G5-NH_2-$TAMRA_1$. It had roughly twice the fluorescence emission of G5-NH_2-$TAMRA_2$, which had twice as much dye, and three times the

fluorescence emission of G5-NH_2-$TAMRA_4$, which had four times as much dye. G5-NH_2-$TAMRA_1$ also had roughly twice the fluorescence emission of stochastically prepared G5-NH_2-$TAMRA_{1.5(avg)}$, which consisted of n = 0, 1, 2, 3, 4 ,5 in percentages of 22, 34, 25, 13, 5, and 1%, respectively. The impact of n is further demonstrated in the FLIM analysis.

The fluorescence lifetime for free TAMRA in water (0.2 μM) was measured to be 2.5 ± 0.1 ns and a similar lifetime value for G5-NH_2-$TAMRA_1$ (0.2 μM) was obtained of 2.3 ± 0.2 ns. In all cases, increased dye:dendrimer ratios resulted in a decreased lifetime value as compared to G5-NH_2-$TAMRA_1$. The change was not linear, and G5-NH_2-$TAMRA_3$ had a lower lifetime value (1.5 ± 0.1 ns) than the G5-NH_2-$TAMRA_4$ (1.7 ± 0.1 ns) (Figure 4.1). Additional unexpected trends in lifetime values occurred when using the samples for cellular uptake and in biological environment modeling studies (*vida infra*). Fluorescence lifetime values for all samples in water, as well as for aqueous solutions with controlled ionic strength and biomolecule concentration, are provided in Table C.2.

Cellular Uptake of Cationic Dendrimers: the impact of dye:dendrimer ratio. Fluorophore:polymer ratio has been reported to influence biological behavior;[22, 24] however, the mechanism of these effects has been obscured by stochastic distributions of dye:dendrimer ratios. In this study, we focus on the real and apparent impacts of dye:dendrimer ratio on cellular uptake. As a model system, we employed mean fluorescence as measured by flow cytometry to quantify uptake in HEK293A cells. Cells were exposed to 0.5 μM G5-NH_2-$TAMRA_n$ (n = 1 - 4, 5+, 1.5_{avg}) for 3 hours at 37 °C and mean fluorescence was determined by measurement of 10,000 cells (Figure 4.2). The raw mean fluorescence data exhibited the largest mean value for G5-NH_2-$TAMRA_1$ and the magnitude continued to decrease with increasing dye:dendrimer ratio; however, our independent measures of the fluorescence intensity of the conjugates (Figure 4.1)

indicated that an accurate assessment of dendrimer uptake required a correction for the relative degree of fluorescence intensity for each conjugate.

In order to determine the correction factors, we measured the absorbance, emission, and lifetime characteristics of 0.1 mg/mL (3.5 μM) G5-NH_2-$TAMRA_n$ (n = 1, 2, 3, 4, 5+, 1.5_{avg}) solutions in a variety of aqueous solutions to model potential interactions from both salt and biomolecules. The measurements were performed in aqueous solution (Figure 4.1), NaCl, PBS, and undiluted fetal bovine serum (FBS). We also included controls containing bovine serum albumin (BSA) and glucose in water (at concentrations present in our FBS control) to independently evaluate the impact of these two components. Ficoll was used as a control for biomolecule crowding effects. The impact of interaction with negatively charged macromolecules was modeled using 1:1 and 1:10 N:P ratios of both plasmid DNA (pDNA) and antisense DNA (asDNA) (N is the number of dendrimer primary amines and P is the number of DNA phosphates). Lastly, we employed HEK293A cell lysate at 100,000 cells per mL as a final, comprehensive control solution (Figures S2 and S3). The cell lysate was prepared by osmotically lysing cells followed by sonication. This lysate contains all of the cell lipids and protein and is detergent free, and thus differs from conventional lysates. For all conditions studied, G5-NH_2-$TAMRA_1$ exhibited the most intense fluorescence emission. In order to compare the emission intensities for the various conjugates under a given model condition, we defined the brightest emission of G5-NH_2-$TAMRA_1$ as 1 and determined the relative fraction of emission for the remaining conjugates (Table 4.2). The overall trend was a decrease in emission with increasing dye:dendrimer ratio. The overall magnitude of the non-quenched fluorescence varied greatly with the addition of the second dye (G5-NH_2-$TAMRA_2$), ranging from 93% for ficoll to 42% for PBS. When considering just the G5-NH_2-$TAMRA_n$ (n = 1, 2, 3, 4)

fluorescence, the change in intensity as a function of n was monotonic; however, when the more complex n = 1.5_{avg} and n = 5+ samples were considered, multiple deviations in the monotonic trend were associated with both samples. The origins of this complex fluorescence emission behavior are not clear. The data show the difficulty in extrapolating behavior for such heterogeneous mixtures of conjugated fluorophores. Fluorescence lifetime measurements for G5-NH_2-$TAMRA_1$ (2.3 ± 0.2 ns) and TAMRA (2.5 ± 0.1 ns) in water were essentially identical, and lifetimes decreased, as expected for the decrease in emission intensity, as a function of n. Based on these studies, we employed the fluorescence correction factors determined from aqueous solution, FBS solution (which also matched trends observed for the cell-based lifetime studies, *vida infra*), and cell lysate in order to correct the mean fluorescence values obtained from flow cytometry.

Table 4.2. Fluorescence emission intensity characterization summary for G5-NH_2-$TAMRA_n$ material.

	Fluorescence Ratios for Control Solutions of 200 µM G5-NH_2-$TAMRA_n$							
	water	PBS	NaCl	BSA	ficoll	pDNA	FBS	asDNA
G5-$(TAMRA)_{1.5avg}$-NH_2	0.54	0.53	0.7	0.69	0.93	0.59	0.54	0.77
G5-$(TAMRA)_0$-NH_2	-	-	-	-	-	-	-	-
G5-$(TAMRA)_1$-NH_2	1	1	1	1	1	1	1	1
G5-$(TAMRA)_2$-NH_2	0.53	0.42	0.45	0.83	0.93	0.81	0.72	0.77
G5-$(TAMRA)_3$-NH_2	0.43	0.24	0.27	0.57	0.59	0.44	0.43	0.47
G5-$(TAMRA)_4$-NH_2	0.34	0.17	0.17	0.42	0.33	0.25	0.29	0.44
G5-$(TAMRA)_{5+}$-NH_2	0.22	0.18	0.21	0.42	0.51	0.2	0.26	0.31

For each condition the intensity for G5-NH_2-$TAMRA_1$ is defined as 1 and the fractional intensity observed for each n = 2, 3, 4, 5+ and 1.5_{avg} is indicated.

Application of the fluorescence emission correction factors (Table 4.2) to the mean fluorescence data obtained from flow cytometry (Figure 4.2) resulted in the trends in mean fluorescence

illustrated in Figure 4.3. For each correction factor, the data for G5-NH_2-$TAMRA_1$ (G5-T_1) was normalized to the intensity observed for raw emission data. All three corrections trend in the same direction and indicate that the uptake of the n ≥ 2 conjugates is significantly underestimated when only raw mean fluorescence data is considered. Indeed, the data indicate that *uptake does not decrease as a function of n* as implied by comparison of the raw mean fluorescence intensities. Rather, n ≥ 2 conjugates give greater uptake than does the n = 1 conjugate. These data also suggest that studies with dye conjugates overestimate the uptake rates of dye-free G5 PAMAM dendrimer into cells, although the rates may be a reasonable estimate for dendrimer containing other moieties of similar hydrophobicity, such as drugs. Lastly, these data indicate that the use of raw mean fluorescence data to quantify dye uptake *in vivo* using stochastic dye:dendrimer, or more generally dye:polymer, conjugates can lead to errors of at least a factor of 3-5 if the biological fractionation effects on the materials are unknown.

Application of Dendrimer-TAMRA Conjugates for Fluorescence Lifetime Imaging Microscopy (FLIM). The G5-NH_2-$TAMRA_n$ (n = 1, 2, 3, 4, 5+, and 1.5_{avg}) conjugates varied in terms of fluorescence intensity as a function of n (Figures 1-3). The variation of intensity with n indicates that interpreting the uptake of materials into the cell using relative brightness in the confocal fluorescence images will not give reliable results (Figure 4.4). In this case, HEK293A cells were treated with 1 μM G5-NH_2-$TAMRA_n$ (n = 1, 2, 3, 4, 5+, and 1.5_{avg}) conjugates for 3 hours. All treated cells exhibited a punctate distribution of fluorophore uptake (TAMRA = green), which was in general agreement with the flow cytometry data (Figures 2 & 3). The mixtures G5-NH_2-$TAMRA_{5+}$ (Figure 4.4g) and G5-NH_2-$TAMRA_{1.5avg}$ (Figure 4.4h) were expected to contain fluorescent particles with intensity levels varying by up to a factor of 5.

Therefore, even within a given cell or field of cells, relative intensity variation may not be correlated with extent of uptake.

FLIM offers an alternative method of fluorescence image contrast that is generally insensitive to intensity-based artifacts. In addition, the fluorescence lifetimes measured are sensitive to the microenvironment including pH, ion concentration, and molecular association.[32] FLIM images were obtained for the same locations as the confocal microscopy data presented in Figure 4.4. The G5-NH_2-$TAMRA_{1.5avg}$ treated sample (Figure 4.5h) gave an average lifetime of 0.7 ± 0.2 ns which is significantly lower than the 1.9 ± 0.1 ns obtained for aqueous solution. This value is also substantially lower than observed for all other samples with the exception of G5-NH_2-$TAMRA_4$. The G5-NH_2-$TAMRA_1$ treated cells exhibited uniformly higher lifetimes of 1.8 ± 0.5 ns (Figure 4.5c), which itself was substantially lower than the 2.3 ± 0.2 ns observed in aqueous solution. Despite the fact that the G5-NH_2-$TAMRA_{1.5avg}$ sample contained 34% G5-NH_2-$TAMRA_1$, the 1.8 ns lifetimes associated with T_1 material did not appear in the cell images (Figure 4.5h). The G5-NH_2-$TAMRA_{5+}$ treated cells also exhibited amongst the highest lifetime value with an average of 1.6 ± 0.6 ns. Surprisingly, this value was greater than the average values observed for G5-NH_2-$TAMRA_n$ (n = 2, 3, 4), as well as for the G5-NH_2-$TAMRA_{5+}$ aqueous value of 1.2 ± 0.1 ns. The images from Figure 4.5 are provided in large form in Figure C.4. Images of individual cells measured using a 40x oil objective with an additional optical zoom of 6.25x are provided in Figure C.5 and the graphical abstract to further illustrate the various intracellular lifetimes observed with these materials. The lifetimes in the zoomed images show a similar trend as the non-zoomed images. The zoomed-in images highlight the punctate distribution of the G5-TAMRA within cells. Further experiments with markers for cellular organelles are needed to determine if samples with different dye:dendrimer ratios are transported

to different organelles. The observation that most of the samples exhibited dynamic quenching in the cell, resulting from possible environmental differences such as pH, ionic strength, or biomolecule interactions, was expected. It was surprising that the G5-NH_2-$TAMRA_{1.5avg}$ treated cells did not show the full range of lifetimes represented by the dye:dendrimer ratios present and that the lifetime of G5-NH_2-$TAMRA_{5+}$ increased in cells, indicating a reduction in dynamic quenching.

In order to gain a greater understanding of how these changes in lifetime varied as a function of n, a series of control experiments were carried out. Fluorescence lifetimes were measured for solutions of G5-NH_2-$TAMRA_n$ (n = 1, 2, 3, 4, 5+, and 1.5_{avg}) in cell lysate, 1X PBS, 137 mM NaCl, 0.3 mM BSA, 7.0 mM glucose, 0.001 mM ficoll, and undiluted fetal bovine serum (FBS) (Figure 4.6). Additional lifetime measurements were made for aqueous solutions using pH 3 and 5 buffers and for aggregates of G5-NH_2-$TAMRA_n$ (n = 1, 2, 3, 4, 5+, and 1.5_{avg}) generated by mixing with anionic oligonucleotides (both plasmid and antisense DNA) (Figures S6 and S7). The undiluted FBS was used to generate a high concentration of biomolecules comparable to that found in the cellular environment. The concentrations of NaCl, BSA, and glucose were set to the levels of the FBS control. Ficoll was set at 5 equiv per dendrimer. 1x PBS is a standard buffer system with an overall salt concentration similar to blood and the same NaCl concentration as the FBS.

The FBS control best matched the cell FLIM data as it gave both the increase in dynamic quenching (lower lifetime) of the G5-NH_2-$TAMRA_1$ material and the decrease in dynamic quenching (higher lifetime) observed for G5-NH_2-$TAMRA_{5+}$ (Figure 4.6). In order to understand how the components of FBS might lead to these lifetime changes, solutions were tested containing salt (PBS, NaCl) and biomolecule components (BSA, glucose) as well as a

ficoll. The results point to a complex mixture of static and dynamic quenching mechanisms present in the G5-NH_2-$TAMRA_n$ conjugates. For G5-NH_2-$TAMRA_1$, NaCl and PBS alone or the presence of ficoll did not generate a significant change in fluorescence lifetime; however, both BSA and glucose did cause a change. For G5-NH_2-$TAMRA_{5+}$, NaCl, PBS, BSA, and ficoll all caused a significant increase in fluorescence lifetime, although glucose did not. For both G5-NH_2-$TAMRA_n$ (n = 2, 3), little change in fluorescence lifetime was observed for any simple controls, although cell lysate caused a significant increase in lifetime for n =3. For G5-NH_2-$TAMRA_4$, all conditions but FBS and cell lysate were observed to decrease lifetime. Since fluorescence lifetime is also known to change for a fluorophore based on pH,[33] the conjugates were also measured in pH =3, 5, and 7 aqueous buffers. Treatment of G5-NH_2-$TAMRA_1$ with pH 3 and 5 buffers caused no change in lifetime, whereas both buffers resulted in an increase in lifetime for G5-NH_2-$TAMRA_{5+}$ (Figure C.6, Table C.3). No clear lifetime trends were observed for the impact of aggregate formation induced by plasmid and antisense DNA, although a decrease in lifetime for G5-NH_2-$TAMRA_1$ and an increase in lifetime for G5-NH_2-$TAMRA_{5+}$ were again observed (Figure C.7, Table C.3). These observations can be compared to the measurements of TAMRA fluorescence lifetime of 2.28 ± 0.01 ns in buffer and 2.48 ± 0.01 ns on a DNA aptamer.[34]

The cell FLIM data can be rationalized in part based upon the control experiments. The most surprising result, the increase of fluorescence lifetime for G5-NH_2-$TAMRA_{5+}$ in HEK293A cells, was reproduced under a variety of control conditions. This behavior may result from a dye-dye static quenching interaction present in a fraction of the G5-NH_2-$TAMRA_{5+}$ sample. Upon addition of salt and biomolecules, the dye-dye interactions may be broken up leading to a lifting of the static quenching and the observation of a new, longer lifetime value. In addition,

the salt and biomolecule interaction with the dye may change the nature of the dynamic quenching that leads to the 1.2 ± 0.1 ns lifetime in aqueous solution, which could also lead to an increase in observed lifetime. This balancing of effects only appears operative for n ≥ 5 dyes per G5 PAMAM dendrimer.

Many previous studies have demonstrated that the punctate G5 PAMAM dendrimer distribution in cells arise from localization into endosomes and lysomes;[35] however, the control data for pH effects (Figure C.6) does not explain the decrease in lifetimes observed in the FLIM images (Figures 4.5, C.S4). Based on our series of control experiments, it appears that changes in ionic strength or interactions with other biomolecules present in the endosomes or lysomes are more likely causes of the decreased fluorescence lifetimes for these dye:dendrimer conjugates in the HEK293A cells.

CONCLUSIONS

G5-NH_2-$TAMRA_n$ (n=1-4, 5+, 1.5_{avg}) samples have been synthesized and characterized by UPLC, ^{1}H NMR, and MALDI-TOF-MS. The absorbance, fluorescence emission, and fluorescence lifetime properties have been measured in aqueous solution as well as in a variety of biologically relevant control conditions. By preparing this set of dye:dendrimer conjugates with well-defined dye:dendrimer ratios, we hope to elucidate the behaviors of the stochastic mixtures of dye:dendrimer ratios typically employed to understand cationic polymer uptake and localization.

During the course of this study we showed that dendrimer uptake varied as a function of n. In addition, knowledge of how fluorescence intensity for G5-NH_2-$TAMRA_n$ varies as a function of n is required for properly understanding the relative degree of uptake. These observations raise

the greatest concerns for studies in which a stochastic mixture can be "separated" by the interaction with the biological systems, ie exhibit a hydrophobic dependency on biodistribution,[15, 19, 25, 26] and when biological tissues are evaluated for uptake by fluorescence without knowledge of the fraction of the dye:polymer conjugate present. Thus, for materials containing stochastic dye:polymer distributions, hypothesis (H1) that the uptake of cationic polymer can be quantified by the change in mean fluorescence of cells should be used with caution. For low Stokes shift dyes similar to TAMRA and fluorescein, H1 is not valid.

The FLIM studies of G5-NH_2-$TAMRA_n$ resulted in a surprising set of lifetime images. In particular, the observation of both decreasing and increasing lifetimes for a given environmental condition as a function of n was not expected. In addition, the magnitudes of changes seen as a function of n for a given control environment was similar to the magnitude of change observed for constant n as a function of changing the environment. This indicates the interpretations of fluorescence lifetimes as resulting from changes in biological environment must be approached with great caution for stochastic dye:polymer conjugates, particularly if biological fractionation of the samples has taken place. In contrast to the initial hypothesis (H2), the components of a stochastic distribution of dye:polymer ratios do not have a similar collective trend in terms of environmental lifetime response. Furthermore, with respect to H3, variation in dye:polymer ratio is found to have a similar magnitude of impact on fluorescence lifetime as changes in the biological environment.

Upon testing the three hypotheses, it is clear that caution needs to be taken when using dye:polymer mixtures to determine cellular uptake and fluorescence lifetime. One good solution for achieving linear intensity profiles is the use of large Stokes shift dyes, as discussed by Mier et al.[16] The strategy of using a stochastic mixture that contains very little of zero dye and one dye

on the polymer, as delineated by Schroeder et al., can also provide a solution.[17] However, many scientifically and technologically important dyes (i.e. TAMRA, fluorescein, AlexaFluors, etc.) have small Stokes shifts, and dye substitution is not always a favorable option. Since dye:polymer ratio impacts biodistribution and function,[9-12, 15-17, 19-27] creation of a high mean stochastic ratio is not a general solution to the problem. In these cases, either direct synthesis of precise dye:polymer materials[36-38] or physical separation to obtain precise dye:polymer ratios[7, 8, 14, 29] is needed for quantitative uptake or lifetime studies.

EXPERIMENTAL PROCEDURES

Chemicals and Methods. Biomedical grade G5 PAMAM dendrimer was purchased from Dendritech Inc. and purified using rp-HPLC to give a molecular weight fraction free of trailing generations (G1-G4) as well as G5 dimers and higher oligomers.[28] Trifluoroacetic acid, HPLC grade water, GE PD-10 Sephadex columns, and HPLC grade acetonitrile were purchased from Fisher-Scientific and used as received. 5-carboxy tetramethylrhodamine succinimydyl ester (TAMRA) was purchased from Life Technologies. A 500 MHz Varian NMR instrument was used for all ^{1}H and ^{19}F NMR measurements. All MALDI-TOF MS measurements were performed on a Bruker Ultraflex III with sinapinic acid matrix (Sigma Aldrich) and sodium trifluoroacetate (Fischer Scientific) salt sample preparation. Serum-free DMEM (SFM) from life technologies was employed for cell culture of HEK293A cells, which were obtained from ATCC. Complete medium was made by adding 50 mL of fetal bovine serum (FBS) and 5 mL 100× of penicillin−streptomycin to 500 mL of SFM.

Conjugation of TAMRA to G5 PAMAM Dendrimer. TAMRA (0.0121 g, 0.023 mmol, 4.5 equiv) was dissolved in dimethyl sulfoxide (3.0 mL) and added dropwise to a stirred solution of

G5 PAMAM dendrimer (0.1390 g, 0.0050 mmol, 1.0 equiv) dissolved in water (30.0 mL). The mixture was stirred at 20 °C overnight and purified using a GE PD-10 sephadex column. A pink solid was obtained after removal of solvent (75% yield). The product was characterized using ^{1}H NMR, UV-Vis absorption and fluorescence spectroscopy, analytical rp-UPLC, and MALDI-TOF MS.

Isolation of Material Containing Precise TAMRA/Dendrimer Ratios. Semi-preparative rp-HPLC isolation was carried out on a Waters Delta 600 HPLC. For analysis of the dendrimer and conjugates, a C18 silica-based rp-HPLC column (250 x 21.20 mm, 10μm particles) connected to a C18 guard column (50 x 21.20 mm) was used. The mobile phase for elution of the conjugates was a linear gradient beginning with 95:5 (v/v) water/acetonitrile and ending with 65:35 (v/v) water/acetonitrile over 28 minutes at a flow rate of 12.00 mL/min. Trifluoroacetic acid (TFA) at 0.10 wt % concentration in both water and acetonitrile was used as a counter ion to make the dendrimer surfaces hydrophobic. Elution traces of the dendrimer-ligand conjugate were obtained at 210 nm. A concentration of 24 mg/mL per injection was used. 120 fractions of 6 seconds duration were collected starting at 9 minutes and 30 seconds. Selection of fractions for combination to yield the precise TAMRA:dendrimer ratios was based upon analysis of the chromatogram in Origin-Pro. Each isolated combination of fractions was reinjected onto an analytical UPLC to determine purity of the sample. ^{1}H NMR spectra are provided in Figure C.8.

Analytical reverse phase Ultra Performance Liquid Chromatography (rp-UPLC). Purity of G5-NH_2-$TAMRA_n$ materials was assessed at 210 nm (dendrimer absorption wavelength) using a Waters Acquity UPLC system controlled by Empower 2 software. A C18 silica-based column (Phenomenex) was employed with a mobile phase linear gradient beginning with 95:5 (v/v) water/acetonitrile and ending with 55:45 (v/v) water/acetonitrile over 17 minutes at a flow rate of

3.0 mL/min. Trifluoroacetic acid (TFA) at 0.14 wt % concentration in water and acetonitrile was used as a counter ion to make the dendrimer surfaces hydrophobic.

Absorption and Emission Measurements. Fluorescence (Fluoromax-4) and UV-Vis (Shimadzu UV-1601) measurements were taken at a concentration of 0.1 mg/mL. For all measurements, the concentration of the solutions were 0.1 mg/mL and within an error of ±0.02. For the fluorescence measurements an excitation of 530 nm and emission of 580 nm were used with a slit width of 2 nm.

MALDI-TOF-MS Measurements. Three solutions were prepared: 1) 10 mg/mL dendrimer in water 2) 20 mg/mL sinapinic acid in 1:1 (v/v) acetonitrile: water and 3) 20 mg/mL sodium trifluoroacetate in water. These were then combined in a ratio of 10:2:1 of matrix:dendrimer:salt solution. The plate was spotted with 1 µL volumes of solution and allowed to dry. At least 100 scans were averaged per measurement and a smoothing factor of 12 channels was employed.

Cell Culture Materials. DMEM high glucose with sodium pyruvate and glutamine (Life Technologies Inc) was the base media. Complete media was made by adding 50 mL of FBS, 5 mL of Non-essential Amino Acids (Thermo Scientific) and 5 mL of penicillin-streptomycin to 500 mL DMEM. PBS (1X) without Ca^{2+} and Mg^{2+} was obtained from Life Technologies. Cells were maintained at 37 °C with 5% CO_2 in a humidified atmosphere and subcultured by trypsinization (Life Technologies).

Measurement of G5-NH_2-$TAMRA_n$ Binding and Uptake in HEK293A cells using Flow Cytometry. HEK 293 A cells were seeded in 12 well plates (Fisher Scientific, 3.8 cm^2) at a density of 150,000 cells per well in 1 mL of complete DMEM and incubated overnight at 37 °C

with 5% CO_2. The complete media was removed prior to incubation with G5-NH_2-$TAMRA_n$. The cells were then rinsed with 1 mL of PBS, followed by addition of 0.8 mL of SFM. The cells were incubated for three hours at 37 °C with 0.5 μM G5-NH_2-$TAMRA_n$ (n = 0-4, 5+, 1.5_{avg}) (~5.0 μL volume of 2 mg/mL solution added to each well). Each treatment was run in triplicate, and 4 independent biological repeats were performed. After incubation with G5-NH_2-$TAMRA_n$ material, the HEK293A cells were rinsed with PBS and harvested for flow cytometry by trypsinization. Trypsinization was performed by incubation with 200 μL of trypsin for 2 minutes at 37 ºC. After 2 minutes, 0.8 mL cold PBS was added to each well to inhibit the trypsin, and the suspensions were then centrifuged for 5 minutes at 2000 rpm. Cell pellets were resuspended in 400 μL of PBS. Cell fluorescence was measured using a BD C6 Accuri flow cytometer by collecting 10,000 events per sample. The cells were excited using a 488 nm laser and emission at the 585 ± 20 nm region was measured. Differences were determined according to a post hoc Games-Howell test using predictive analytics SPSS software. This statistical test was chosen because it does not assume equal variance, which we deemed most relevant for comparing multiple biological replicates of HEK 293A cells (* used in figures indicates a p value < 0.05).

Cell Preparation for Confocal and Fluorescence Lifetime Microscopy. HEK 293 A cells were seeded in 2 well confocal chambers (Nunc Labtek II, 4 cm^2) at a density of 50,000 cells per well in 1.5 mL of complete DMEM and incubated overnight at 37 °C with 5% CO_2. The complete media was removed prior to incubation with G5-NH_2-$TAMRA_n$. The cells were then rinsed with 1 mL of PBS, followed by addition of 0.5 mL serum free DMEM. Cells were incubated with 1 μM G5 TAMRA in serum free DMEM for 3 hours. The cells were then rinsed with PBS three times and fixed using 2% paraformaldehyde. The fixed cells were rinsed 3 times

with PBS, two drops of prolong gold solution containing DAPI was added, and a 1.5 thickness coverslip was placed on each sample.

Confocal Fluorescence Microscopy. Confocal microscopy was performed using Leica SP5 inverted confocal microscope using a 40x oil immersion objective. The section thickness was set at 1 μm. The excitation wavelength used was 555 nm, and the emission from 585 nm to 700 nm was measured.

Time Domain Fluorescence Lifetime Imaging Microscopy (FLIM) of G5-NH_2-$TAMRA_n$ in HEK 293A Cells using a Multi Photon Laser. Lifetime imaging for HEK293A cells was performed using a LEICA inverted SP5 confocal microscope in the multiphoton mode. The source was a Mai-Tai laser with a 20 MHz frequency. The excitation wavelength was 850 nm with 2.2 W power. A PMT detector and TCSPC counter were used to measure lifetime. Images shown were taken at approximately mid-cell height by first taking an image in the x-z plane and using the DAPI signal to estimate cell heights (about 8 μm for the HEK293A cells). The z position was then set to this value, and the x-y plane images shown in Figure 4.5 were obtained. Taking images too near the confocal chamber or coverslip surface induced low lifetime artifacts. Measurements were taken until a maximum of 1000 photons were measured for each pixel. The lifetime histograms and exponential fitting were performed using Symphotime software (Picoquant Inc). The FLIM images of cells presented here show the average lifetime per pixel calculated using the FastFLIM algorithm in Symphotime. For solution lifetimes, single exponential lifetimes were used. It has been reported that the lifetime of TAMRA changes with temperature.[39] In our experiments, the MP laser could heat samples and change lifetimes. To test for this, the lifetimes for free TAMRA and G5-NH_2-$TAMRA_1$ were measured using two sequential four minute scans (the average time to image a field of cells) to test if heating during

image acquisition was affecting measured lifetime values. For free TAMRA, the sequentially measured lifetime values were 2.37 and 2.36 ns. For G5-NH_2-$TAMRA_1$, the values were 2.46 and 2.40 ns. These results indicate that change in lifetime due to temperature is not a cause for concern in our study.

Fluorescence Lifetime Imaging Microscopy (FLIM) Measurement of G5-NH_2-$TAMRA_n$ lifetime using Single Photon Laser Excitation. Lifetime imaging in solution was performed using an Olympus IX-81 time resolved confocal microscope using avalanche photodiodes. The source was a SC-400-6-PP supercontinuum laser with 20 MHz frequency. The excitation wavelength was 530 nm with 6.0 W power. An APD detector and TCSPC counter were used to measure lifetime. The lifetime histograms and exponential fitting were performed using ALBA software. Single exponential fitting was performed to obtain solution lifetimes. The mean fluorescence intensity and fluorescence lifetime of each sample was measured. One-way ANOVA followed by Games-Howell post hoc analysis was performed to test if the means were significantly different.

Solution Conditions to Measure Control Fluorescence Lifetimes FLIM. Control measurements in water, 1X PBS, undiluted FBS (Thermo Fisher Scientific), NaCl (137mM), BSA (23 mg/mL), glucose (1.25 mg/mL), and ficoll (60 mg/mL) were performed using 200 µM G5-NH_2-$TAMRA_n$. Polyplex solutions were mixed at an N:P of 10:1 and 1:1 at a concentration of 500 nM G5-NH_2-$TAMRA_n$ based on published protocols.[40]

Preparation of Cell Lysate. HEK 293A cell lysate was prepared by washing a confluent plate of cells with 1X PBS. The cells were then treated with 2 mL trypsin for 2 min at 37° C. The trypsinization was stopped by adding 8 mL of complete DMEM. The cells were triturated and

counted using a hemocytometer. The cells were centrifuged at 1400 g for 2 min and the supernatant was removed. The cells were then suspended in DI water such that there were 5 million cells per mL and sonicated in a bath sonicator for 15 min. The absence of intact cells was checked using a light microscope. For use in experiments, the lysate was diluted to 100,000 cells/mL. This protocol was used rather than typical cell lysate protocols in order to avoid detergents, which interfere with fluorescence lifetime solution measurements, and to include all cell lipid.

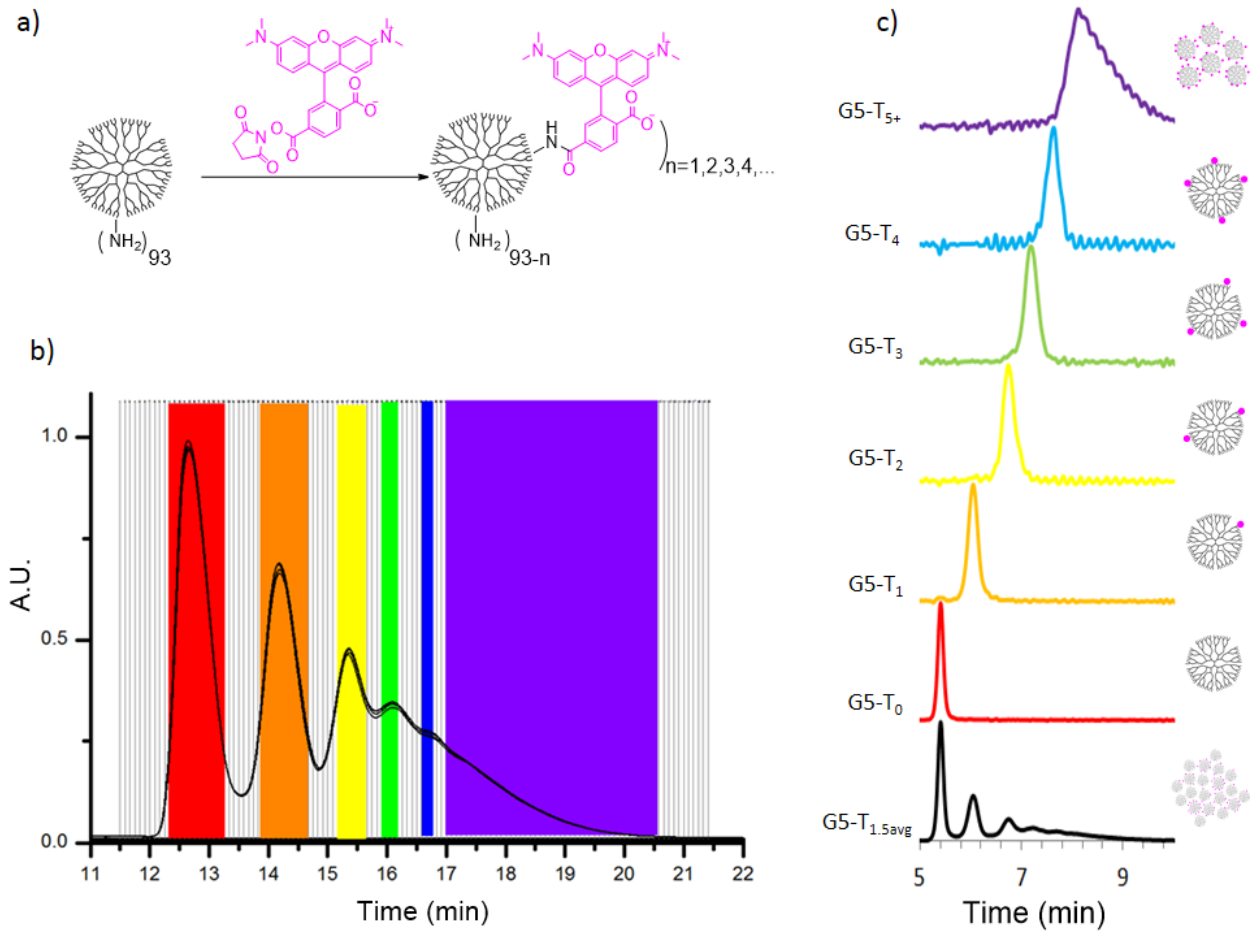

Scheme 4.1 Synthesis, isolation, and characterization of G5-NH_2-$TAMRA_n$ samples. a) Stochastic conjugation of TAMRA to G5 PAMAM dendrimer b) Isolation of G5-NH_2-$TAMRA_n$ employing semi-preparative rp-HPLC c) Reinjection of combined fractions on analytical rp-UPLC to determine purity. n = 1.5_{avg} (black), 0 (red), 1 (orange), 2 (yellow), 3 (green), 4 (blue), and 5+ (purple).

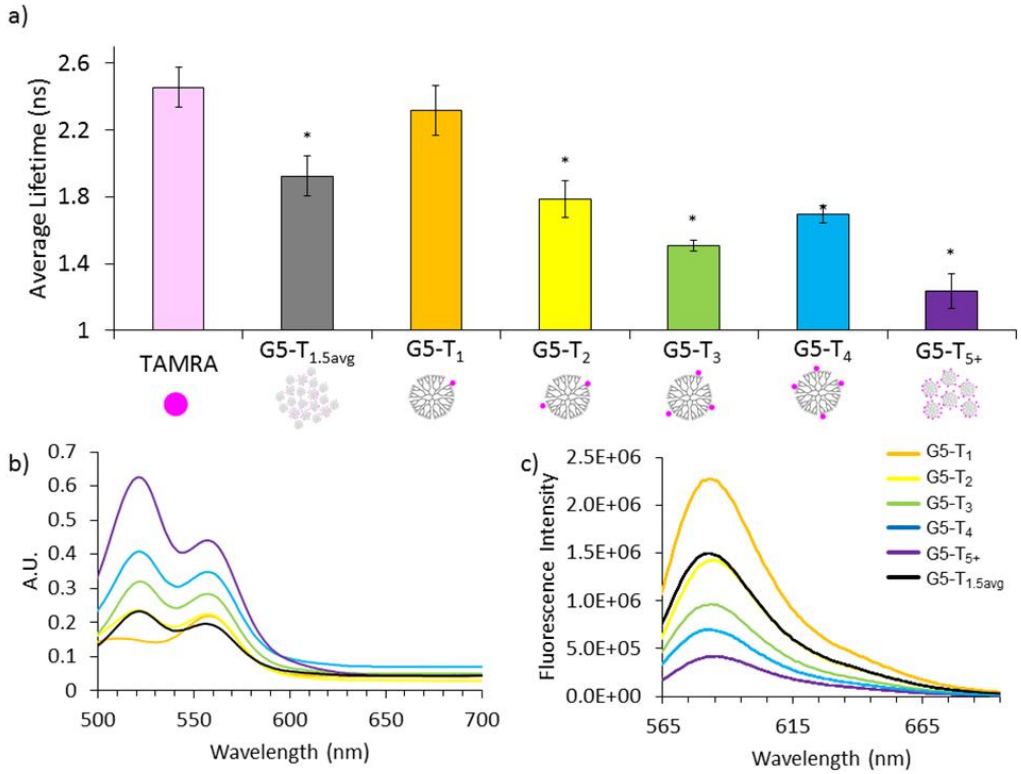

Figure 4.1. Photophysical properties of G5-NH_2-$TAMRA_n$ in aqueous solution. a) Fluorescence lifetime values, b) absorption spectra, and c) emission spectra of 0.1 mg/mL G5-NH_2-$TAMRA_n$ (n = 0, 1, 2, 3, 4, 5+, 1.5_{avg}) in aqueous solution. A significant decrease in lifetime value (denoted by *) was observed for samples with n > 1 as compared to free TAMRA dye (pink) and G5-NH_2-$TAMRA_1$. The absorption increases while the emission decreases with increasing n. See Table C.4 for p values.

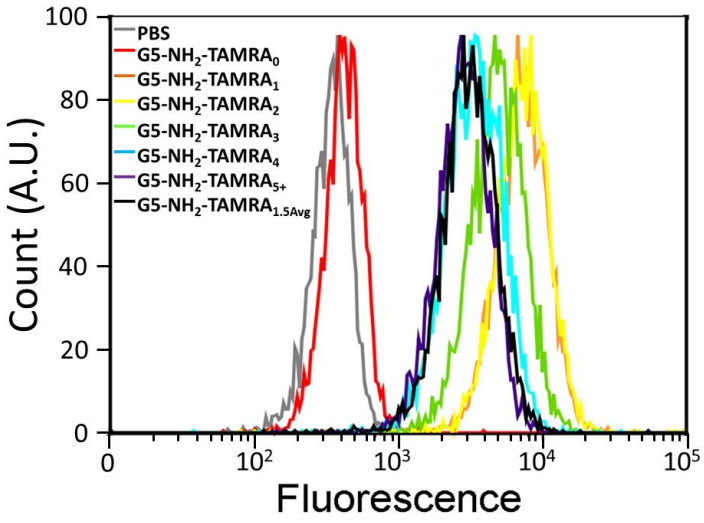

Figure 4.2. Cellular Uptake of G5-NH_2-$TAMRA_n$ in HEK293A cells. Flow cytometry of one repeat for the G5-NH_2-$TAMRA_n$ (n = 0, 1, 2, 3, 4, 5+, 1.5_{avg}) samples showing cell count versus fluorescence intensity.

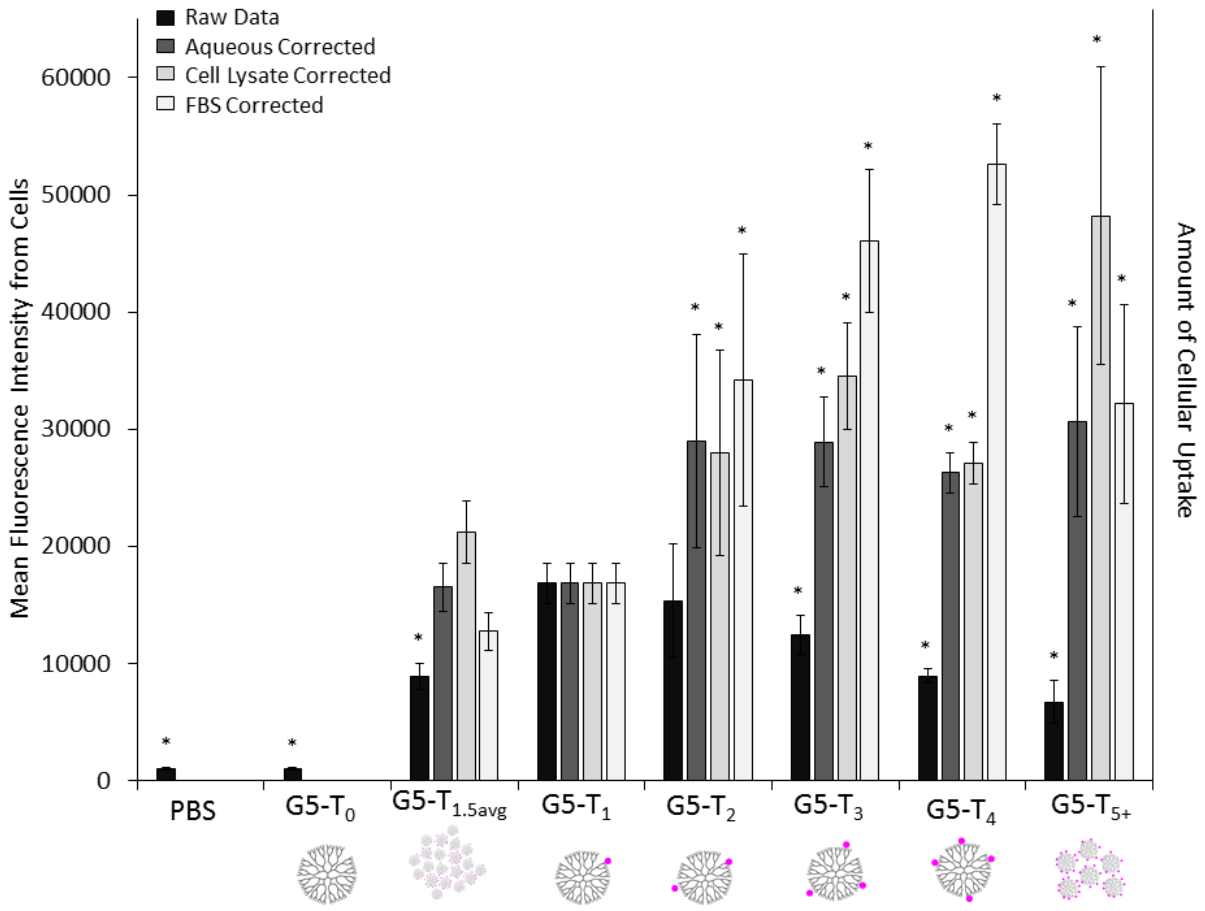

Figure 4.3. Cellular uptake of G5-NH_2-$TAMRA_n$ corrected for fluorescence differences. Uptake and binding of G5-NH_2-$TAMRA_n$ as measured by flow cytometry after 3 hours of incubation with HEK293A cells. The bar graphs illustrate the uptake trend as measured by raw mean fluorescence data and the trends after correction using relative fluorescence emission in aqueous solution, FBS solution, and cell lysate. All correction factors are summarized in Table 4.2 from the data shown in Figures 1c, S2, and S3). Significance for differences in G5-NH_2-$TAMRA_n$ fluorescence intensity (denoted by *) as compared to G5-NH_2 –$TAMRA_1$ intensity was assessed using a Games-Howell analysis (see Table C.4 for p values).

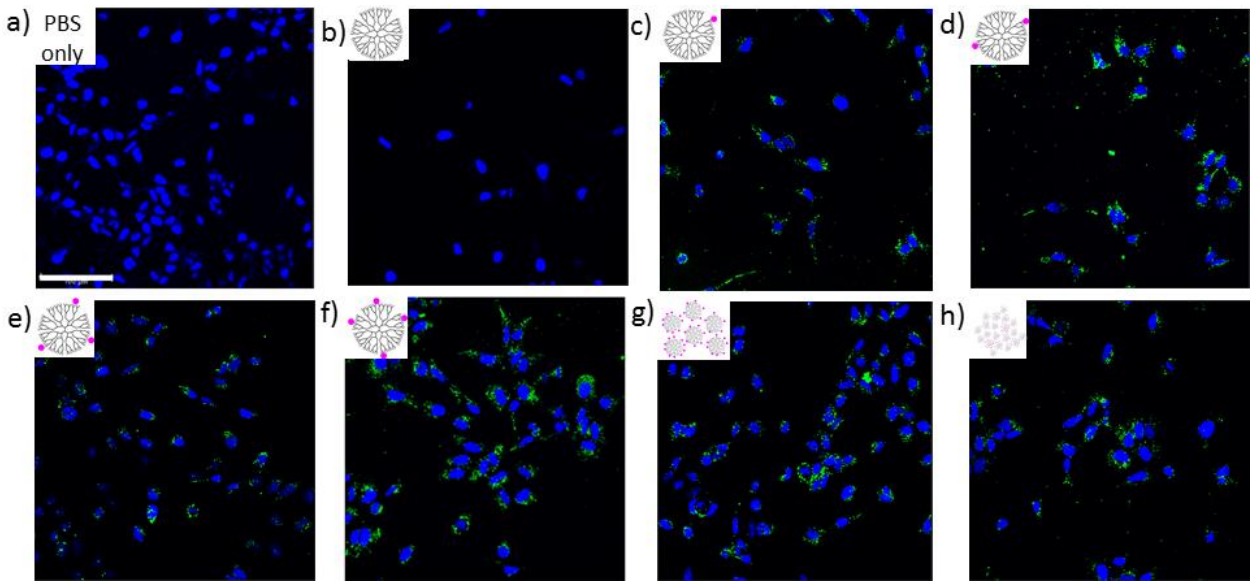

Figure 4.4. Confocal Microscopy Images of HEK293A cells incubated with G5-NH_2-$TAMRA_n$. Confocal Microscopy Images of HEK293A cells incubated for three hours with a) PBS only b) G5-NH_2 c) G5-NH_2-$TAMRA_1$ d) G5-NH_2-$TAMRA_2$ e) G5-NH_2-$TAMRA_3$ f) G5-NH_2-$TAMRA_4$ g) G5-NH_2-$TAMRA_{5+}$ h) G5-NH_2-$TAMRA_{1.5avg}$. TAMRA fluorescence is shown in green. The fluorescence deriving from DAPA-stained cell nuclei is shown in blue. Images were obtained with a 40x oil immersion objective. The same set of image locations is presented in Figure 4.5 using FLIM. Scale bar is 100 μm.

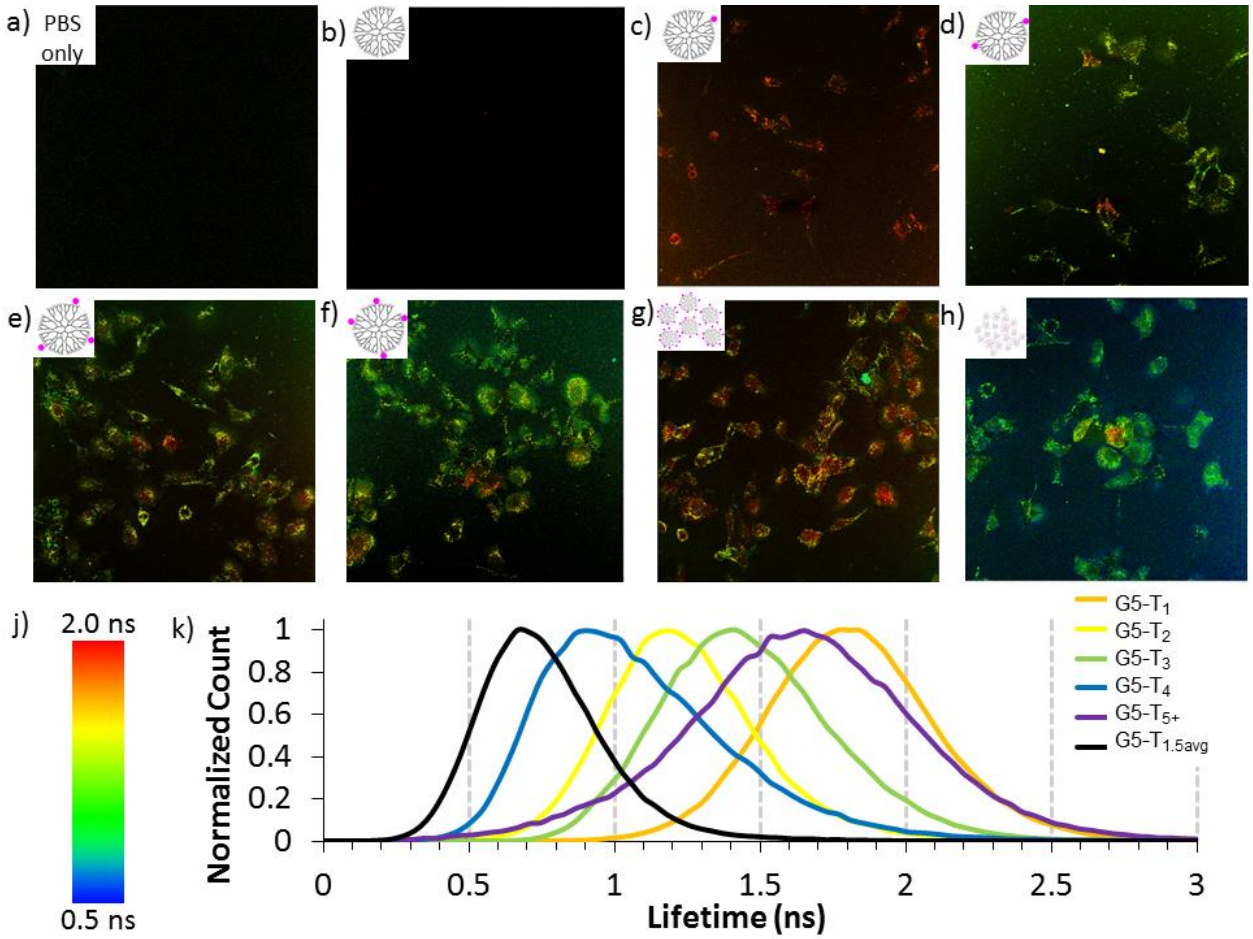

Figure 4.5. FLIM images of HEK293A cells incubated with G5-NH_2-$TAMRA_n$. FLIM images of HEK293A cells incubated for three hours with a) PBS only b) G5-NH_2 c) G5-NH_2-$TAMRA_1$ d) G5-NH_2-$TAMRA_2$ e) G5-NH_2-$TAMRA_3$ f) G5-NH_2-$TAMRA_4$ g) G5-NH_2-$TAMRA_{5+}$ h) G5-NH_2-$TAMRA_{1.5avg}$. j) Color code for FLIM images. k) Histograms of fluorescence lifetimes for FLIM images. Images were obtained with a 40x oil immersion objective. The same set of image locations is presented in Figure 4.4 using confocal fluorescence microscopy.

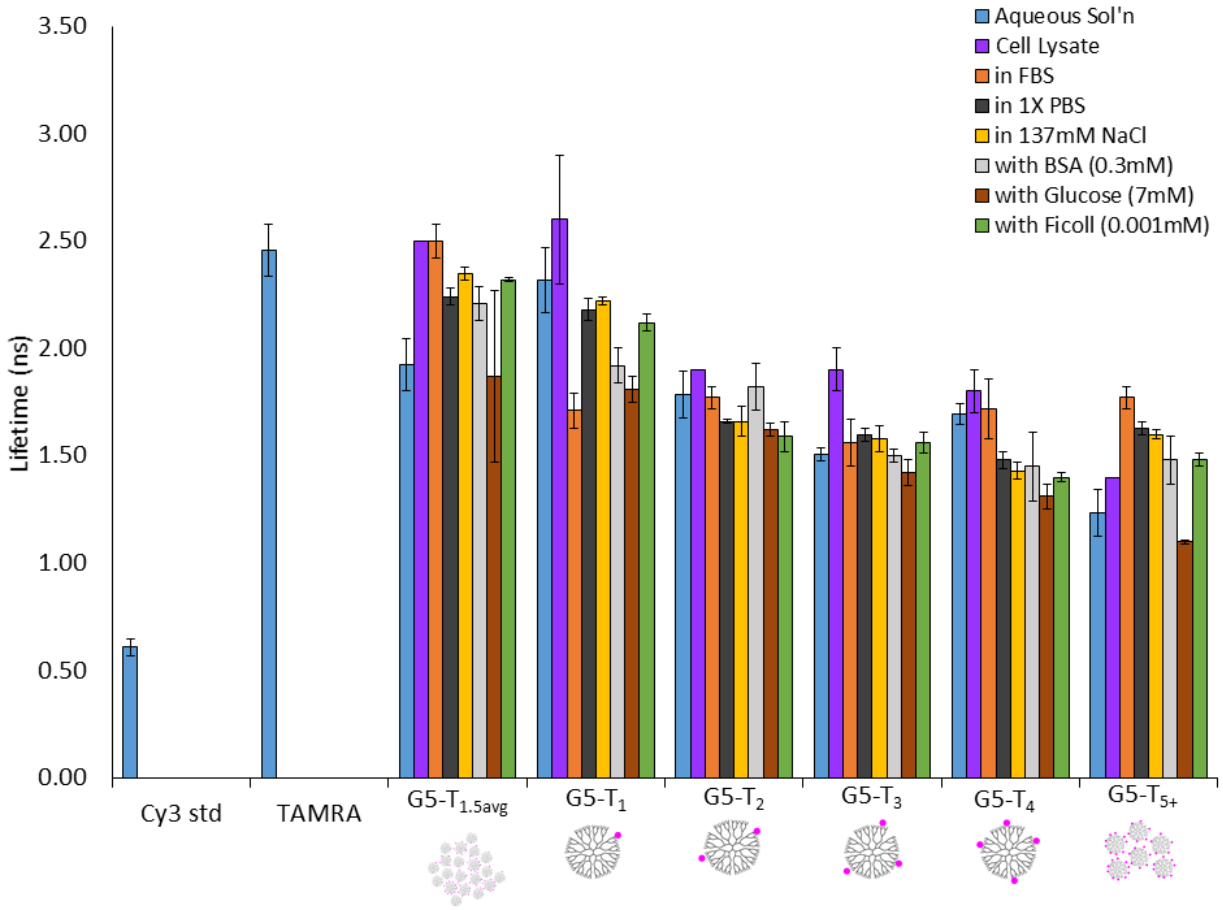

Figure 4.6. Fluorescence lifetime measurements of G5-NH_2-$TAMRA_n$ in aqueous solution under various conditions. Cy3 and TAMRA dyes in water were used as calibration standards. See Table C.2 for summary of numerical values.

REFERENCES

1. Larson, N.; Ghandehari, H., Polymeric Conjugates for Drug Delivery. *Chem. Mater.* **2012,** *24* (5), 840-853.

2. Lee, C. C.; MacKay, J. A.; Frechet, J. M. J.; Szoka, F. C., Designing dendrimers for biological applications. *Nature Biotech.* **2005,** *23*, 1517-1526.

3. Haag, R.; Kratz, F., Polymer Therapeutics: Concepts and Applications. *Angew. Chem. Int. Ed.* **2006,** *2006* (45), 1198-1215.

4. Mintzer, M. A.; Grinstaff, M. W., Biomedical applications of dendrimers: a tutorial. *Chem. Soc. Rev.* **2011,** *40* (1), 173-190.

5. Mintzer, M. A.; Simanek, E. E., Nonviral Vectors for Gene Delivery. *Chem. Rev.* **2009,** *109* (2), 259-302.

6. Chen, M. J.; Yin, M. Z., Design and development of fluorescent nanostructures for bioimaging. *Prog. Polym. Sci.* **2014,** *39* (2), 365-395.

7. Mullen, D. G.; Fang, M.; Desai, A.; Baker, J. R.; Orr, B. G.; Holl, M. M. B., A Quantitative Assessment of Nanoparticle-Ligand Distributions: Implications for Targeted Drug and Imaging Delivery in Dendrimer Conjugates. *Acs Nano* **2010,** *4* (2), 657-670.

8. Mullen, D. G.; Banaszak Holl, M. M., Heterogeneous ligand-nanoparticle distributions: a major obstacle to scientific understanding and commercial translation. *Acc. Chem. Res.* **2011,** *44*, 1135-1145.

9. Alexis, F.; Pridgen, E.; Molnar, L. K.; Farokhzad, O. C., Factors affecting the clearance and biodistribution of polymeric nanoparticles. *Mol. Pharmaceutics* **2008,** *5* (4), 505-515.

10. Duan, X. P.; Li, Y. P., Physicochemical Characteristics of Nanoparticles Affect Circulation, Biodistribution, Cellular Internalization, and Trafficking. *Small* **2013,** *9* (9-10), 1521-1532.

11. Moyano, D. F.; Goldsmith, M.; Solfiell, D. J.; Landesman-Milo, D.; Miranda, O. R.; Peer, D.; Rotello, V. M., Nanoparticle Hydrophobicity Dictates Immune Response. *J. Am. Chem. Soc.* **2012,** *134* (9), 3965-3967.

12. van Dongen, M.; Dougherty, C. A.; Banaszak Holl, M. M., Multivalent Polymers for Drug Delivery and Imaging: The Challenges of Conjugation. *Biomacromolecules* **2014,** *15*, 3215-3234.

13. Duhamel, J., Global Analysis of Fluoresence Decays to Probe the Internal Dynamics of Fluorescently Labeled Macromolecules. *Langmuir* **2014,** *30*, 2307-2324.

14. Dougherty, C. A.; Furgal, J. C.; van Dongen, M. A.; Goodson, T.; Holl, M. M. B.; Manono, J.; DiMaggio, S., Isolation and Characterization of Precise Dye/Dendrimer Ratios. *Chem. Eur. J.* **2014,** *20* (16), 4638-4645.

15. Pansare, V. J.; Hejazi, S.; Faenza, W. J.; Prud'homme, R. K., Review of Long-Wavelength Optical and NIR Imaging Materials: Contrast Agents, Fluorophores, and Multifunctional Nano Carriers. *Chem. Mater.* **2012,** *24* (5), 812-827.

16. Wangler, C.; Moldenhauer, G.; Saffrich, R.; Knapp, E. M.; Beijer, B.; Schnolzer, M.; Wangler, B.; Eisenhut, M.; Haberkorn, U.; Mier, W., PAMAM Structure-Based Multifunctional Fluorescent Conjugates for Improved Fluorescent Labelling of Biomacromolecules. *Chem. Eur. J.* **2008,** *14* (27), 8116-8130.

17. Kim, Y.; Kim, S. H.; Tanyeri, M.; Katzenellenbogen, J. A.; Schroeder, C. M., Dendrimer Probes for Enhanced Photostability and Localization in Fluorescence Imaging. *Biophys. J.* **2013,** *104* (7), 1566-1575.

18. Opitz, A. W.; Czymmek, K. J.; Wickstrom, E.; Wagner, N. J., Uptake, effux, and mass transfer coefficient of fluorescent PAMAM dendrimers into pancreatic cancer cells. *Biochem. Biophys. Acta* **2013,** *1828*, 294-301.

19. He, C. B.; Hu, Y. P.; Yin, L. C.; Tang, C.; Yin, C. H., Effects of particle size and surface charge on cellular uptake and biodistribution of polymeric nanoparticles. *Biomaterials* **2010,** *31* (13), 3657-3666.

20. Santos, J. L.; Oliveira, H.; Pandita, D.; Rodrigues, J.; Pego, A. P.; Granja, P. L.; Tomas, H., Functionalization of poly(amidoamine) dendrimers with hydrophobic chains for improved gene delivery in mesenchymal stem cells. *J. Controlled Release* **2010,** *144* (1), 55-64.

21. Shakhbazau, A.; Isayenka, I.; Kartel, N.; Goncharova, N.; Seviaryn, I.; Kosmacheva, S.; Potapnev, M.; Shcharbin, D.; Bryszewska, M., Transfection efficiencies of PAMAM dendrimers correlate inversely with their hydrophobicity. *Int. J. Pharm.* **2010,** *383* (1-2), 228-235.

22. Vuorimaa, E.; Urtti, A.; Seppanen, R.; Lemmetyinen, H.; Yliperttula, M., Time-resolved fluorescence spectroscopy reveals functional differences of cationic polymer-DNA complexes. *J. Am. Chem. Soc.* **2008,** *130* (35), 11695-11700.

23. Ketola, T. M.; Hanzlikova, M.; Urtti, A.; Lemmetyinen, H.; Yliperttula, M.; Vuorimaa, E., Role of Polyplex Intermediate Species on Gene Transfer Efficiency: Polyethylenimine-DNA Complexes and Time-Resolved Fluorescence Spectroscopy. *J. Phys. Chem. B.* **2011,** *115* (8), 1895-1902.

24. Yoo, H.; Juliano, R. L., Enhanced delivery of antisense oligonucleotides with fluorophore-conjugated PAMAM dendrimers. *Nucleic Acids Res.* **2000,** *28* (21), 4225-4231.

25. Seib, F. P.; Jones, A. T.; Duncan, R., Establishment of subcellular fractionation techniques to monitor the intracellular fate of polymer therapeutics I. Differential centrifugation fractionation B16F10 cells and use to study the intracellular fate of HPMA copolymer-doxorubicin. *J. Drug Target.* **2006,** *14* (6), 375-390.

26. Yang, Y.; Sunoqrot, S.; Stowell, C.; Ji, J. L.; Lee, C. W.; Kim, J. W.; Khan, S. A.; Hong, S., Effect of Size, Surface Charge, and Hydrophobicity of Poly(amidoamine) Dendrimers on Their Skin Penetration. *Biomacromolecules* **2012,** *13* (7), 2154-2162.

27. Perumal, O. P.; Inapagolla, R.; Kannan, S.; Kannan, R. M., The effect of surface functionality on cellular trafficking of dendrimers. *Biomaterials* **2008,** *29* (24-25), 3469-3476.

28. van Dongen, M. A.; Desai, A.; Orr, B. G.; Baker, J. R.; Holl, M. M. B., Quantitative analysis of generation and branch defects in G5 poly(amidoamine) dendrimer. *Polymer* **2013,** *54* (16), 4126-4133.

29. Mullen, D. G.; Borgmeier, E. L.; Desai, A. M.; van Dongen, M. A.; Barash, M.; Cheng, X. M.; Baker, J. R.; Holl, M. M. B., Isolation and Characterization of Dendrimers with Precise Numbers of Functional Groups. *Chem. Eur. J.* **2010,** *16* (35), 10675-10678.

30. Selwyn, J. E.; Steinfeld, J. I., Aggregation Equilibria of Xanthene Dyes. *J. Phys. Chem.* **1972,** *76* (5), 762-774.

31. van Dongen, M.; Orr, B. G.; Banaszak Holl, M. M., Diffusion NMR Study of Generation Five PAMAM Dendrimer Materials. *J. Phys. Chem. B.* **2014,** *118*, 7195-7202.

32. Chen, L. C.; Lloyd, W. R.; Chang, C. W.; Sud, D.; Mycek, M. A., Fluorescence Lifetime Imaging Microscopy for Quantitative Biological Imaging. *Methods Cell Biol.* **2013,** *114*, 457-488.

33. Lin, H.-J.; Herman, P.; Lakowicz, J. R., Fluorescence Lifetime-Resolved pH Imaging of Living Cells. *Cytometry Part A* **2003,** *52A*, 77-89.

34. Unruh, J. R.; Gokulrangan, G.; Wilson, G. S.; Johnson, C. K., Fluoresence Properties of Fluorescein, Tetramethylrhodamine and Texas Red Linked to a DNA Aptamer. *Photochem. Photobiol.* **2005,** *81*, 682-690.

35. Thomas, T. P.; Majoros, I.; Kotlyar, A.; Mullen, D.; Holl, M. M. B.; Baker, J. R., Cationic Poly(amidoamine) Dendrimer Induces Lysosomal Apoptotic Pathway at Therapeutically Relevant Concentrations. *Biomacromolecules* **2009,** *10* (12), 3207-3214.

36. Xu, Z. J.; He, B. C.; Shen, J.; Yang, W. T.; Yin, M. Z., Fluorescent water-soluble perylenediimide-cored cationic dendrimers: synthesis, optical properties, and cell uptake. *Chemical Communications* **2013,** *49* (35), 3646-3648.

37. Ornelas, C.; Lodescar, R.; Durandin, A.; Canary, J. W.; Pennell, R.; Liebes, L. F.; Weck, M., Combining Aminocyanine Dyes with Polyamide Dendrons: A Promising Strategy for Imaging in the Near-Infrared Region. *Chem. Eur. J.* **2011,** *17* (13), 3619-3629.

38. Ornelas, C.; Pennell, R.; Liebes, L. F.; Weck, M., Construction of a Well-Defined Multifunctional Dendrimer for Theranostics. *Org. Lett.* **2011,** *13* (5), 976-979.

39. Vámosi, G.; Gohlke, C.; Clegg, R. M., Fluorescence Characteristics of 5-Carboxytetramethylrhodamine Linked Covalently to the 5' End of Oligonucelotides: Multiple Conformers of Single-Stranded and Double-Stranded Dye-DNA Oligomers. *Biophys. J.* **1996,** *71*, 972-994.

40. Rattan, R.; Vaidyanathan, S.; Wu, G. S. H.; Shakya, A.; Orr, B. G.; Holl, M. M. B., Polyplex-Induced Cytosolic Nuclease Activation Leads to Differential Transgene Expression. *Mol. Pharmaceutics* **2013,** *10* (8), 3013-3022.

Chapter 5 Cationic Vector Intercalation into the Lipid Membrane Enables Intact Polyplex DNA Escape from Endosomes for Gene Delivery

Submitted to the journal Molecular Pharmaceutics for publication

INTRODUCTION

Non-viral vectors have been extensively investigated for the delivery of plasmid DNA (pDNA) for gene therapy and biopharmaceutical manufacturing with limited successes.[1–6] Despite years of research, there is no consensus on cellular pathways and the physicochemical properties of vectors that enable successful transport of plasmid DNA (pDNA) to the nucleus, as is necessary for protein expression. Proposed factors critical for nuclear transport of pDNA include 1) endosomal release[1,4,5,7–9] 2) protection from nucleases[10,11] 3) release of pDNA from vector[8] 4) transport to specific internal organelles[12–14] 5) cell division and/or interaction with other nuclear pore or cytosolic components.[15–19]

Cationic polymer-pDNA complexes (polyplexes) enter cells by adsorption-mediated endocytosis and accumulate in endosomes.[20–23] Endosomal release of pDNA followed by entry into the nucleus has been widely held to be critical for successful gene expression.[1,4,5,7–9] The popular "proton sponge hypothesis" points to the buffering activity of cationic vectors as the critical parameter responsible for endosomal release and the therapeutic activity of nucleotides.[4,5,7–9] However, studies tracking the colocalization of vector and pDNA labeled with pH sensitive fluorophores in single endosomes do not support this hypothesis.[24,25] Moreover,

Hennink et al. synthesized a newpolymer with better buffering capacity and observed that the polymer did not exhibit good transfection abilities.[26] Furthermore, the proton sponge model also does not attribute a vector property for the entry of pDNA into the nucleus. Although some studies have pointed to cell division as a pathway for nuclear entry,[15,17,27,28] other studies have found that expression can occur without cell division.[18,29–33] To understand pDNA transport to the nucleus, microscopy studies have tracked the transport of pDNA to multiple organelles such as endosomes, lysosomes, endoplasmic reticulum (ER) and Golgi apparatus.[12–14] However, the relative importance of pDNA transport to these organelles in enabling protein expression is unknown. The degradation of DNA within a cell further complicates the tracking of DNA using fluorescence techniques, as it is unknown if the DNA observed in a given organelle has been protected successfully from the action of nucleases.

In this study, we used an oligonucleotide FRET probe (OMB) to track the location of both *intact* and cleaved DNA material. We chose this strategy because degradation of pDNA by cytosolic nucleases has been proposed to be one of the factors limiting gene delivery to the nucleus.[11,34–36] Therefore, information about the intactness of the DNA as function of cellular location, including organelles, would enable us to identify transport pathways involved in successful protein expression. To correlate differences in transport of intact DNA to protein expression, we used the vectors jetPEI and G5 PAMAM dendrimers which show a >10 fold difference in protein expression. The results obtained by employing this OMB inform us about the following key hypotheses (H1 and H2) related to optimal vector design:

H1: The limiting step for gene delivery is the endosomal release of DNA. Therefore, vectors that most effectively release of DNA from endosomes allow more gene expression. OMBs delivered using jetPEI were released into the cytosol in a higher fraction of cells (88 ± 5 %) than OMBs

delivered using G5 PAMAM (9 ± 1 % %). Thus, the fraction of cells showing diffuse distribution is proportional to fraction of cells in which protein expression was induced by jetPEI (80 ± 10 %) and G5 PAMAM polyplexes (4 ± 1 %).

H1a: Endosomal release occurs via vectored-mediated pH buffering (proton sponge hypothesis)

H1b: Vector intercalation into, and destabilization of, the endosomal membrane drives endosomal release.

Adding L-PEI to cells 3 h after incubation with G5 PAMAM polyplexes induced a diffuse OMB distribution, fluorescence in the nucleus and also increased expression by 10X as compared to G5 PAMAM alone. The new expression level is comparable to L-PEI or jetPEI polyplexes. This data indicates that L-PEI need only be present in the cells. L-PEI is not required to be part of the internal cargo from the initial absorptive endocytosis of the polyplex. This result is consistent with H1b and inconsistent with H1a.

H2: Vectors that optimize other factors such as cellular uptake of polyplexes, protection of DNA from nucleases and transport DNA to specific organelles cells allow more protein expression. JetPEI polyplexes provide a similar degree of uptake into cells as compared to G5 PAMAM polyplexes, protect DNA for a shorter duration and show similar levels of transport to the ER and Golgi apparatus despite having >10 fold higher protein expression. Thus, this study reinforces the generally held view that uptake and nuclease protection are necessary, but not a sufficient, criterion for efficient gene expression. The intracellular location rather than the relative amount of *intact* DNA is the critical factor.

The results (when combined with previously published data on vector-cell membrane interactions[37]) indicate that the ability of free vectors to interact with lipid bilayers is the key physicochemical property that enables polyplexes to overcome the limiting steps of endosomal release and entry to the nucleus from the cytosol (Scheme 1). The results also point to a strategy in which the DNA delivery into endosomes and subsequent release of DNA are achieved by two different vectors. Since endosomal escape is also important for other intracellular protein therapeutics, the results could also help design better carriers for protein delivery.[38,39]

RESULTS

Proof of concept: OMB exhibits FRET in solution and FRET is abolished by S1 nuclease treatment

To elucidate the relative importance of different transport pathways, we designed a single stranded oligonucleotide molecular beacon (OMB) that reports the location of both *intact* and *cleaved* DNA. The OMB contains a FRET dye pair AF488 and AF594 (AF488-CCTCGTCCATACCCAAGAAGGAAGCGAGG-AF-594, Figure 5.1) with a nuclease sensitive loop. We quantified the extent of FRET (Intactness, *I*) using equation 1. The detailed OMB design (Figure D.1) and FRET quantification (Figure D.2), proof of concept (Figure D.3) and potential errors (Figures D.4-5) are provided in supplemental material.

$$I = \frac{AF594_{FRET} - Noise}{AF594_{direct}} * 100 \; = \frac{I_{D\ ex,Aem} - I_{noise}}{I_{A\ ex,Aem}} * 100 \qquad (1)$$

The OMB FRET properties were tested in aqueous solution (Figure D.3). The OMB exhibits FRET (Intactness = 12) in the absence of S1 nuclease and the FRET emission decreases (Intactness = 0.2) to background levels in the presence of S1 nuclease.

Successful Protein Expression is due to Release from Endosomes and not Because of Transport to Other Organelles

In order to relate differences in the transport of intact DNA to gene expression, we used the vectors jetPEI and G5 PAMAM since they show a >20 fold difference in protein expression. JetPEI and G5 PAMAM polyplexes containing green fluorescent protein (GFP) pDNA induced expression in 80 ± 10 % and 4 ± 1% of transfected HEK 293A cells, respectively (Figure 5.1e). In order to understand the cellular distribution of the OMB, cells were treated with mixed polyplexes containing a 50:50 mixture of blank pDNA and OMB and imaged using confocal microscopy. Microscopy experiments used blank pDNA of similar size to the GFP pDNA because GFP fluorescence emission is in the same range as AF488 and can confound images. 88 ± 5 % of the cells incubated with jetPEI polyplexes show a diffuse OMB distribution throughout the cytosol (Figure 5.1a). By way of contrast, only 9 ± 1 % of cells incubated with G5 PAMAM polyplexes show a diffuse OMB distribution in the cytosol (Figure 5.1b). An intactness map of OMB in the cytosol generated by using equation 1 on a pixel by pixel basis showed that OMBs released into the cytosol were *intact* (Figure 5.1c-d). Overall, the fraction of cells displaying *intact* OMB diffusely distributed in the cytosol at 4 h (Figure 5.1a-b) was similar to the fraction of cells expressing GFP for both jetPEI and G5 PAMAM (Figure 5.1e). The fraction of cells exhibiting OMB distribution and the fraction expressing GFP was significant significantly higher for jetPEI than G5 PAMAM ($p < 0.001$ and power = 1).

The release of intact DNA in the cytosol from G5 PAMAM and jetPEI polyplexes was measured at different time points (1 ,2 , 4, 8, 12, and 24 h) (Figure 5.2 – single cells, Figure D.6 – multiple cells). For jetPEI polyplexes, the release of intact DNA into the cytosol started at 2 h and persisted until at least 8 h (Figure 5.2). Although the quick release of the beacon from the

jetPEI polyplexes is critical for gene expression, the release also results in the degradation of the OMBs in the cell. By way of contrast, OMBs delivered by G5 PAMAM are significantly more intact at all time points (Figure 5.2c) but completely *ineffective* for gene expression because they remain localized in endosomes. The quick degradation of OMB delivered using jetPEI was also confirmed in a population of cells using flow cytometry (Figures D.S7, 8). Thus, these population-level results are consistent with the observations and conclusions obtained using confocal fluorescence microscopy.

In order to test if there were differences in the amount of *intact* OMB present in other organelles, we stained cells using organelle markers for ER (ER tracker blue) and Golgi apparatus (wheat germ agglutinin-AF 350, WGA). Figures D.S9 and 10 illustrate the colocalization of *intact* and *cleaved* OMBs delivered using jetPEI and G5 PAMAM with ER tracker blue and WGA. Colocalization was quantified using Mander's coefficients combined with manual thresholding to ensure that background noise did not confound colocalization coefficients.[40] A two sample t-test was used to test if the colocalization of the *intact* or *cleaved* OMB signals with organelle markers were significantly different (Table I and II in Appendix D). For Golgi apparatus, the intact OMB channel (AF 594 FRET) alone showed a lower colocalization with the wheat germ agglutinin when delivered using jetPEI. This can be explained by the fact that OMBs delivered by jetPEI are released into the cytosol. Similarly, the overlap of AF 488 channel (cleaved OMB) and AF 594 direct channel (all OMB) with ER marker was significantly higher for jetPEI. Once again, this difference can be explained by the release of OMB into the cytosol when delivered using jetPEI. Thus, differences in colocalization are due to release of OMB into cytosol and colocalization with ER and Golgi markers do not appear related to the 20-fold difference in expression efficiency.

Loading pDNA in endosomes using G5 PAMAM and Releasing them Using L-PEI Increases Protein Expression

The results quantitatively show that successful endosomal escape distinguishes effective vectors from ineffective vectors. We then probed if endosomal escape can be mediated by a vector different from the vector used to form polyplexes. We discovered that adding L-PEI at various time points to cells incubated with G5 PAMAM polyplexes (along with, 1 h before or 1 h after G5 PAMAM polyplex addition) induced OMB release into the cytosol, movement of OMB into the nucleus, and increased protein expression by >10 fold (Figure 5.3). L-PEI was used instead of jetPEI because it provided similar expression to jetPEI (a proprietary version of L-PEI) and avoids unknown components present in jetPEI. In the experiment in which L-PEI was co-incubated with G5 PAMAM, previously published NMR and fluorescence results suggest that L-PEI will exchange with the G5 PAMAM polyplexes prior to cellular uptake.[41,42] The L-PEI containing polyplexes then change the OMB cellular distribution from that expected for G5 PAMAM polyplexes and increased protein expression.[41,42] To avoid this polymer exchange process, cells were incubated with free L-PEI before or after incubation with G5 PAMAM polyplexes and this still resulted in the same diffuse OMB distribution and increased protein expression. In the pre and post-incubation experiments the cells were washed with complete media and fresh media was added before the addition of polyplexes or free L-PEI. In all cases, the fraction of cells displaying OMB in the cytosol was greater than the fraction of cells expressing GFP (Figure 5.3m). In the experiments described above, the concentration of L-PEI was the same as that present in N:P 10 polyplexes. We also tested if lower concentrations of L-PEI could achieve a similar increase in gene expression. Free L-PEI can increase the fraction of cells expressing GFP by 10X even at the concentration equivalent of an N:P = 1:1 L-PEI

polyplex (Figure D.11). Finally, the presence of OMB in the nucleus is also consistent with earlier reports that polyplexes can interact with nuclear membranes and that L-PEI further facilitated the entry of the nucleotides into the nucleus.[19,32,43,44]

Since decreasing polymer concentrations can improve cell survival, we also tested to see if the load-release strategy could be exploited to increase bulk protein production using a luciferase system. Figure 5.3n shows that pure L-PEI polyplexes at N:P = 3:1 show no gene expression. However, the addition of L-PEI to cells treated with G5 PAMAM polyplexes (N:P = 3) shows 8X more luciferase expression. At higher N:P ratios, pure L-PEI polyplexes provide the same or higher luciferase activity as the two step process. Thus, experiments in Figure 5.3 show that endosomal release and nuclear entry of DNA is mediated by free vector as opposed to intact polyplexes.

We also tested if adding other cationic vectors can induce endosomal release and increased gene expression. The addition of extra G5 PAMAM to cells along with, before or after incubation with G5 PAMAM polyplexes resulted in a 2-fold increase in fraction of cells displaying OMB in the cytosol but < 2-fold increase in the fraction of cells expressing GFP (Figure 5.4a-c,g). For this reason, another cationic material was selected that gives high expression efficiency polyplexes. The co-incubation of lipofectamine and G5 PAMAM polyplexes resulted in a > 10-fold increase in cells displaying *intact* OMB cytosol, nuclear permeabilization and cells expressing GFP (Figure 5.4e,h) but pre- or post-treatment of cells with lipofectamine did not induce a diffuse OMB distribution and only increased expression by 2-fold (Figure 5.4d,f,h). It is likely in the co-incubation case, the lipofectamine exchanged some G5 PAMAM present in polyplexes to form Lipofectamine polyplexes.[41,42] These results suggest that lipofectamine is most effective when initially incorporated into the endosome along with the polyplex and that

trafficking from the plasma membrane to internal membrane and inducing endosomal permeability release is less effective than L-PEI.

DISCUSSION

The readily cleaved single strand sequence of the OMB (Figure D.1) is a good model for the single stranded "hot spots" in pDNA identified by Prazeres et al. and Rattan et al. as being particularly susceptible to nuclease attack.[11,45,46] The dye pair was selected for photostability and because the dyes show optimal FRET with minimal bleed through. Specifically, the absorption spectrum of AF594 shows significant overlap with the emission spectrum of AF488 which ensures good FRET transfer. On the other hand, the emission of AF488 has minimal overlap with AF594 emission. These dyes are convenient for studying beacon degradation in populations of cells using flow cytometry and for tracking beacon transport using confocal fluorescence microscopy in single cells. Moreover, the choice of dyes allows us to combine the OMB with organelle markers containing absorbance maxima in the UV or far-red range to study the intracellular location of the OMB by using dyes. When the OMB is intact, excitation of AF488 results in partial energy transfer to AF594 giving both green (525-580 nm) and red (620-700 nm) emission.

A potential drawback of the OMB probe is its small size (30 bases) compared to a pDNA (5000 bases). The very different molecular weights change the diffusion characteristics within the cytosol as shown by Zuhorn et al.[7] Despite this drawback, the OMB does reflect the relative ability of the different vectors to facilitate release and subsequent expression of intact genetic material. We considered the possibility of pDNA-based FRET probes for these studies. Kataoka et al. previously used a pDNA labeled with Fluorescein and Rhodamine to study the degree of relaxation of pDNA present in polyplexes.[8] They observed that pDNA delivered using linear PEI

was more relaxed than pDNA delivered using branched PEI. Although this study provided information regarding pDNA unpacking, it did not address the question nuclease-induced cleavage and whether the pDNA was still viable for expression. Methods have been described in literature that would allow the insertion of FRET pair of dyes to specific nuclease sensitive sequences within pDNA.[47–49] However, a major drawback with this approach is the promiscuity of nuclease and the vast number of cleavage sites observed on pDNA.[11] Hence, the intactness reported by a pDNA beacon with just one or two FRET sites would greatly over report the true intactness, and there viability, of the pDNA. Indeed, almost all cleaved pDNA would be reported as intact and viable when it was in fact no longer active on the expression pathway. This challenge is the major reason we have employed a small single strand sequence that models pDNA single strand "hot spots".[11,45,46]

Previous studies have observed that the addition of free L-PEI to cells treated with L-PEI polyplexes increased protein expression and the removal of L-PEI decreased protein expression.[36,50–52] Shubert et al. showed that L-PEI polyplex formulations with N:P ratios ≥ 10 which show the best transfection have more than 70% free L-PEI.[53] Similarly, Baker et al. also co-incubated DEAE-Dextran to improve transfection by G5 PAMAM polyplexes.[3] Although these studies showed the ability of free vectors to increase protein expression, there is no consensus on their mechanism of action. Some previous studies had suggested that free PEI helped overcome the inhibitory effect of cell surface glycosaminoglycans on cellular uptake.[22,23] Our results suggest that the enhanced expression obtained by adding free L-PEI is due to the facilitation of endosomal escape and transport of DNA into the nucleus. The results also (summary in Figure Figure D.12) suggest that endosomal release is not mediated by intact

polyplexes inside endosomes but mediated by free vectors released from polyplexes that have intercalated into endosomal membranes.

The importance of endosomal release in gene delivery seen in our results is broadly consistent with the proton sponge hypothesis. However, the ability of L-PEI to induce the endosomal release of DNA when delivered separately is inconsistent with the proton sponge hypothesis as it suggests that endosome rupture is mediated by the buffering activity of polyplexes from within the endosome.[4,5,9,21] Moreover, the inability of G5 PAMAM, which has a high buffering capacity, to mediate endosomal release of intact pDNA is also inconsistent with the hypothesis. Moreover, recent studies report that endosomal release leaves behind intact endosomes.[7,54] The intact endosomes are not consistent with the more dramatic rupture of vesicles proposed by proton sponge. Thus, an alternate physicochemical property of L-PEI that can explain its ability to permeabilize both endosomal and nuclear membranes, and which leaves behind intact endosomes, needs to be identified.

We propose that high partition constants of free vectors in lipid bilayers and their ability to disrupt lipid bilayers are critical for successful gene delivery. Although the importance of polyplex-membrane interactions in enabling gene expression have been investigated and no correlation was observed, [11,19,37,44,55] a reanalysis indicates that *free vector-cell membrane interactions* reported from our previous studies are related to gene expression.[11,37] Specifically, L-PEI permeabilized cell membranes of HEK 293A at concentrations 5X lower than G5 PAMAM and had a 1.6X higher equilibrium partition constant in the plasma membrane than G5 PAMAM.[37] Moreover, the ability of free vectors (but not polyplexes) to induce increased permeability in HeLa cells also predicts their ability to induce gene expression.[11] Thus, the ability of free L-PEI to induce endosomal release can be explained by L-PEI's ability to

intercalate into and permeabilize the endosomal membrane. However, it is unclear if the increase in nuclear transport of DNA is mediated by the action of free L-PEI or polyplexes. The doubling time of HEK 293A cells is > 24h.[33] The presence of intact OMB in the nucleus as early as 2h and the degradation of DNA within 8h in the cytosol both support the argument that cell division is not the major means of transport of DNA to the nucleus. Zuhorn et al. also reported distribution of both free 20-mer DNA and L-PEI in the cytosol and the rapid import of small oligonucleotides in the nucleus, which does not leave enough time for nuclear transport mediated by cell division.[7] Other studies have also observed polyplex/polymer mediated nuclear membrane permeability.[44] Free vectors and polyplexes could reach the nuclear membrane by either free diffusion or by lipid recycling. Verkman et al. have shown that polymers under 500 kD are capable of diffusion in the cytosol but diffusion is very slow for bare DNA.[43,56] Escande et al. showed that polyplexes were transported 10 fold more effectively to nuclei than bare DNA.[32] Our previous study showed that cationic polymers can associate with cell membranes for several minutes. This also allows for the possibility of their transport to other cell organelles by means of lipid recycling pathways. Finally, the distribution of cationic vectors to other cell organelles can also explain the cytotoxicity induced by these materials by increasing mitochondrial membrane permeability.

It is unclear if the membrane intercalation model can explain gene expression by lipofectamine since endosomal release and nuclear transport of DNA was only achieved if vector was delivered along with DNA. Further studies that quantify the interaction of lipofectamine (and other lipid vectors) with the cell plasma membrane can inform us if the membrane intercalation model can explain the effectiveness of lipid vectors.

CONCLUSION

In conclusion, we propose a model for transfection and expression by cationic polymers in which intercalation of free vector into the lipid membranes promotes endosomal release, nuclear entry and gene expression in the following steps (Scheme 1):

1. Polyplexes delivered to the cell release free vector, smaller polyplexes, and free DNA either near the cell membrane or inside vesicles[41,42,57]
2. Free cationic vector released from polyplexes intercalates into endosomal membranes. The presence of vector *in the membrane* allows endosomal release.
3. Free cationic vector or polyplexes permeabilize the nuclear membrane and enables the pDNA to enter the nucleus and express the gene of interest

Cationic vector – cell membrane interactions have generally been viewed as a property important only in the context of complexing DNA and inducing cytotoxicity. By way of contrast, our studies suggest that the charge mediated vector-cell membrane interaction is the critical parameter that mediates release of intact DNA into the cytosol and that is a critical step for successful gene expression. The results also highlight a two-step strategy for gene delivery in which a less cytotoxic agent is used to load cargo into endosomes and lower concentrations of a more cytotoxic agent are added to induce endosomal release. This two-step strategy may also be extended to promote the endosomal release of other therapeutic cargo such as peptides, proteins and small molecules.

EXPERIMENTAL METHODS

Materials: G5 PAMAM dendrimers were obtained from Dendritech, Inc. (Midland, MI). jetPEI and L-PEI were obtained from Polysciences, Inc (Warrington, PA). Other reagents were obtained

from Fisher Scientific unless specified otherwise. DMEM High Glucose with Sodium Pyruvate and Glutamine (Life technologies, Cat. No: 11995) was the base media. Complete media was made by adding 50 mL of Fetal Bovine Serum, 5 mL of Non-essential Amino Acids (Thermo Scientific) and 5mL of Penicillin-Streptomycin to 500 mL DMEM. PBS (1X) without Ca^{2+} and Mg^{2+} was obtained from Life Technologies. Luciferase plasmid (pGL4.51) were purchased from Promega Corp. HEK293A cells (a sub-clone of HEK293) were obtained from ATCC (Cat. No. CRL-1573). The cell line was tested negative for mycoplasma, expanded and cryopreserved in liquid nitrogen (Cat. No. 6601; Takara Bio; Kyoto, Japan).

FRET Beacons and Control Beacons: Molecular beacon DNA sequence 5'-CCTCGTCCATACCCAAGAAGGAAGCGAGG -3' which is sensitive to nucleases functionalized with FRET pair dyes Alexa-Fluor (AF) 488 and AF594 at the 5' and 3' ends respectively was custom synthesized by Integrated DNA technologies. For the 5' modification Alexa 488 Azide was clicked on to the DNA modified with DBCO moiety. This click reaction as copper free. The 3' addition of AF594 was an NHS ester coupling. Two control beacons were also purchased. These consisted of the same sequence but had either AF488 or AF594 attached to them. The dyes in the single labeled oligonucleotides were both NHS ester coupled to the amines on the ends of the DNA.

Cell Culture: HEK 293 A cells at 50,000 cells/well in 1 mL of complete media were incubated overnight in either a two well confocal chamber or in a 24 well plate over-night. The cells were transfected with jetPEI^{TM}, G5 PAMAM, or L-PEI polyplexes and incubated at 37^{o} C in 450 μL of serum free media.

Polyplex preparation and Transfection: Polyplexes containing 1 μg of total DNA with N:P ratio of 10 were made by adding equal volumes of polymer to DNA in water. The polyplexes

contained 0.5 µg of beacon DNA and 0.5 µg of plasmid DNA. The mixture was allowed to incubate for 20 minutes. Here, N and P represent the cationic amine groups in the vector and the anionic phosphate groups in the DNA, respectively. At N:P=10, polyplexes are positively charged. HEK 293 A cells were grown in complete DMEM over night at a density of 50,000 cells/well. For transfection, 50 µL of polyplex solution was added to 50,000 cells plated in 450 µL of serum free DMEM. Transfected cells were incubated with beacons for 3 h in serum free DMEM. After 3 h, the media was aspirated and replaced with complete DMEM. Confocal microscopy of the cells between 0-3 h was performed in the serum free DMEM containing polyplexes. This contributed to a higher background signal in these images.

Gene Expression: Gene expression abilities of vectors were tested by transfecting cells with plasmid coding for GFP. HEK 293 A cells were plated overnight in 24 well sterile plates at a density of 50000 cells per well. Polyplexes containing 1 µg of pDNA with N:P ratio of 10 were made by adding equal volumes of polymer to pDNA in water. The mixture was allowed to incubate for 20 minutes. For transfection, 50 µL of polyplex solution was added to 50,000 cells plated in 450 µL of serum free DMEM. Transfected cells were incubated with beacons for 3 h in serum free DMEM. After 3 h, the media was aspirated and replaced with complete DMEM.

For some experiments probing the role of free vectors, additional vector was added along with polyplexes and allowed to incubate for 3 h. To probe if free vectors added at a different time from polyplexes could impact gene expression, we also incubated cells with vectors before (1 h) or after (1 h) incubation with polyplexes. The amount of free vector added was the amount present in polyplexes of N:P ration of 10:1. The serum free media was replaced before or after the incubation with free vectors and the cells were washed three times with serum containing

media. Thus, the media only had either polyplexes or fee vector at any given time. Three biological repeats were performed for each experiment and results report mean and standard deviation.

Luciferase assay: Luciferase assay was purchased from Promega Corp. (Cat # 1500) and the assay was performed as per manufacturer's instructions. Briefly, the cells were washed with PBS. The cells were then lysed using cell culture lysis reagent by adding 100 µL of 1X reagent to each well. 20 µL of lysed cell solution was added to a 96 well luminescence plate. 100 µL of luciferase assay substrate was added to each well and the luminescence was measured using a luminometer (Synergy HT) with an integration time of 10 s.

FRET Confocal Microscopy: Confocal was performed using a Leica SP5 inverted microscope with a 63x objective. The AF488 and AF594 dyes were excited using a tunable white light laser with excitation wavelengths of 488 nm and 594 nm respectively. To measure FRET, images were obtained in a sequence of frames. For the first frame, the cells were excited using the 488 nm laser and the emission between 525-560 nm and between 620-670 nm were collected. For the second frame, the cells were excited using 594 nm wavelength and emission between 525-560 nm and between 620-670 nm were collected. Proof of concept experiments using beacons in solution was also performed using the same protocol except for the fact that a drop of solution placed on a coverslip served as the sample.

FRET flow cytometry: For flow cytometry, media was removed and cells were washed with Ca^{2+} and Mg^{2+} free PBS. 200 µL of trypsin was added to each well and incubated for 2 mins. After 2 min, 800 µL of cold PBS (with Ca^{2+} and Mg^{2+}) was added. The cells were then

centrifuged for 5 min at 2000 rpm. The supernatant was removed and the cells were suspended in 400 µL of PBS (without Ca^{2+} and Mg^{2+}). Flow cytometry was performed using a Synergy head flow cytometer (BD Biosciences). First, the cells were excited using the 488 nm laser and the emission between 525-560 nm and between 620-670 nm were collected. A few milliseconds later, the same cells were excited using 594 nm wavelength and emission between 525-560 nm and between 620-670 nm were collected.

Flow Cytometry to measure GFP Expression: Cells were suspended in PBS as described for the FRET flow cytometry. Flow cytometry was performed using a Accuri C6 flow cytometer. The cells were excited using the 488 nm laser and the emission between 525-560 nm was collected. A total of 10,000 events were collected per sample. Three replicates were performed for each experiment. The results are shown as an average and standard deviation.

Quantification of Intactness:

Confocal microscopy (Intactness maps): In this study, the Intactness (I) was calculated using equation 1. The average FRET signal from the AF594 dye from a box of 4 neighboring pixels was divided by the average signal from AF594 excited by 594 nm from the same four pixels. This FRET efficiency measure was then plotted on a pixel-by-pixel basis to obtain a FRET image.

Flow cytometry: Equation1 was also used for quantifying Intactness from flow cytometry. However, there was no pixel-by-pixel averaging. The numerator was the AF594 signal due to FRET and the denominator was AF594 signal due to direct excitation by 594 nm laser. The Intactness (eq 1) for polyplexes formed with only AF594 was 0.03% for both G5 PAMAM and jetPEI.

Statistical analyses for Intactness: Data from 20 magnified images of cells were used to obtain average FRET indices. Samples were normally distributed and had equal variances. Two-sample t-test (two sided) was used to compare the FRET indices of OMB delivered using jetPEI and G5 PAMAM at each time point. Power test was performed post-hoc and reported with the results. One-way ANOVA followed by Tukey-HSD post-hoc test was performed to test if the mean intactness of OMB delivered using either jetPEI or G5 PAMAM was different across different time points.

Colocalization with Organelle Markers: ER (ER tracker blue) and Golgi (Wheat germ agglutinin-AF 350) purchased from Life Technologies Inc. were used to assess the localization of the intact and cleaved beacons. Wheat germ agglutinin has been shown to be bind to the n-acetylglucoseamines and sialic acids that are rich in the Golgi apparatus.[58] The cells were incubated with the labels as per manufacturer's instructions. The cells labeled with ER tracker were excited using a 405 nm laser and beacons were excited using the 488 nm and 594 nm lasers respectively. The cells labeled with WGA-AF350 were excited using a two photon laser at 750 nm and the beacons were excited using single photon 488 nm and 594 nm confocal setup. The emission ranges were 425-600 nm for the ER tracker blue and 400-500 nm for the wheat germ agglutinin. The excitation and emission were performed in a frame by frame manner. For example, an entire frame was imaged by exciting the organelle labels with the 405 nm laser and emission was collected in the wavelength range appropriate for each label.

Mander's Coefficients: Just Another Colocalization Plug-in (JACoP) in ImageJ[40] was used to quantify the colocalization of the beacon signal with the organelle markers. The plugin allows the user to set a threshold to distinguish the beacon signal from background. Mander's coefficient are then determined to quantify colocalizaton. Briefly, the formula for Mander's

coefficients for two fluorophores G and R respectively are described in equation 3 and 4.[59] M1 quantifies the overlap of G with R and M2 quantifies the overlap of R with G. A Manders colocalization closer to 1 indicates more overlap and coefficients closer to 0 indicates less overlap.

$$M_1 = \frac{\sum R_{icoloc}}{\sum R_{iTotal}} \quad \text{where } R_{iColoc} = R_i \text{ if } G_i > 0 \text{ and } R_{iColoc} = 0, \text{ if } G_i = 0$$

$$M_2 = \frac{\sum G_{icoloc}}{\sum G_{iTotal}} \text{ where } G_{iColoc} = G_i \text{ if } R_i > 0 \text{ and } G_{iColoc} = 0, \text{ if } R_i = 0$$

Statistical analyses for Mander's Coefficients: Data from 15 magnified images of cells were used to obtain average Mander's coeffcients. The experiments are designed such that a 2 fold difference in colocalization can be detected with a power greater than 0.8. Samples were normally distributed and had equal variances. Two-sample t-test (two sided) was used to compare the Mander's coefficients. Power test analysis was performed post-hoc and reported in supplemental material along with the results.

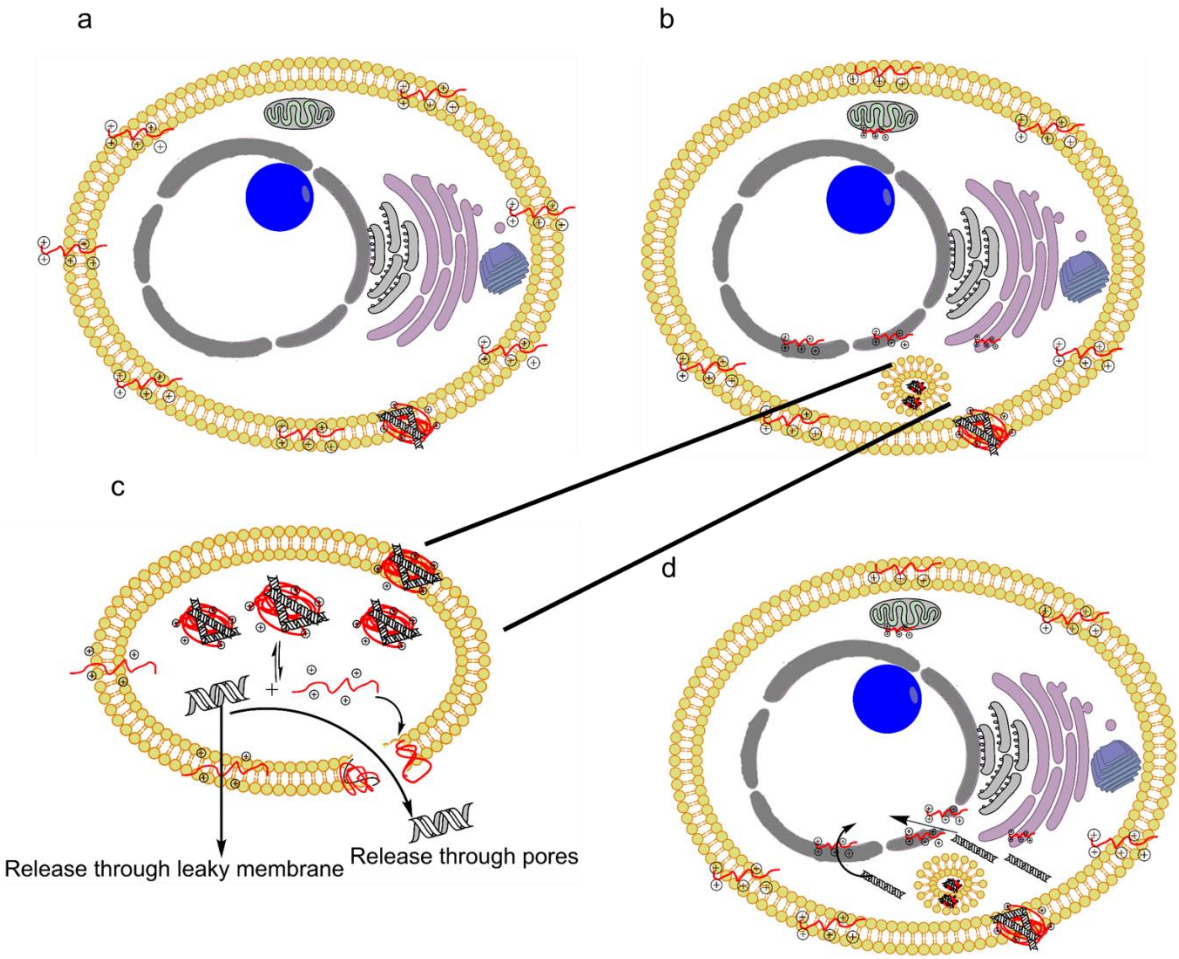

Scheme 5.1. Endosomal Release by Membrane Intercalation of Free Cationic Polymers. (a) Free cationic polymer intercalates into the plasma membrane and/or is released from associated polyplexes. (b) Cationic polymer is dispersed into internal cellular membranes via lipid recycling pathways. Polyplexes are endocytosed. (c) Cationic polymer intercalated into endosomal membranes induces membrane permeability and facilitates release of genetic material into the cytosol. (d) We hypothesize that cationic polymer associated with the nuclear membrane via lipid recycling and/or cytosolic pathways induces permeabilization and facilitates transport into the nucleus.

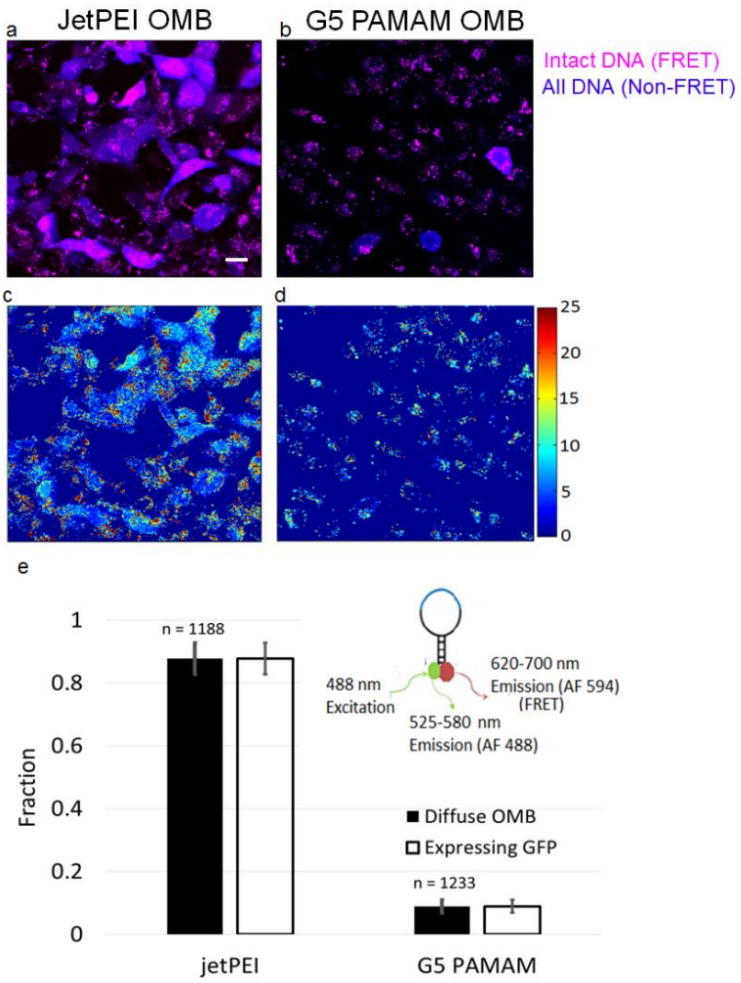

Figure 5.1. The relationship of intact OMB released in the cytosol to GFP expression in HEK 293A cells. (a)OMB delivered using jetPEI polyplexes (N:P 10:1) exhibits diffuse distribution at 4h. (b) OMB delivered using G5 PAMAM polyplexes (N:P 10:1) were confined to vesicles with few cells showing diffuse OMB distribution. (c) The intactness map derived from image (a) shows diffuse, *intact* OMB in the cytosol (d) The intactness map derived from image (b) shows *intact* OMBs confined to vesicles. The Intactness map scale for (c) and (d) is provided to the right of image (d). (e) The fraction of cells (n = total number of cells counted from 10 images each obtained from 3 biological replicates) showing diffuse OMB distribution in the cytosol (jetPEI = 88 ± 5 %, G5 PAMAM = 9 ± 2 %) corresponds to the fraction of cells expressing GFP (jetPEI = 80 ± 5 %, G5 PAMAM 4 ± 1 %). Inset shows OMB employed for FRET studies.

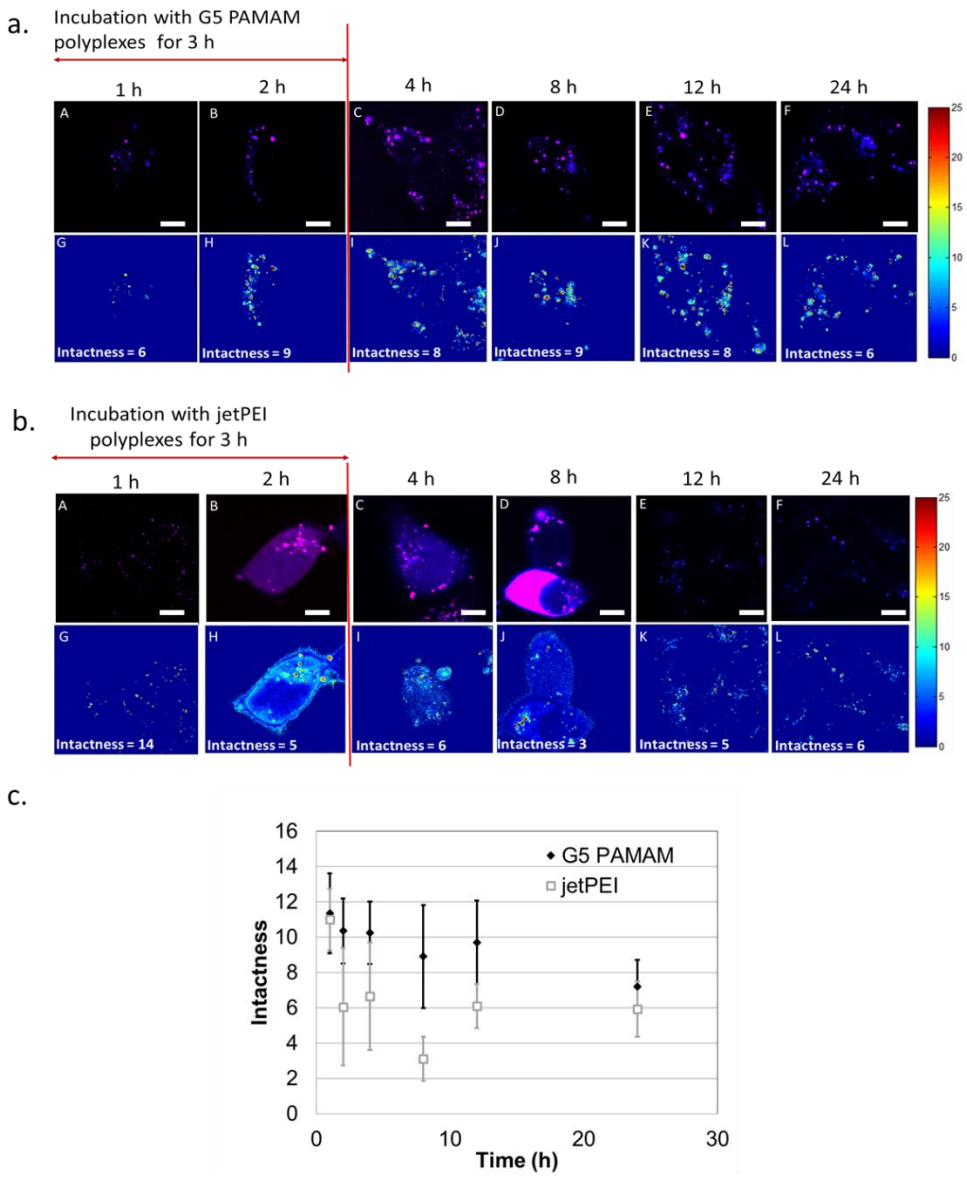

Figure 5.2. Release and degradation of OMB over time in HEK 293A cells. (a) OMBs delivered using G5 PAMAM polyplexes (N:P 10:1) were confined to vesicles for 24 h. (b) OMB delivered using jetPEI polyplexes (N:P 10:1) were confined to vesicles at 1 h but gave a diffuse distribution of *intact* OMB in the cytosol from 2 to 8 h. The intact OMB in the cytosol dissipated by 12 h (panels G-L) and the remaining intact OMB was confined to vesicles. The Intactness map scale for panels (G-L) is provided to the right of images (a) and (b). (c) The average intactness for both jetPEI and G5 PAMAM delivered OMBs decreased over time. For jetPEI, ANOVA followed by Tukey's post-hoc test showed that the average intactness was significantly lower after 2 h due to release of the OMB into the cytosol. Even though the delivery of OMB with jetPEI resulted in lower *intactness* at all time points after 1 h compared to G5 PAMAM (two sided t-test, n=20, $p < 0.001$, power = 1), the ability of jetPEI to release *intac*t DNA into the cytosol enables ~ 20 fold higher gene expression.

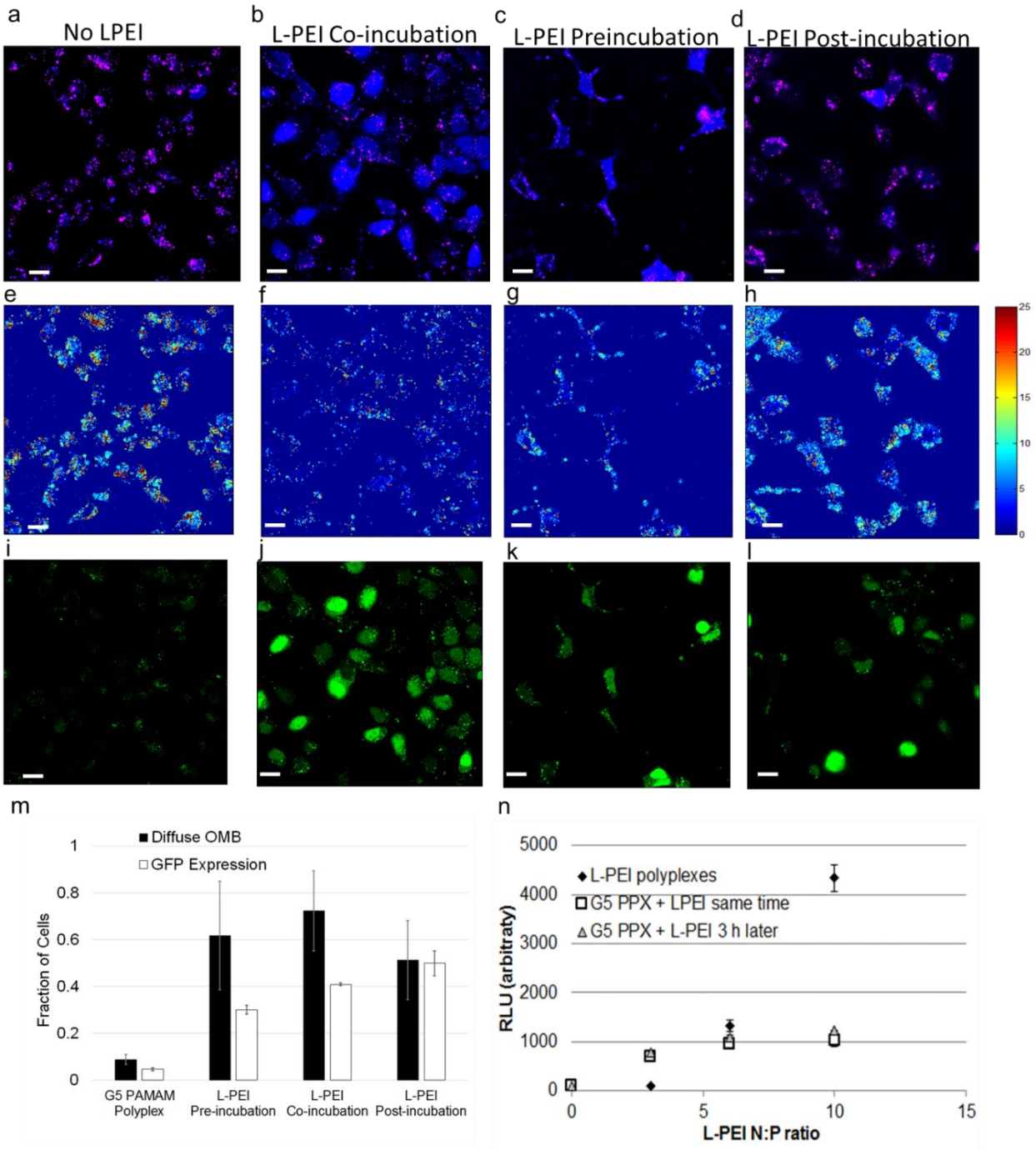

Figure 5.3. **Free L-PEI mediates endosomal release in HEK 293A cells.** (a) Incubation with G5 PAMAM N:P 10:1 polyplexes containing OMB and blank pDNA for 3 h results in confinement of OMB to vesicles. (b) Co-incubation of cells with G5 PAMAM polyplexes and free L-PEI results in diffuse, cytosolic OMB distribution. (c) Pre-treatment of cells with L-PEI for 1 hr prior to G5 PAMAM polypex incubation results in diffuse, cytosolic OMB distribution. (d) Treatment of cells with L-PEI for 1 h following 3 h G5 PAMAM polyplex incubation results in diffuse, cytosolic OMB distribution. (e-h) Intactness maps derived from images a-d are given

as e-h, respectively. The Intactness map scale for (e-h) is provided to the right of image h. (i) Fluorescence emission of AF488 (FRET donor) for cells exposed to G5 PAMAM polyplex only does not exhibit nuclear localization (j –l) Fluorescence emission of AF488 for cells with free L-PEI added demonstrates nuclear localization. (m) Pre-incubation, co-incubation and post-incubation of L-PEI with G5 PAMAM polyplexes increases both fraction of cells displaying diffuse OMB and fraction of cells expressing GFP by >10-fold. (n) Transfection with luciferase plasmids using L-PEI (N:P = 3:1, 6:1, 10:1) or G5 PAMAM polyplexes (N:P = 3:1). Cells treated with G5 PAMAM polyplexes and then exposed to free L-PEI showed ~ 8X more luciferase expression. For flow cytometry experiments, data are presented as mean± standard deviation of three biological replicates. For all images (a, c, e, g) blue indicates = all DNA, pink = intact OMB (AF 594 emission by FRET). Scale bar is 20 µm.

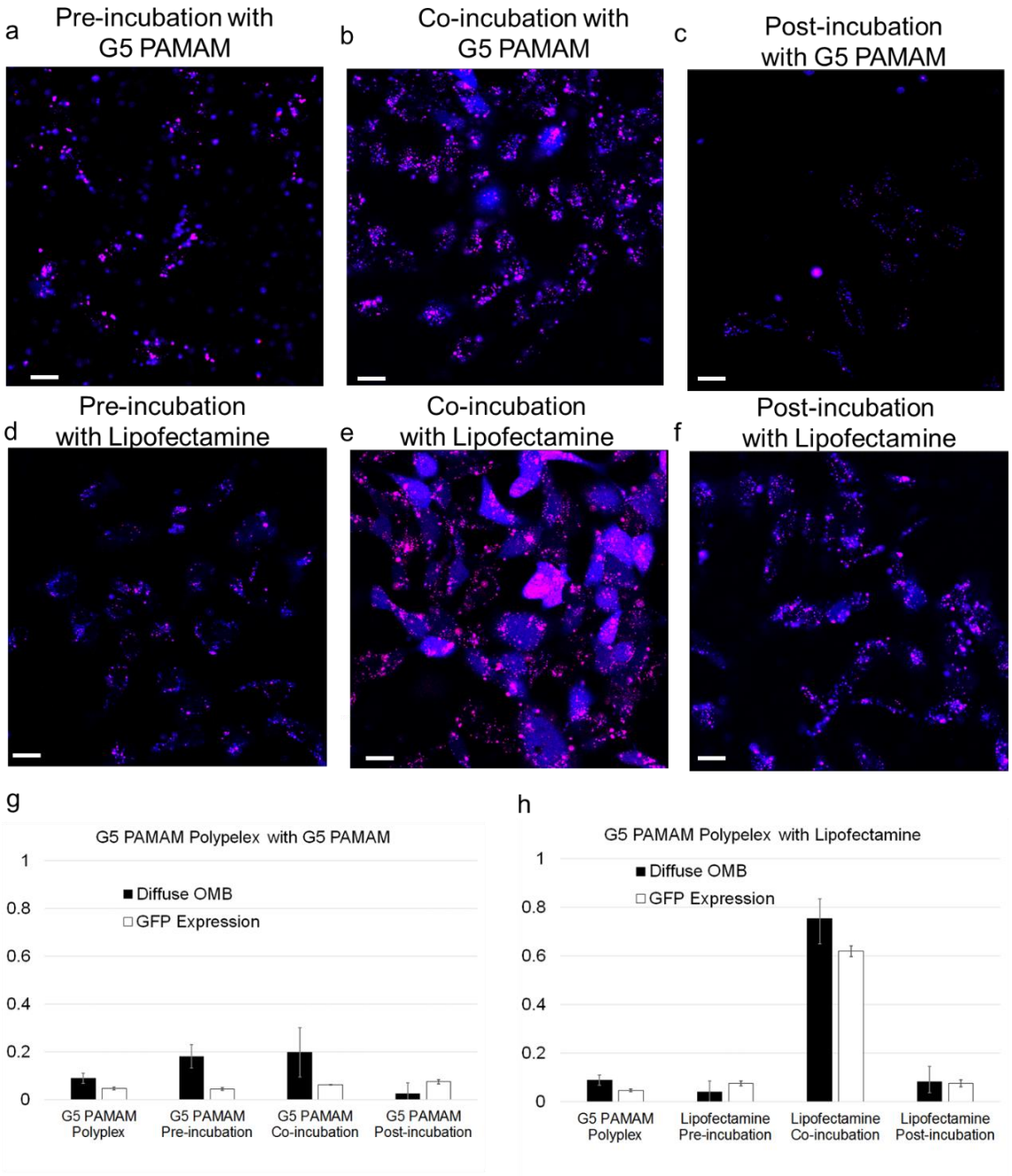

Figure 5.4. Addition of free G5 PAMAM and lipofectamine to HEK 293A cells treated with G5 PAMAM polyplexes. (a) Treatment with free G5 PAMAM for 1 h followed by treatment with G5 PAMAM N:P 10:1 polyplexes for 3 h. (b) Co-incubation of free G5 PAMAM with G5 PAMAM polyplexes for 3 h. (c) Incubation with G5 PAMAM polyplexes for 3 h followed by 1 h treatment with free G5 PAMAM. (d) Treatment with free lipofectamine for 1 h followed by treatment with G5 PAMAM N:P 10:1 polyplexes for 3 h. (e) Co-incubation of free lipofectamine with G5 PAMAM polyplexes for 3 h. (f) Incubation with G5 PAMAM polyplexes for 3 h followed by 1 h treatment with free lipofectamine. (g) Treatments (a-c) followed by measurement of GFP expression after 24 h. A 2-fold increase in GFP expression was observed.

(h) Treatments (d-f) followed by measurement of GFP expression after 24 h. Little change in expression levels were observed except for a >10-fold increase for lipofectamine co-incubation. For flow cytometry quantification of GFP expression (g, h), data are presented as mean± standard deviation of three biological replicates. In the fluorescence images, blue indicates all OMB and pink indicates intact OMB (AF 594 emission by FRET). Scale bar is 20 μm.

REFERENCES:

(1) Nguyen, J.; Szoka, F. C. Nucleic Acid Delivery: The Missing Pieces of the Puzzle? *Acc. Chem. Res.* **2012**, *45*, 1153–1162.

(2) Burke, P. A.; Pun, S. H.; Reineke, T. M. Advancing Polymeric Delivery Systems Amidst a Nucleic Acid Therapy Renaissance. *ACS Macro Lett.* **2013**, *2*, 928–934.

(3) Kukowska-Latallo, J. F.; Bielinska, A. U.; Johnson, J.; Spindler, R.; Tomalia, D. A.; Baker, J. R. Efficient Transfer of Genetic Material into Mammalian Cells Using Starburst Polyamidoamine Dendrimers. *Proc. Natl. Acad. Sci.* **1996**, *93* , 4897–4902.

(4) Boussif, O.; Lezoualc'h, F.; Zanta, M. A.; Mergny, M. D.; Scherman, D.; Demeneix, B.; Behr, J. P. A Versatile Vector for Gene and Oligonucleotide Transfer into Cells in Culture and in Vivo: Polyethylenimine. *Proc. Natl. Acad. Sci. U. S. A.* **1995**, *92*, 7297–7301.

(5) Behr, J.-P. The Proton Sponge: A Trick to Enter Cells the Viruses Did Not Exploit. *Chim. Int. J. Chem.* **1997**, *51*, 1–2.

(6) Yin, H.; Kanasty, R. L.; Eltoukhy, A. A.; Vegas, A. J.; Dorkin, J. R.; Anderson, D. G. Non-Viral Vectors for Gene-Based Therapy. *Nat Rev Genet* **2014**, *15*, 541–555.

(7) ur Rehman, Z.; Hoekstra, D.; Zuhorn, I. S.; Rehman, Z. ur; Hoekstra, D.; Zuhorn, I. S. On the Mechanism of Polyplex-and Lipoplex-Mediated Delivery of Nucleic Acids: Real-Time Visualization of Transient Membrane Destabilization Without Endosomal Lysis. *ACS Nano* **2013**, *7*, 3767–3777.

(8) Itaka, K.; Harada, A.; Yamasaki, Y.; Nakamura, K.; Kawaguchi, H.; Kataoka, K. In Situ Single Cell Observation by Fluorescence Resonance Energy Transfer Reveals Fast Intra-Cytoplasmic Delivery and Easy Release of Plasmid DNA Complexed with Linear Polyethylenimine. *J. Gene Med.* **2004**, *6*, 76–84.

(9) Akinc, A.; Thomas, M.; Klibanov, A. M.; Langer, R. Exploring Polyethylenimine-Mediated DNA Transfection and the Proton Sponge Hypothesis. *J. Gene Med.* **2005**, *7*, 657–663.

(10) Pollard, H.; Toumaniantz, G.; Amos, J. L.; Avet-Loiseau, H.; Guihard, G.; Behr, J. P.; Escande, D. Ca2+-Sensitive Cytosolic Nucleases Prevent Efficient Delivery to the Nucleus of Injected Plasmids. *J. Gene Med.* **2001**, *3*, 153.

(11) Rattan, R.; Vaidyanathan, S.; Wu, G. S.-H.; Shakya, A.; Orr, B. G.; Banaszak Holl, M. M. Polyplex-Induced Cytosolic Nuclease Activation Leads to Differential Transgene Expression. *Mol. Pharm.* **2013**, *10*, 3013–3022.

(12) Reilly, M. J.; Larsen, J. D.; Sullivan, M. O. Polyplexes Traffic through Caveolae to the Golgi and Endoplasmic Reticulum En Route to the Nucleus. *Mol. Pharm.* **2012**, *9*, 1280–

1290.

(13) Fichter, K. M.; Ingle, N. P.; McLendon, P. M.; Reineke, T. M. Polymeric Nucleic Acid Vehicles Exploit Active Interorganelle Trafficking Mechanisms. *ACS Nano* **2013**, *7*, 347–364.

(14) Ingle, N. P.; Xue, L.; Reineke, T. M. Spatiotemporal Cellular Imaging of Polymer-pDNA Nanocomplexes Affords in Situ Morphology and Trafficking Trends. *Mol. Pharm.* **2013**, *10*, 4120–4135.

(15) Brunner, S.; Sauer, T.; Carotta, S.; Cotten, M.; Saltik, M.; Wagner, E. Cell Cycle Dependence of Gene Transfer by Lipoplex, Polyplex and Recombinant Adenovirus. *Gene Ther.* **2000**, *7*, 401–407.

(16) Lechardeur, D.; Lukacs, G. L. Nucleocytoplasmic Transport of Plasmid DNA: A Perilous Journey from the Cytoplasm to the Nucleus. *Hum. Gene Ther.* **2006**, *17*, 882–889.

(17) Mortimer, I.; Tam, P.; MacLachlan, I.; Graham, R. W.; Saravolac, E. G.; Joshi, P. B. Cationic Lipid-Mediated Transfection of Cells in Culture Requires Mitotic Activity. *Gene Ther.* **1999**, *6*, 403–411.

(18) Dowty, M. E.; Williams, P.; Zhang, G.; Hagstrom, J. E.; Wolff, J. a. Plasmid DNA Entry into Postmitotic Nuclei of Primary Rat Myotubes. *Proc. Natl. Acad. Sci. U. S. A.* **1995**, *92*, 4572–4576.

(19) Grandinetti, G.; Reineke, T. M. Exploring the Mechanism of Plasmid DNA Nuclear Internalization with Polymer-Based Vehicles. *Mol. Pharm.* **2012**, *9*, 2256–2267.

(20) Jewell, C. M.; Lynn, D. M. Surface-Mediated Delivery of DNA: Cationic Polymers Take Charge. *Curr. Opin. Colloid Interface Sci.* **2008**, *13*, 395–402.

(21) Thomas, M.; Klibanov, A. M. Non-Viral Gene Therapy: Polycation-Mediated DNA Delivery. *Appl. Microbiol. Biotechnol.* **2003**, *62*, 27–34.

(22) Hanzlíková, M.; Ruponen, M.; Galli, E.; Raasmaja, A.; Aseyev, V.; Tenhu, H.; Urtti, A.; Yliperttula, M. Mechanisms of Polyethylenimine-Mediated DNA Delivery: Free Carrier Helps to Overcome the Barrier of Cell-Surface Glycosaminoglycans. *J. Gene Med.* **2011**, *13*, 402–409.

(23) Ruponen, M.; Honkakoski, P.; Tammi, M.; Urtti, A. Cell-Surface Glycosaminoglycans Inhibit Cation-Mediated Gene Transfer. *J. Gene Med.* **2004**, *6*, 405–414.

(24) Kulkarni, R. P.; Mishra, S.; Fraser, S. E.; Davis, M. E. Single Cell Kinetics of Intracellular, Nonviral, Nucleic Acid Delivery Vehicle Acidification and Trafficking. *Bioconjug. Chem.* **2005**, *16*, 986.

(25) Benjaminsen, R. V; Mattebjerg, M. A.; Henriksen, J. R.; Moghimi, S. M.; Andresen, T. L. The Possible "proton Sponge" Effect of Polyethylenimine (PEI) Does Not Include Change in Lysosomal pH. *Mol. Ther.* **2012**, *21*, 149–157.

(26) Funhoff, A. M.; van Nostrum, C. F.; Koning, G. A.; Schuurmans-Nieuwenbroek, N. M. E.; Crommelin, D. J. A.; Hennink, W. E. Endosomal Escape of Polymeric Gene Delivery Complexes Is Not Always Enhanced by Polymers Buffering at Low pH. *Biomacromolecules* **2004**, *5*, 32–39.

(27) Grosse, S.; Thévenot, G.; Monsigny, M.; Fajac, I. Which Mechanism for Nuclear Import

of Plasmid DNA Complexed with Polyethylenimine Derivatives? *J. Gene Med.* **2006**, *8*, 845–851.

(28) Tseng, W.-C.; Haselton, F. R.; Giorgio, T. D. Mitosis Enhances Transgene Expression of Plasmid Delivered by Cationic Liposomes. *Biochim. Biophys. Acta - Gene Struct. Expr.* **1999**, *1445*, 53–64.

(29) Dean, D. A. Import of Plasmid DNA into the Nucleus Is Sequence Specific. *Exp. Cell Res.* **1997**, *230*, 293–302.

(30) Wilson, G. L.; Dean, B. S.; Wang, G.; Dean, D. A. Nuclear Import of Plasmid DNA in Digitonin-Permeabilized Cells Requires Both Cytoplasmic Factors and Specific DNA Sequences. *J. Biol. Chem.* **1999**, *274* , 22025–22032.

(31) Ludtke, J. J.; Sebestyen, M. G.; Wolff, J. A. The Effect of Cell Division on the Cellular Dynamics of Microinjected DNA and Dextran. *Mol Ther* **2002**, *5*, 579–588.

(32) Pollard, H.; Remy, J.-S.; Loussouarn, G.; Demolombe, S.; Behr, J.-P.; Escande, D. Polyethylenimine but Not Cationic Lipids Promotes Transgene Delivery to the Nucleus in Mammalian Cells. *J. Biol. Chem.* **1998**, *273* , 7507–7511.

(33) Matz, R. L.; Erickson, B.; Vaidyanathan, S.; Kukowska-Latallo, J. F.; Baker, J. R.; Orr, B. G.; Banaszak Holl, M. M. Polyplex Exposure Inhibits Cell Cycle, Increases Inflammatory Response, and Can Cause Protein Expression without Cell Division. *Mol. Pharm.* **2013**, *10*, 1306–1317.

(34) Lechardeur, D.; Sohn, K. J.; Haardt, M.; Joshi, P. B.; Monck, M.; Graham, R. W.; Beatty, B.; Squire, J.; O'Brodovich, H.; Lukacs, G. L. Metabolic Instability of Plasmid DNA in the Cytosol: A Potential Barrier to Gene Transfer. *Gene Ther.* **1999**, *6*, 482–497.

(35) Rattan, R.; Bielinska, A. U.; Banaszak Holl, M. M. Quantification of Cytosolic Plasmid DNA Degradation Using High-Throughput Sequencing: Implications for Gene Delivery. *J. Gene Med.* **2014**, *16*, 75–83.

(36) Ruponen, M.; Arkko, S.; Urtti, A.; Reinisalo, M.; Ranta, V.-P. Intracellular DNA Release and Elimination Correlate Poorly with Transgene Expression after Non-Viral Transfection. *J. Control. Release* **2009**, *136*, 226.

(37) Vaidyanathan, S.; Anderson, K. B.; Merzel, R. L.; Jacobovitz, B.; Kaushik, M. P.; Kelly, C. N.; van Dongen, M. A.; Dougherty, C. A.; Orr, B. G.; Banaszak Holl, M. M. Quantitative Measurement of Cationic Polymer Vector and Polymer–pDNA Polyplex Intercalation into the Cell Plasma Membrane. *ACS Nano* **2015**, *9*, 6097–6109.

(38) Fu, A.; Tang, R.; Hardie, J.; Farkas, M. E.; Rotello, V. M. Promises and Pitfalls of Intracellular Delivery of Proteins. *Bioconjug. Chem.* **2014**, *25*, 1602–1608.

(39) Li, M.; Tao, Y.; Shu, Y.; LaRochelle, J. R.; Steinauer, A.; Thompson, D.; Schepartz, A.; Chen, Z.-Y.; Liu, D. R. Discovery and Characterization of a Peptide That Enhances Endosomal Escape of Delivered Proteins in Vitro and in Vivo. *J. Am. Chem. Soc.* **2015**, *137*, 14084–14093.

(40) Bolte, S.; Cordelieres, F. P. A Guided Tour into Subcellular Colocalization Analysis in Light Microscopy. *J. Microsc.* **2006**, *224*, 213–232.

(41) Prevette, L. E.; Nikolova, E. N.; Al-Hashimi, H. M.; Banaszak Holl, M. M. Intrinsic

Dynamics of DNA-Polymer Complexes: A Mechanism for DNA Release. *Mol. Pharm.* **2012**, *9*, 2743–2749.

(42) Shakya, A.; Dougherty, C. A.; Xue, Y.; Al-Hashimi, H. M.; Banaszak Holl, M. M. Rapid Exchange Between Free and Bound States in RNA–Dendrimer Polyplexes: Implications on the Mechanism of Delivery and Release. *Biomacromolecules* **2016**, *17*, 154–164.

(43) Lukacs, G. L.; Haggie, P.; Seksek, O.; Lechardeur, D.; Freedman, N.; Verkman, A. S. Size-Dependent DNA Mobility in Cytoplasm and Nucleus. *J. Biol. Chem.* **2000**, *275*, 1625–1629.

(44) Grandinetti, G.; Smith, A. E.; Reineke, T. M. Membrane and Nuclear Permeabilization by Polymeric pDNA Vehicles: Efficient Method for Gene Delivery or Mechanism of Cytotoxicity? *Mol. Pharm.* **2012**, *9*, 523–538.

(45) Ribeiro, S. C.; Monteiro, G. A.; Prazeres, D. M. F. The Role of Polyadenylation Signal Secondary Structures on the Resistance of Plasmid Vectors to Nucleases. *J. Gene Med.* **2004**, *6*, 565–573.

(46) Azzoni, A. R.; Ribeiro, S. C.; Monteiro, G. A.; Prazeres, D. M. F. The Impact of Polyadenylation Signals on Plasmid Nuclease-Resistance and Transgene Expression. *J. Gene Med.* **2007**, *9*, 392–402.

(47) Matovina, M.; Seah, N.; Hamilton, T.; Warren, D.; Landy, A. Stoichiometric Incorporation of Base Substitutions at Specific Sites in Supercoiled DNA and Supercoiled Recombination Intermediates. *Nucleic Acids Res.* **2010**, *38*, e175.

(48) Luzzietti, N.; Knappe, S.; Richter, I.; Seidel, R. Nicking Enzyme-Based Internal Labeling of DNA at Multiple Loci. *Nat. Protoc.* **2012**, *7*, 643–653.

(49) Lee, W.; von Hippel, P. H.; Marcus, A. H. Internally Labeled Cy3/Cy5 DNA Constructs Show Greatly Enhanced Photo-Stability in Single-Molecule FRET Experiments. *Nucleic Acids Res.* **2014**, *42*, 5967–5977.

(50) Boeckle, S.; von Gersdorff, K.; van der Piepen, S.; Culmsee, C.; Wagner, E.; Ogris, M. Purification of Polyethylenimine Polyplexes Highlights the Role of Free Polycations in Gene Transfer. *J. Gene Med.* **2004**, *6*, 1102–1111.

(51) Dai, Z.; Gjetting, T.; Mattebjerg, M. A.; Wu, C.; Andresen, T. L. Elucidating the Interplay between DNA-Condensing and Free Polycations in Gene Transfection through a Mechanistic Study of Linear and Branched PEI. *Biomaterials* **2011**, *32*, 8626–8634.

(52) Yue, Y.; Jin, F.; Deng, R.; Cai, J.; Chen, Y.; Lin, M. C. M.; Kung, H.-F.; Wu, C. Revisit Complexation between DNA and Polyethylenimine - Effect of Uncomplexed Chains Free in the Solution Mixture on Gene Transfection. *J. Control. Release* **2011**, *155*, 67–76.

(53) Perevyazko, I. Y.; Bauer, M.; Pavlov, G. M.; Hoeppener, S.; Schubert, S.; Fischer, D.; Schubert, U. S. Polyelectrolyte Complexes of DNA and Linear PEI: Formation, Composition and Properties. *Langmuir* **2012**, *28*, 16167–16176.

(54) Wittrup, A.; Ai, A.; Liu, X.; Hamar, P.; Trifonova, R.; Charisse, K.; Manoharan, M.; Kirchhausen, T.; Lieberman, J. Visualizing Lipid-Formulated siRNA Release from Endosomes and Target Gene Knockdown. *Nat Biotech* **2015**, *33*, 870–876.

(55) Prevette, L. E.; Mullen, D. G.; Holl, M. M. B. Polycation-Induced Cell Membrane

Permeability Does Not Enhance Cellular Uptake or Expression Efficiency of Delivered DNA. *Mol. Pharm.* **2010**, *7*, 870.

(56) Seksek, O.; Biwersi, J.; Verkman, A. . Translational Diffusion of Macromolecule-Sized Solutes in Cytoplasm and Nucleus. *J. Cell Biol.* **1997**, *138*, 131–142.

(57) Shi, J.; Chou, B.; Choi, J. L.; Ta, A. L.; Pun, S. H. Investigation of Polyethylenimine/DNA Polyplex Transfection to Cultured Cells Using Radiolabeling and Subcellular Fractionation Methods. *Mol. Pharm.* **2013**.

(58) Sawa, M.; Hsu, T.-L.; Itoh, T.; Sugiyama, M.; Hanson, S. R.; Vogt, P. K.; Wong, C.-H. Glycoproteomic Probes for Fluorescent Imaging of Fucosylated Glycans in Vivo. *Proc. Natl. Acad. Sci. U. S. A.* **2006**, *103*, 12371–12376.

(59) Manders, E. M. M.; Verbeek, F. J.; Aten, J. A. Measurement of Co-Localization of Objects in Dual-Colour Confocal Images. *J. Microsc.* **1993**, *169*, 375–382.

APPENDIX A

Supplemental figures for

Detergent Induction of HEK 293A Cell Membrane Permeability Measured Under Quiescent and Superfusion Conditions Using Whole Cell Patch Clamp

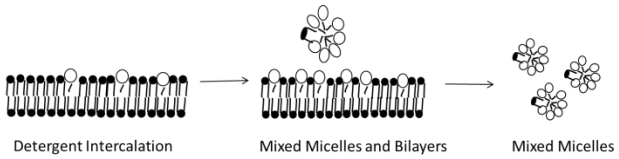

Figure A.1. The Solubilization of Lipid Membrane by Detergents. The solubilization of lipid membrane by detergents has been described to proceed in three phases: 1) The intercalation of detergents in the bilayer 2) Above a critical concentration, mixed bilayers and mixed micelles are formed 3) On complete solubilizaition, mixed micelles containing detergent and lipids are formed.

A

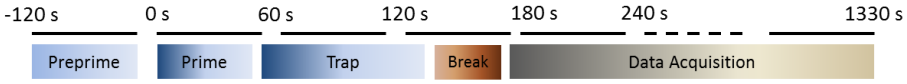

B

Phase	Main Channel	Traps	Traps and Compounds	Compounds
Preprime	1 psi (0-92 s) 0.3 psi (92-120 s)	5 psi (0-90 s) 1.5 psi (90-115 s)	6 psi (115-120s)	
Prime	1 psi (0-30 s) 0.4 psi (30-55 s)	6 Hg (50-55 s)	5 psi (0-20 s) 2 psi (20-50 s)	Not used
Trap	Pulse: 0 psi for 4.2s 0.25 psi for 0.8 s 15 such pulses	6 Hg (0-85 s)	Not used	Not used
Break	0.2 psi (0-20 s)	6 Hg (0-5 s) 10 Hg (5-15 s) 6 Hg (15-20 s)	Not used	Not used
Data Acquisition	0.16 psi (Duration of experiment)	6 Hg (Duration of experiment)	Not used	6 psi

C

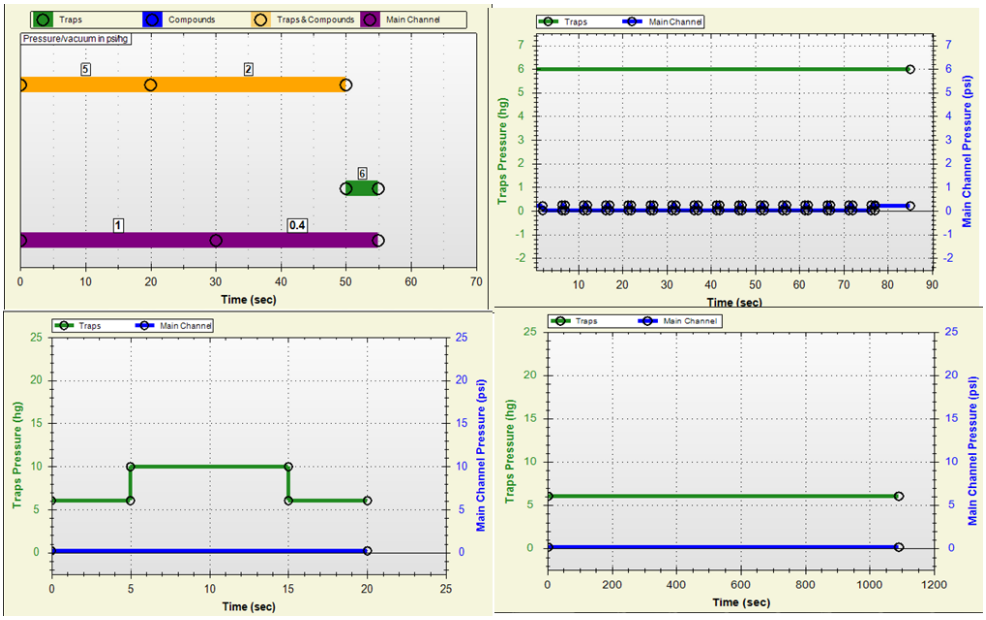

Figure A.2. Operation of IonFlux 16^{TM}. A shows the order and relative durations of the 4 phases in the experiment. B summarizes the pressure settings at the different phases. C is a graphic representation of the pressure settings.

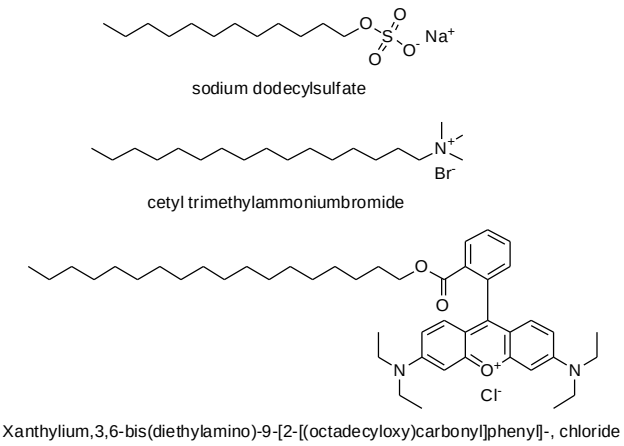

Figure A.3. The detergents used in this experiements . The detergents used in this study are anionic sodium dodecylsulfate and cationic cetyl trimethylammoniumbromide. The fluorescent agent xanthylium, 3,6-bis(diethylamino)-9-[2-(octadecyloxy)carbonyl]phenyl]-,chloride (Octadecyl Rhodamine B, ORB) was used because it is amphiphilic and is known to intercalate in membranes.

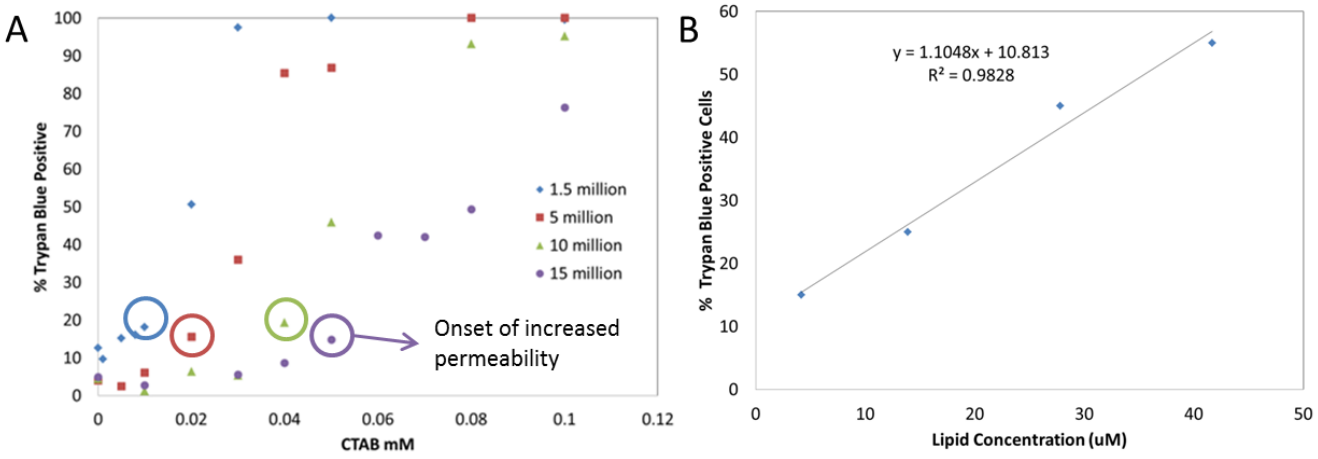

Figure A.4. Description of Partition Constant Calculation Using Trypan Permeability . 1.5 – 15 million cells were treated with different concentrations of CTAB for 15 minutes. The cells were centrifuged and resuspended in ECS. 10 µL of cell suspension was added to 10 µL of trypan blue and 80 µL of PBS. The number of trypan blue positive cells was then counted using a hemocytometer. **A**. Percent of trypan blue positive cells after treatment with CTAB. Circles

indicate the point of onset of increased permeability to trypan blue as an example of point of onset of lipid perturbation. **B**. CTAB concentration at the onset of increase in percent of trypan blue positive cells with respect to lipid concentration. The partition constant was thus evaluated similar to experiments reported in literature. The ratio of detergent to lipid in the bilayer (R_b) was 1.1 ± (0.1). The intercept was 11± (3) mM. The partition constant was calculated to be 48,000 M^{-1}.

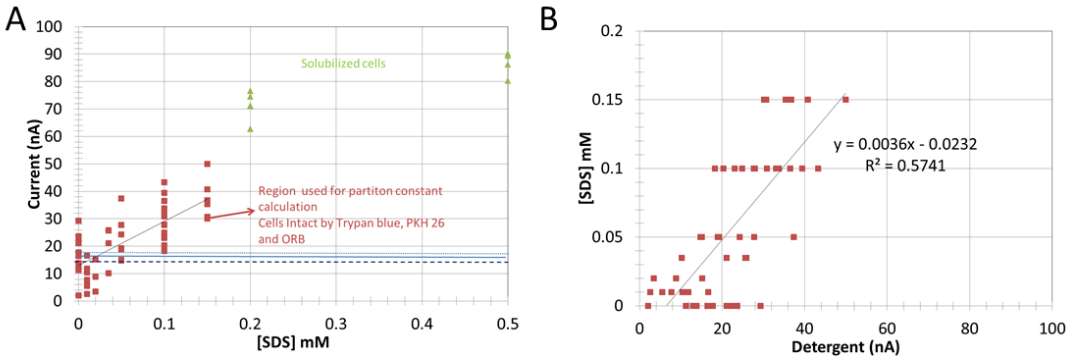

Figure A.5. Description of Partition Constant Calculation Using Trypan Permeability. Due to variability in current data, the partition constant for patch clamp study was evaluated in a manner different from studies in literature. **A** shows currents when 1.5 million cells were treated with increasing concentrations of SDS. Data from region I where cells exhibit currents of about 50 nA was used for further analysis. **B** shows the inverse of plot A. The slope in **B** gives the detergent necessary to increase the current by 1 nA. The detergent necessary to increase the current by 15 nA was calculated using the slope from the linear regression in **B**. This was plotted with respect to the lipid concentration (figure 9 B) in order to obtain estimates for R_b and K.

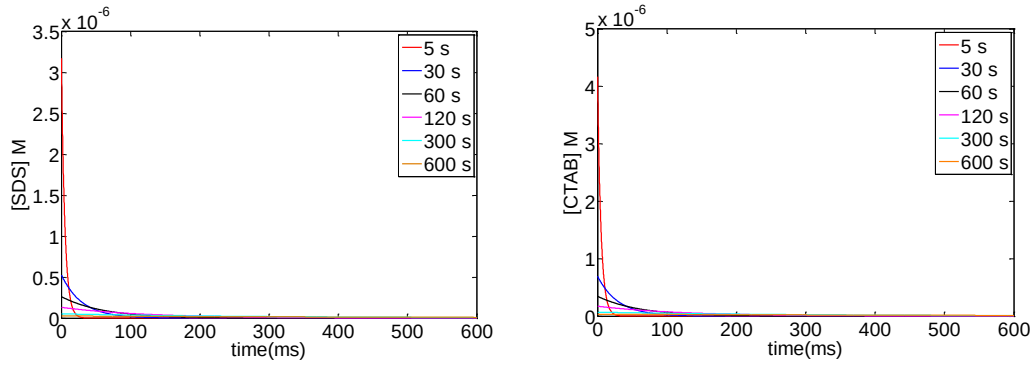

Figure A.6. Modeling Release of Detergents from Microfluidic Channel Walls. We assumed that a monolayer of detergent molecules was adsorbed on the surface of the microfluidic channel. SDS and CTAB were modeled to have surface areas of 0.3 and 0.4 nm^2 respectively[1,2]. We modeled the concentration of detergent that cells would be exposed to assuming exponential release of the detergent from the surface with time constants ranging from 5 s to 600 s. The highest concentrations of detergent for release profiles with different time constants for SDS and CTAB range from 0.02 - 3 µM and 0.04 – 4 µM CTAB respectively. Thus, cells are exposed respectively to SDS and CTAB at concentrations 70-10,000 fold and 3 -250 fold less than the concentrations necessary to induce membrane permeability in the kinetic experiments.

Analysis of errors for partition constant:

The partition constant K is calculated using our estimates for R and D_w. Thus, uncertainties in the estimation of R and D_w both contribute to the estimation of K. The first step in estimating the error in the estimation of K is to estimate the uncertainty associated with the values of R and D_w. This is followed by an error propagation formula to estimate the error in K.[3]

Step 1: The standard errors for the slope (R) and intercept (D_w) presented in figure 9B are calculated

In Figure 9B, detergent concentration at 15 nA increase in current (Y) is plotted versus lipid concentration (X) and the data is fit to a line (equation a)

$$Y_{fit} = b_0 + b_1 * X \quad \text{(a)}$$

The variability of the observed Y values around the regression line is given by equation b.

$$s = \sqrt{\frac{(\sum Y_{observed} - Y_{fit})}{n-2}} \quad \text{(b)}$$

Standard error for the estimates for slope (b_1) and intercept (b_0) were calculated using equations c and d.

$$SE_{b_0} = s * \sqrt{\frac{1}{n} + \frac{\bar{X}^2}{(X-\bar{X})^2}} \quad \text{(c)}$$

$$SE_{b_1} = \frac{s}{\sqrt{(X-\bar{X})^2}} \quad \text{(d)}$$

Step 2: Calculation of error in K due to errors in the measurement of R and D_w

Partition constant is calculated as in equation e

$$K = \frac{R + \delta R}{(R + \delta R + 1) * (D_w + \delta D_w)} = \frac{1}{\frac{D_w \pm \delta D_w}{R \pm \delta R} + (D_w \pm \partial D_w)}$$

According to reference 3,

$$\frac{A \pm \delta A}{B \pm \delta B} = \frac{A}{B} \pm \frac{B}{A} \left(\frac{\partial A}{A} + \frac{\delta B}{B}\right)$$

Thus the estimate for K simplifies to

$$K = \frac{1}{\left(\frac{D_W}{R} + D_W\right) \pm \left[\frac{D_W}{R}\left(\frac{\delta D_W}{D_W} + \frac{\delta R}{R}\right) + \delta D_W\right]} \quad \text{(e)}$$

REFERENCES:

1. de Aguiar, H. B.; Strader, M. L.; de Beer, A. G.; Roke, S. Surface Structure of Sodium Dodecyl Sulfate Surfactant and Oil at the Oil-in-Water Droplet liquid/liquid Interface: A Manifestation of a Nonequilibrium Surface State. *J Phys Chem B* **2011**, *115*, 2970-2978.

2. Ravera, F.; Ferrari, M.; Liggieri, L.; Loglio, G.; Santini, E.; Zanobini, A. Liquid–liquid Interfacial Properties of Mixed nanoparticle–surfactant Systems. *Colloids Surf. Physicochem. Eng. Aspects* **2008**,*323*, 99.

3. Bevington, P. R., *In Data Reduction and Uncertainty Analysis for the Physical Sciences* ; McGraw-Hill: New York, 1969.

APPENDIX B

Supplemental Material for Chapter 3

Quantitative Measurement of Cationic Polymer Vector and Polymer/pDNA Polyplex Intercalation into the Cell Plasma Membrane

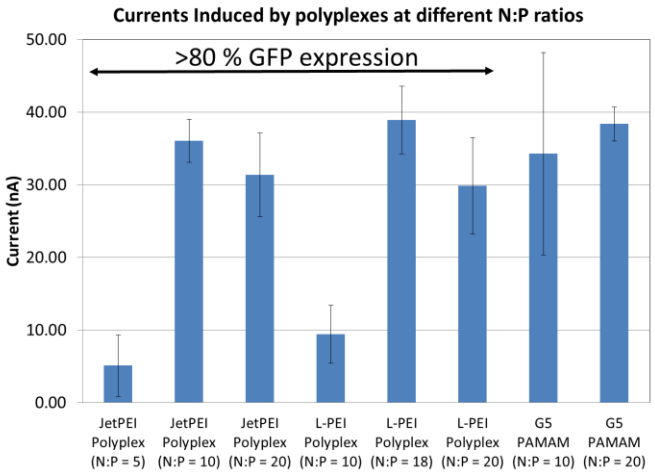

Figure B.1. Current Induced by Polyplexes at different N:P ratios.

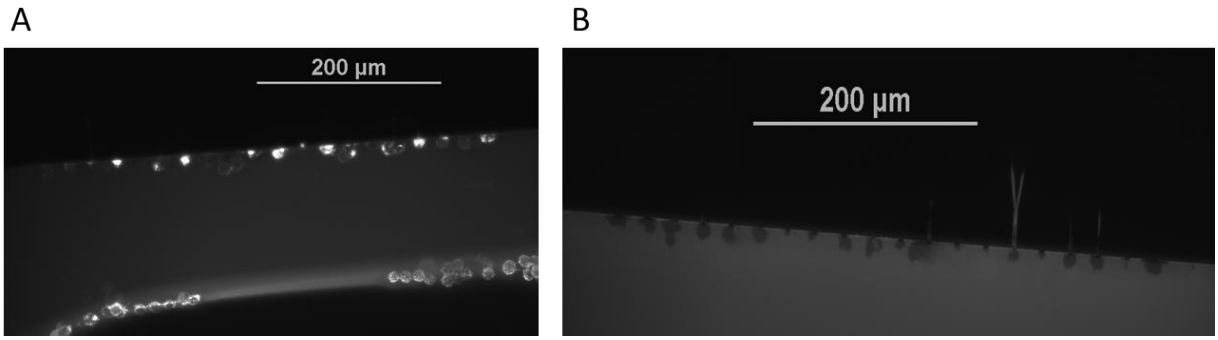

Figure B.2. Cells Treated Using Polymers are Intact. A. Exposure of cells to amine-terminated G5-NH_2-$TAMRA_1$ shows the presence of fluorescent material in cells along with an increase in current by patch clamp. B. Exposure of cells to G5-Ac-$TAMRA_1$ does not result in increased current and also does not stain cells.

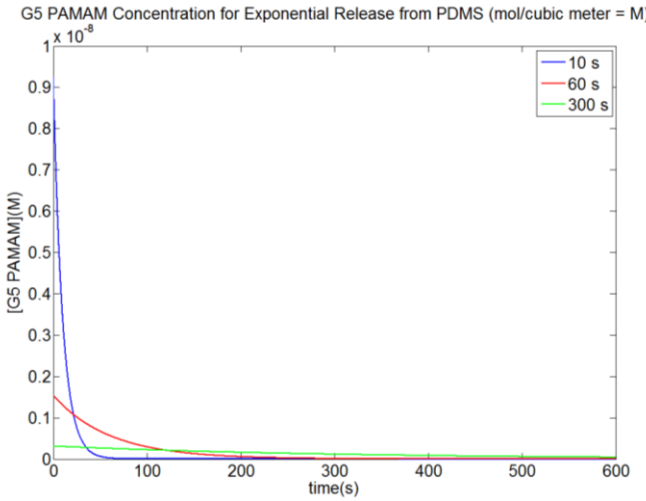

Figure B.3. Modeling Release of G5 PAMAM from Microfluidic Channel Wall. Assuming an exponential release of G5 PAMAM stuck on the walls of the channel and a surface area of 72 nm^2 [1] for G5 PAMAM, the concentration of G5 PAMAM was 9 nM which is 50 X less than the concentration necessary to induce increased membrane conductivity. If we assume similar release dynamics and surface area for L-PEI, the concentration would still be 12 X less than the concentrations necessary to induce increased membrane conductivity.

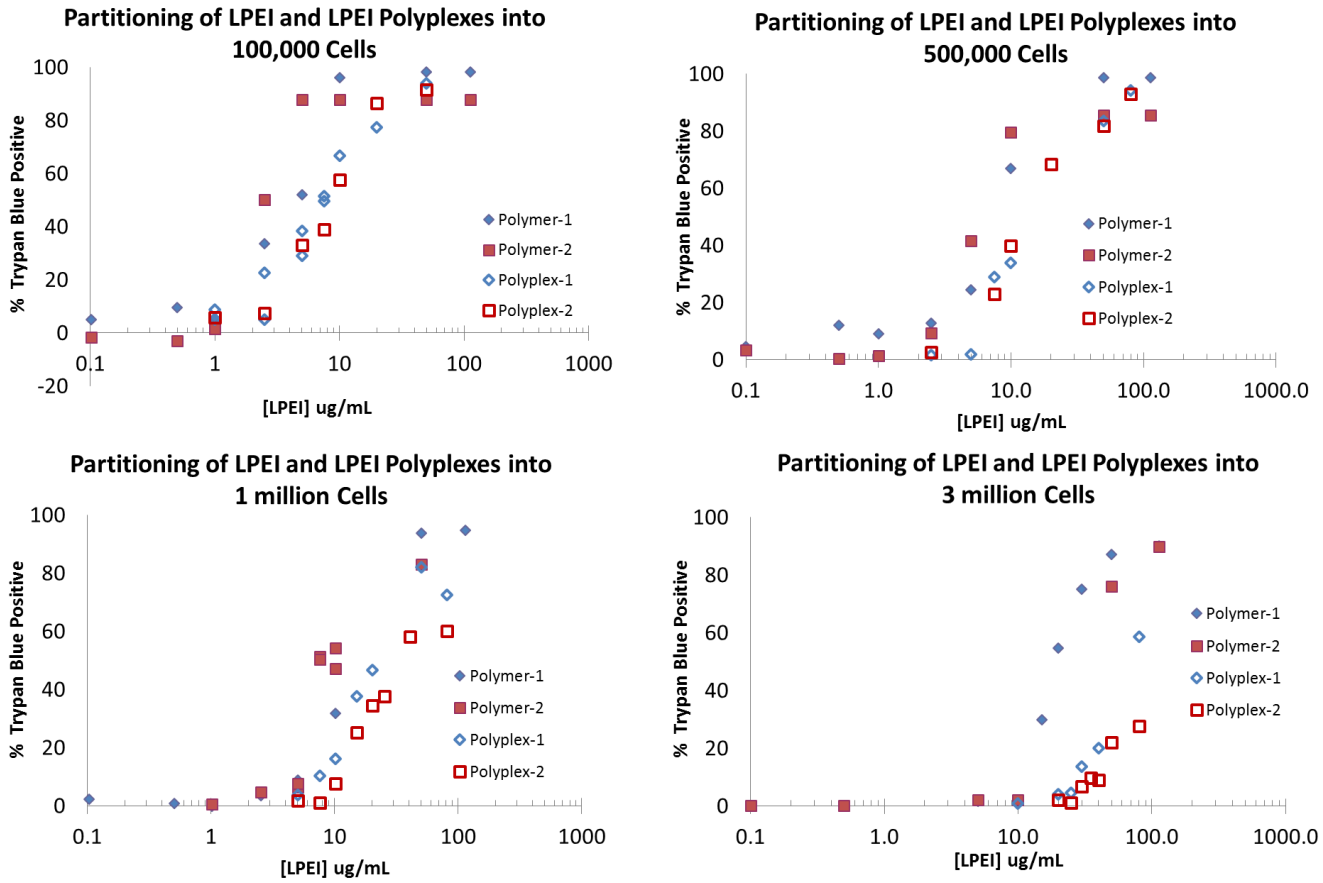

Figure B.4. Trypan blue permeability induced by L-PEI and L-PEI polyplexes for different cell numbers. It is seen that the concentration of L-PEI necessary to induce increased trypan blue permeability increases as the cell count increases. Polyplexes also induce permeability at higher concentrations than free polymers.

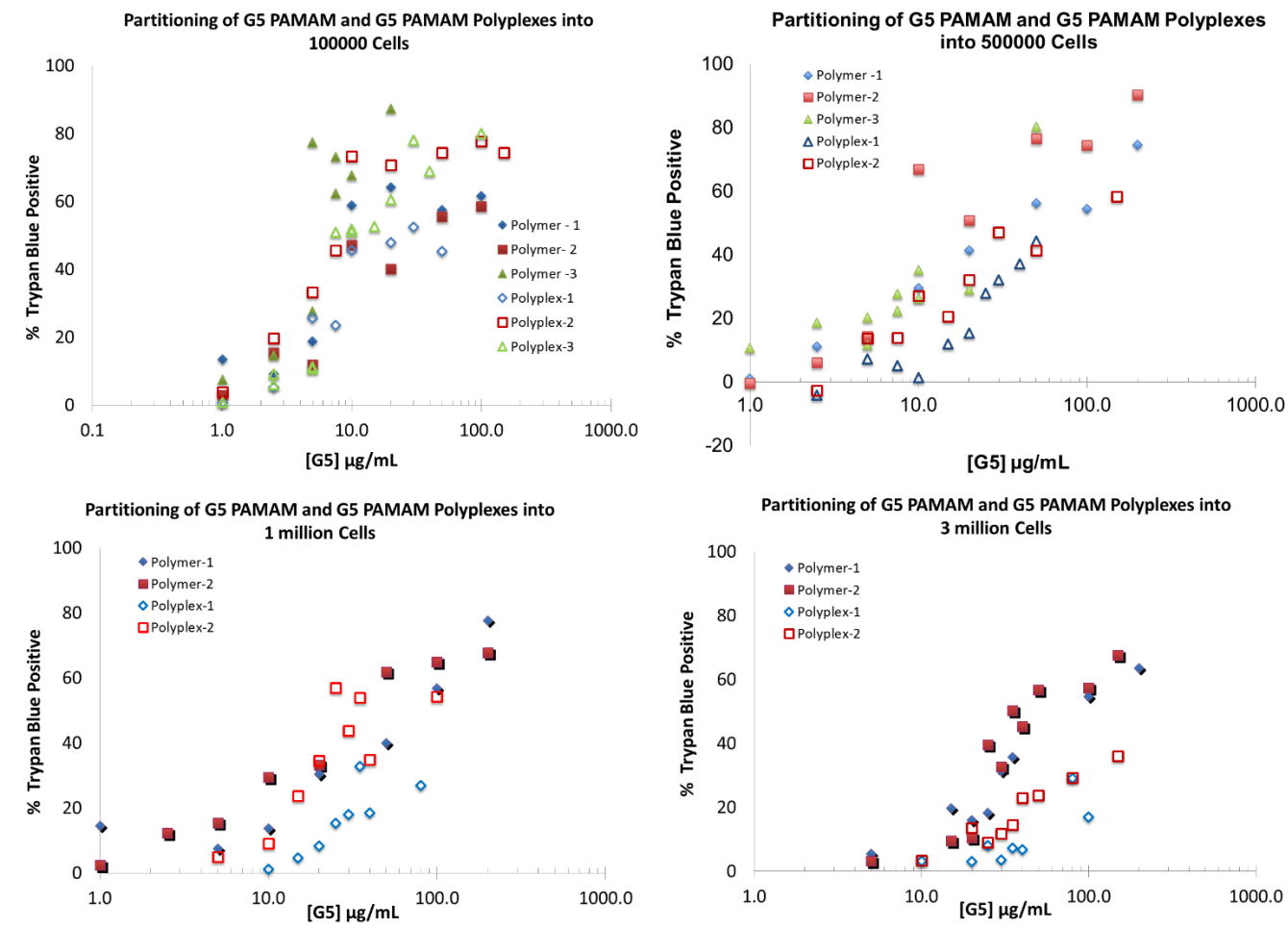

Figure B.5. Trypan blue permeability induced by G5 PAMAM and G5 PAMAM polyplexes for different cell numbers. It is seen that the concentration of G5 PAMAM necessary to induce increased trypan blue permeability increases as the cell count increases.

.

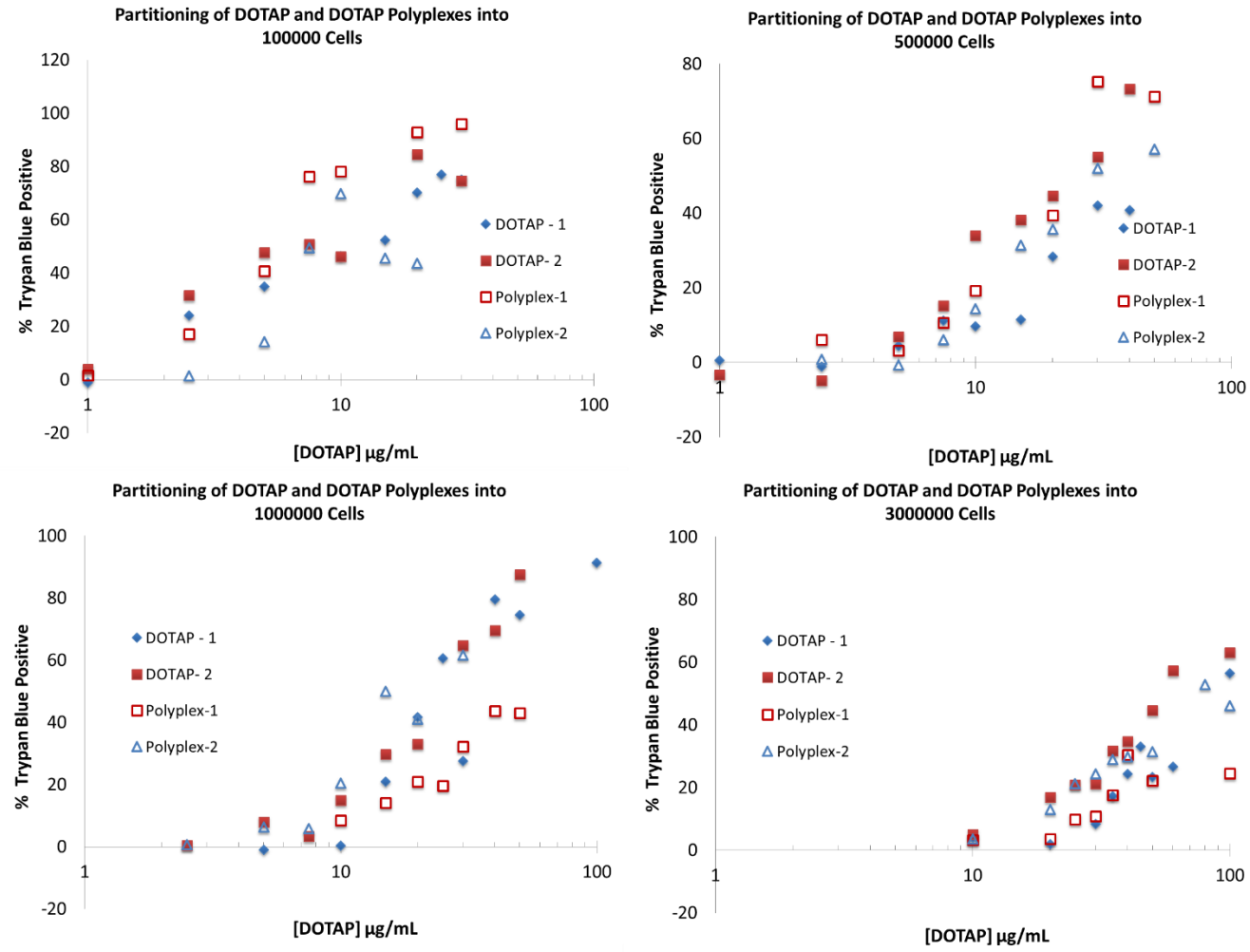

Figure B.6. Trypan blue permeability induced by DOTAP and DOTAP polyplexes for different cell numbers. It is seen that the concentration of DOTAP necessary to induce increased trypan blue permeability increases as the cell count increases.

Mathematical Model for Polymer Partition Constant:

We used previously reported partition models[2–5,6] for measuring the partition constants of free L-PEI, G5 PAMAM, and their respective polyplexes with HEK 293A cells. Briefly, the concentration of polymers required to induce a given magnitude of membrane permeability is linearly related to the lipid concentration. At a fixed membrane perturbation level, the amount of total detergent in the system is constant as presented in Equation 1 where P_b denotes polymer in bilayer and P_w the polymer in water.

$$P_{total} = P_b + P_w \quad (1)$$

R_b is the ratio of polymer to lipid (L) in the bilayer for a given level of membrane disruption as given in Equation 2.[2–5] Substitution of Equation (2) into Equation (1) results in Equation 3.

$$R_b = \frac{P_b}{L} \quad (2)$$

$$P_{Total} = R_b * L + P_w \quad (3)$$

The partitioning of polymer into the lipid membrane can be described by a model in which the mole fraction of detergent in the bilayer (X_b) is related to the polymer in water (P_w) through a partition constant (K), as shown in Equation 4. [2–5]

$$X_b = \frac{P_b}{P_b + L} = K * P_w \quad (4)$$

The substitution of Equations 2 and 4 into equation 3 results in Equation 5. [2–5]

$$P_T = R_b * L + \frac{R_b}{(R_b + 1) * K} \quad (5)$$

The polymer concentration at the onset of membrane permeability (as determined by the trypan blue assays) was plotted against lipid concentration (Figure 11). The lipid concentration in cells was estimated from literature to be 10^9 lipid molecules per cell membrane.[7] The slope and intercept of this line were R_b and P_w, respectively (Equation 3). The partition constant (K) was then estimated using Equation 6.

$$K = \frac{\text{slope}}{(\text{slope} + 1) * \text{intercept}} \quad (6)$$

Analysis of errors for partition constant:

The partition constant *K* is calculated using our estimates for *R* and P_w. Thus, uncertainties in the estimation of *R* and P_w both contribute to the estimation of *K*. The first step in estimating the error in the estimation of *K* is to estimate the uncertainty associated with the values of *R* and P_w. This is followed by an error propagation formula to estimate the error in *K*.[8]

Step 1: The standard errors for the slope (*R*) and intercept (P_w) presented in figure 11 are calculated

In Figure 10, the polymer concentration at the onset of trypan blue uptake above the baseline (Y) is plotted versus lipid concentration (X) and the data is fit to a line (Equation a)

$$Y_{fit} = b_0 + b_1 * X \ \ldots \text{(a)}$$

The variability of the observed Y values around the regression line is given by Equation b.

$$s = \sqrt{\frac{(\sum Y_{observed} - Y_{fit})}{n-2}} \ \ldots \text{(b)}$$

Standard error for the estimates for slope (b_1) and intercept (b_0) were calculated using equations c and d.

$$SE_{b_0} = s * \sqrt{\frac{1}{n} + \frac{\bar{X}^2}{(X-\bar{X})^2}} \ \ldots \text{(c)}$$

$$SE_{b_1} = \frac{s}{\sqrt{(X-\bar{X})^2}} \ \ldots \text{(d)}$$

Step 2: Calculation of error in K due to errors in the measurement of R and P_w

Partition constant is calculated as in Equation e

$$K = \frac{R + \delta R}{(R + \delta R + 1) * (D_w + \delta D_w)} = \frac{1}{\frac{D_w \pm \delta D_w}{R \pm \delta R} + (D_w \pm \partial D_w)}$$

According to reference 2,

$$\frac{A \pm \delta A}{B \pm \delta B} = \frac{A}{B} \pm \frac{B}{A} \left(\frac{\partial A}{A} + \frac{\delta B}{B}\right)$$

Thus the estimate for K simplifies to

$$K = \frac{1}{\left(\frac{D_w}{R} + D_w\right) \pm \left[\frac{D_w}{R}\left(\frac{\delta D_w}{D_w} + \frac{\delta R}{R}\right) + \delta D_w\right]} \ldots \text{(e)}$$

Effect of Electrostatic Interactions Between Vectors/Polyplexes and Plasma Membrane on Partition Constants:

It is well documented that that the concentration of charged molecules near the surface of the charged cell membrane is not necessarily equal to the bulk detergent concentration in the aqueous phase.[5,9,10] In this section, we have tried to estimate if the concentration of the vectors/polyplexes near the cell membrane surface could be significantly different from the bulk concentration. According to Borukhov *et al*., the maximum concentration of a polyelectrolyte of radius a near a charged membrane surface is $1/a^3$ molecules/m^3.[11] For a polymer of radius 2.5 nm, this results in 6 *10^{25} molecules/m^3 near the surface. A bulk concentration of 500 nM results in 3*10^{20} molecules/m^3. Thus, if the experiment were performed in the absence of other ions, the polymer/polyplex concentrations near the surface of the cell could be five orders of magnitude greater than the polymer/polyplex bulk concentration. The width of such a saturated layer of

polymer (l^*) can be calculated according to Equation i, where σ is the surface charge density of the cell membrane, e is the charge of an electron and z is the number of charges in a polymer.[11]

$$l^* = \frac{a^3\sigma}{z*e} \quad \text{(i)}$$

We estimated the surface charge density of a cell membrane by assuming 10^9 lipid molecules per cell membrane[7] and charges on 30% of the lipids.[12] For a cell of radius 10 μm, this resulted in a charge density of $2*10^{18}$ electrons/m^2. The G5 PAMAM has 93 primary amines with a pKa of 10.6. Since a majority of the primary amines would be protonated at pH 7.4, we assumed z = 50, resulting in l^*=0.6 nm. Thus, the higher surface concentration of the polymers would extend only up to 0.6 nm from the lipid bilayer surface. The presence of charged species in solution besides the polymers/polyplexes must also be considered. The cells and polymers in these experiments are first exposed to the ECS buffer before incubation of the cells with the polymers. The concentrations of NaCl and other salts present in the ECS buffer are about six orders of magnitude greater than the polymer concentrations. The Debye length (λ) for NaCl of molarity M is independent of the surface charge of the cell membrane and can be calculated using Equation ii. [13] Any charge that is farther than the Debye length is shielded from interaction with the bilayer.[14]

$$\lambda\ (nm) = \frac{0.304}{\sqrt{M}} \quad \text{(ii)}$$

The Debye length for sodium ions is 0.8 nm. The Debye length and l^* are both < 1 nm. Thus, the membrane surface charge cannot induce changes in polymer concentration beyond 1 nm. Since the polymers and polyplexes are larger than 1 nm, it is unlikely that the polymer/polyplex concentration near the surface would be significantly different from their bulk concentration. Therefore, it is likely that the charged species closest to the membrane would be sodium ions. Changes in the local concentration of polymers near the surface of the lipid bilayer would be minimal due to charge screening by the buffer salts present in solution. Thus, the bulk polymer concentrations in our systems would be minimally affected by the electrostatic interactions with the cell membrane.

Mathematical model of cells trapped in the Ion-Flux 16:

In order to understand possible origins of the variation in the DOTAP data in Fig 3.2c we modeled the patch sites as a group of impedances in parallel. The impedance of the open channel was 16 MΩ based on measurements using an unpatched plate. The 20 cells trapped in the patch site were modeled as parallel impedances of 200 MΩ. For a holding voltage of -70 mV, this resulted in a current of – 7 nA, which is in the range of currents commonly seen in our experiments. We modeled a cell completely saturated by cationic polymer as having a 40 MΩ impedance. This impedance was selected because it results in currents of -35 nA when all the cells are saturated with the polymer. Cells treated with cationic polymers exhibited currents between 30-40 nA.

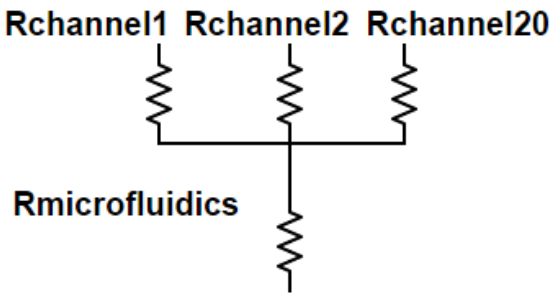

One possibility for obtaining the different current states observed in Fig 2c for DOTP is the presence of a "DOTAP-sensitive" subpopulation of cells. For this hypothesis, one can calculate the fraction of the patch population required to obtain a membrane current of about -20 nA. This would be about 10 cells of 20 in the patch site dominating the observed currents. The likelihood of this self-organization occurring in the patch region from a random mixture of cell is extremely low and therefore the hypothesis was rejected.

An alternative hypothesis is that a mixtures of responses by the 20 cells to the saturating DOTAP exposure provides the observed average current; however, this hypothesis does not account for the binary current response and the absence of measured current traces with magnitudes between -10 and -20 nA.

REFERENCES:

(1) Majoros, I. J.; Williams, C. R.; Becker, A. C.; Baker, J. R. Surface Interaction and Behavior of Poly(amidoamine) Dendrimers: Deformability and Lipid Bilayer Disruption. *J. Comput. Theor. Nanosci.* **2009**, *6*, 1430–1436.

(2) Heerklotz, H.; Seelig, J. Correlation of Membrane/Water Partition Coefficients of Detergents with the Critical Micelle Concentration. *Biophys. J.* **2000**, *78*, 2435–2440.

(3) Lichtenberg, D.; Ahyayauch, H.; Alonso, A.; Goni, F. M. Detergent Solubilization of Lipid Bilayers: A Balance of Driving Forces. *Trends Biochem. Sci.* **2013**, *38*, 85–93.

(4) Lasch, J. Interaction of Detergents with Lipid Vesicles. *BBA - Rev. Biomembranes* **1995**, *1241*, 269–292.

(5) Heerklotz, H. Interactions of Surfactants with Lipid Membranes. *Q. Rev. Biophys.* **2008**, *41*, 205–264.

(6) Vaidyanathan, S.; Orr, B. G.; Banaszak Holl, M. M. Detergent Induction of HEK 293A Cell Membrane Permeability Measured under Quiescent and Superfusion Conditions Using Whole Cell Patch Clamp. *J. Phys. Chem. B* **2014**, *118*, 2112–2123.

(7) Bruce Alberts, Alexander Johnson, Julian Lewis, Martin Raff, Keith Roberts, and P. W. Molecular Biology of the Cell. In; Garland Science: New York, 2002.

(8) Bevington, P. R. *Data Reduction and Error Analysis for the Physical Sciences*; 1969; Vol. 336.

(9) Beck, A.; Li-Blatter, X.; Seelig, A.; Seelig, J. On the Interaction of Ionic Detergents with Lipid Membranes Thermodynamic Comparison of N-Alkyl-$^{+}N(CH_3)_3$ and N-Alkyl-SO_4^{-}. *J. Phys. Chem. B* **2010**, *114*, 15862–15871.

(10) Tan, A.; Ziegler, A.; Steinbauer, B.; Seelig, J. Thermodynamics of Sodium Dodecyl Sulfate Partitioning into Lipid Membranes. *Biophys. J.* **2002**, *83*, 1547–1556.

(11) Borukhov, I.; Andelman, D.; Orland, H. Adsorption of Large Ions from an Electrolyte Solution: A Modified Poisson–Boltzmann Equation. *Electrochim. Acta* **2000**, *46*, 221–229.

(12) Koizumi, K.; Tamiya-Koizumi, K.; Fujii, T.; Okuda, J.; Kojima, K. Comparative Study of the Phospholipid Composition of Plasma Membranes Isolated from Rat Primary Hepatomas Induced by 3'-Methyl-4-Dimethylaminoazobenzene and from Normal Growing Rat Livers. *Cancer Res.* **1980**, *40* , 909–913.

(13) Israelachvili, J. N. *Intermolecular and Surface Forces*; Elsevier, 2011.

(14) Dill, Ken A and Bromberg, S. Salt Ions Shield Charged Objects. In *Molecular Driving Forces: Statistical Thermodynamics in Chemistry and Biology*; **2010**; p. 436.

APPENDIX C

Supplemental Material for

Fluorophore:Dendrimer Ratio Impacts Cellular Uptake and Intracellular Fluorescence Lifetime

Table C.1. Characterization summary for G5-NH_2-$TAMRA_n$ material.

	Yield (mg)	MALDI-TOF-MS m/z ratio	% Yield	Equivalents of TFA	Average Number of Dyes	
					UPLC	Proton NMR
G5-$(TAMRA)_{1.5(AVG)}$-NH_2	121.0	27500	86	0.32	1.5	5.9
G5-NH_2-$(TAMRA)_0$	1.0	24600	27*	0.79	0.0	0.0
G5-NH_2-$(TAMRA)_1$	5.2	24300	21*	0.05	1.0	0.9
G5-NH_2-$(TAMRA)_2$	2.5	25900	28*	0.20	2.0	1.8
G5-NH_2-$(TAMRA)_3$	3.5	26400	23*	5.24	3.0	3.3
G5-NH_2-$(TAMRA)_4$	4.6	26800	23*	5.90	4.0	4.5
G5-NH_2-$(TAMRA)_{5+}$	15.3	28900	23*	1.35	6.8	6.9

*** % Yield calculated based on fractional amount of each species present in G5-NH_2-$(TAMRA)_{1.5AVG}$ as determined by peak fitting the rp-UPLC trace.**

Table C.2. Fluorescence lifetime for solutions that mimic cell conditions. All values are in ns with standard deviations obtained from at least three independent measurements give in parentheses. The data corresponds to Figures 1 and 6.

	water	FBS	PBS	NaCl	ficoll	BSA	glucose	DCS
Cy3	0.61 (0.04)	-	-	-	-	-	-	-
TAMRA	2.46 (0.04)	-	-	-	-	-	-	-
G5T$_{1.5avg}$	1.92 (0.12)	2.5 (0.08)	2.24 (0.04)	2.35 (0.03)	2.32 (0.01)	2.21 (0.08)	1.87 (0.04)	2.51 (0.03)
G5T$_1$	2.32 (0.15)	1.71 (0.08)	2.18 (0.05)	2.22 (0.02)	2.12 (0.04)	1.92 (0.08)	1.81 (0.06)	1.86 (0.04)
G5T$_2$	1.78 (0.11)	1.77 (0.05)	1.66 (0.01)	1.66 (0.07)	1.59 (0.07)	1.82 (0.11)	1.62 (0.03)	1.88 (0.11)
G5T$_3$	1.51 (0.03)	1.56 (0.11)	1.6 (0.03)	1.58 (0.06)	1.56 (0.05)	1.5 (0.03)	1.42 (0.06)	1.82 (0.13)
G5T$_4$	1.70 (0.05)	1.72 (0.14)	1.48 (0.04)	1.43 (0.04)	1.4 (0.02)	1.45 (0.16)	1.31 (0.06)	1.38 (0.05)
G5T$_{5+}$	1.23 (0.11)	1.77 (0.05)	1.63 (0.03)	1.6 (0.02)	1.48 (0.03)	1.48 (0.11)	1.1 (0.01)	2.51 (0.03)

Table C.3. Fluorescence lifetimes for polyplex and pH solution conditions (Figures S6 and S7). All values are in ns with standard deviations obtained from at least three independent measurements give in parentheses.

	pDNA 1:1	pDNA 10:1	oligo 1:1	oligo 10:1	Buffer pH=3	Buffer pH=5
G5T$_{1.5avg}$	2.07 (0.02)	2.05 (0.21)	2.03 (0.07)	2.11 (0.12)	-	-
G5T$_1$	2.05 (0.05)	1.76 (0.05)	1.32 (0.11)	1.83 (0.09)	2.32 (0.11)	2.18 (0.06)
G5T$_2$	1.98 (0.03)	1.67 (0.06)	1.56 (0.12)	1.65 (0.10)	2.38 (0.05)	2.05 (0.07)
G5T$_3$	1.52 (0.32)	1.5 (0.11)	1.16 (0.12)	1.43 (0.20)	2.08 (0.04)	1.84 (0.03)
G5T$_4$	1.74 (0.04)	1.46 (0.08)	1.13 (0.05)	1.48 (0.16)	1.96 (0.02)	1.71 (0.05)
G5T$_{5+}$	1.18 (0.06)	1.55 (0.14)	1.59 (0.16)	1.24 (0.21)	1.5 (0.02)	1.57 (0.03)

Table C.4. P-values from Games-Howell analysis of flow cytometry data. Significance based on $p < 0.05$ for both Figures 1 and 3.

	Flow Cytometry				Lifetime
	p-value for Raw Data	p-value for Aqueous Corrected	p-value for DCS corrected	p-value for FBS corrected	p-value for Aqueous Solution
TAMRA dye	-	-	-	-	-
G5-NH_2-$(TAMRA)_1$	-	-	-	-	0.681
G5-NH_2-$(TAMRA)_2$	0.997	0.004	0.033	0.044	0.014
G5-NH_2-$(TAMRA)_3$	0.010	0.001	0.013	0.024	0.015
G5-NH_2-$(TAMRA)_4$	0.005	0.033	0.001	0.001	0.020
G5-NH_2-$(TAMRA)_{5+}$	0.002	0.044	0.026	0.027	0.001
G5-NH_2-$(TAMRA)_{1.5(AVG)}$	0.009	0.965	0.854	0.307	0.022
PBS	0.002	0.002	0.002	0.002	-
G5-NH_2-$(TAMRA)_0$	0.002	0.002	0.002	0.002	-

Figure C.1. MALDI-TOF-MS spectra of G5-NH_2-$TAMRA_n$ materials. Numbers for m/z ratios for each sample are reported in Table S1.

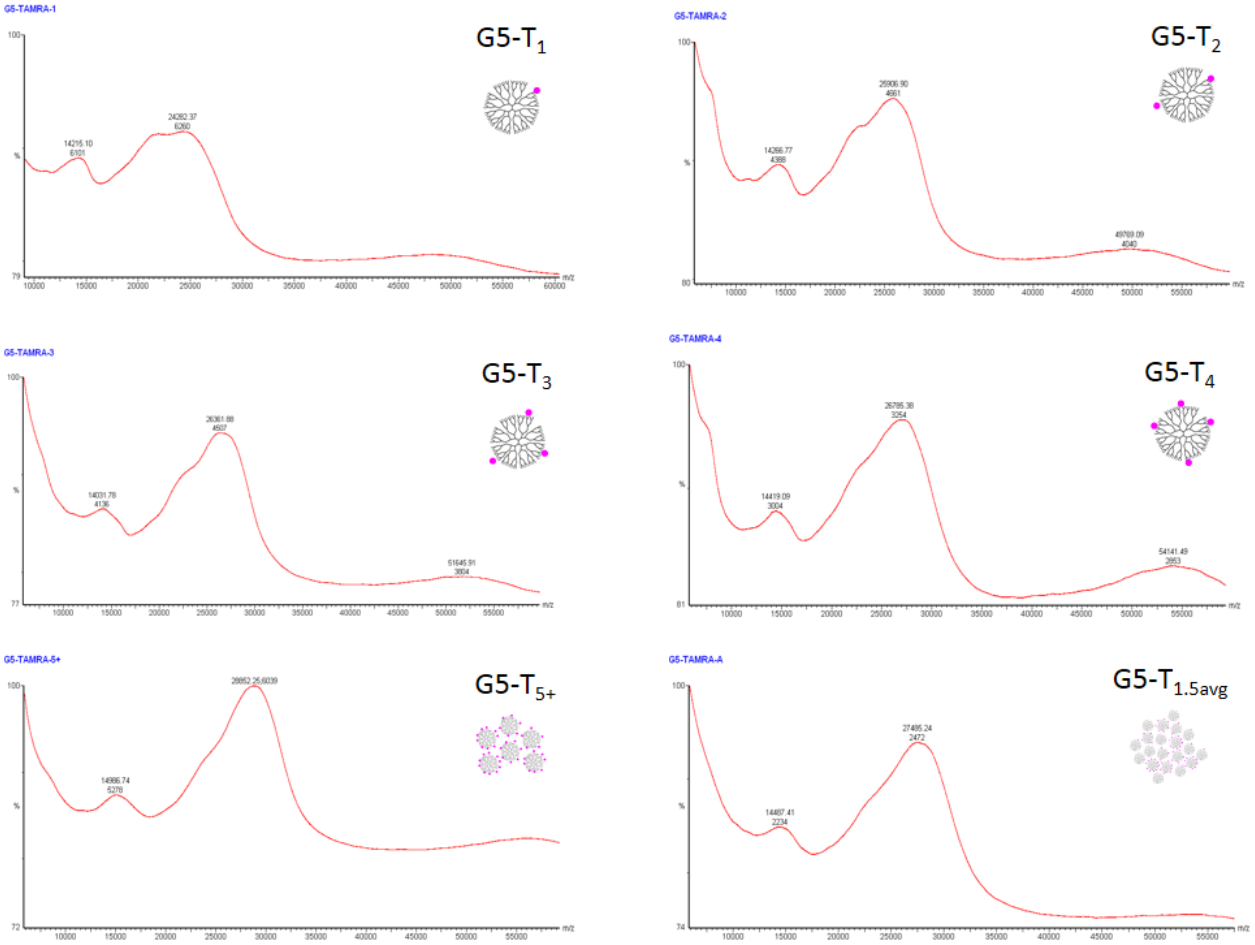

Figure C.2. Fluorescence emission intensities of 0.1 mg/mL samples of G5-NH_2-$TAMRA_n$ (n=1, 2, 3, 4, 5+, and 1.5_{avg}) for the various control solutions.

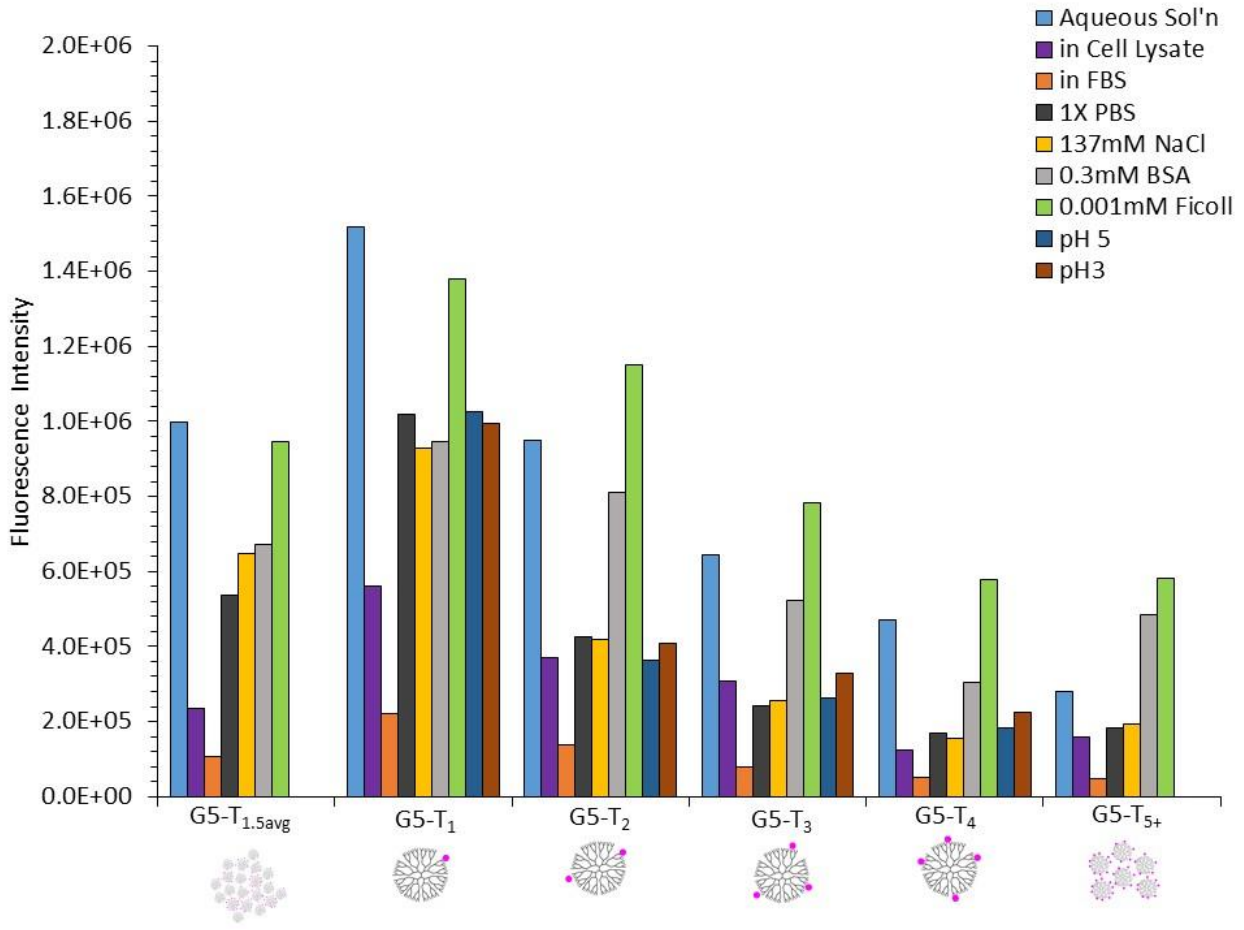

Figure C.3. Fluorescence emission spectra of G5-NH_2-$TAMRA_n$ in various solutions. Fluorescence emission spectra of G5-NH_2-$TAMRA_n$ in solution with various controls in comparison to materials in aqueous solution. PBS, FBS, NaCl, DNA, BSA, and ficoll show similar fluorescence intensity ratios to those obtained in water (Figure 1c). n=1 (orange), n=2 (yellow), n=3 (green), n=4 (blue), n=5+ (purple), and $n=1.5_{avg}$ (black).

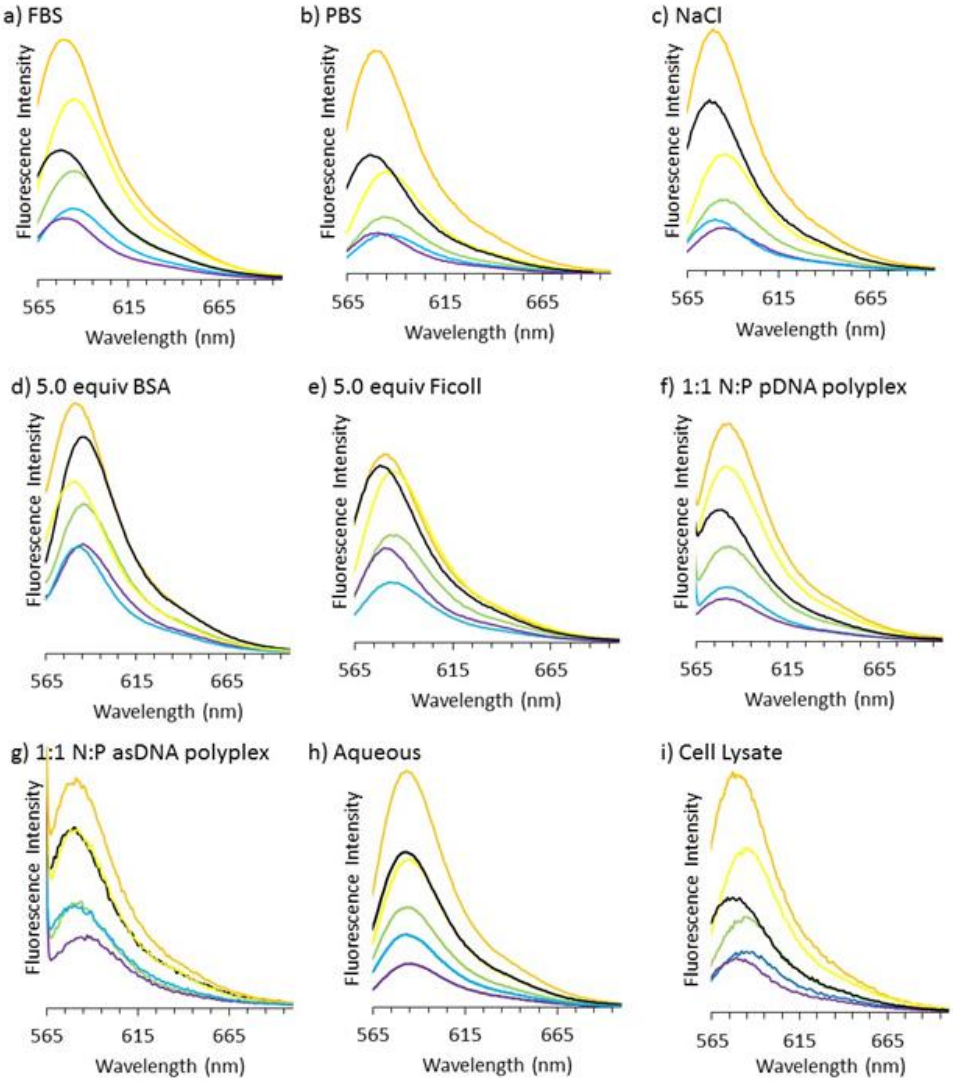

Figure C.4. Large form of images in Figure 5. FLIM of G5-NH_2-$TAMRA_n$ in HEK 293A cells. a) PBS control b) n=0, c) n=1, d) n=2, e) n=3, f) n=4, g) n=5+, h) $n=1.5_{ave}$. Images size is 139 x 139 μm.

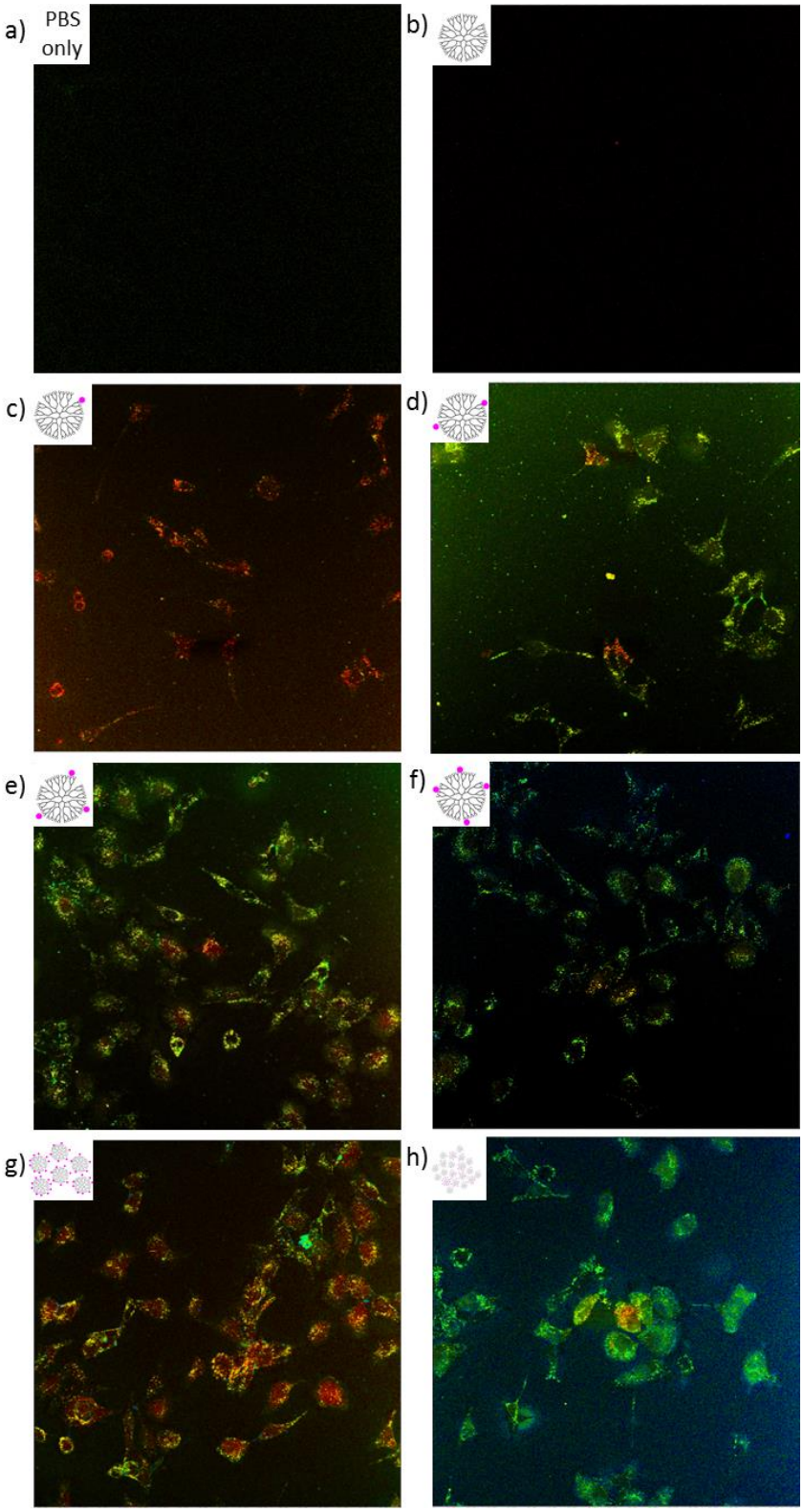

Figure C.5. FLIM images of HEK293A cells from Figure 4. a) G5-NH_2-$TAMRA_1$ b) G5-NH_2-$TAMRA_2$ c) G5-NH_2-$TAMRA_3$ d) G5-NH_2-$TAMRA_4$ e) G5-NH_2-$TAMRA_{5+}$ f) G5-NH_2-$TAMRA_{1.5(avg)}$ after an incubation of 3 hours (40x objective, 6.5 zoom). The images are lifetime color coded with high to low lifetimes going from red (2.0 ns) to blue (0.5 ns). All samples show more intense fluorescence in punctate spots. Scale bar is 20 μm.

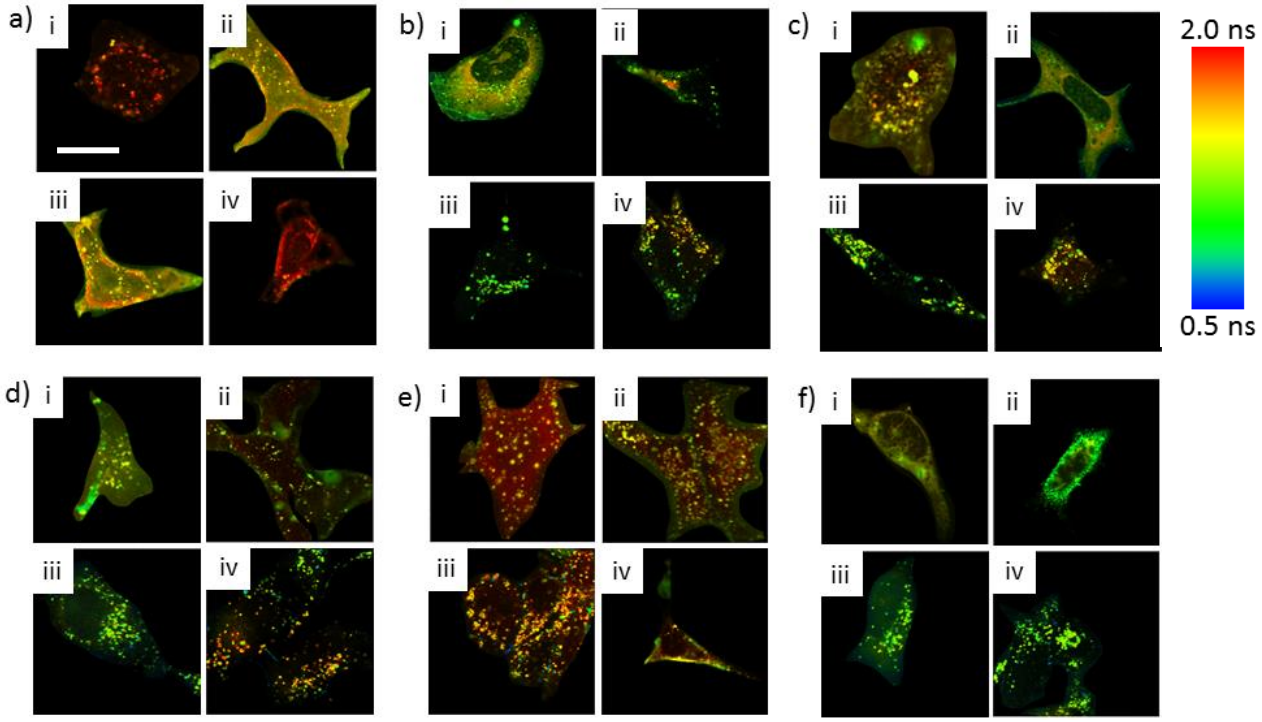

Figure C.6. Fluorescence lifetimes controls in buffers. Solution fluorescence lifetime controls for cell data comparing aqueous fluorescence lifetimes to lifetimes of materials in buffers at a pH = 3 and pH = 5. See Table S3 for summary of numerical values.

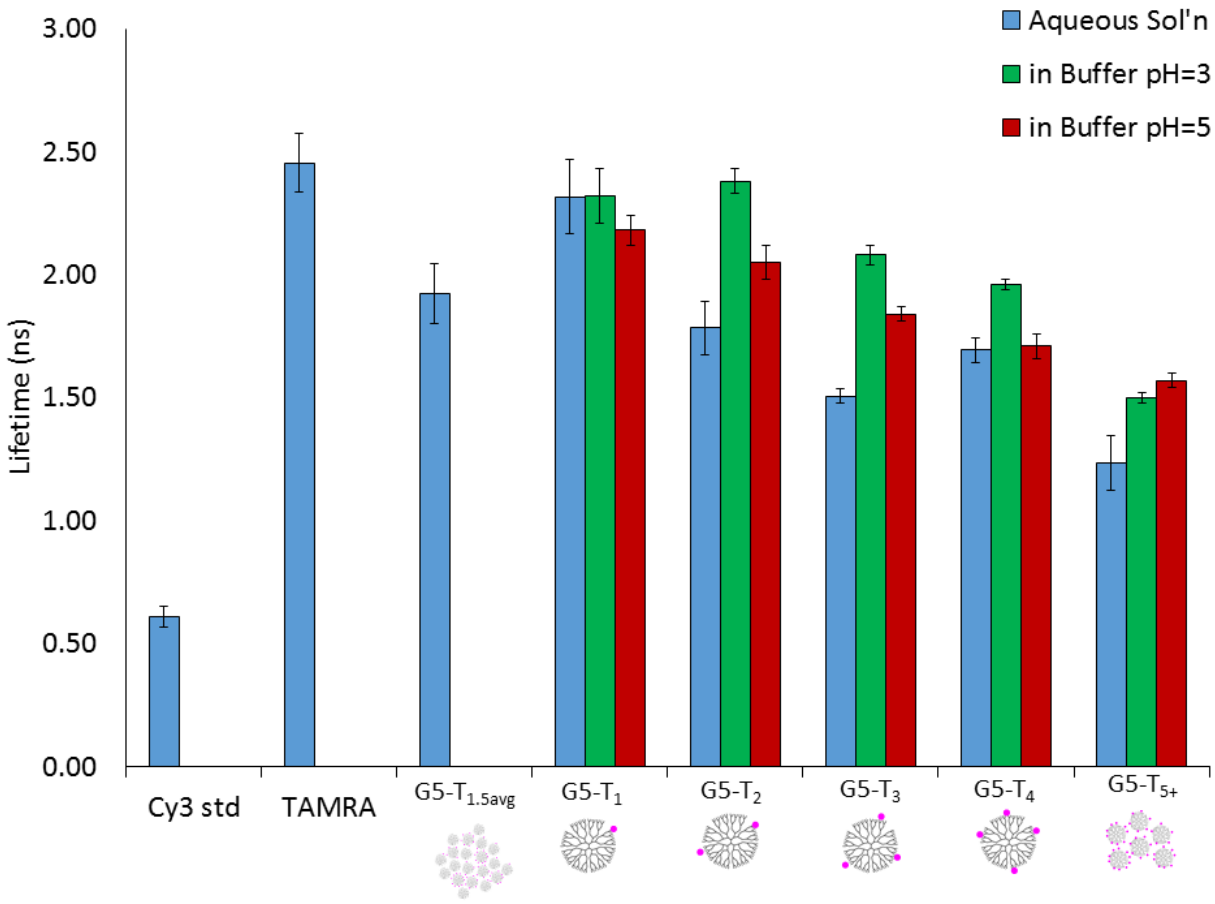

Figure C.7. Fluorescence lifetime of G5-NH_2-$TAMRA_n$:DNA polyplexes in aqueous solution. See Table S3 for summary of numerical values.

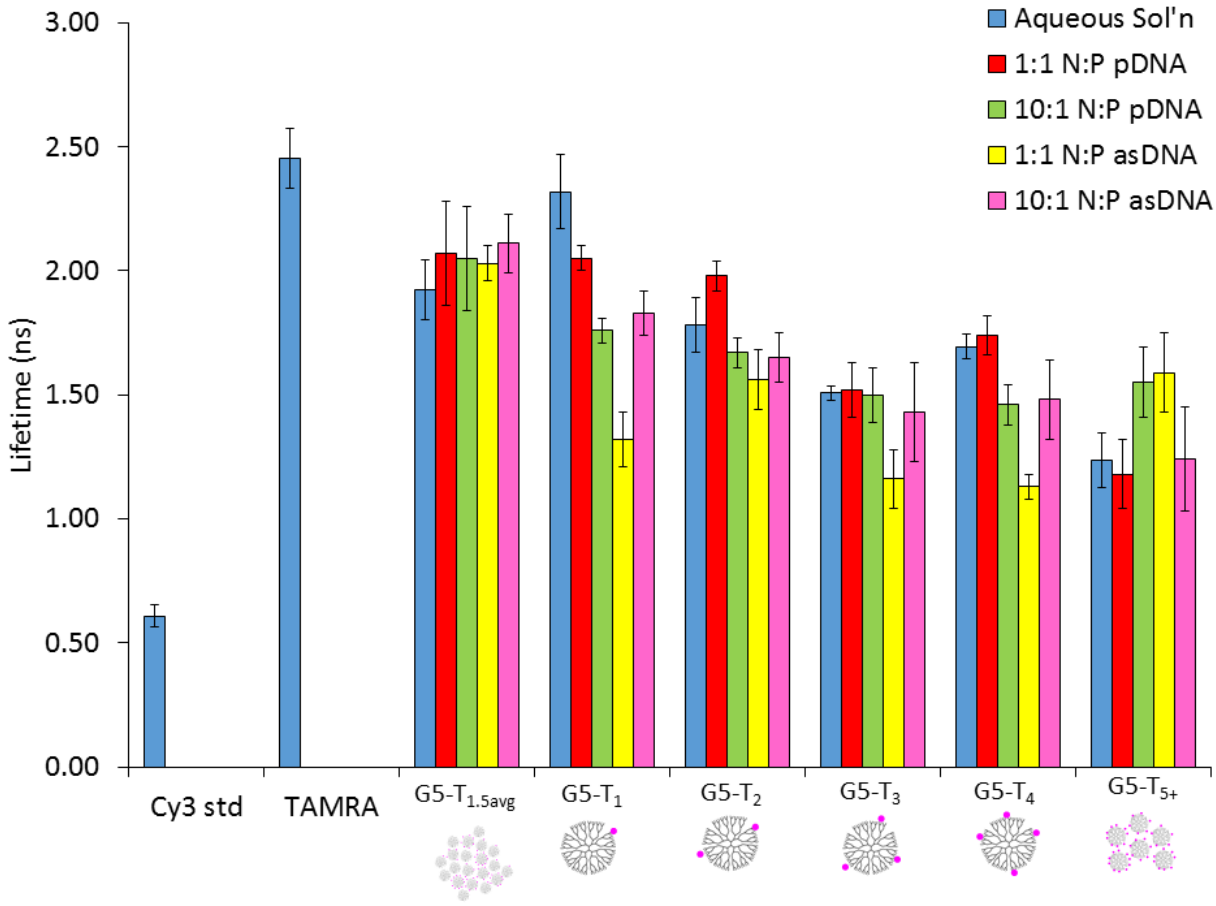

Figure C.8. ^{1}H NMR Spectra of G5-NH_2-$TAMRA_n$ materials in D_2O at 500 MHz. n = 0, 1, 2, 3, 4, 5+, and avg = 1.5.

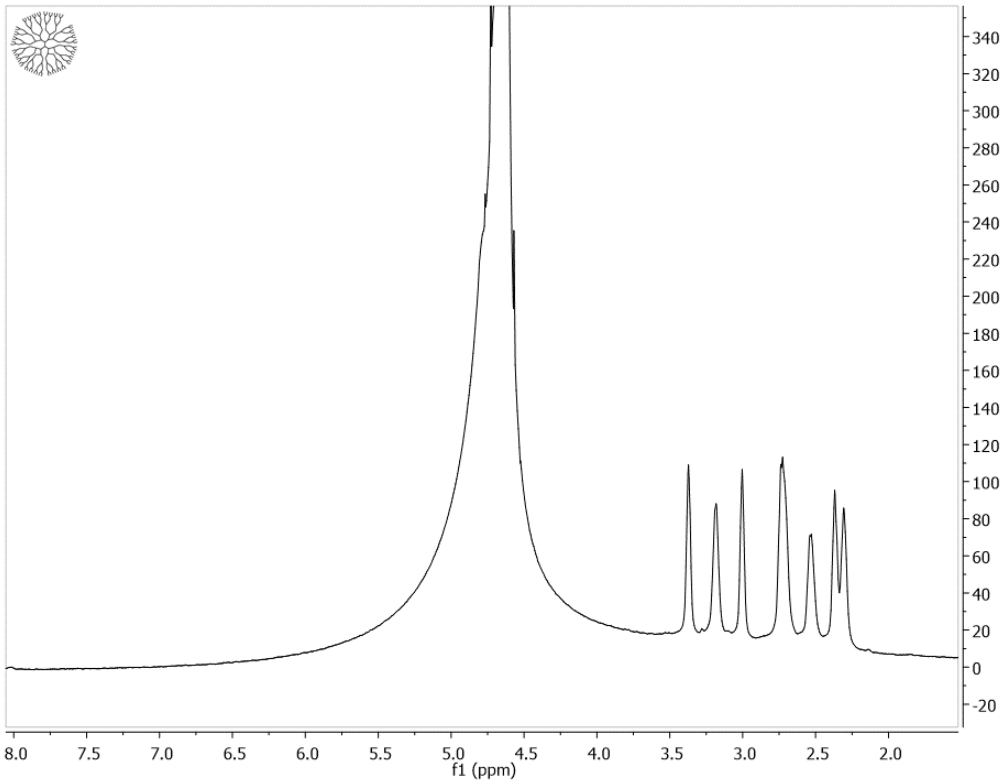

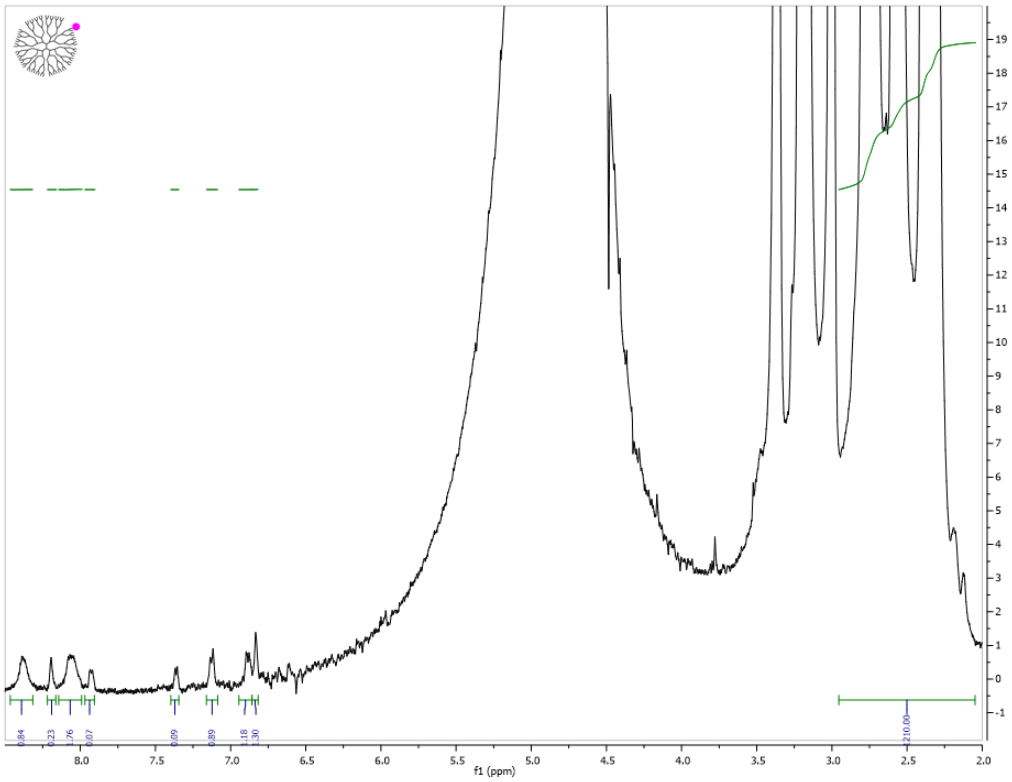
f1 (ppm)

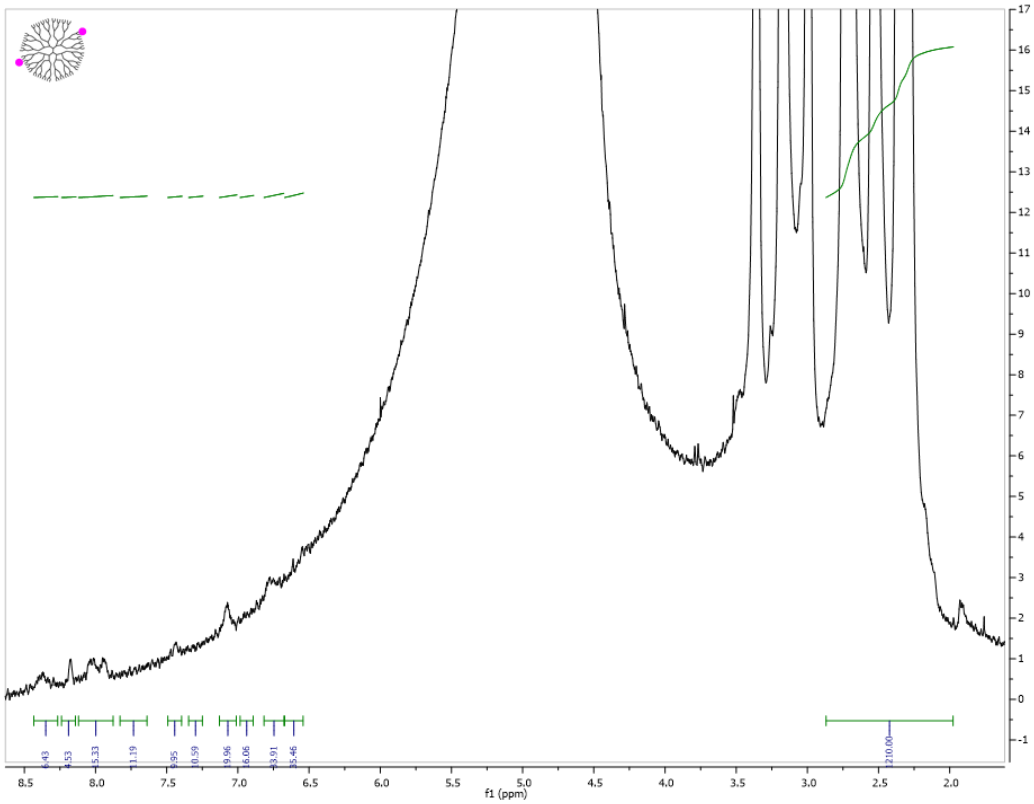
f1 (ppm)

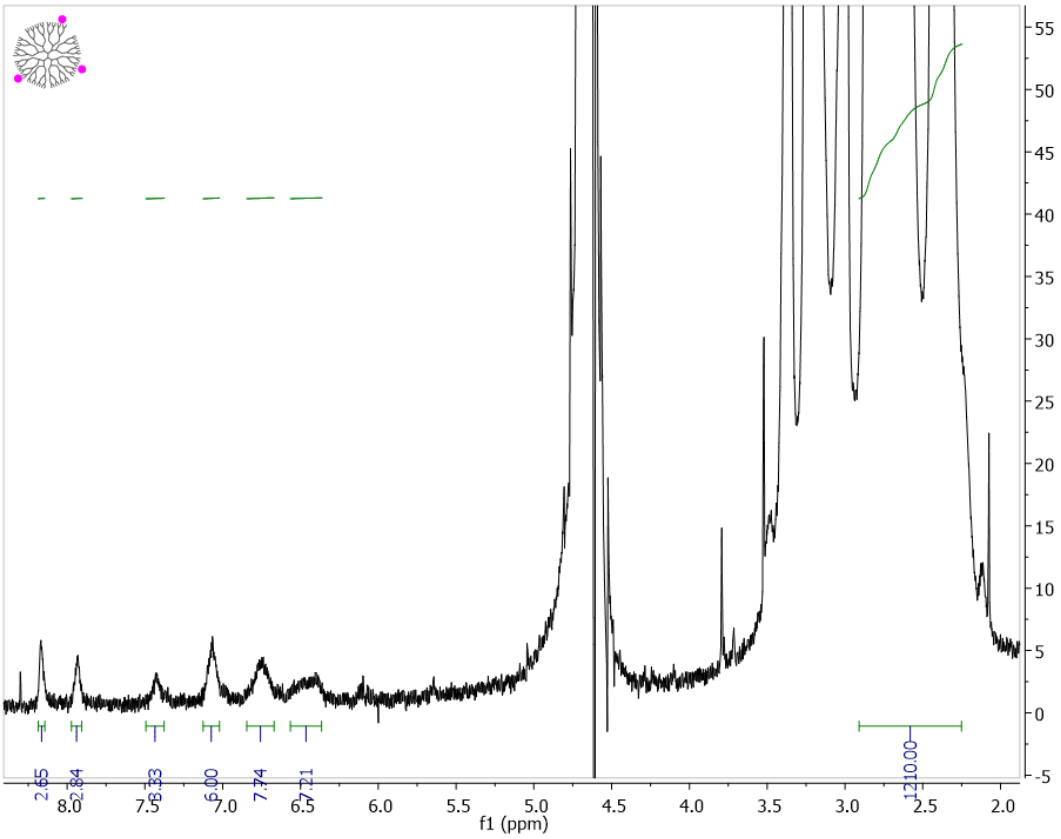
2.65
2.84
6.33
6.00
7.74
7.21
10.00
f1 (ppm)

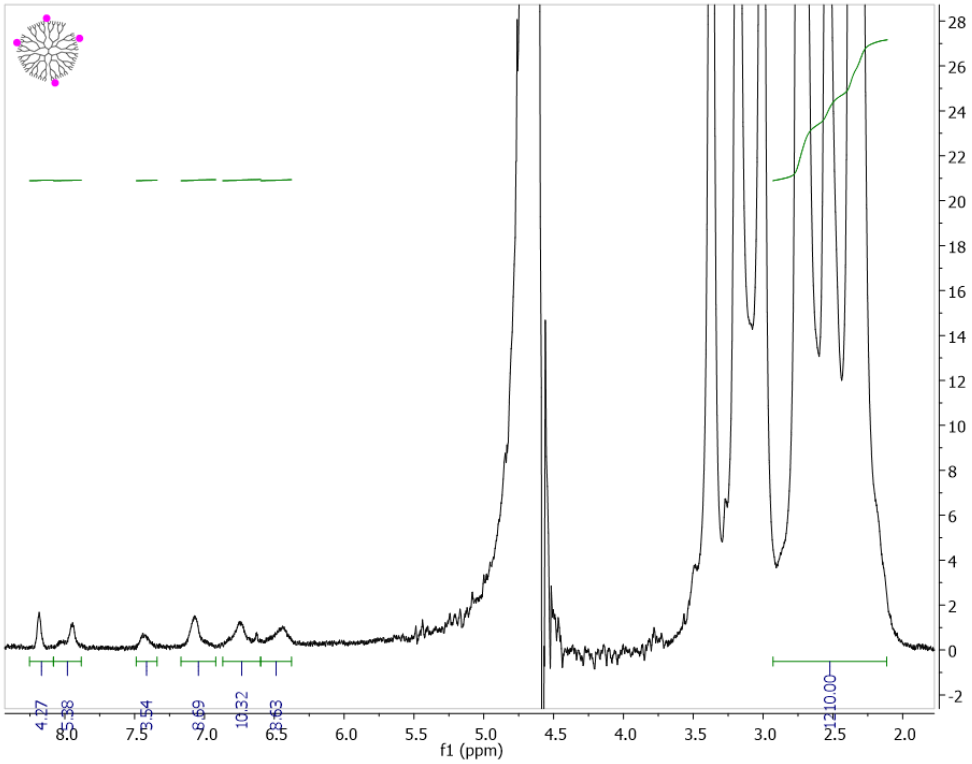
4.27
4.38
5.54
8.69
10.32
8.63
10.00
f1 (ppm)

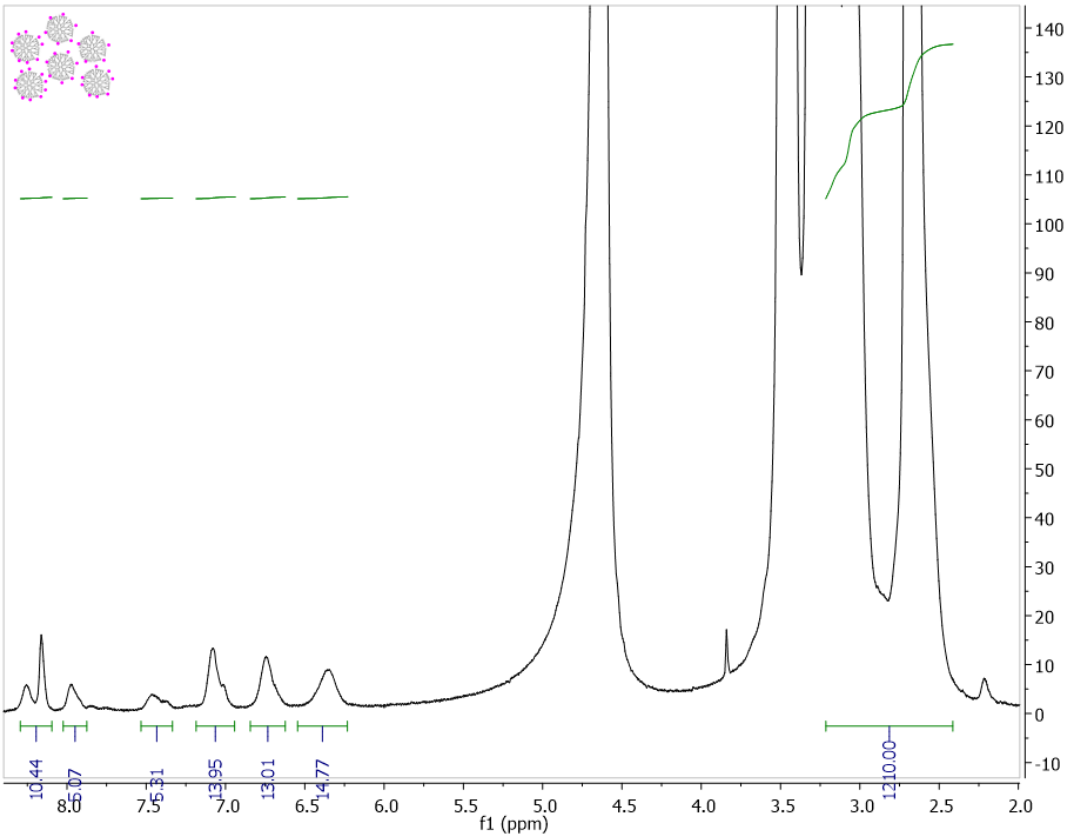
10.44
5.07
5.31
13.95
13.01
14.77
10.00
f1 (ppm)

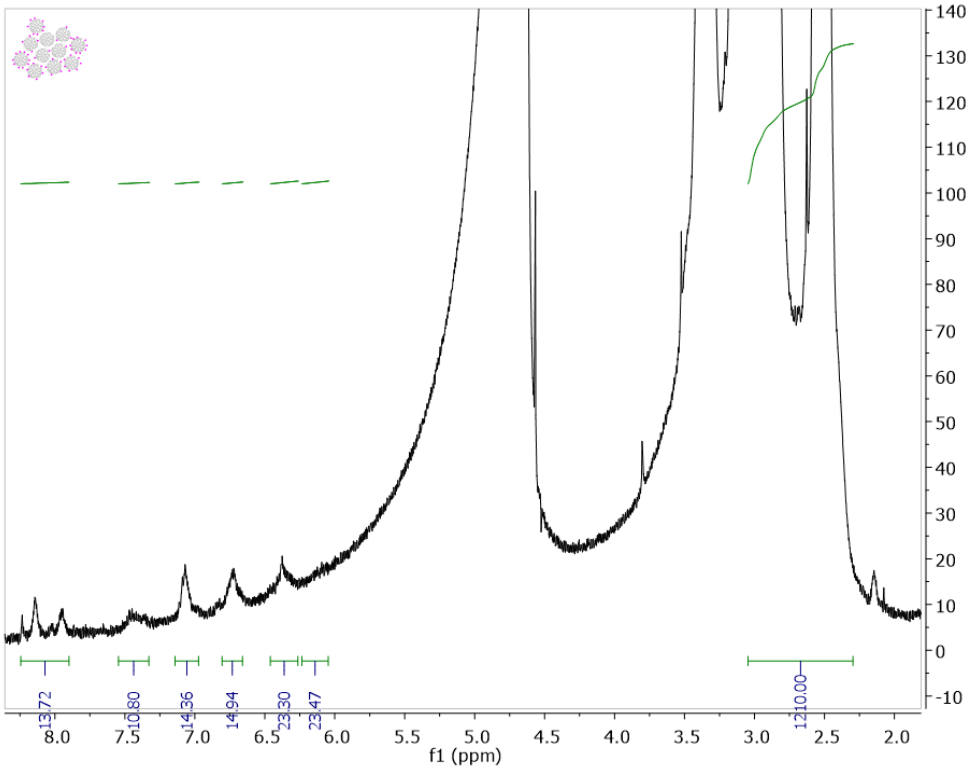
140
130
120
110
100
90
80
70
60
50
40
30
20
10
0
-10
13.72
10.80
14.36
14.94
23.30
23.47
12
10.00
8.0
7.5
7.0
6.5
6.0
5.5
5.0
4.5
4.0
3.5
3.0
2.5
2.0
f1 (ppm)

APPENDIX D

Supplemental Material for

Cationic Vector Intercalation into the Lipid Membrane Enables Intact Polyplex DNA Escape from Endosomes for Gene Delivery

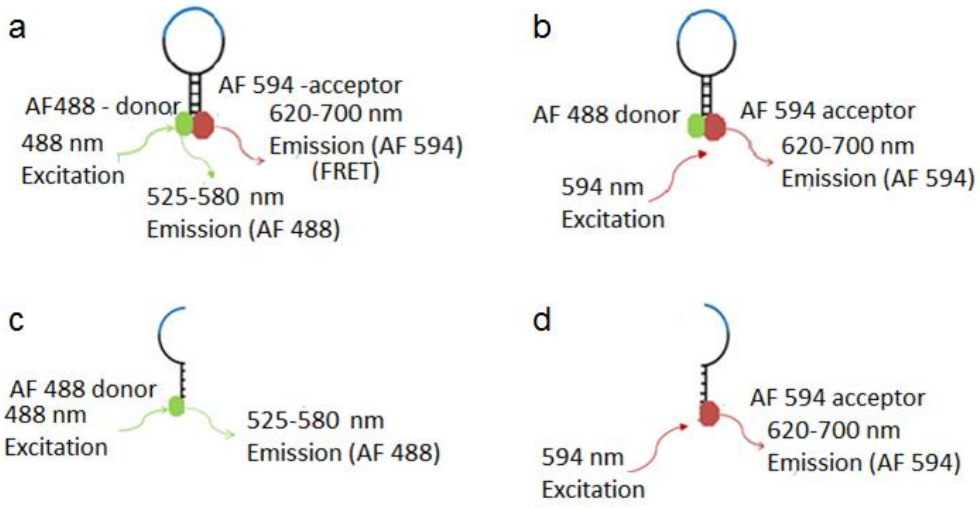

Figure D.1. Summary of oligonucleotide molecular beacon (OMB) probe response as a function of structural state and excitation wavelength. (a) Intact beacon shows both FRET red emission (620-700 nm) and green emission (525-580 nm) when excited by 488 nm laser.(b) Excitation of intact beacon by 594 nm laser allows quantification of cleaved beacon by providing a non-FRET level of emission from the AF594 dye. (c) Cleaved beacon exhibits green emission (525-580 nm) upon 488 nm laser excitation. (d) Cleaved beacon exhibits red emission (620-700 nm) upon 594 nm laser excitation.

Quantifying FRET: Several indices to quantify FRET (Intactness, I) using intensities of the FRET donor and acceptor have been described in the past . [9] These include equations A and 1:

$$I = \frac{I_{D\ ex,Aem}}{I_{Dex,Aem}+I_{Dex,Dem}} * 100 \quad \text{(A)}$$

$$I = \frac{I_{D\ ex,Aem}-I_{noise}}{I_{A\ ex,Aem}} * 100 \qquad (1)$$

In the subscripts A denotes FRET acceptor (AF594), D denotes FRET donor (AF488), ex denotes excitation and em denotes emission. For example, $I_{D\ ex,\ A\ em}$ means donor (AF488) is excited and emission from acceptor (AF594) is measured. Preliminary studies indicated that the Intactness measured using the equation A was dependent on the polymer used to make polyplexes. This difference is due to the fact that AF594 but not AF 488 was quenched significantly by jetPEI (Figure D.S2a-b). However, the Intactness measured using equation 1 was insensitive to quenching by the polymers (Figure D.S2b) since equation 1 uses only the intensities of the acceptor emission. Hence, all subsequent work uses equation 1 to quantify FRET.

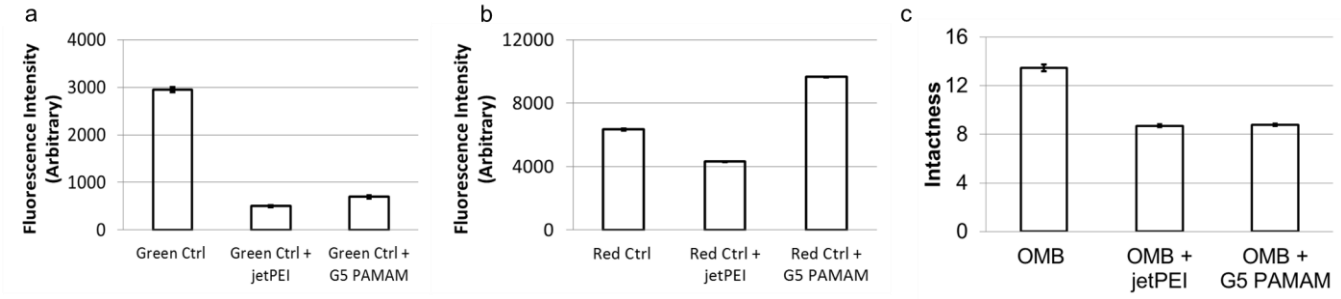

Figure D.2. OMB FRET in the presence of polymers. (a) A decrease in fluorescence emission in the 525-580 nm range is observed for beacons containing only AF488 in the presence of jet PEI or G5 PAMAM (485 nm excitation).(b) An increase in fluorescence emission in the 620-700 nm range is observed for beacons containing only AF 594 in the presence of G5 PAMAM (590 nm excitation). (c) Equation 1 was used to quantify FRET because it is unchanged by the changes in emission of AF594 induced by the vectors. As shown in panel C, this method showed similar FRET in the presence of both jetPEI and G5 PAMAM vectors.

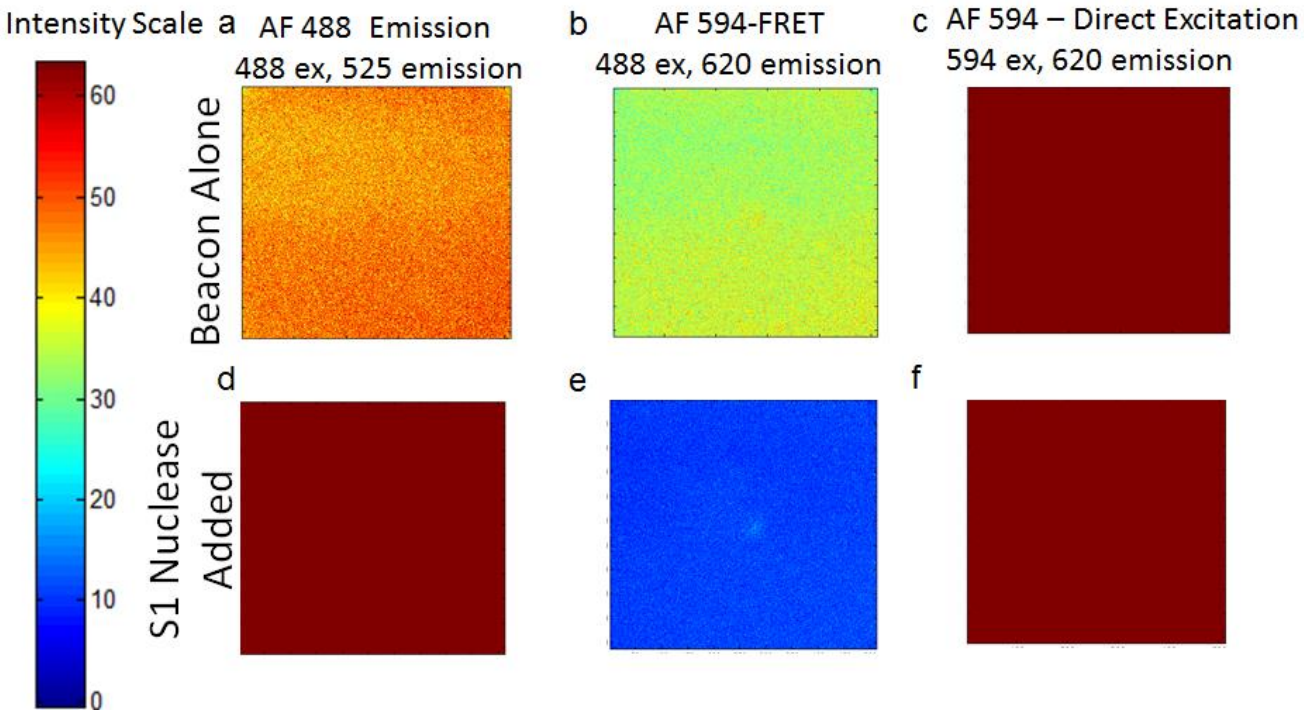

Figure D.3. OMB was dissolved in 1X - S1 nuclease buffer and the fluorescence assessed using a microscope. Color bar on the left indicates intensity of emission. (a) The excitation of the solution using a 488nm laser resulted in emission in the 525-580 nm channel. (b) When excited using the 488 nm laser, OMB emission was also observed in the 620-700 nm channel as expected. (c) The emission of AF 594 excited using a 594 nm laser was also measured. (d) When S1 nuclease was added to the same droplet, AF488 emission increased since energy was no longer being transferred by FRET. (e) FRET emission by AF594 also reduced to ~ 0 after the addition of S1 nuclease. (f) AF594 emission due to excitation by 594 nm laser did not change.

FRET from Cleaved Beacons

A factor that could confound the experiments is the possibility that cleaved beacons are held together by the polymer resulting in a FRET signal. To test for this possibility, cells were incubated with polyplexes containing both single labeled AF488 and AF594. Figures D.S4 and D.S5 shows that polyplexes made using a mixture of singly labeled beacons containing AF488 and AF594 can exhibit some FRET signal. However, the Intactness for these samples was 3

compared with 7-10 for jetPEI and G5 PAMAM beacons at 4h. Thus our controls confirm that the results obtained from the flow cytometry experiments and confocal experiments were representative of beacon cleavage within the cell.

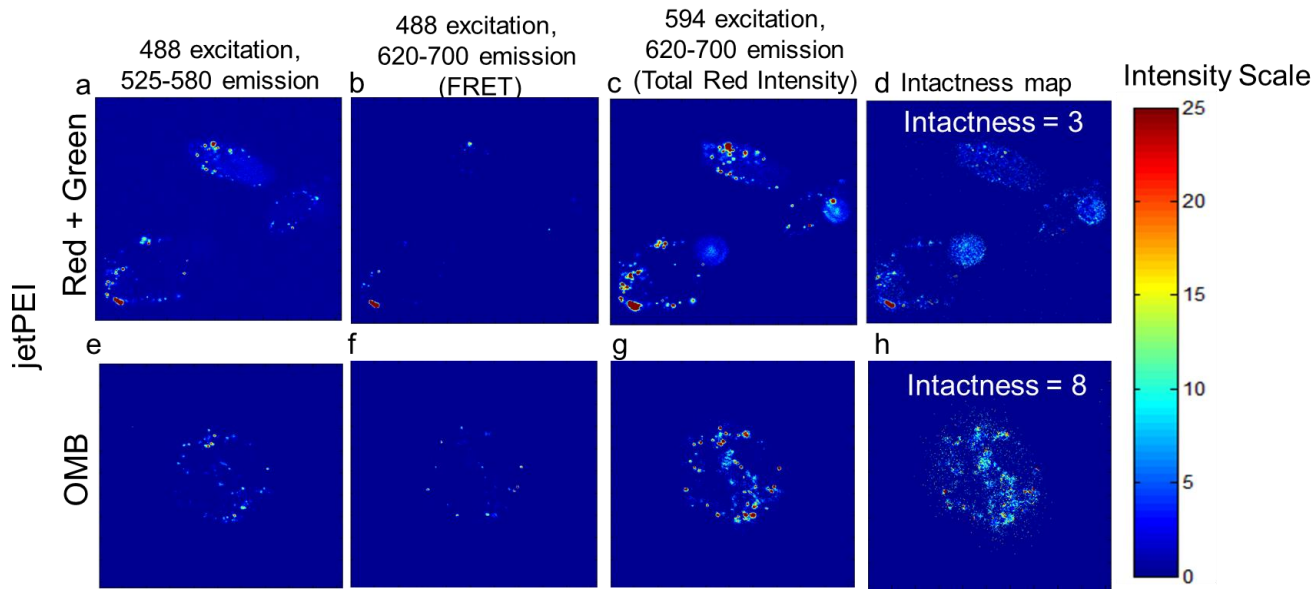

Figure D.4. FRET from mixed jetPEI polyplexes containing AF488 and AF594. FRET may occur between AF 488 and AF 594 from neighboring beacon molecules when present in the polyplex and can result in an elevated measure of intactness of the beacon. To test for this possibility, controls experiments were performed in which cells were treated with polyplexes made with a mixture of singly labeled beacons containing only AF 488 dyes and AF 594 dyes (1 ug each) for 3 h. (a) AF488 emission from polyplexes. (b) AF594 emission by excitation with 488 nm. These polyplexes with a mixture of singly labeled beacons still show some FRET signal inside cells. (c) AF594 emission by excitation with 594 nm. (d) Intactness map of mixed polyplexes shows an average value of 3. (e-g) As a comparison, fluorescence from the same channels are shown for a regular OMB. (f) Average intactness for a regular OMB is 8.

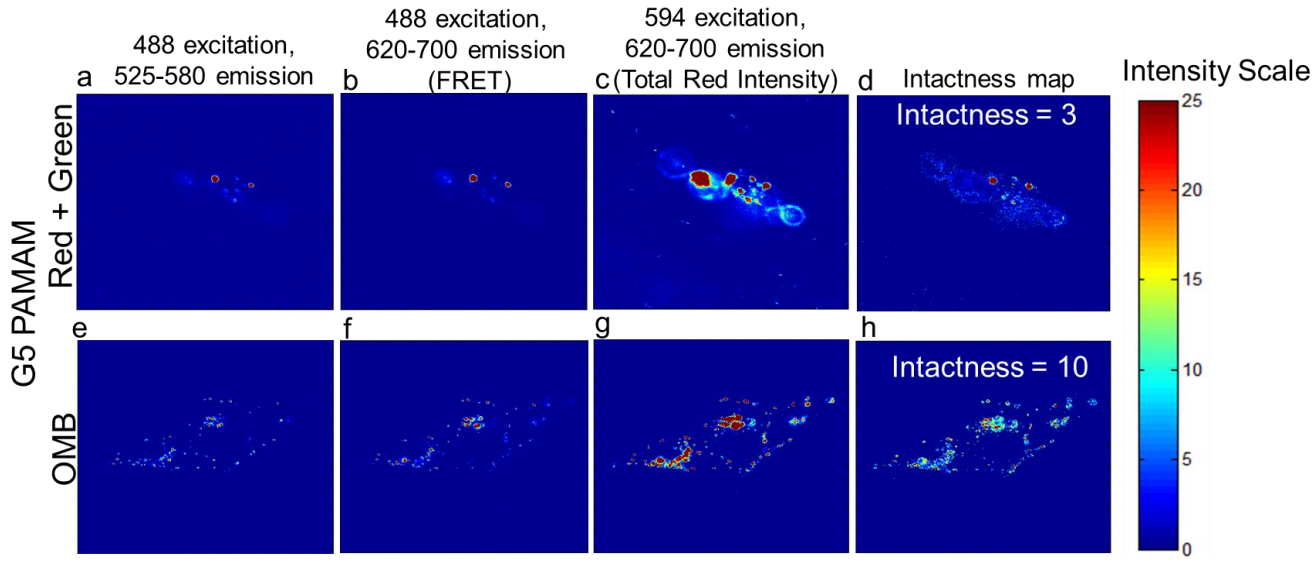

Figure D.5. FRET from mixed G5 PAMAM polyplexes containing AF488 and AF594. FRET may occur between AF 488 and AF 594 from neighboring beacon molecules when present in the polyplex and can result in an elevated measure of intactness of the beacon. To test for this possibility, controls experiments were performed in which cells were treated with polyplexes made with a mixture of singly labeled beacons containing only AF 488 dyes and AF 594 dyes (1 ug each) for 3 h. (a) AF488 emission from polyplexes. (b)AF594 emission by excitation with 488 nm. These polyplexes with a mixture of singly labeled beacons still show some FRET signal inside cells. (c) AF594 emission by excitation with 594 nm. (d) Intactness map of mixed polyplexes shows an average value of 3. (e-g) As a comparison, fluorescence from the same channels are shown for a regular OMB. (f) Average intactness for a regular OMB is 10.

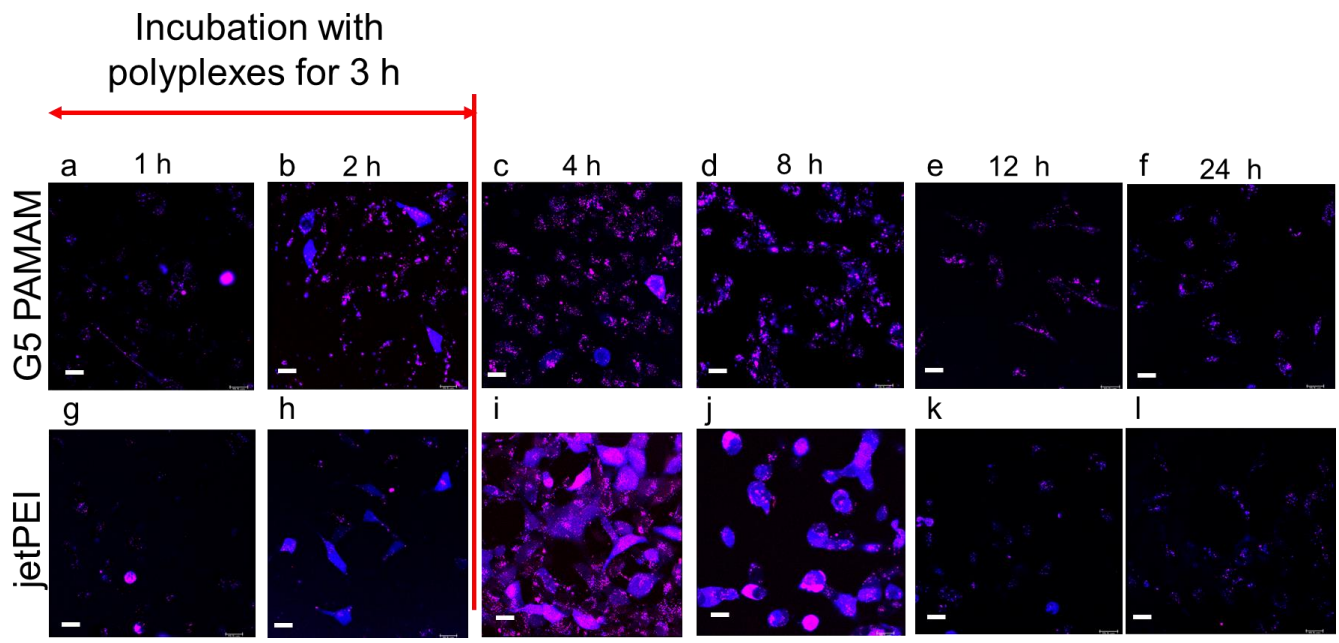

Figure D.6. Release and degradation of OMB over time in multiple cells. (a-f) HEK 293A cells exposed for 4 h to either G5 PAMAM polyplexes (N:P 10:1) formed using 0.5 µg OMB and 0.5 µg blank pDNA. OMB fluorescence was imaged using a confocal microscope. OMBs delivered using G5 PAMAM were mostly confined to vesicles and were intact in the punctate regions for 24 h. (g-l) OMB delivered using jetPEI polyplexes exhibited a punctate distribution at 1 h. At 2h, 4h and 8 h, a diffuse distribution of intact OMB in the cytosol was observed which dissipated by 12 h.The OMB left in punctate spots at 12 and 24 h had a substantial fraction of intact OMBs. Scale bar represents 20 µm for all images.

A quantitative analysis of cytosolic DNA cleavage in a cell population

Degradation of the OMB in a cell population was quantifed using flow cytometry. HEK 293A cells were incubated with G5 PAMAM and jetPEI polyplexes (N:P 10:1) formed using a 1:1 mixture (0.5 µg each) of OMB and blank pDNA for 3 h and analyzed using flow cytometry (Figure D.S7) at 4 h. In order to quantify the difference in FRET intensity as function of polymer vector, the experiment was performed using a flow cytometer that contained both 488 nm and 594 nm lasers. In this experiment, cells were first exposed to the 488 nm laser and emission from 525-580 nm was collected. The same cells were then exposed to a 594 nm laser and emission

from 620-700 nm was then collected. This allowed us to quantify FRET emission using equation 1. Results in Figure D.S7 show that the FRET signal from cells treated using G5 PAMAM beacons was higher than the FRET signal from cells treated using jetPEI polyplexes. The Intactness (eq 1) for the OMBs formed using G5 PAMAM and jetPET at 4 h were 20% and 7%, respectively (Figure D.S4). Figure D.S8 also shows results from cells at 30 min, 4 h and 16 h after incubation with polyplexes using a different flow cytometer with only a 488 nm laser. In cells exposed to polyplexes for 16 h, the level of FRET decreased. Nevertheless, G5 PAMAM polyplexes exhibited higher FRET that jetPEI polyplexes.

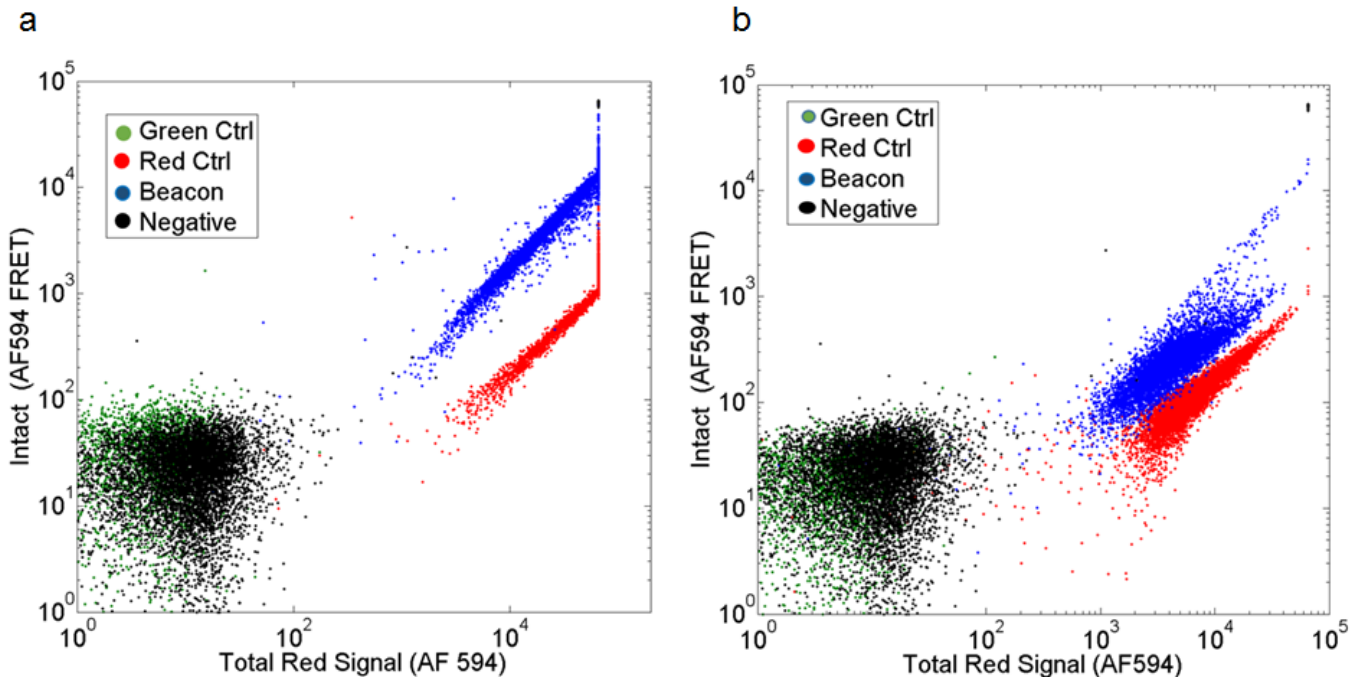

Figure D.7. OMB degradation in a population of cells. (a) HEK 293A cells treated for 4 hours with G5 PAMAM polyplexes (N:P = 10:1) formed using a 1:1 ratio of OMB and blank pDNA (0.5 µg each). The x-axis shows fluorescence emission (620-700 nm) upon 594 nm excitation. The y-axis shows the FRET fluorescence emission (620-700 nm) signal upon 488 nm excitation. (b) HEK 293A cells treated for 4 hours with jetPEI polyplexes (N:P = 10:1) formed using a 1:1 ratio of OMB and blank pDNA (0.5 µg each). jetPEI polyplexes (N:P 10:1) Polyplexes formed using G5 PAMAM exhibit 10x greater FRET signal than those formed with jet PEI as judged by the relative y-shift of the blue and red cell distributions.

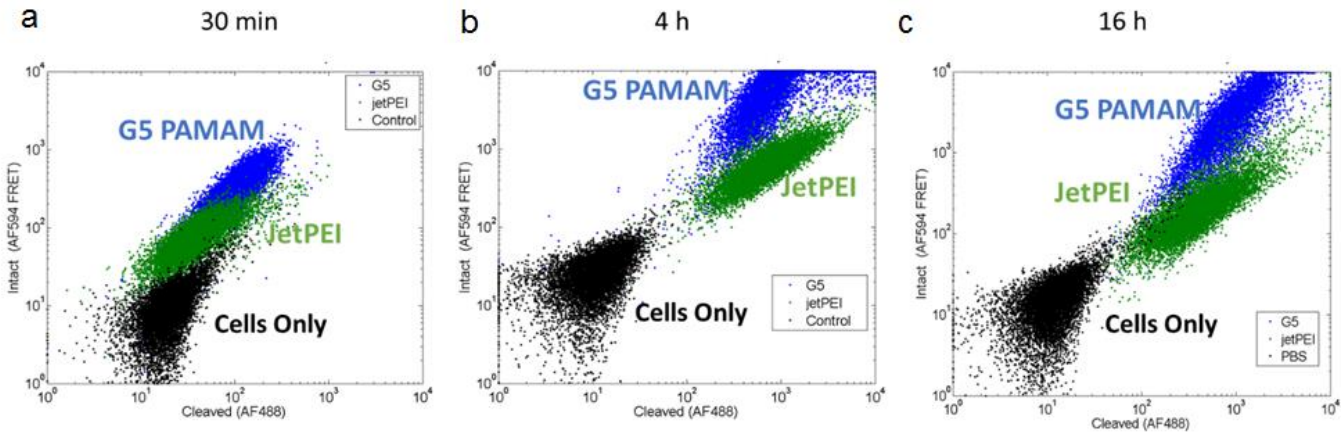

Figure D.8. OMB Degradation Over Time Studied Using Flow Cytometry. (a) HEK 293A cells exposed for 30 minutes to either G5 PAMAM or jet PEI polyplexes (N:P 10:1) formed using 0.5 μg of oligonucleotide molecular beacon and 0.5 μg blank pDNA. The x-axis shows fluorescence emission (525-580 nm) upon 488 nm excitation. The y-axis shows the FRET fluorescence emission (620-700 nm) signal upon 488 nm excitation. OMBs delivered using jetPEI show less AF594 FRET emission than beacons delivered using G5 PAMAM. (b) HEK293A cells exposed to G5 PAMAM or jetPEI polyplexes for 3 h in serum free media followed by 1 h incubation in complete media. OMBs delivered using jetPEI show less AF594 FRET emission than beacons delivered using G5 PAMAM. (c) HEK293A cells exposed to G5 PAMAM or jetPEI polyplexes for 3 h in serum free media followed by 13 h incubation in complete media. OMBs delivered using jetPEI show less AF594 FRET emission than beacons delivered using G5 PAMAM.

Colocalization of OMB with Organelle Markers

In order to test if there were differences in the amount of intact OMB present in the endoplasmic reticulum (ER) and Golgi apparatus, we stained cells using organelle markers for ER (ER tracker blue) and Golgi apparatus (wheat germ agglutinin-AF 350, WGA). Figures D.S9 and D.S10 illustrate the colocalization of beacons with ER tracker blue and WGA. Colocalization was quantified using Mander's coefficients combined with manual thresholds to ensure that background noise did not confound colocalization coefficients.[10] M1 (fraction of organelle markers that overlap with OMB) and M2 (fraction of OMB that overlap with the organelle marker) have been calculated for both FRET signal (intact beacons) and AF488 or AF594 signal

by direct excitation (the sum of intact and cleaved beacons). Since the organelle markers are widespread, a higher fraction of beacon signal was colocalized with the organelle markers. Hence, M2 was greater than M1 for all cases. We observed that the colocalization of OMB with ER was higher than the colocalization with the Golgi for both L-PEI and G5 PAMAM polyplexes. Two sample t-test was used to test if the colocalization of the OMB delivered using jetPEI and G5 PAMAM with organelle markers were significantly different. The results are presented in tables I and II. The experiments are designed such that a 2 fold difference in colocalization can be detected with a power greater than 0.8. In cases where the t-test showed a significant difference in colocalization of OMB, the power was ≥ 0.8. For cases where the means were not significantly different, the power was lower.

a. G5 PAMAM

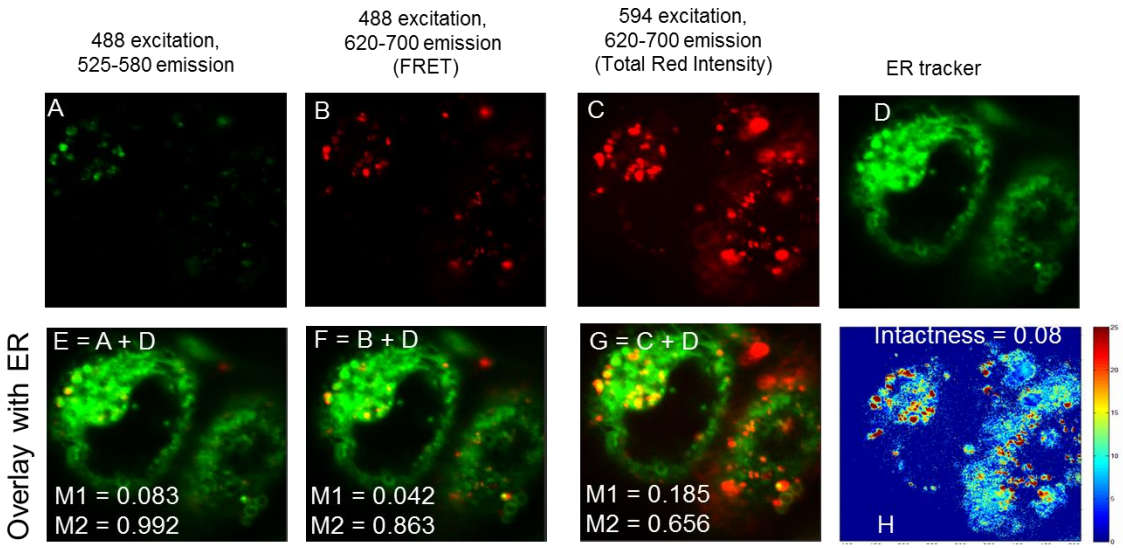

b. jetPEI

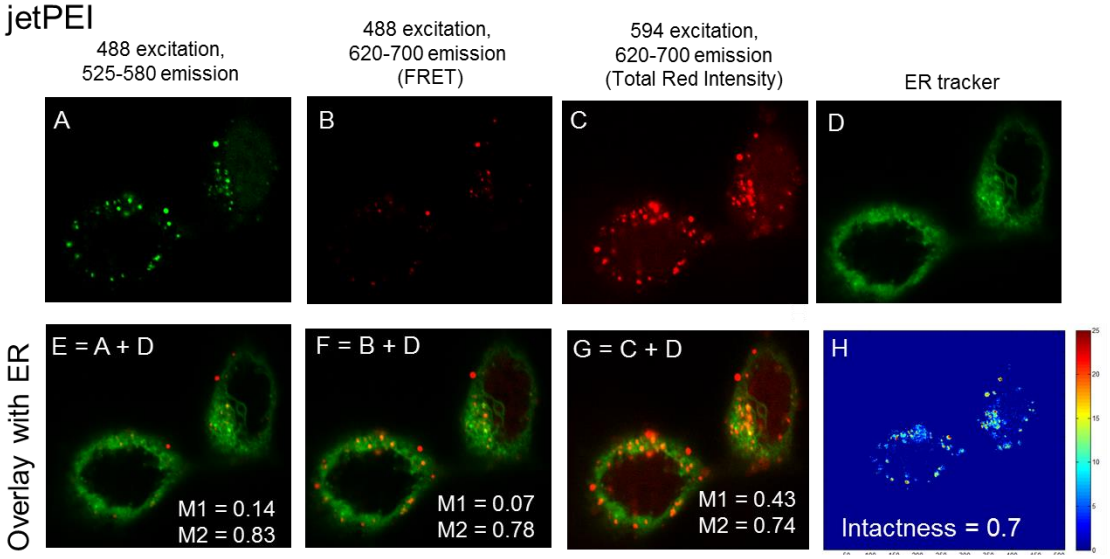

c. Average Mander's coefficients from multiple cells

A

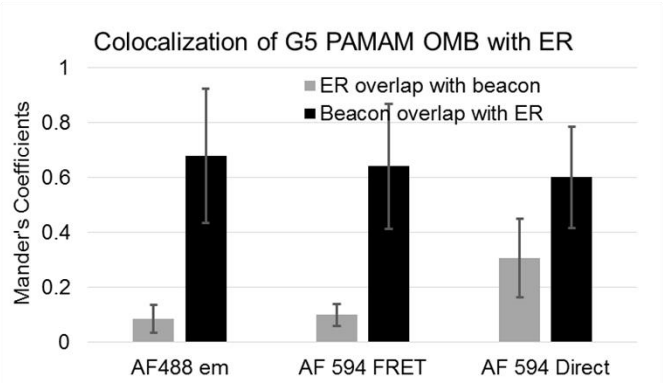

B

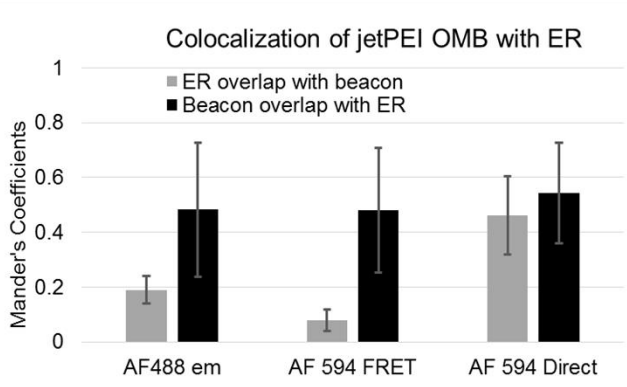

Figure D.9. Colocalization of OMB with ER tracker blue. (a) Images A-D show the signal from beacons and ER tracker respectively for beacons delivered using G5 PAMAM. Images E-G show the overlay of A, B and C with D. (b) Images show the signal from the beacons and ER for beacons delivered using jetPEI. For beacons delivered using both jetPEI and G5 PAMAM, a large fraction of intact (B) and cleaved beacons (A) are distributed close to the ER (D) as indicated by the Mander's coefficients (M2). JetPEI beacons also show a diffuse distribution throughout the cell. (c) Since the diffuse beacons do not colocalize with ER, the average Mander's coefficients presented in B for jetPEI beacons are less than the average Mander's coefficients presented for G5 PAMAM beacons in A.

Table D.1. Colocalization of OMB with ER tracker

	AF 488	**AF594 FRET**	**AF594 direct**	
M1	0.0126	0.1075	0.0324	p value
	1	0.5	0.8	power
M2	0.0531	0.0754	0.4761	pvalue
	0.8	0.8	0.1	power

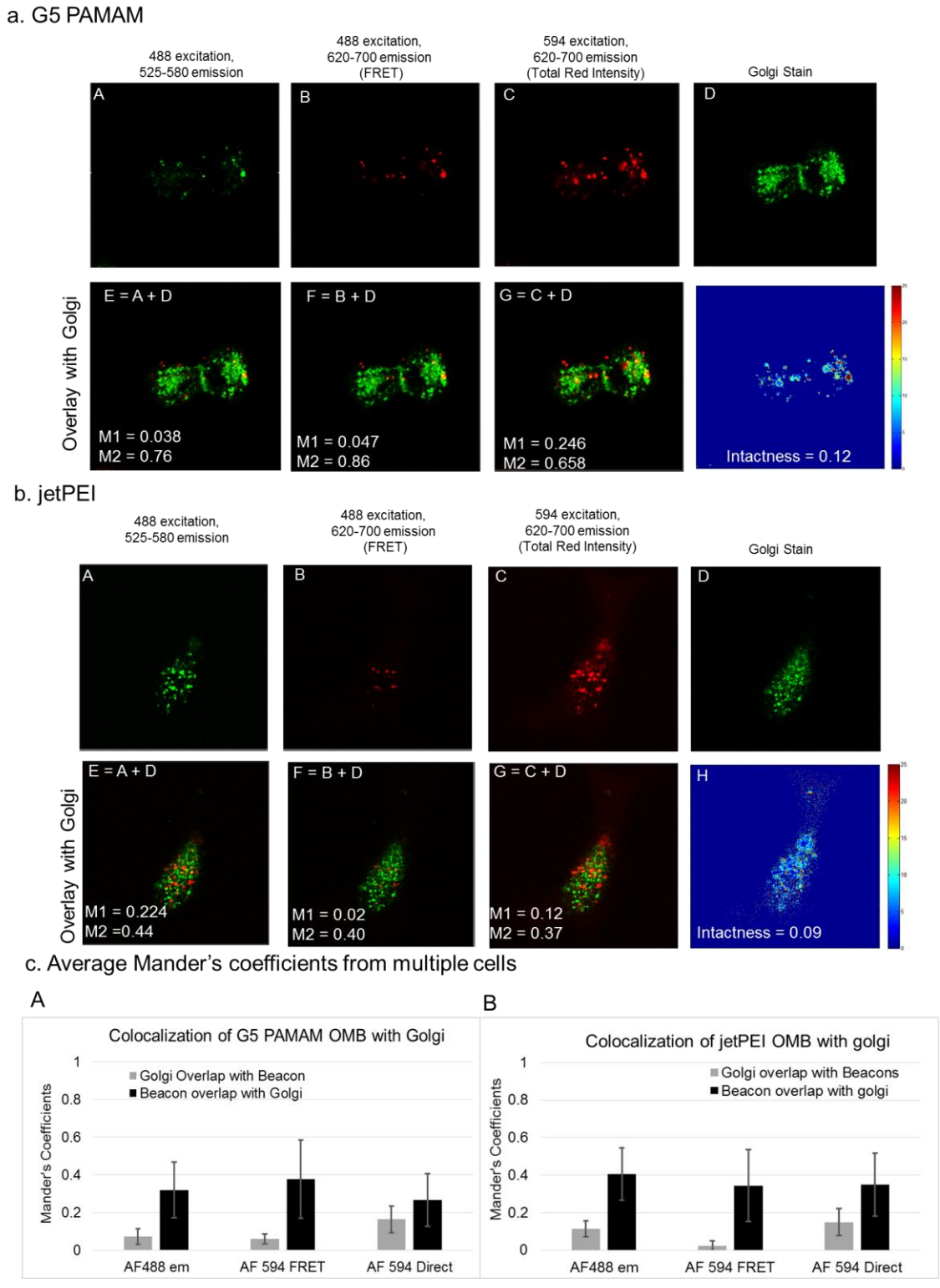

Figure D.10. Colocalization of OMB with golgi stain (WGA-AF350). (a) Images A-D show the signal from beacons and wheat germ agglutinin (golgi marker) respectively for beacons delivered using G5 PAMAM. Images E-G show the overlay of A, B and C with D. (b) Images show the

signal from the beacons and ER for beacons delivered using jetPEI. More overlap is seen between the beacon and and wheat germ agglutinin (golgi marker) for jetPEI polyplexes. (c) For both G5 PAMAM polyplexes and jetpEI polyplexes, the fraction of beacons overlapping with golgi signal were less than the average fraction of beacons overlapping with ER tracker. Interestingly, the fraction of beacons overlapping with golgi was less for jetPEI polyplexes than G5 PAMAM polyplexes.

Table D.2. Colocalization of OMB with WGA

	AF 488	**AF594 FRET**	**AF594 direct**	
M1	0.088	<0.0001	0.6879	p value
	0.5	1	0.08	power
M2	0.1716	0.6872	0.2131	pvalue
	0.5	0.09	0.3	power

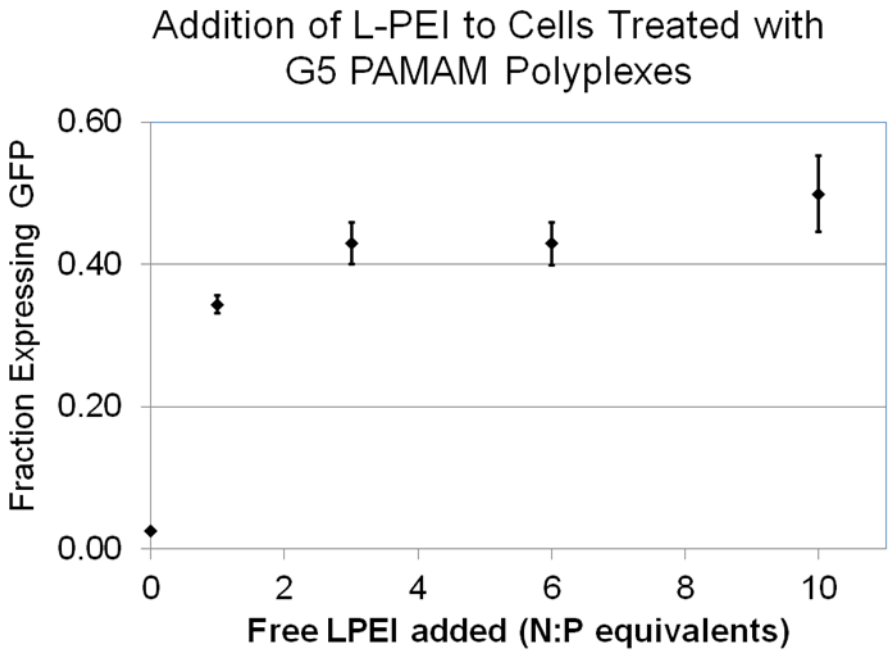

Figure D.11. Addition of free L-PEI to cells incubated with G5 PAMAM polyplexes for 3 h. The addition of free L-PEI at concentration seen in L-PEI polyplexes with N:P ratio of 1:1 was siufficient to increase the percent of cells expressing GFP by 10X to 34 ± 1 % compared to cells exposed to G5 PAMAM polyplexes alone. Addition of more free L-PEI did not increase fraction of cells expressing GFP substantially.

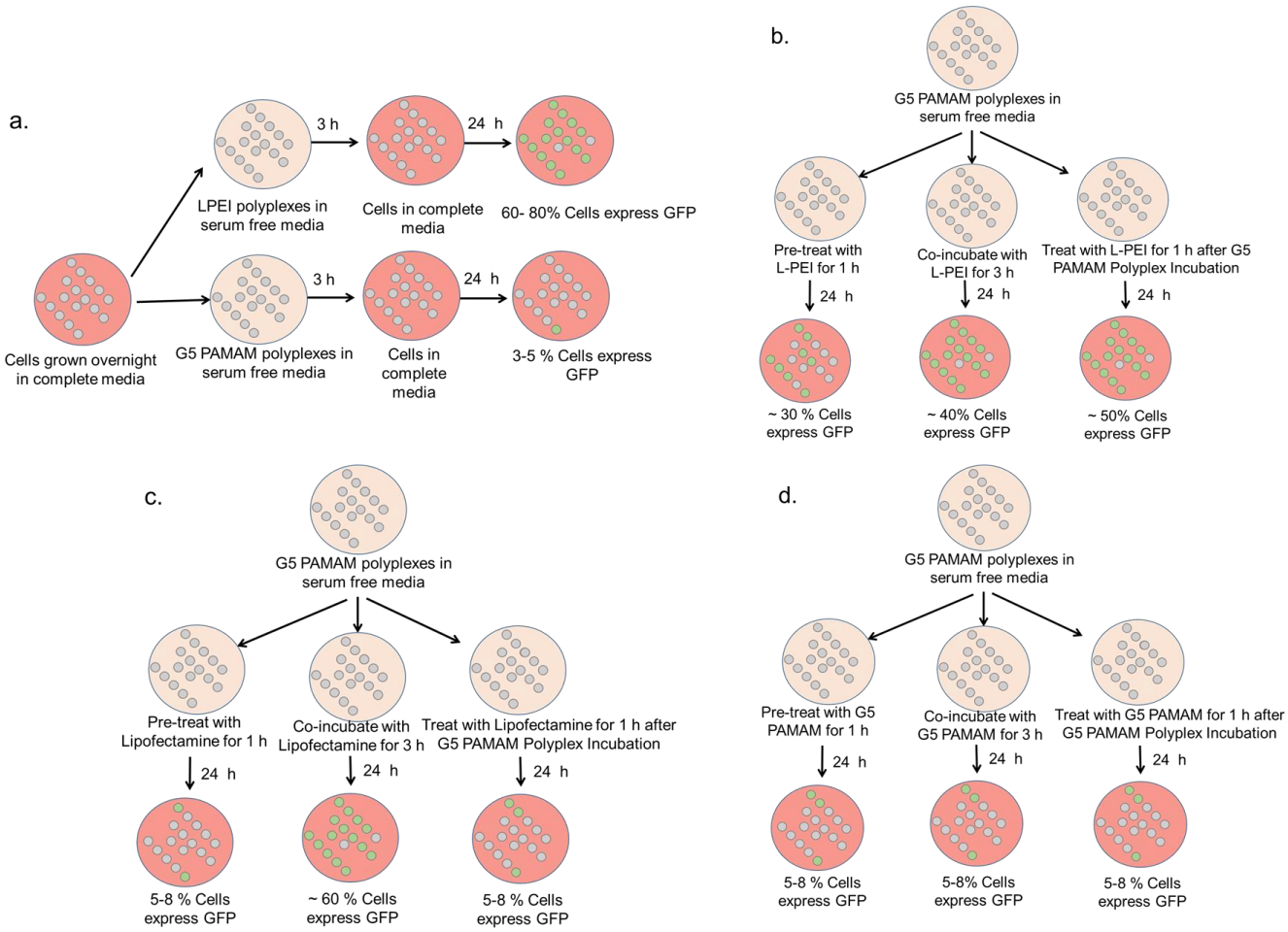

Figure D.12. Summary of experiments that tested GFP expression in cells. (a) 60-80% of HEK 293A cells treated with L-PEI polyplexes (N:P = 10) showed GFP expression. Under 5% of cells treated with G5 PAMAM polyplexes (N:P = 10) showed gene expression.(b) Adding L-PEI to cells treated with G5 PAMAM polyplexes resulted in increased genen expression. (c) Lipofectamine only increased expression dramatically if co-incubated with G5 PAMAM polyplexes. (d) Adding extra G5 PAMAM does not increase gene expression.

References:

1. Rattan, R. *et al.* Polyplex-Induced Cytosolic Nuclease Activation Leads to Differential Transgene Expression. *Mol. Pharm.* **10,** 3013–3022 (2013).

2. Ribeiro, S. C., Monteiro, G. A. & Prazeres, D. M. F. The role of polyadenylation signal secondary structures on the resistance of plasmid vectors to nucleases. *J. Gene Med.* **6,** 565–573 (2004).

3. Azzoni, A. R., Ribeiro, S. C., Monteiro, G. A. & Prazeres, D. M. F. The impact of polyadenylation signals on plasmid nuclease-resistance and transgene expression. *J. Gene Med.* **9,** 392–402 (2007).

4. ur Rehman, Z. *et al.* On the Mechanism of Polyplex-and Lipoplex-Mediated Delivery of Nucleic Acids: Real-Time Visualization of Transient Membrane Destabilization Without Endosomal Lysis. *ACS Nano* **7,** 3767–3777 (2013).

5. Itaka, K. *et al.* In situ single cell observation by fluorescence resonance energy transfer reveals fast intra-cytoplasmic delivery and easy release of plasmid DNA complexed with linear polyethylenimine. *J. Gene Med.* **6,** 76–84 (2004).

6. Matovina, M., Seah, N., Hamilton, T., Warren, D. & Landy, A. Stoichiometric incorporation of base substitutions at specific sites in supercoiled DNA and supercoiled recombination intermediates. *Nucleic Acids Res.* **38,** e175 (2010).

7. Luzzietti, N., Knappe, S., Richter, I. & Seidel, R. Nicking enzyme-based internal labeling of DNA at multiple loci. *Nat. Protoc.* **7,** 643–653 (2012).

8. Lee, W., von Hippel, P. H. & Marcus, A. H. Internally labeled Cy3/Cy5 DNA constructs show greatly enhanced photo-stability in single-molecule FRET experiments. *Nucleic Acids Res.* **42,** 5967–77 (2014).

9. Zal, T. & Gascoigne, N. R. J. Photobleaching-Corrected FRET Efficiency Imaging of Live Cells. *Biophys. J.* **86,** 3923–3939 (2004).

10. Bolte, S. & Cordelieres, F. P. A guided tour into subcellular colocalization analysis in light microscopy. *J. Microsc.* **224,** 213–232 (2006).